AD-A019 049

THE DEVELOPMENT OF AN ADVANCED ANTI-ICING/DEICING
CAPABILITY FOR U. S. ARMY HELICOPTERS. VOLUME II.
ICE PROTECTION SYSTEM APPLICATION TO THE UH-1H
HELICOPTER

J. B. Werner

Lockheed-California Company

Prepared for:

Army Air Mobility Research and Development Laboratory

November 1975

THE DEVELOPMENT OF AN ADVANCED ANTI-ICING/DEICING CAPABILITY FOR U. S. ARMY HELICOPTERS

Volume II - Ice Protection System Application to the UH-1H Helicopter

Lockheed-California Company
Box 511
Burbank, Calif. 91520

November 1975

Final Report for Period 30 June 1973 - 30 June 1975

EUSTIS DIRECTORATE POSITION STATEMENT

This Directorate concurs in the findings presented in this report
and recommends use of the information contained herein to enhance
the design and development of ice protection systems for rotary-wing
aircraft.

The main thrust of this effort was to accurately quantify design
criteria for helicopter ice protection systems and to identify and
evaluate the most promising rotor blade ice protection concept. Many
concepts have been analyzed, and the cyclic-electrothermal concept
was identified as the most promising for application to future and
existing Army helicopters.

Although the cyclic-electrothermal blade deicing concept appears to be
the most feasible for application to helicopter rotor blades in the
near future, the penalties for ice protection are significant. Addi-
tionally, this deicing concept has been subjected only to limited
simulated icing tests. Although this flight testing was adequate to
demonstrate concept feasibility, additional simulated and natural ice
testing is mandatory to finalize system control parameters and to re-
solve problem areas identified to date.

This directorate will continue investigation of ice protection con-
cepts that show promise of minimizing system penalties.

The Project Engineer for this effort was Richard I. Adams of the
Military Operations Technology Division.

REPORT DOCUMENTATION PAGE

READ INSTRUCTIONS
BEFORE COMPLETING FORM

1. REPORT NUMBER	2. GOVT ACCESSION NO.	3. RECIPIENT'S CATALOG NUMBER
USAAMRDL-TR-75-34B		

4. TITLE (and Subtitle)

THE DEVELOPMENT OF AN ADVANCED ANTI-ICING/
DEICING CAPABILITY FOR U. S. ARMY HELICOPTERS,
Volume II - Ice Protection System Application to the
UH-1H Helicopter

5. TYPE OF REPORT & PERIOD COVERED

Final Report for Period 30 June
1973 to 30 June 1975

6. PERFORMING ORG. REPORT NUMBER

LR 27180

7. AUTHOR(s)

J. B. Werner

8. CONTRACT OR GRANT NUMBER(s)

DAAJ02-73-C-0107

9. PERFORMING ORGANIZATION NAME AND ADDRESS

Lockheed-California Company
Box 511
Burbank, Calif. 91520

10. PROGRAM ELEMENT, PROJECT, TASK
AREA & WORK UNIT NUMBERS

62209A 1F262209AH76 00
002 EK

11. CONTROLLING OFFICE NAME AND ADDRESS

Eustis Directorate
U. S. Army Air Mobility R&D Laboratory
Fort Eustis, Va. 23604

12. REPORT DATE

November 1975

13. NUMBER OF PAGES

220

14. MONITORING AGENCY NAME & ADDRESS (if different from Controlling Office)

15. SECURITY CLASS. (of this report)

Unclassified

15a. DECLASSIFICATION/DOWNGRADING
SCHEDULE

16. DISTRIBUTION STATEMENT (of this Report)

Approved for public release; distribution unlimited.

17. DISTRIBUTION STATEMENT (of the abstract entered in Block 20, if different from Report)

18. SUPPLEMENTARY NOTES

Volume II of a 2-volume report.

19. KEY WORDS (Continue on reverse side if necessary and identify by block number)

Ice	Electrothermal Deicing
Snow	Protection
Deicing System	Ice Prevention
Advanced Rotary-Wing Aircraft	Freezing Point Depressant
UH-1H	

20. ABSTRACT (Continue on reverse side if necessary and identify by block number)

The work which has been accomplished under this program is reported in two volumes. The first
volume, Design Criteria and Technology Considerations, discusses (1) icing severity level analysis
and recommended design criteria, (2) adverse weather protection technology, (3) a trade-off
comparison between different types of ice protection systems for various categories of helicopters,
and (4) a technology development program for an advanced electrothermal deicing system. This
volume describes the application of the recommended electrothermal deicing system to a UH-1H
test aircraft. It provides a detailed description of the modifications to the basic aircraft

DD FORM 1473 EDITION OF 1 NOV 65 IS OBSOLETE

Block 20. Abstract continued.

(including the flight test instrumentation) and the results of the ground and flight test program for that aircraft conducted in the winter of 1974-75

SUMMARY

The work which has been accomplished under this program is reported in
two volumes. The first volume, Design Criteria and Technology Consid-
erations, discusses (1) icing severity level analysis and recommended
design criteria, (2) adverse weather protection technology, (3) a trade-
off comparison of different types of ice protection systems for various
categories of helicopters, and (4) a technology development program for
an advanced electrothermal deicing system. This volume, Ice Protection
System Application to the UH-1H Helicopter, describes the application of
the recommended electrothermal deicing system to a UH-1H test aircraft.
It provides a detailed description of the modifications to the basic air-
craft (including the flight test instrumentation) and the results of the
ground and flight test program for that aircraft conducted in the winter
of 1974-75.

Meteorological design criteria are provided for freezing rain and
drizzle, snow, and supercooled droplets (icing). It is shown that the
minimum (99th percentile criterion) temperature for freezing rain is
$14^{\circ}F$, that the liquid water content does not exceed 0.32 grams per
cubic meter and that the droplet diameter ranges from 400 to 1200 microns.
The 99th percentile snowfall criterion ranges from 1.6 grams per cubic
meter at $15^{\circ}F$ to 2.1 grams per cubic meter at $35^{\circ}F$. It is recommended
that the existing FAA (and equivalent military specification) be used
for the severity of supercooled droplets under continuous maximum icing
conditions and that the 99th percentile severity be used for intermittent
maximum conditions.

The technology review focuses upon protection against supercooled
clouds, the normal icing problem. It is shown that protection against
freezing rain is not justified and that snow can be accommodated by

proper basic design with negligible penalty. The principal emphasis in technology is on main and tail rotor blade protection. It is concluded that electrothermal cyclic deicing offers the best solution for existing and future helicopters and that the same basic design is suitable for both all-metal and composite blade construction. It is shown that the most critical problem with the electrothermal system is obtaining a reliable blade heater assembly, and this has been identified as the key development task. The timer/controller/power distribution subsystem recommended for use with the cyclic deicing system is a hybrid solid-state/electromechanical design incorporating extensive electrical fault sensing and protection.

Protection requirements for engine inlets, windshields, radomes, flight probes, and weapons and sensors are also discussed, and the state of the art of ice detectors and severity level instrumentation is defined. Engine inlet protection is highly dependent upon the inlet design, and it is shown that several existing designs apparently do not require a protection system. Windshield protection utilizing electrical anti-icing by a transparent conductive film is recommended. The need for radome ice protection depends upon the type of radar employed and its location on the aircraft, and often the radar performance penalties associated with an ice protection system exceed the penalties due to ice. Flight probe anti-icing designs are currently more than satisfactory. The need for weapon system ice protection needs to be experimentally evaluate, as there is no available information. Sensor windows, e.g., those of cameras, IR sights, and weapon sights, need protection when they are subject to icing, but it is shown that the only feasible method of protection is a cover door or an engine bleed air heating system.

A trade-off has been performed for windshield ice protection, and the results show that the electrical system is superior.

The trade-off analysis compares five systems of rotor blade ice protection systems for seven helicopter types. The five systems are: the electrothermal cyclic deicing system, the chemical freezing point depressant (alcohol) system, and three variations of circulating liquid loop anti-icing utilizing engine exhaust gas heat. Weight, performance penalties, reliability, and production, operating and maintenance costs have been developed. In addition, system weight and performance penalties have been evaluated for the systems for freezing rain requirements as well as supercooled droplets, and the electrothermal and chemical system requirements have also been evaluated as a function of icing severity. The results show that based upon year-around penalties and an icing encounter duration of 1 hour, the chemical freezing point depressant system is the lightest and cheapest system for all but the two heaviest helicopter types (with electrothermal system second or first). If, however, maximum mission time is used as the basis for calculating year-around system weight and penalties, the electrothermal deicing system is shown to have less penalty for helicopters with a TOGW in excess of 16,000 lb. Based upon performance and logistics considerations, however, the electrothermal system is recommended for all types of helicopters.

The materials, processes, quality controls, and structural criteria and properties are described for main and tail rotor deicer heater blankets. Recommended materials are described, and it is shown that the resulting structural properties are satisfactory. Electroformed nickel is recommended for the erosion shield, and a stainless steel etched foil design is recommended for the heating element. The through-scan ultrasonic inspection technique is recommended for bonding verification on the rotor blade as the last production step.

The electrothermal deicing system which has been developed and demonstrated on the UH-1H helicopter requires 13.4 kilowatts for the main

rotor blades (two) and 4 kilowatts for the tail rotor. The main rotor blade is divided into six spanwise sections for cyclic deicing, with the heating sequence from the tip to blade root. Power density varies from 12 watts/in² at the tip to 26 watts/in² at the root. The entire tail rotor is deiced at 20 watts/in². The main rotor gyro stabilizer bar and tip weight is anti-iced (continuously heated during icing conditions) at 5 watts/in² and requires 2 kw. The windshields are also anti-iced with electric heat (using a tin oxide coating) and require 5.4 kw. A new ac electrical system is installed using a 20/30 kva generator. This system also has the capability of providing a variable voltage in accordance with icing severity: 160 volts (line-to-line) for light icing, 200 volts (the nominal value) for moderate icing, and 230 volts for heavy icing.

The helicopter underwent 15 hours of airworthiness and electrical systems flight testing at Edwards Air Force Base, California, and 15 hours at Moses Lake, Washington, behind the CH-47 Helicopter Icing Spray System (HISS). A total of 35 flight hours and 19 ground operating hours were obtained on the aircraft. All structural loads measured were found to be within limits, and aircraft handling qualities were better than those for the basic aircarft (reduced main rotor boost-off control force requirements).

Icing tests behind the tanker were made at ambient temperatures as low as -4°F and at liquid water contents up to 0.75 gram per cubic meter. Complete shedding of the ice from the main rotor blade was observed at temperatures down to $+5^{\circ}$F, but shedding was reported to be incomplete inboard of station 83 (where the doublers start) at an ambient of -4°F. No tail rotor icing was observed. Windshield and stabilizer anti-icing power appeared to be adequate. It is recommended that further flight testing be conducted to achieve a greater variety of conditions: hover behind the Canadian National Research Council Spray Rig at Ottawa, Ontario, behind the HISS, and in natural icing.

PREFACE

This program to determine adverse weather protection requirements was conducted by the Lockheed-California Company under Contract DAAJO2-73-C-0107 to the Eustis Directorate, US Army Air Mobility Research and Development Laboratory (USAAMRDL) Fort Eustis, Virginia.

The program was performed during the period 30 June 1973 through 30 June 1975. Technical monitoring of the project for USAAMRDL was by Richard I. Adams.

The Lockheed program was under the technical direction of J. B. Werner, Senior Research and Development Engineer. Additional Lockheed personnel making major technical contributions to the program included J. T. Alpern, W. A. Anderson, H. Carr, R. H. Cotton, M. J. Cronin, A. M. James, R. M. Johnston, J. E. Rhodes, G. M. Ryan, J. Schmidt, K. K. Schmidt, V. S. Sorenson, and J. H. Van Wijk.

Simulated icing tests were conducted by the US Army Aviation Engineering Flight Activity (USAAEFA), Edwards Air Force Base, California. Major technical contributions were made by Maj. Robert K. Merrill, Project Officer and Engineering Test Pilot, Capt. Louis Kronenberger, Flight Test Engineer, and Capt. Leonard Hanks, chase plane pilot and icing test consultant.

TABLE OF CONTENTS

Preceding page blank

LIST OF ILLUSTRATIONS

13

LIST OF TABLES

1.0 INTRODUCTION

The ice protection technology review and trade-off study discussed in
Volume I of this report concluded that the electrothermal cyclic deicing
system is the concept which should be applied to those helicopters
having missions which require all-weather operation. As part of this
program, therefore, an advanced electrothermal deicing system has been
designed, built, and flight tested on an Army UH-1H aircraft. This
volume describes the ice protection system which has been installed,
the other associated modifications to the aircraft, the instrumentation
and flight test data acquisition system, the test procedure, and test
results.

Preliminary system design started in January, 1974, and ground testing
of the completed and installed system on the aircraft started at the
contractor's plant in Burbank, California, in December, 1974. Air-
worthiness and system checkout tests were completed by the contractor
at the Army Aviation Engineering Flight Activity facility at Edwards
Air Force Base on February 28, 1975, and the aircraft was then ferried
to Moses Lake, Washington for simulated icing tests behind the CH-47
Helicopter Icing Spray System (HISS). Testing at Moses Lake was
completed on March 31, 1975.

2.0 ICE PROTECTION SYSTEM DESCRIPTION

Figure 1 schematically shows the changes which have been made to the standard aircraft. An electrothermal cyclic deicing system has been installed on the main and tail rotor blades,   ! a heating blanket to provide anti-icing also has been installed over the stabilizer bar arm and tip weight. In addition, the plastic pilot's and copilot's windshields have been replaced with laminated glass heated windshields. These additions and changes to the aircraft resulted in the addition of appropriate ice protection control systems and a new ac generating system to supply the electrical power demands.

Two different types of ice detector (and icing severity) systems and OAT (outside air temperature) probes also have been installed to provide inputs to both cockpit instruments and the main and tail rotor automatic deicing controller.

No changes were made to the engine air inlet system, as experience indicated that engine power has not been affected by ice buildups on the inlet screens of the UH-1H aircraft.

The subsections below describe in detail the additions and modifications which have been made to the aircraft.

2.1 MAIN AND TAIL ROTOR

2.1.1 Main Rotor

The installation of the electrothermal cyclic deicing heaters on the main rotor blade is shown schematically in Figure 2. Each blade is divided spanwise into 6 zones; and both blades are powered simultaneously so as to provide symmetrical ice shedding. Heating starts at the tip (Zone I) and proceeds sequentially inboard to the root (Zone VI). The upper surface is heated to approximately 12% chord (2.75 inches

19
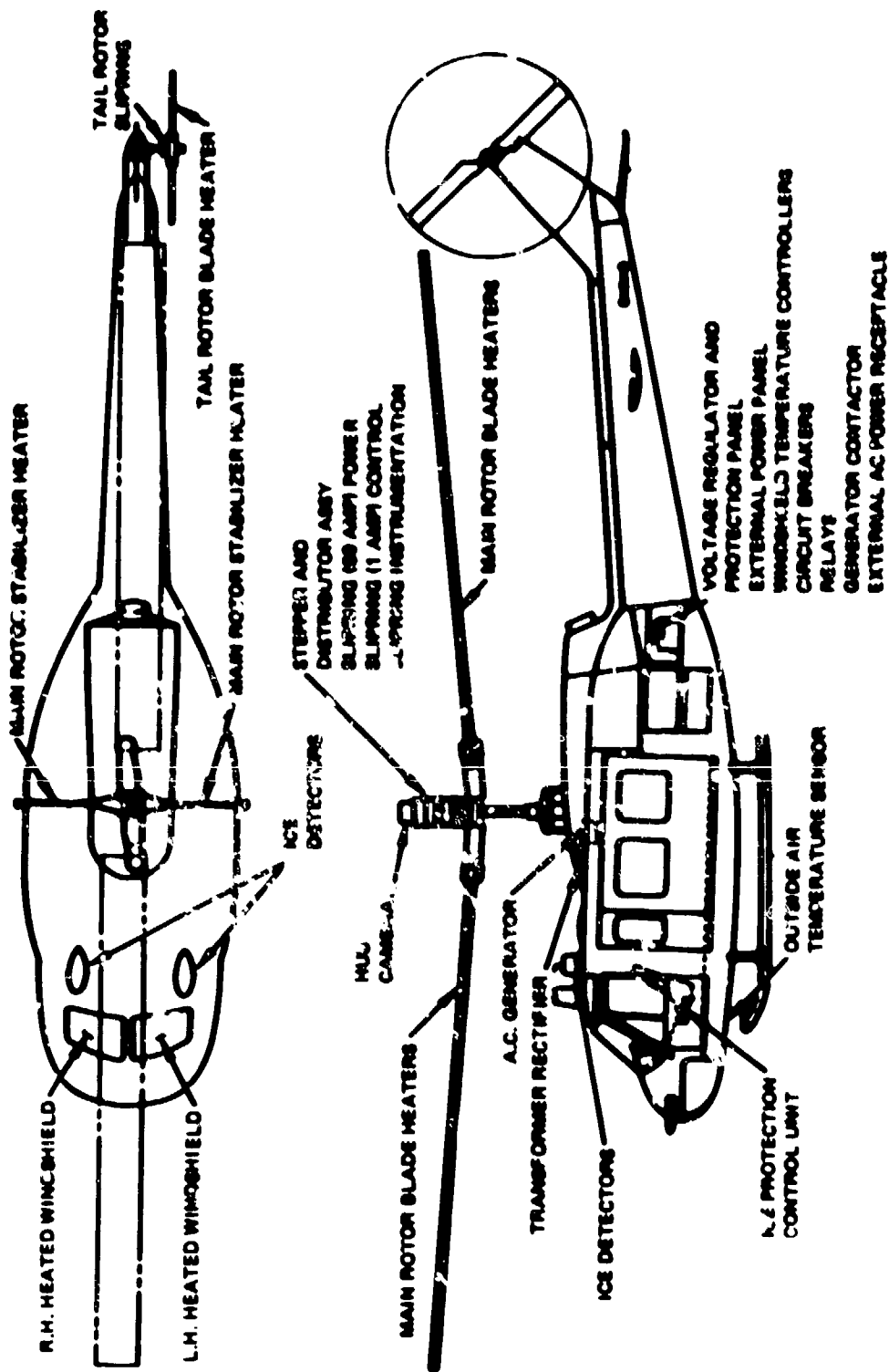
Figure 1. Advanced Ice Protection System Modification to UH-1H.
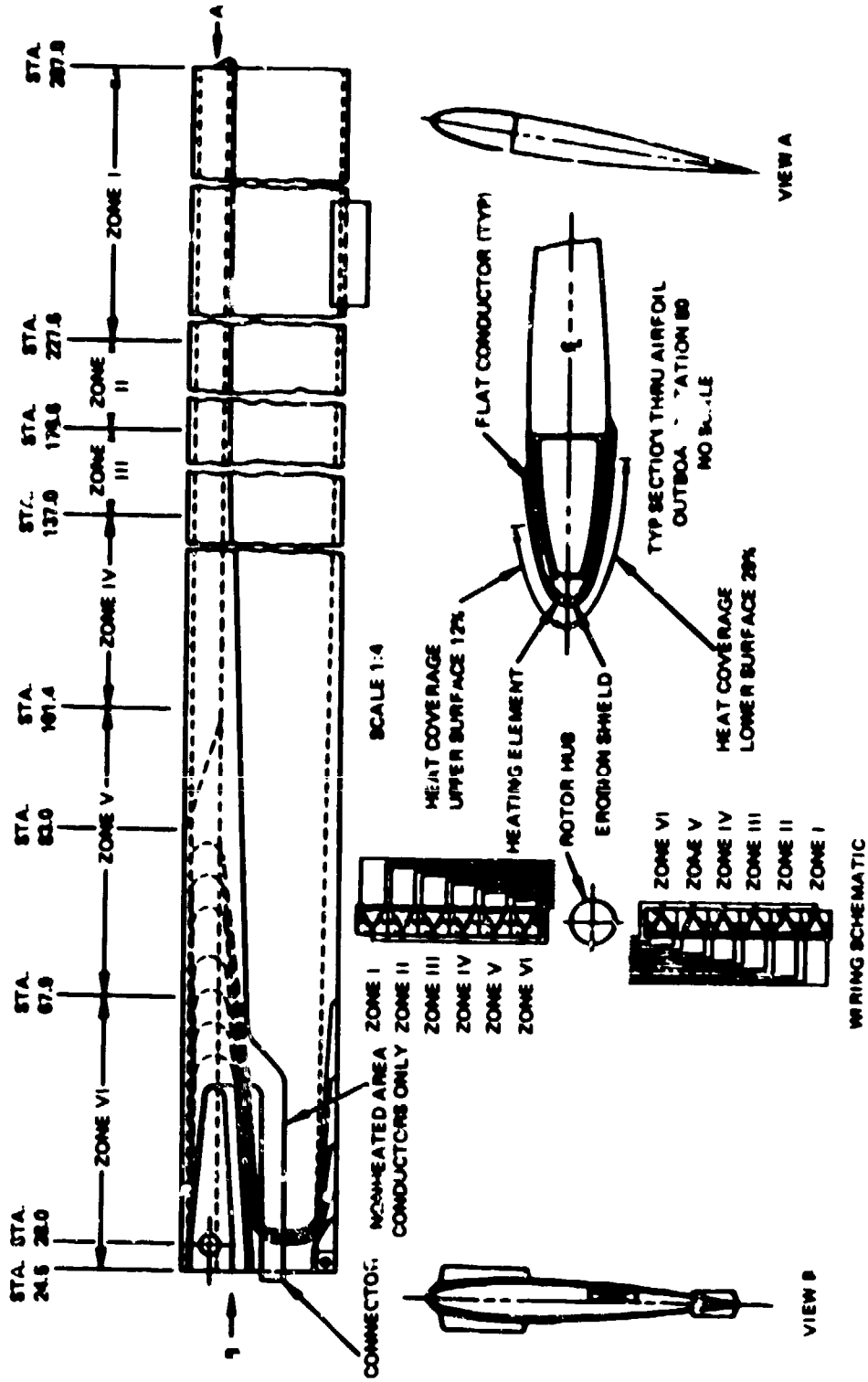
Figure 2. Main Rotor Blade Heater Blanket.

back from the leading edge), and the lower surface is heated to approximately 29% chord (6.45 inches back from the leading edge).

The power density is varied from tip to root as shown in Figure 5, and each zone uses the same total power: 6.7 kw/blade (per zone).

The power variation takes into account the kinetic heating effect which varies as the square of the blade radius (thus tending to reduce the required temperature rise outboard), and the "cooling effect" (the heat transfer coefficient), which varies as the square root of the blade radius (thus tending to increase the rate of heating required outboard for a given required temperature rise). The required power all time and the operation of the blade deicing control system is described in Section 2.2.

There are two basic heating areas on the main rotor: the basic blade area from rotor station 83 to the tip (approximately 17 feet) and an inner section which covers the rotor over the doubler area (sta. 23 to sta. 83).

The cross section of the deicer heater installation is shown in Figure 4. The erosion shield for the outer 17 feet of the main blade is 0.030 inch 1/4 H 301 stainless steel, and the erosion shield for the inner 5 feet (the doubler area) is 0.010 inch 7075 aluminum. The blade heater consists of an erosion shield, an epoxy/fiberglass dielectric layer between the erosion shield and the heater element (which is of etched foil made from 0.005 inch stainless steel), and inner fiberglass epoxy layers. The existing stainless steel and cobalt erosion shield is removed from the blade in order to minimize the blade weight change. The blade is then built back to contour with a fiberglass epoxy layer filler. The complete deicer boot erosion shield assembly is then bonded to the existing filler built-up blade.
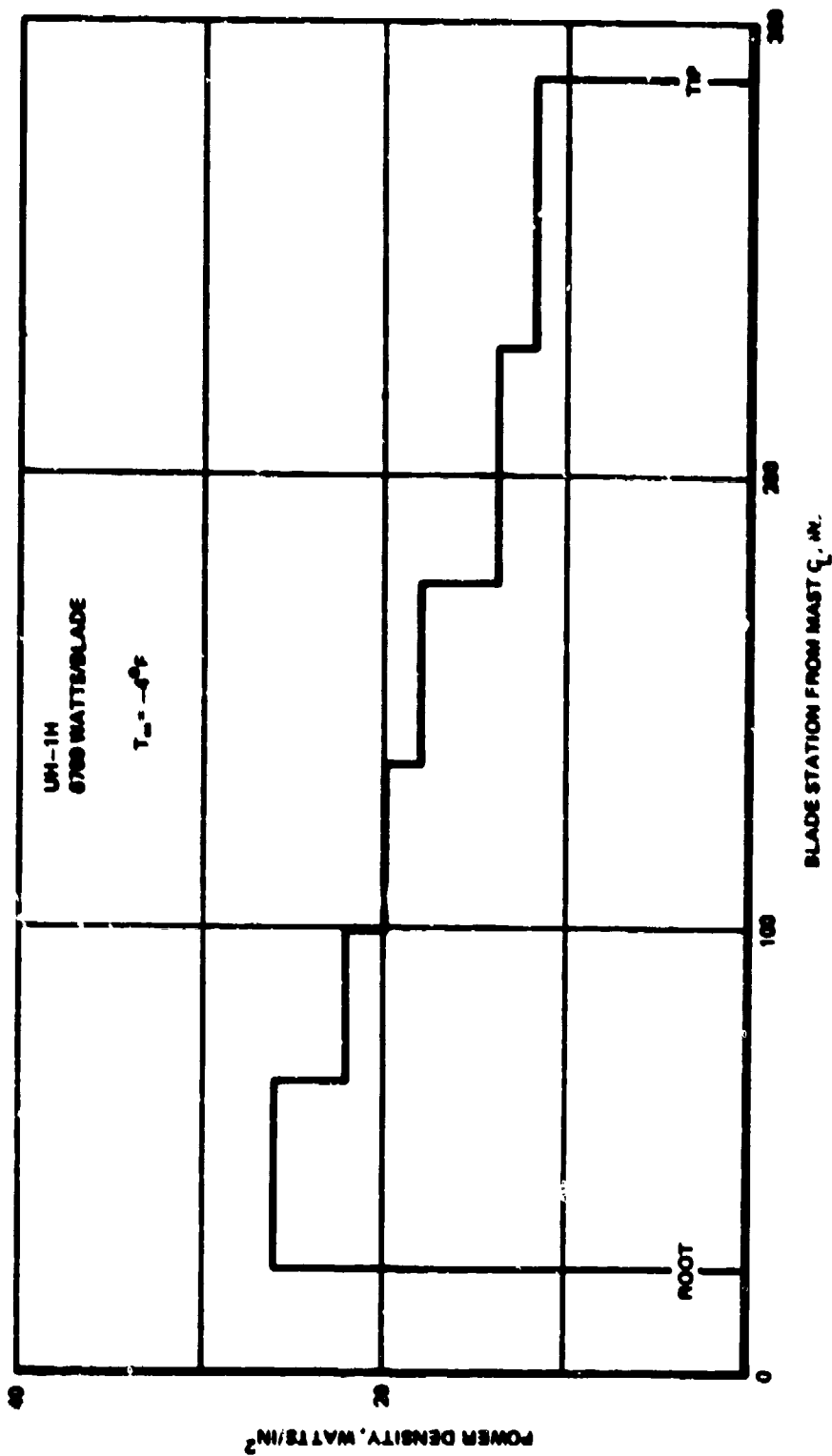
Figure 3. Main Rotor Blade Spanwise Power Density Distribution.

23

EROSION SHIELD .030 STAINLESS STEEL FOR MAIN ROTOR
NICKEL TAPERED FROM 0.030 AT LEADING EDGE TO 0.010
AT AFT EDGE FOR TAIL ROTOR

BLADE
STRUCTURE

0.010 INSULATION

0.005 HEATER RIBBON

0.035 INSULATION

CROSS SECTION
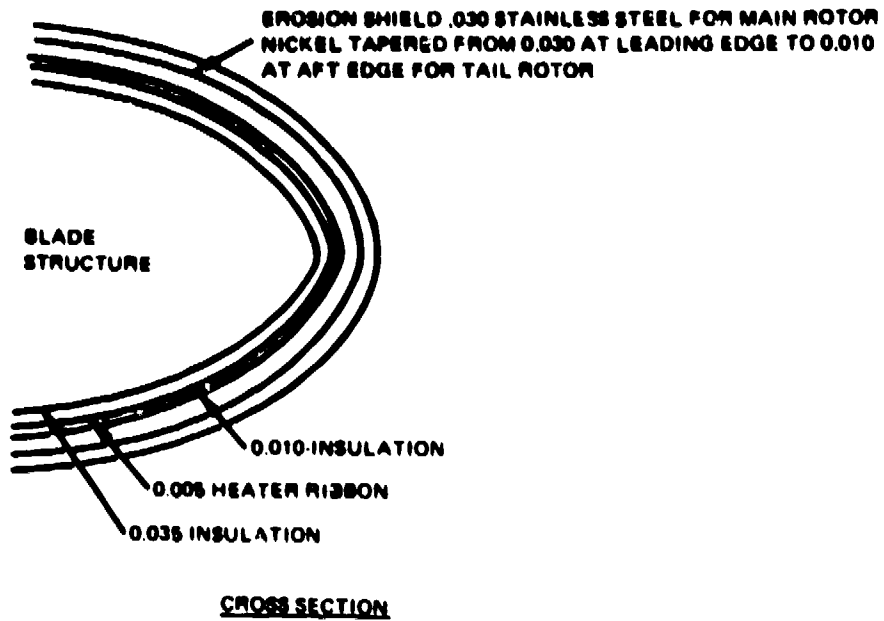
NOTE: ALL DIMENSIONS IN INCHES

0.050 +0.010 TYP GAP

0.197 +0.010 TYP RIBBON

INSTALLATION PATTERN
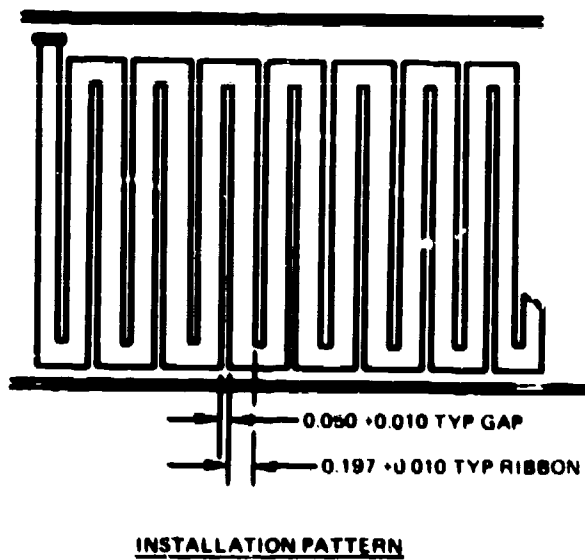
Figure 4. Rotor Blade Heater Design.

Although the heated area extends back to 12% chord on the upper surface, the erosion shield extends further aft due to the need to provide area for the copper braid power feed conductors to the various segments. The erosion shield extends a constant 6.83 inches back on the lower surface between stations 288 (blade tip) and 83, the start of the doublers. The shield extends back a constant 5.20 inches on the upper surface between stations 288 and 155 and tapers uniformly back to 6.43 inches at station 83. The heated area over the doubler is irregular.

The blade heater uses three-phase power (at a nominal voltage of 200 volts, line-to-line), and each phase powers a different spanwise area of each zone. A common copper braid ground return is used on the lower surface behind the heated area but under the erosion shield. Since the boot basically extends almost 0.090 inch outside the existing blade contour, a fiberglass fairing is provided behind the erosion shield. This extends back approximately 1 inch.

Power leads extend out of the deicer boot in straps at the inboard end and then terminate in waterproof connectors for cable assemblies leading into a power distribution stepper switch on top of the rotor mast.

The stepper switch provides the cycling to the six zones, so only four power leads need to go through the sliprings and then into the fuselage through a hollow tube in the center of the transmission shaft. The slipring assembly housing (Figure 5) contains not only the sliprings but instrumentation components (page 46) and the mounting for a camera which was used for obtaining inflight motior pictures of one rotor blade. A total of 24 sliprings were provided on the main rotor to provide for rotor deicing (4), stabilizer bar anti-icing (2), camera operation (6), and instrumentation (12).

2.1.2 Tail Rotor

The tail rotor deicer boot and 'nner fill layers are similar to that of the main rotor. On the tail rotor, only the basic blade has a deicer heater; there is no deicing coverage for the inboard doubler area. The erosion shield is electroformed nickel tapered from 0.030 inch at the leading edge to 0.010 inch at the trailing edge.

The tail rotor blade heated area extends from stations 20.68 to station 50. Protection extends aft to 10% chord on the "outboard" surface (1 inch) and to 25% chord on the "inboard" surface (2.3 inches). The erosion shield, however, actually extends aft 2 inches on the "outboard" surface and 3.05 inches on the inboard surface and spanwise to the tip (station 51). As on the main rotor blades, an aerodynamic fairing extends behind the erosion shield.

Since the heated area on the tail rotor is smaller than a zone on the main rotor, the entire tail rotor is deiced as an entity, at a uniform nominal power intensity of 20 watts/in^2 at 200 vAC. Thus, no stepper switch is required for the tail rotor.

Figure 6 shows the tail rotor slipring assembly. It contains 4 power and 12 instrumentation rings.

2.1.3 Stabilizer Bar

The stabilizer bar is continuously heated during icing to provide an anti-icing capability, at 5 watts per square inch (Figure 7). Control of the stabilizer and the counterweight heaters is again from the pilot's control panel, and the switch is normally ON. Unlike the main and tail rotor elements which are three phase, the stabilizer heater is single phase - connected across one pair of lines of the three-phase ac system. Separate sliprings in the main rotor mast and circuit breakers are used for the stabilizer bar.

Figure 5. Main Rotor Slipring Assembly.

Figure 6. Tail Rotor Slipring Assembly.

27

STA.

TAPER TO 0.75 IN. DIAMETER

1.5 IN. DIAMETER, BASIC BAR

SYMMETRICAL ABOUT ℄

HEATER BLANKET LENGTH

36.9 IN.
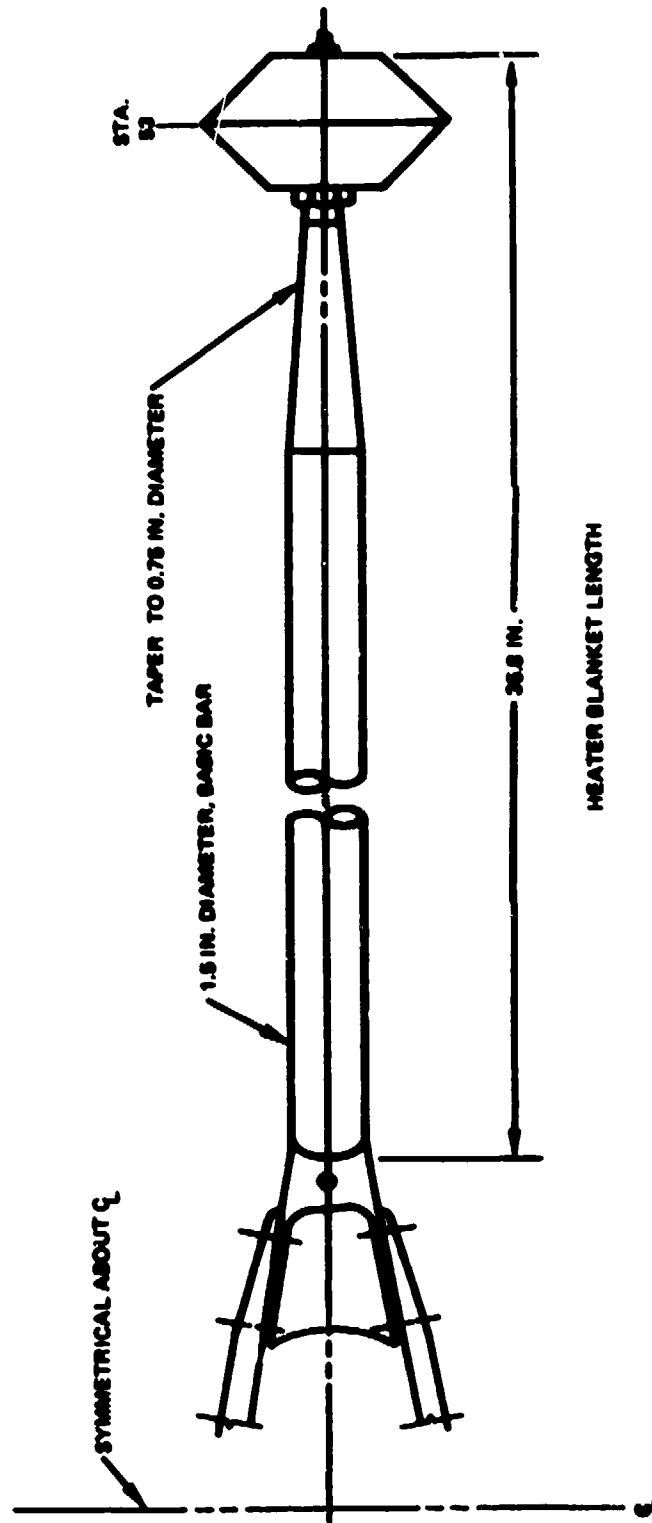
Figure 7. Sketch of Heater Blanket Coverage For Stabilizer Bar.

2.2 ELECTRICAL DESCRIPTION

As noted in Section 2.1, the main rotor blade is divided into six heated areas or zones, each drawing equal power. The power demand of the main rotor is approximately 13.2 kva under moderate (200 Vac) icing conditions. The tail rotor blades, as mentioned previously, are deiced simultaneously. Their normal power demand is approximately 4.0 kva (moderate icing). Additional ac electrical loads on the aircraft are the stabilizer bar (3 kva approximate) and the two heated windshields. The windshield load is 5.2 kva, bringing the total anti/deicing peak load (at 200 v) to approximately 25.4 kva. The systems can also be used at 160 volts or 230 volts, as discussed below, with corresponding total power requirement of 16.3 kw or 33.6 kw, respectively.

2.2.1 Power Generation System

Since the basic UH-1H is equipped with only two 28-volt, 300-amp, dc generators (one a starter-generator), a new 20/30 kva ac generator is used to meet the new icing loads and other electrical loads in the helicopter. The generator selected is a Bendix model 28B23-15. It is one of a few machines that fits on the 5 inch bolt circle pad of the dc generator and which also operates at the same nominal drive speed of 6600 rpm. For reliability reasons, a brushless configuration of this generator is used. While the generator is designed to use blast-air cooling, it is operated in the UH-1H with a self-cooled internal fan since the generator is designed to operate with $120^{\circ}C$ cooling air.

The new three-phase 200/115-volt ac generator is installed at the 12 o'clock position on the transmission pad. The pad is normally occupied by a 28-volt dc 300-amp generator. Because of this substitution, the available redundant dc power generation capability would have been deleted from the vehicle. Thus, another modification of the UH-1H

basic power system consisted of the installation of a 28-volt, 200-amp, transformer rectifier (T/R) unit. This unit is located on top of the fuselage next to the ac generator and under the movable cowling, as shown in Figure 8.

The dc system has been rewired to make the starter generator the primary generator (instead of the standby generator which it is in the basic vehicle). With this change, the transformer-rectifier unit now operates as the standby dc system.

All new electrical components and items associated with the ice protection system have been located in the electrical load center except for the control panels in the cockpit and a power stepper switch located on the main rotor head assembly (for distributing power sequentially to the six main rotor heating zones). The load-center components include circuit breakers, relays, ac deicer power relay box, voltage regulators, terminal strips, etc. All these have been installed with a minimum of change to the basic layout of the existing components. Also located in this area is a new three-phase external ac power receptacle to permit checkout of the ice protection system on the ground without running the engine.

2.2.2 System Operation and Control

Control of the deicing system is accomplished from two panels mounted at the aft end of the control pedestal in the cockpit. These panels (Figure 9) are known as the pilot's control panel and the deicing control panel. Functionally, all control resides in these two units. The pilot's control panel establishes the operational mode of the system (and monitors its performance), while the controller acts as an automatic processor, accepting the pilot's data inputs and those of the OAT (outside air temperature) and LWC (liquid water content) sensor systems.

Figure 8.   AC Generator and Transformer Rectifier Installation.
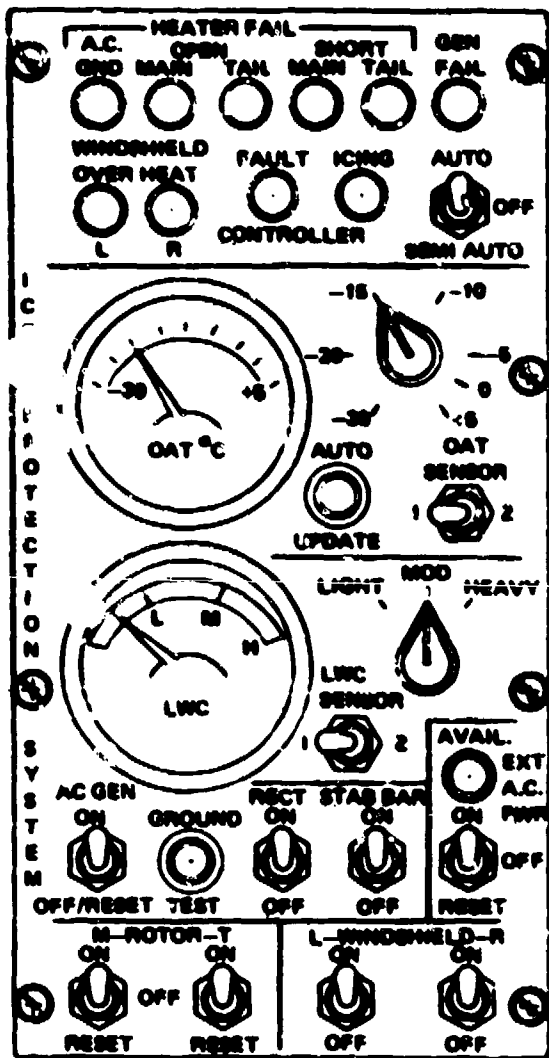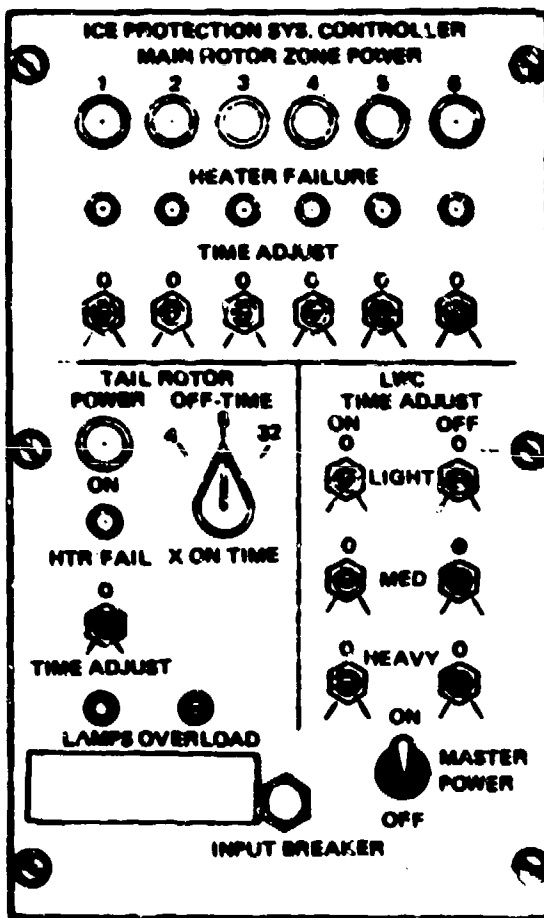
a. PILOT'S CONTROL PANEL.   b. DE-ICING CONTROL PANEL.

Figure 9.   Ice Protection Control Panels.

The deicing control system has two operational modes: automatic and semiautomatic. These are selectable by the pilot, and the only difference between the two is that the deicing schedule for the system in the "semiauto" mode is controlled manually. To do this, the pilot uses the information displayed on the OAT and LWC instruments and operates the OAT and LWC controls which are in juxtaposition with them. The necessary ON/OFF times are scheduled by the controller (even in the "semiauto" position). In the "auto" position the deicing schedule is established directly by the outside environment sensor system (outside air temperature and icing severity). In the "auto" position, the OAT selector switch and the icing severity selector switch have no effect on the performance of the deicing system. The instruments, however, continue to display the outside icing environment.

Operationally, the system is designed to require minimum attention by the flight crew. All switches could typically be in the position shown in Figure 8. With the exception of the "external power switch," all switches would normally be in the position shown (ON). A master power switch located in the lower right corner of the deicing control panel has control over all dc power to the sensors and to the controller/processor system.

The system is adaptive to the deicing environment in such a way that the power density (watts/in^2) applied to the heaters is proportional to the icing severity: the lower the icing severity, the lower the power density applied to the heater elements. Conversely, the heavier the icing environment, the higher the power density. This method of changing the watts/in^2 is effected by changing the voltage produced by the ac generator. The purpose of this type of control is to preserve the life of the generator by subjecting it to the high loading conditions only when the helicopter is flying in heavy *icing conditions. The life of the generator (aside from bearings,

_____

*See Volume 1 for definition of icing severity levels.

etc.) is related to the average (root-mean-square) heating of the insulation system. Operating the generator in this manner will lower the average temperature of the windings and substantially extend the life of the generator as well as minimize the torque loading on the transmission pad.

While an infinitely variable voltage control would have been more desirable, it would have been more complex, so three fixed voltage levels are used. These relate to the varying icing severity conditions as follows:

Icing Condition*	Voltage
Heavy	230 v (line-to-line)
Moderate	200 v (line-to-line)
Light	160 v (line-to-line)

These voltages give a power range of 2:1 from light to heavy icing conditions. When the voltage/power intensity levels change, it is also necessary that related changes be made to the "heater-on" periods. The ON-time is basically determined by the temperature differential below freezing and is proportional to it (the lower the outside air temperature, the longer the ON-time). For any condition where the voltage is increased (watt intensity increase), the rate of temperature-rise at the blade surface also increases. As a result, for a given temperature rise requirement, a shorter ON-time is programmed at the higher voltage levels. The controller timing logic operates in such a way that the LWC factor controls ON-time as an inverse-proportion function of icing severity: the worse the icing severity, the shorter the required ON-time, thus permitting faster cycling. As ice accretes

---

*As read on the penel LWC meter.

34

on the blades at a rate proportional to the icing severity, it is
beneficial if the cycle time (time to heat all blade elements) is
shortened at the more severe icing conditions. Figures 10 and 11
show the matrix of OAT versus LWC for the different voltage levels
for the main and the tail rotors, respectively.

Since the ON-time schedule was established by an analytical evaluation
of the spectrum of icing conditions, it is possible that some of the
calculated values may differ from actual operating requirements. Three
adjustment controls, therefore (located vertically on the lower right
quadrant of the controller panel), provide a $\pm$ 50% control of the
ON-time settings. Once these adjustments are made, there will be little
need to use these controls again, and they would not be required for a
production unit.

Another aspect of the deicing schedule is to provide for an OFF-period
between each heating cycle. The OFF period associated with each of
the three icing severities is set between the following ranges:

Icing Condition	OFF-Period (Min.)
Heavy	0.2 - 3.0
Moderate	0.7 - 10.0
Light	1.0 - 15.0

These adjustable settings are also located on the lower right quadrant
of the controller panel. The initial adjustments were set at 2, 5, and
14 minutes, respectively.

While the LWC sensor system will detect rapid and frequent changes in
icing conditions, it is undesirable for the generator voltage to fluc-
tuate following these instantaneous sensor responses. To inhibit this,
a "muting" period is built into the controller to insure that the
heating parameters do not change oftener than once in 5 minutes.* The

*This time interval can be adjusted

35

AS MEASURED DURING TEST PROGRAM

(Y-axis) AVERAGE MAIN ROTOR TIME ON PER ZONE, SEC

(X-axis) DEICING OAT SETTING, °C

LWC SETTING – LIGHT

MODERATE

HEAVY
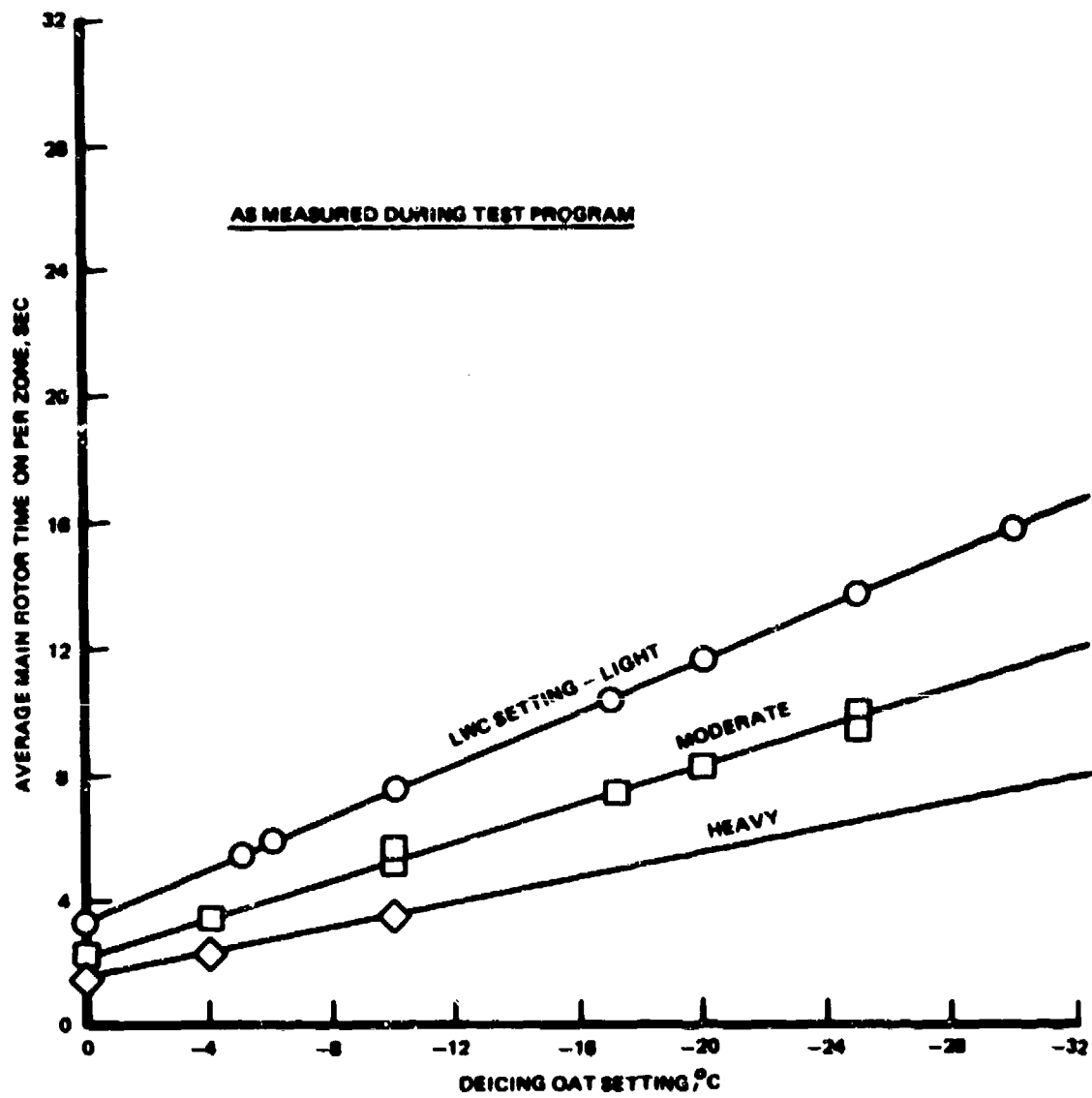
Figure 10. Schedule of Main Rotor Power ON-Time.

36
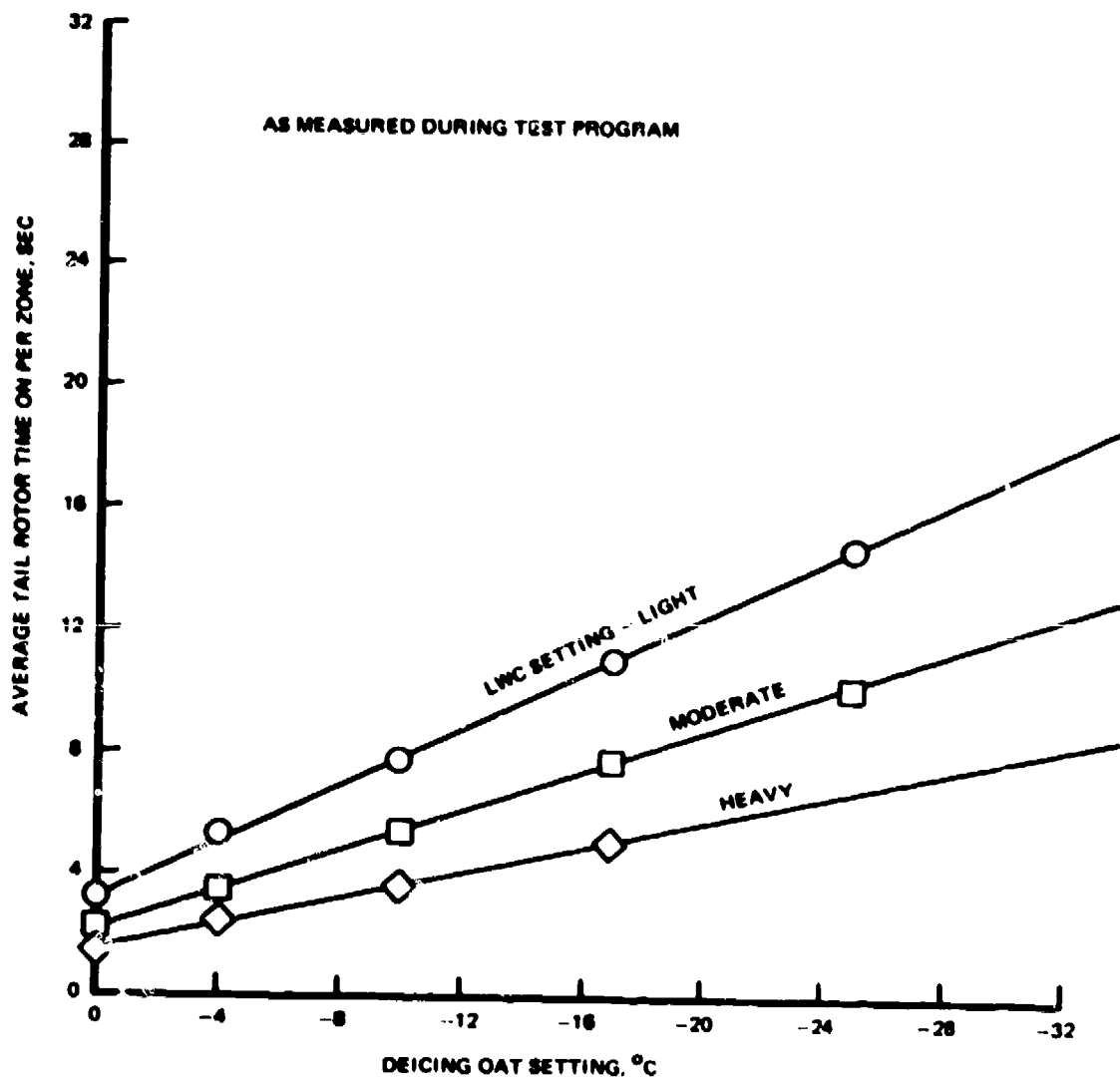
Figure 11. Schedule of Tail Rotor Power ON-Time.

control parameters that will be affected by a change in the icing condition will be:

- The voltage level of generator

- The ON-time established for the main and tail rotor heater elements

- The OFF-period between each cycle (for the main rotor)

If, however, the pilot finds that he has entered a more severe icing condition than the system has been controlling to, he can use an "update" control button which is provided on the center of the pilot's control panel. When this button is pressed, the old timing cycle will be immediately terminated; the cycle will return to the "start" position; the ON periods will be reduced; and the OFF period will be shortened as appropriate for the icing condition being encountered.

Separate timing circuits are used for the main and tail rotor. Tail rotor cycling consists simply of sequential ON and OFF periods, with the OFF period being made a multiple of the ON period. This ratio is established by a three-position selector switch located on the left center of the controller panel. The graduations on the switch are 4, 8, and 32: a selection of "8" would mean that the OFF period on the tail rotor heater elements would be 8 times the heater ON period. The tail rotor ON periods may be adjusted independently of the main rotor; these $\pm$ 50% controls are located in the lower right quadrant of the controller panel. At the initiation of deicing, the main and tail rotor systems would start simultaneously; and sequencing would then depend on the main and tail rotor deicing schedules selected.

Protection, like the function of the control system, is individual and specific to the main and tail rotor systems. Amber fault warning lamps are located on the top portion of the pilot's control panel in the

38

peripheral vision of the pilot. These lights provide indication of
open or short circuits in the main and tail rotor systems. A "ground"
light (top left corner of panel) provides a warning of any line-to-
ground short in the generator system wiring or in the wiring of the
deicing system itself such as a blade element shorting to ground.

Two OAT and two LWC sensor systems are installed, and these are select-
able from the pilot's control panel. The OAT sensors are conventional
resistance wire thermal sensors which furnish data to the controller and
to the OAT indicator. Since both OAT sensors are of the same type, the
only purpose in using two is to provide redundancy. In contrast, the
LWC sensors are of different types, as discussed in Section 2.3.

External ac power is controlled via the pilot's control panel. A mili-
tary starlard receptacle is used, and an "external power monitor" is
installed in the load center to monitor the quality of the external power
supply connected to the vehicle. If the phase rotation of the voltage
or the frequency is not within prescribed limits, power cannot be
applied to the buses. A lamp located on the control panel (Figure 9)
is used to indicate when ac external power is available to the elec-
trical system.

In considering the electrical control system for the rotor blades,
critical attention was focused on those safety aspects wherein a
system failure could result in loss of the aircraft. Such a possibility
could arise if an entire blade heater assembly were to delaminate in
flight and separate from the rotor (the resulting dynamic imbalance
could be catastrophic). One way such an event might occur is as a
result of overheating the blade due to excessively long power ON
time.

Accordingly, a detailed thermal analysis was made in order to establish the degree of thermal margin in the system. The expected time for deicing to occur on the main rotor blade was determined for each of the six deicing zones and for each of the three voltages. Figure 12 shows the results of the analysis (for an ambient temperature of $0^{\circ}F$). Deicing is presumed to occur when the leading edge of the erosion shield reaches $32^{\circ}F$. The sawtooth effect is due to the variation in spanwise heat transfer coefficient, the kinetic temperature rise, and the variation in power density for each zone. Near the inboard end of each segment the kinetic rise is a minimum, and this results in the longest required time to raise the surface temperature to $32^{\circ}F$ for end zone. While Zone 1 has the lowest power density, it still requires the least power ON time. Basically, however, the expected deicing time is 13 seconds at 160 volts, 7 seconds at 200 volts, and 5 seconds at 230 volts. This compares with allowable ON times (from an overheat standpoint) of 22 seconds, 13 seconds, and 8 seconds, respectively. Thus, there is a satisfactory safety margin available for normal system functioning.

It is to be noted that the required deicing time is based upon the highest heat transfer rate (at a given station), which occurs at the leading edge, and overheat is based upon the minimum heat transfer coefficient, which occurs approximately one inch aft of the leading edge on the lower surface. The lowest heat transfer coefficient occurs at the start of boundary layer transition between laminar and turbulent flow (assumed to occur at a local Reynolds number of 500,000). Aft of this location the heat transfer coefficient increases; and forward it is also higher, being a maximum at the stagnation point. The heat transfer coefficient also varies spanwise due to the variation of blade velocity with blade radius. Therefore, a parametric analysis of temperature rise with heat transfer coefficient, power density (watts/in^2), and power ON time was performed. Figure 13 shows the temperature distribution through

40
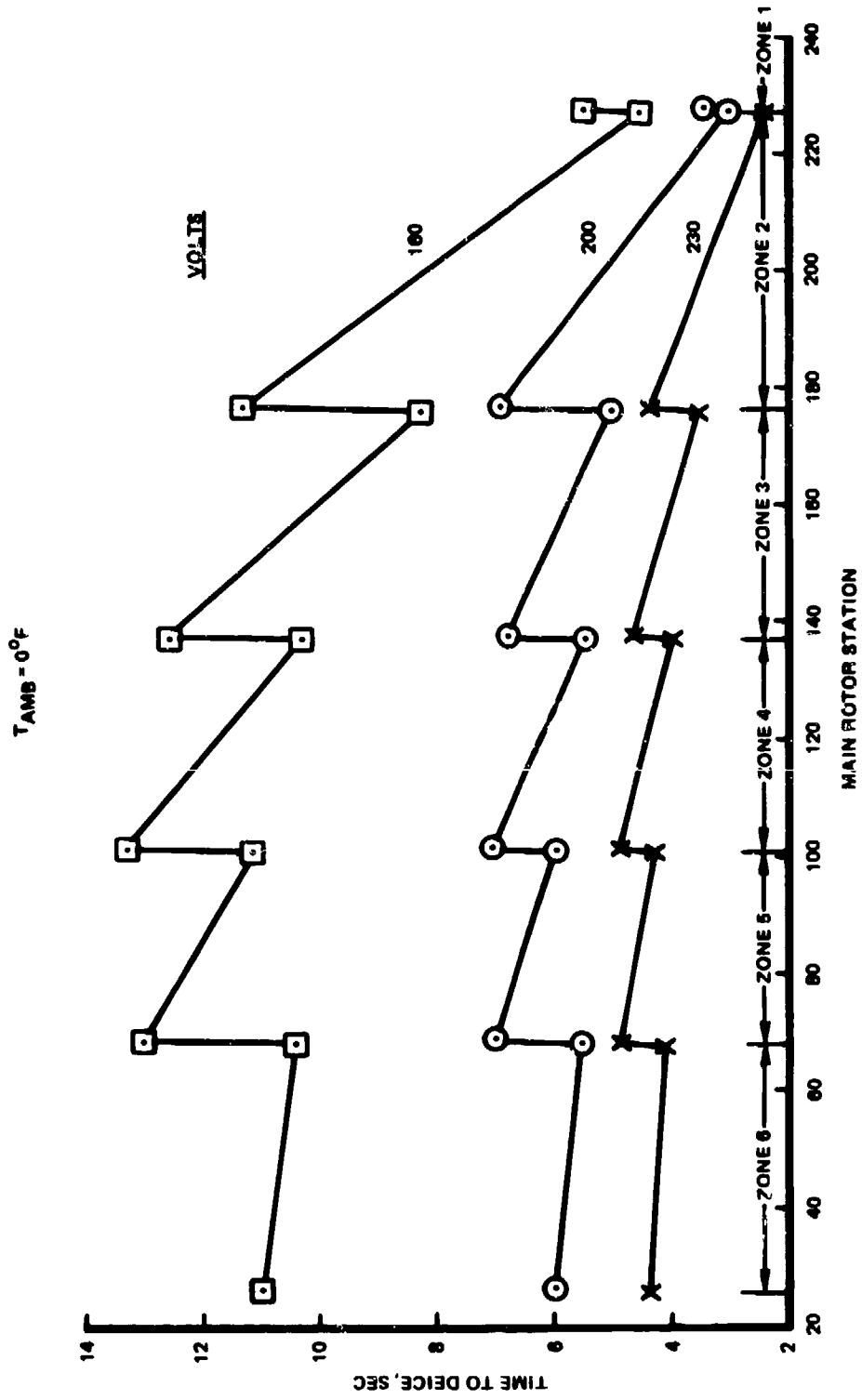
Figure 12. Calculated Effect of Voltage on the Time Required To Deice the Main Rotor.
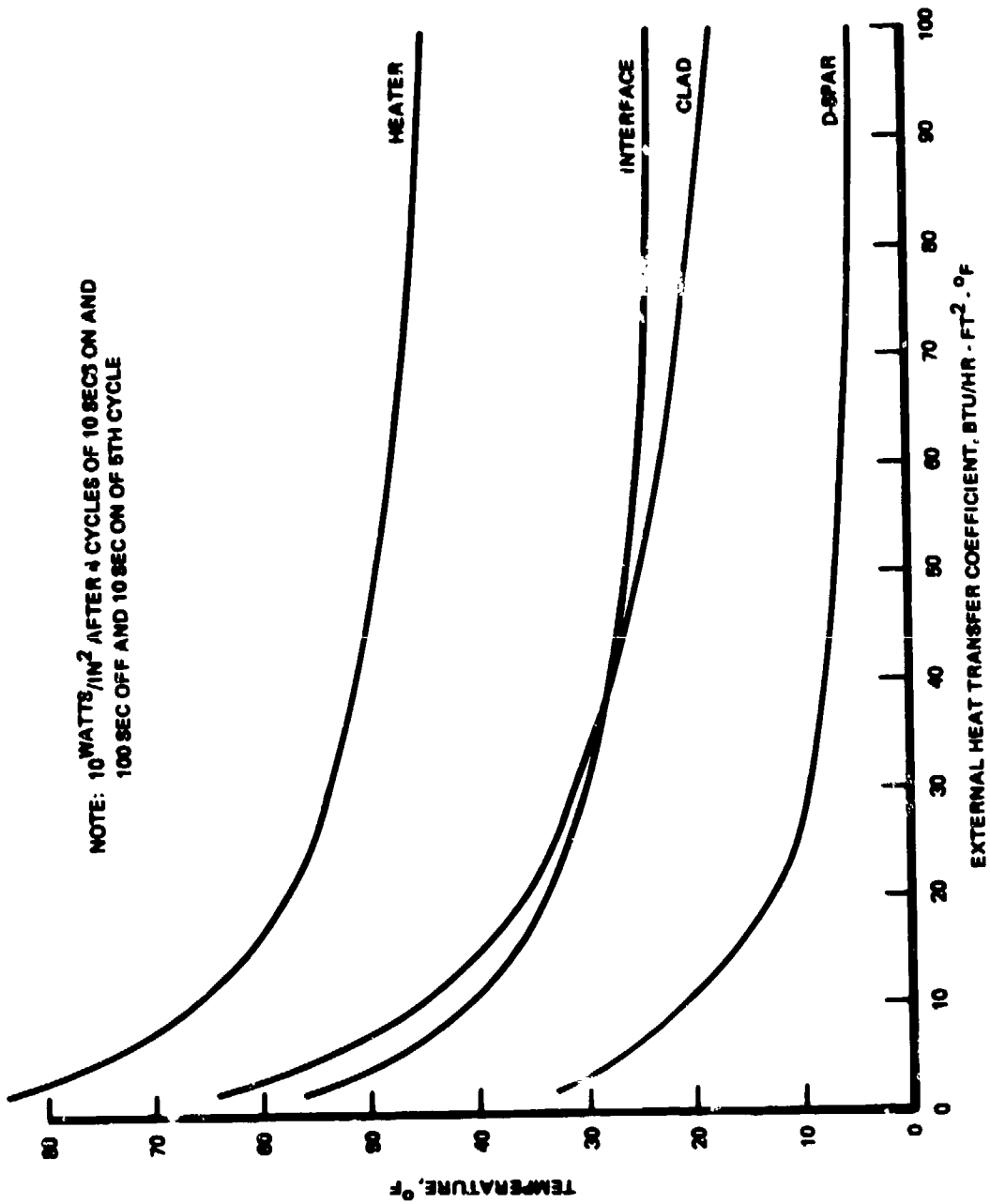
Figure 13. Temperature Distribution in Main Rotor Vs. External Heat
Transfer Coefficient.

the heating element assembly and blade for 10 seconds ON after the
5th deicing cycle (100 seconds OFF between cycles). An OFF time of
100 seconds represents the shortest possible OFF time. Multiple
cycles were examined because a "steady state" cycle is generally not
achieved on the first one due to heat storage in the D-spar. Since the
temperature rise of the system is linear with power density, Figure 13
can be applied for each of the various heating zones along the blade
and for each volt ge by using the correct multiple of 10 watts/in^2
(i.e., the temperature rise for 20 watts/in^2 is double the value shown).

For design purposes, the overheat criteria which have been used are a
maximum allowable heater element temperature of 300°F, a blade surface
(D-spar) temperature of 200°F, and the interface bond line (between
the deicer assembly and the fiberglass layup on the blade) temperature
of 200°F. (Note in Figure 13 the very close relationship between
interface and clad temperature.) To determine maximum permissible
power ON times, an ambient temperature of 50°F was assumed. The
allowable power ON times for each of the three system voltages
(22 seconds at 160 volts, 13 seconds at 200 volts, and 8 seconds at
230 volts) were established at Zone 6 (in the doubler area). Table 1
shows the ciitical temperatures on the other zone locations and indi-
cates a substantial margin outboard.

As a final level of protection against overheating, three instrumentation
thermocouples installed on one of the main rotor blades for thermal
measurements (as a part of the experimental UH-1H flight test program)
were used to provide a warning of any blade problem by illuminating a
caution light in the cockpit.

The thermocouple blade temperature monitoring system as used in the
UH-1H consisted of the following:

43

- Chromel - constantan thermocouple

- Solid state + 32°F reference junction

- Vector - Aydin Co. low-level VCO

- Vector - Aydin Co. mixer-amplifier

- Discriminator

- Voltage comparator

- Cockpit caution light.

TABLE 1. MAXIMUM SYSTEM TEMPERATURES, °F						
	160 Volts		200 Volts		230 Volts	
Zone	Heater Element	Interface	Heater Element	Interface	Heater Element	Interface
1	99	81	112	86	110	83
2	116	92	131	98	127	91
3	143	111	160	117	155	105
4	165	126	184	134	172	119
5	195	146	208	151	186	131
6	300	200	300	200	300	200

The output of the VCO mixer-amplifier receiving the thermocouple input is discriminated by three discriminators which in turn are connected to a voltage comparator circuit. This circuit performs three functions:

1. Sets and detects the overheat temperature points,

2. Performs a logic "OR" on the four temperature signals, and

3. Drives the caution indicator light.

44

The temperature overheat set points are individually adjustable from +125°F to +165°F. Since the thermocouples operate into an "OR" logic gate circuit, any one of the three thermocouples will provide an output signal to operate the caution light system when the reference temperature is exceeded. Further details of the temperature sensing system are discussed in Section 3.0.

2.3 HEATED WINDSHIELD

When operating in cold-weather conditions, it is necessary that both the pilot and copilot have windshield areas that are clear of ice, frost, or fogging so that flight vision can be maintained. The most effective means of maintaining clear vision is to electrically heat the critical area of the windshield. A laminated glass windshield having a transparent electrical resistance heating area was selected as the best means of accomplishing this. Compared to plastic, a glass windshield has much greater heat conductivity and has far superior resistance to windshield wiper abrasion.

Each windshield consists of two thin, curved plies of glass laminated together with a tough polyvinyl butyral plastic interlayer giving a "safety glass" construction. A resin-impregnated fiberglass edge retainer is used for mounting the windshield into the helicopter fuse-lage frame. The windshield is depicted in Figure 14.

The glass plies are made by stacking two sheets of plate glass together and heating until slightly soft, at which point they simultaneously sag to contour on a curved form to provide a matched fit. The curved glass panes are cut to size and edge finished. The glass plies are reheated to approximately 1000°F and rapidly chilled under controlled conditions to give a tough, semitempered condition. Sheets of polyvinyl butyral plastic are placed between the glass plies. Each glass ply is 0.10 inch

45

SENSING ELEMENTS
WITHIN THIS AREA

NESA HEATED AREA

POWER BRAID

RADIUS OPTIONAL (TYP)

BUS BAR

NOTE: DIMENSIONS IN INCHES
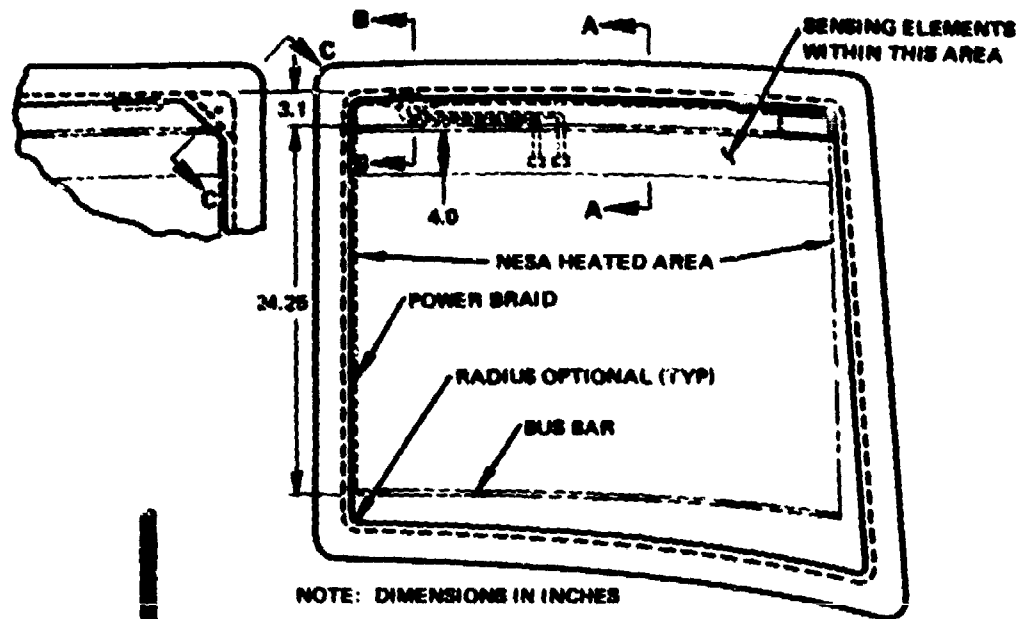
POWER
BRAID

SECTION
C-C

SECTION
A-A

SECTION
B-B

Figure 14. UH-1H Heated Windshield.

46

thick, and the polyvinyl butyral is 0.080 inch thick, giving a
total windshield thickness of 0.280 inch. Polyvinyl butyral was
chosen as the laminating interlayer because of its toughness, excellent
bond to glass, and history of good service. The polyvinyl butyral
has strong adherence to the glass surfaces, and holds the glass frag-
ments from flying in the event of breakage or projectile penetration.

A fiberglass-plastic laminate is installed around the edge of the
glass plies to act as protection for this critical area and to provide
the structure by which the windshield is installed in the helicopter.
Localized mounting stresses are absorbed by the flexibility of this
fiberglass-plastic laminate to avoid point loading the edge of the
glass. The laminate is drilled to accept mounting screws.

The UH-1H windshield is heated in a rectangular section of 800 square
inches across the center of the windshield. Under moderate icing
conditions, the power is at 3.3 watts per square inch, for a total of
2640 watts. The voltage will vary, as it does for the deicing system,
from 160 volts in light icing, to 200 volts in moderate icing, and to
230 volts in heavy icing conditions, as determined by the LwC. If rotor
blade deicing is turned off, the voltage supplied to the windshields
will be 160 volts.* This power level is sufficient to melt off ice
when the helicopter is parked, or to keep ice from forming in the
heated area during any cold weather conditions that could be encountered.
In addition, the heated area would be defogged during humid weather. To
avoid thermal shock, voltage is automatically applied at 160 volts
for one minute, and then automatically set to the voltage corresponding
to icing conditions.

---

*Except when the T/R is required, at which time the voltage will be 200
Vac.

Heating is accomplished by a transparent tin oxide film applied on the inside surface of the outer glass ply. The tin oxide film acts as an electrical resistance heating element. Single phase alternating electrical current is fed through copper braid wires into thin silver strip bus bars along two opposite sides (top and bottom) of the tin oxide film heating area, and then into the tin oxide film.

The tin oxide (NESA) film resistance is made so as to provide a uniform power density. Variations from the average do occur, however, and Figure 15 shows a typical power variation over the surface. The power variations are controlled so that the coldest area will still anti-ice while the hottest area does not overheat. The heat control sensor is located in a region of average power.

Two heat sensors of very fine wire are laminated into the polyvinyl butyral interlayer just behind the tin oxide film. The resistance of the sensors changes with temperature so that the control system can sense when the windshield has reached $78^{\circ}F$ and cycle power ON at that point (OFF at $82^{\circ}F$). Only one sensor is connected, the second identical sensor is a spare in case of failure of the other sensor. The control sensor also acts as an overtemperature control and will light a warning light on the pilot's control panel when the windshield reaches $105^{\circ}F \pm 5^{\circ}F$, and will turn off, and lock out, all power to the affected windshield. The pilot may restore power by momentarily turning the control switch off and then on, should the situation require this action.

The control and power circuits for each windshield are completely separate from each other and from the rotor blade deicing systems. Should a fault develop in the deicing system, or in one windshield, it will always be possible to use at least one panel.

NOTE:

NUMBERS IN EACH
ZONE CORRESPOND
TO WATTS/IN^2 AT
200 VOLTS
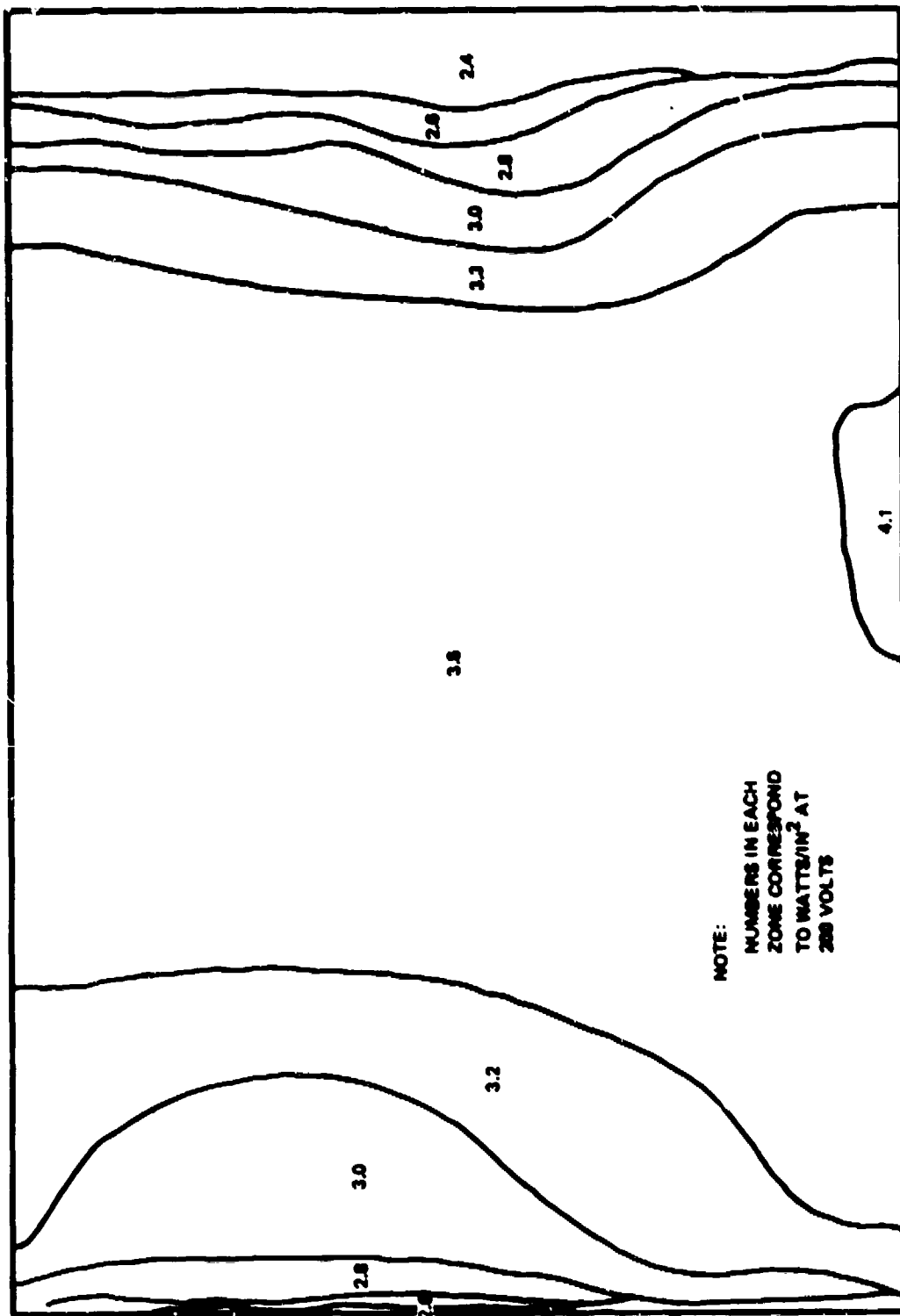
Figure 15. Typical Windshield Power Density Map.

2.4 ICE DETECTION

Two different ice detector/icing severity meter designs are installed
on top of the cabin area. One is the ultrasonic type and the second is
the infrared occlusion type. Both sensors include aspirators using
engine compressor bleed air to induce the ambient cloud across the
detector during hover. The output of either sensor is displayed on
the pilot's control panel through a meter. The detectors are installed
on masts so that the sensors are approximately 12 inches away from the
fuselage. Each of the sensors requires approximately one-half pound
per minute of engine bleed air to operate the aspirator. The principal
benefit of the aspiration is during hover, as there is sufficient ram
airflow across the sensing system during cruise to assure a sensitive
signal.

The output of the ultrasonic system is a continuous analog voltage
which is displayed on the meter in terms of T (trace), L (light),
M (moderate), and H (heavy). The infrared system provides one of
three discrete severity signals corresponding to L, M, or H. (L will
be read with icing intensities up to the threshold of M, etc.)

Figure 16 shows the installation of the two ice detectors on top of the
fuselage.

2.5 SYSTEM WEIGHT

The weight increase resulting from the installation of all new equip-
ment (excluding flight test instrumentation) and the modifications to
the rotor blade is 279 pounds. The weight of the flight test equip-
ment is 567 pounds, resulting in a total aircraft weight increase for
the test configuration of 846 pounds. The weights of the individual
components comprising the anti/deicing system for the test aircraft are
shown in Table 2.

50

ULTRASONIC
ICE DETECTOR

INFRARED
ICE DETECTOR

Figure 16. Ice Detector Installation.

TABLE 2. FLIGHT TEST UH-1H ELECTROTHERMAL DEICING SYSTEM WEIGHT

	Pounds
Main Rotor and Balance Bar Heater Blankets	43
Tail Rotor Heater Blankets	3
Timer/Controller and Stepping Switch	24
Change to All Glass Windshields (2)	34
Main and Tail Rotor Sliprings	25
Cockpit Control Panel	6
Ice Detectors (2) and OAT Probes	9
Wiring, Relays, Circuit Breakers, etc.	95
Change to AC Generator, Including Voltage Regulator	23
Transformer/Rectifier	17
Total Weight	279
Flight Test Instrumentation	567
Total UH-1H Weight Change	846

Table 2 shows that 46 pounds is included for main and tail rotor heater blankets. This weight would normally be adjusted in the blade balance for a new blade design so as to achieve a zero net blade weight increase. In addition, a weight increase of 34 pounds is shown for a change to the heated (glass) windshield. Of this increase, 27 pounds is attributable to the change from plastic to glass, and only 7 pounds (for controls and wiring) is directly attributable to heating of the (two) windshields.

If the UH-1H were retrofitted with ice protection on a production basis, the estimated system weights would be as shown in Table 3. A comparison of the two tables indicates significant component differences for the main rotor blades, sliprings, and electrical generating system. It is postulated that a production blade design would use a tapered nickel erosion shield on the main rotor blades (from 0.030 inch at the leading edge to 0.010 inch at the trailing edge of the shield) instead of the 0.030-inch stainless steel erosion shield on the flight test aircraft; the slipring weight would be reduced by virtue of eliminating the rings required for instrumentation; and the electrical generating system weight could be substantially reduced by utilizing a 12,000-rpm generator instead of the 6600-rpm machine used for the flight test program.

It is also noted that Table 3 itemizes the weight effect of deleting tail rotor ice protection, as flight test experience has shown that the engine exhaust heats the tail sufficiently to prevent tail rotor icing (at least with the standard exhaust configuration).

53

TABLE 3. ESTIMATED UH-1H PRODUCTION DEICING SYSTEM WEIGHT

	Pounds
Main Rotor and Balance Bar Heater Blankets (2).	33
Tail Rotor Blades (2)	3
All Glass Windshields and Controls (2).	34
Generator and Control	-22
Timer/Controller and Stepping Switch	18
Cockpit Control Panel	3
Main and Tail Rotor Sliprings	17
Transformer/Rectifier	18
Ice Detector and OAT System	4
Wiring, Relays, Circuit Breakers and Connectors	85
Total Weight Increase	193
Without Tail Rotor Protection	176

54

3.0 FLIGHT TEST INSTRUMENTATION

Provisions for measuring approximately 45 parameters were incorporated
into the data acquisition system, as identified in Table 4. Instru-
mentation was installed to measure main and tail rotor blade loads, rotor
blade surface temperature, electrical system parameters, and basic
aircraft and engine performance parameters. It is to be noted that
Table 4 identifies approximately 65 measurement items, but these include
4 spare thermocouples and 4 spare strain gauges on the main rotor blade.
The strain gauge locations were selected so as to provide a correlation
with data obtained on previous UH-1 flight test programs and also to
provide an indication of any potential blade dynamic problem. Collec-
tive handle force was also measured to determine the effect of blade
cg shift on boost-off control force requirements. Vibration measure-
ments (accelerometers) were also made to correlate with basic aircraft
data and to determine if a problem exists with new components such
as the ac generator and the main rotor sliprings.

Icing signals from both the ultrasonic and the infrared ice detectors
were also recorded as well as displayed (one at a time) in the cockpit.

The thermocouple locations were selected on the basis of measuring:

- Maximum blade temperatures - in order to provide surveillance
  of potential overheat problems. Maximum blade temperatures
  (at a given rotor station) should occur at the aft end of the
  chordwise laminar boundary layer (the location of minimum
  heat transfer coefficient). It was estimated that this
  location was approximately 1 inch aft of the leading edge
  on the lower surface.

TABLE 4. FLIGHT TEST MEASUREMENT LIST					
Meas. No.	Parameter	Where Recorded or Displayed			
		Tape	Cockpit	A.O.	Scope
	Structural Loads/Vibration				
S7000	M.R. Flapwise Bending @ Sta 35 (R)	X	-	-	X
S7001	M.R. Inplane Bending @ Sta 35 (R)	X	-	-	X
S7002	M.R. Flapwise Bending @ Sta 150 (R)	X	-	-	-
S7003	M.R. Pitch Link Load (Blade Torsion) (R)	X	-	-	X
S7004	C.P. Collective Handle Force	X	-	-	-
S7005	M.R. Flapwise Bending @ Sta 234 (R)	X	-	-	-
S7006	M.R. Inplane Bending @ Sta 150 (R)	X	-	-	-
S7010	T.R. Inplane Bending @ Sta 11 (R)	X	-	-	X
S7011	T.R. Pitch Link Load (Blade Torsion) (R)	X	-	-	X
S7012	T.R. Flapwise Bending @ Sta 21.5 (R)	X	-	-	-
D6000	M.R. Index (R)	X	-	-	-
D6001	T.R. Index (R)	X	-	-	-
D6002	Collective Handle Position	X	-	-	-
A3000	Pilot Sta. Vibration-Vertical	X	-	-	-
A3001	Pilot Sta. Vibration-Lateral	X	-	-	-
A3003	Copilot Sta. Vibration-Vertical	X	-	-	-
A3004	M.R. Gearbox Vibration-Vertical	X	-	-	-
A3005	M.R. Gearbox Vibration-Lateral	X	-	-	-

		Where Recorded or Displayed			
Meas. No.	Parameter	Tape	Cockpit	A.O.	Scope
A3006	M.R. Gearbox Vibration-Longitudinal	X	-	-	-
A3007	AC Generator Vibration-Vertical	X	-	-	-
A3008	AC Generator Vibration-Lateral	X	-	-	-
A3009	T.R. 90° Gearbox Vibration-Vertical	X	-	-	-
A3010	T.R. 90° Gearbox Vibration-Lateral	X	-	-	-
A3012	C.G. Vertical Acceleration	X	X	-	-
A3013	Main Rotor Slipring Assy Horiz. Vibration	X	-	-	-
A3014	Main Rotor Hub Inplane Vibration	X	-	-	-
	Ice Protection System				
R8001	Icing Severity - Ultrasonic	X	X	-	-
R8002	Icing Severity - Infrared	X	X	-	-
T4000	Total Air Temp. (Oat)	X	X	-	-
T4001	M.R. Blade Temp @ Sta 102 @ 1" Lower (R)	X	-	-	-
T4002	M.R. Blade Temp @ Sta 101.25 @ 7" Lower (R)	X	-	-	-
T4003	M.R. Blade Temp @ Sta 178 @ 1" Lower (R)	X	-	-	-
T4004	M.R. Blade Temp @ Sta 169 @ 6" Lower (R)	X	-	-	-
T4005	M.R. Blade Temp @ Sta 83 @ 6" Lower (R)	X	-	-	-
T4006	M.R. Blade Temp @ Sta 82.5 @ 1" Lower (R)	X	-	-	-

		Where Recorded or Displayed			
Meas. No.	Parameter	Tape	Cockpit	A.O.	Scope

TABLE 4. FLIGHT TEST MEASUREMENT LIST (Cont)

Meas. No.	Parameter	Tape	Cockpit	A.O.	Scope
T4007	M.R. Blade Temp @ Sta 45 @ 0.5" Lower (R)	X	–	–	–
T4008	M.R. Blade Temp @ Sta 30 @ L.E. (R)	X	–	–	–
T4010	T.R. Blade Temp @ Sta 35 @ 2" L (R)	X	–	–	–
T4011	T.R. Blade Temp @ Sta 22 @ .75" L (R)	X	–	–	–
T4015	R.H. Windshield Temp(Max Watts/In^2)	X	–	–	–
T4016	R.H. Windshield Temp (Avg. Watts/In^2)	X	–	–	–
T4020	L.H. Windshield Temp (Max Watts/In^2)	X	–	–	–
T4021	L.H. Windshield Temp (Avg Watts/In^2)	X	–	–	–
E9019	M.R. Heater Signal Voltage (Equiv. to Stepper Out Voltage)	X	–	–	–
E9018	M.R. Heater Controller Output Volts (A-CØ)	X	–	–	–
E9020	T.R. Heater Controller Output Volts (A-CØ)	X	–	–	–
E9012	L.H. Windshield Var. Heater Volts (A-CØ)	X	X	–	–
E9013	R.H. Windshield Heater Volts (A-CØ)	X	–	–	–
P5001	Engine Inlet Plenum ΔP (Avg of 3)	X	X	–	–
P5003	Engine Bleed Press @ Aspirator	X	–	–	–
T4026	AC Generator Cooling Air Out Temp	–	X	–	–
T4028	DC Generator Cooling Air Out Temp	–	X	–	–
T4029	Total Air Temp (Rosement)	X	–	X	–

Meas. No.	Parameter	Where Recorded _. Displayed			
		Tape	Cockpit	A.O.	Scope
T4030	AC Generator Cooling Air in Temp	–	X	–	–
E9001	AC Generator Volts (B-CØ)	X	X	–	–
E9003	AC Generator Current (AØ)	X	X	–	--
E9021	AC Generator Volts (Neut-Structure)	X	–	–	–
	Test Condition Parameters				
B2000	Elapsed Time	X	X	–	–
B2001	Air speed	X	*	X	–
B2002	Altitude	X	*	X	–
B2003	Event Marker	X	–	X	–
B2004	Hub Camera Burst Counter	–	X	X	–
B2005	Civil Time	–	X	X	–
R8004	Engine Torque Pressure (ΔP)	–	*	X	–
R8005	Rotor RPM/Eng RPM	–	*	X	–
R8006	Fuel Quantity	–	*	–	–
R8007	N_1 (Gas Generator RPM)	–	*	X	–
T4027	EGT (Sensitive, Digital)	–	–	X	–

TABLE 4. FLIGHT TEST MEASUREMENT LIST (Cont)

Notes:

(R) = Rotating Meas.
 * = Presently ships equipment

- Minimum blade temperature - in order to provide information
  on the temperature rise required for deicing, as the coldest
  chordwise location i ...., determine the energy required
  for ice removal. The coldest area could be either the
  leading edge or the aft edge of the heated area where the
  boundary layer would be expected to be turbulent (high heat
  transfer coefficient).

- Special "problem" areas. There is a 1/4-inch "unheated" area
  on either side of the production skin splice at station 83
  that could tend to be a potential ice anchor location.

Figure 17 shows the location of the main and tail rotor blade thermocouples.

- Windshield temperature (both pilot and copilot panels) at
  locations corresponding to both average power density and
  maximum power density. In addition, the thermocouples had
  to be located so that they were out of the area of windshield
  wiper travel.

Also utilized during the program but not shown in Table 4 were tempera-
ture indicating stickers (templates). Up to 100 at a time were
installed on the main and tail rotor blade heaters and stabilizer
bar heaters to supplement the thermocouples. These stickers (Fig-
ure 18) indicate the peak temperature experienced during a test and
are useful in providing an indication of overheat and for providing addi-
tional information on the heat transfer properties of the airstream
over the rotor blades and gyro stabilizer bar.

A 16mm motion picture camera was mounted above the main rotor system,
turning with the rotor and bore-sighted along the No. 1, or instrumented,
blade to record ice accretion/ice shedding on that blade. The lens
and automatic exposure control (AEC) were enclosed in a metal housing
to protect these parts from the icing environment. The lens and AEC

60
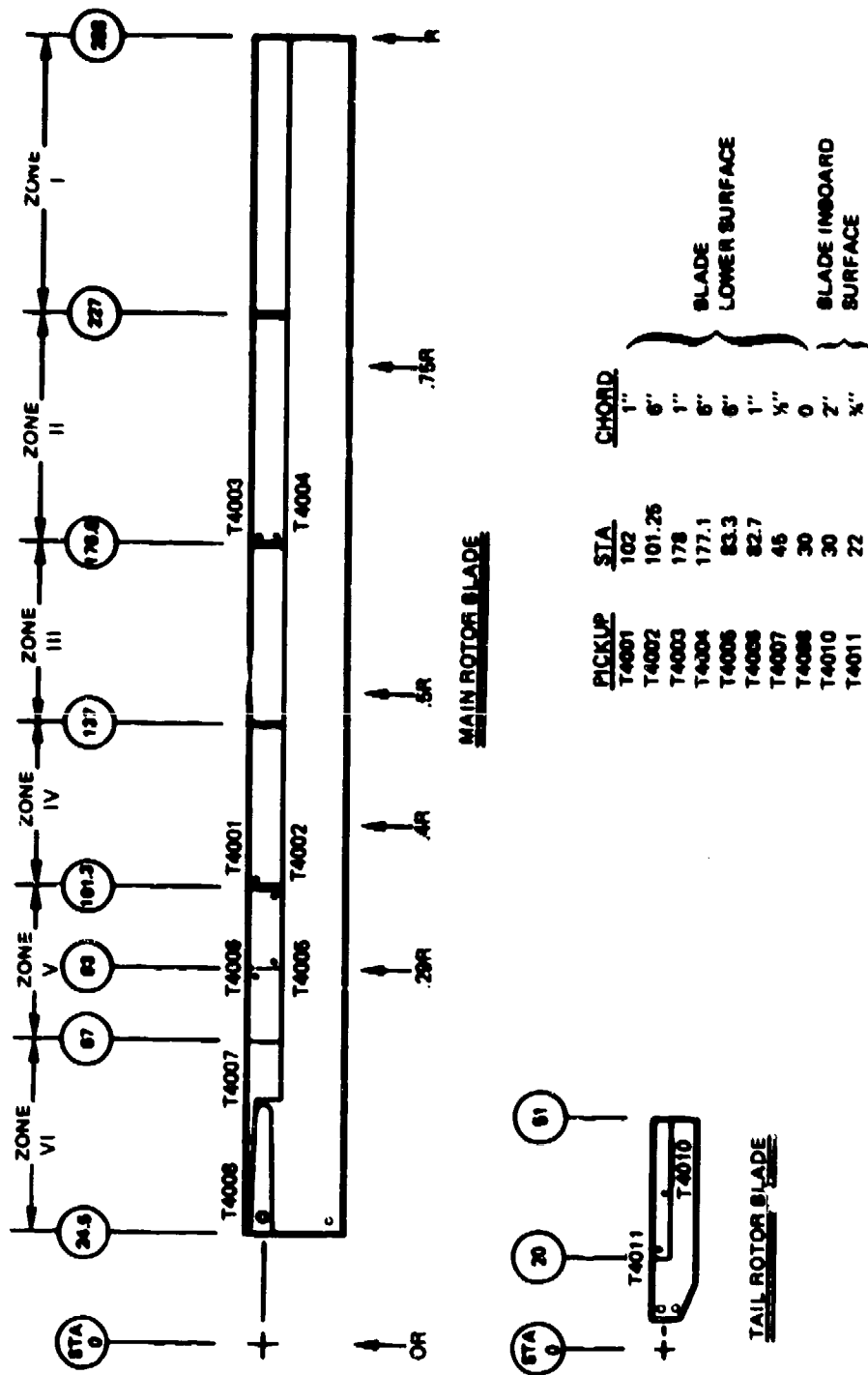
Figure 17. Main and Tail Rotor Blade Thermocouple Locations.

61
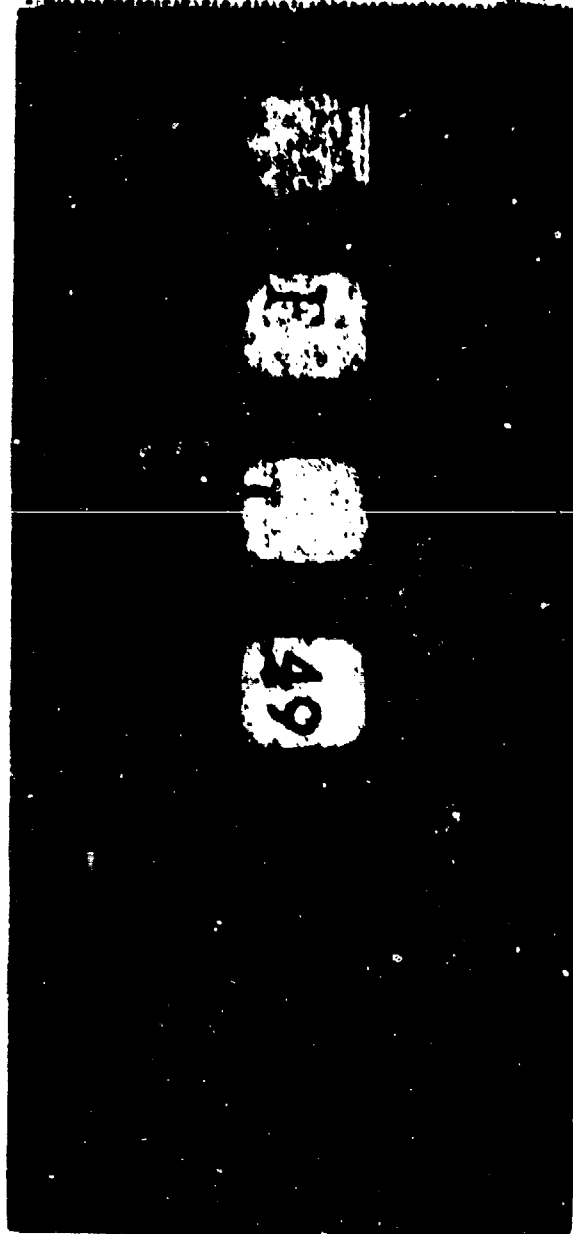
Figure 18.   Temperature Sensitive Indicating Sticker.

viewed the blade through a window which was electrically anti-iced, in a manner similar to standard aircraft anti-iced windscreens. A temperature sensor, embedded within the glass, provided a temperature signal to a monitor/control circuit which turned electrical power to the window on at $10^{\circ}C$ and off at $27^{\circ}C$, thus cyclically heating the unit. Control and switching logic electronics were also contained within the lens and AEC protective cover assembly. Figure 19 shows the camera installation atop the main rotor slipring/instrumentation housing.

The electrical system parameters were measured primarily for diagnostic purposes to assist in troubleshooting in the event of system malfunction.

Engine inlet plenum pressure was measured in order to monitor the effect of possible ice buildup on the engine inlet screens.

The primary data acquisition system installed in the aircraft was a 14-track frequency modulation (FM) tape recorder. This was supplemented by a small photopanel and added specialized instruments in the cockpit. Four on-board oscilloscopes were also utilized to monitor in flight potentially critical main and tail rotor loads in real time. A block diagram of the complete data acquisition system is shown in Figure 20. As shown, the major subassemblies of the data acquisition system are:

- Main and tail rotor sliprings.

- Proportional bandwidth voltage controlled oscillator (VCO) chassis and power supply assemblies mounted in the rotating portion of the main and tail rotor systems.

- A 16mm camera mounted above and rotating with the main rotor to record ice accretion/ice shedding on one blade.

63
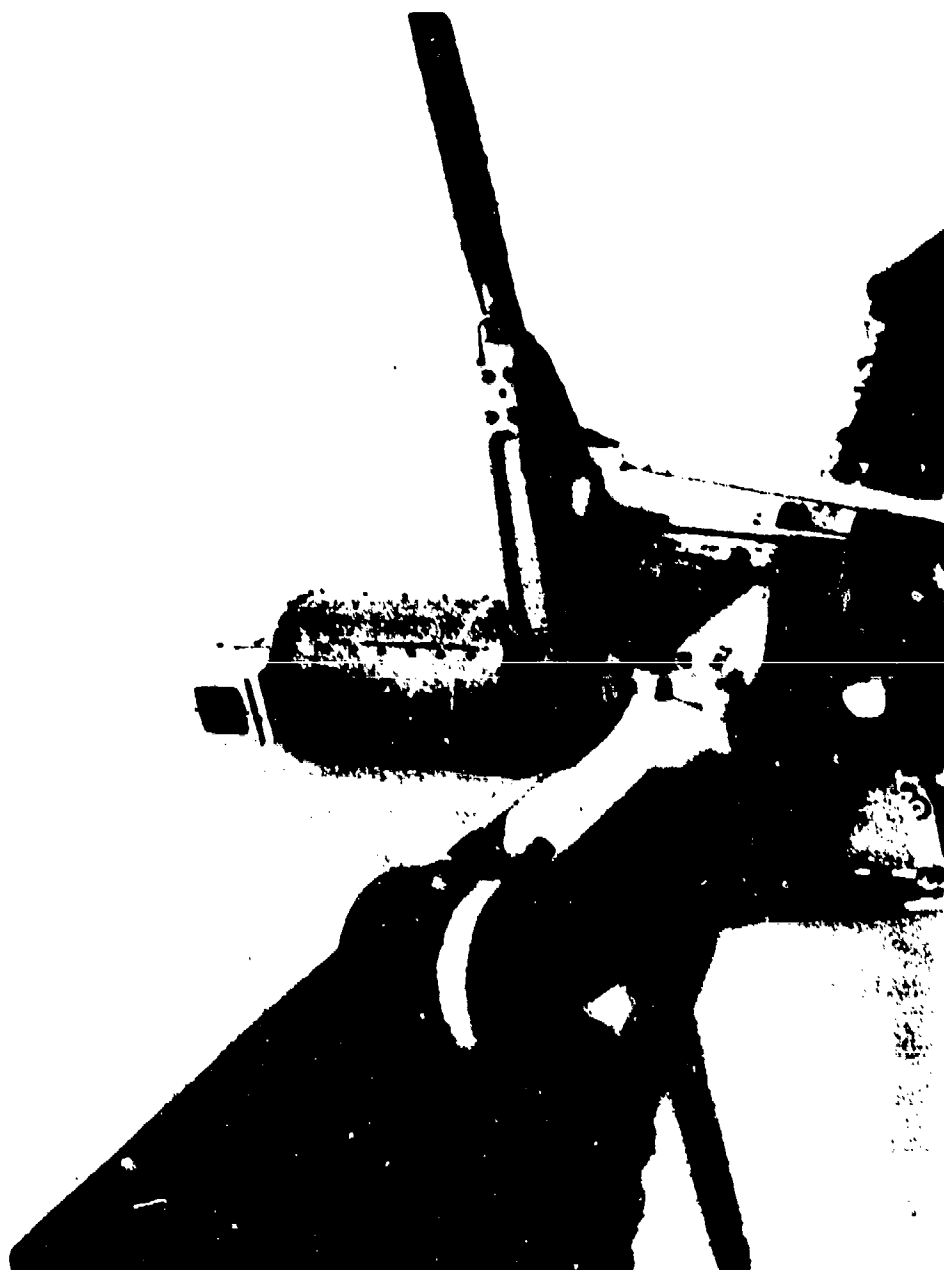
Figure 19. Hub Camera Installation.
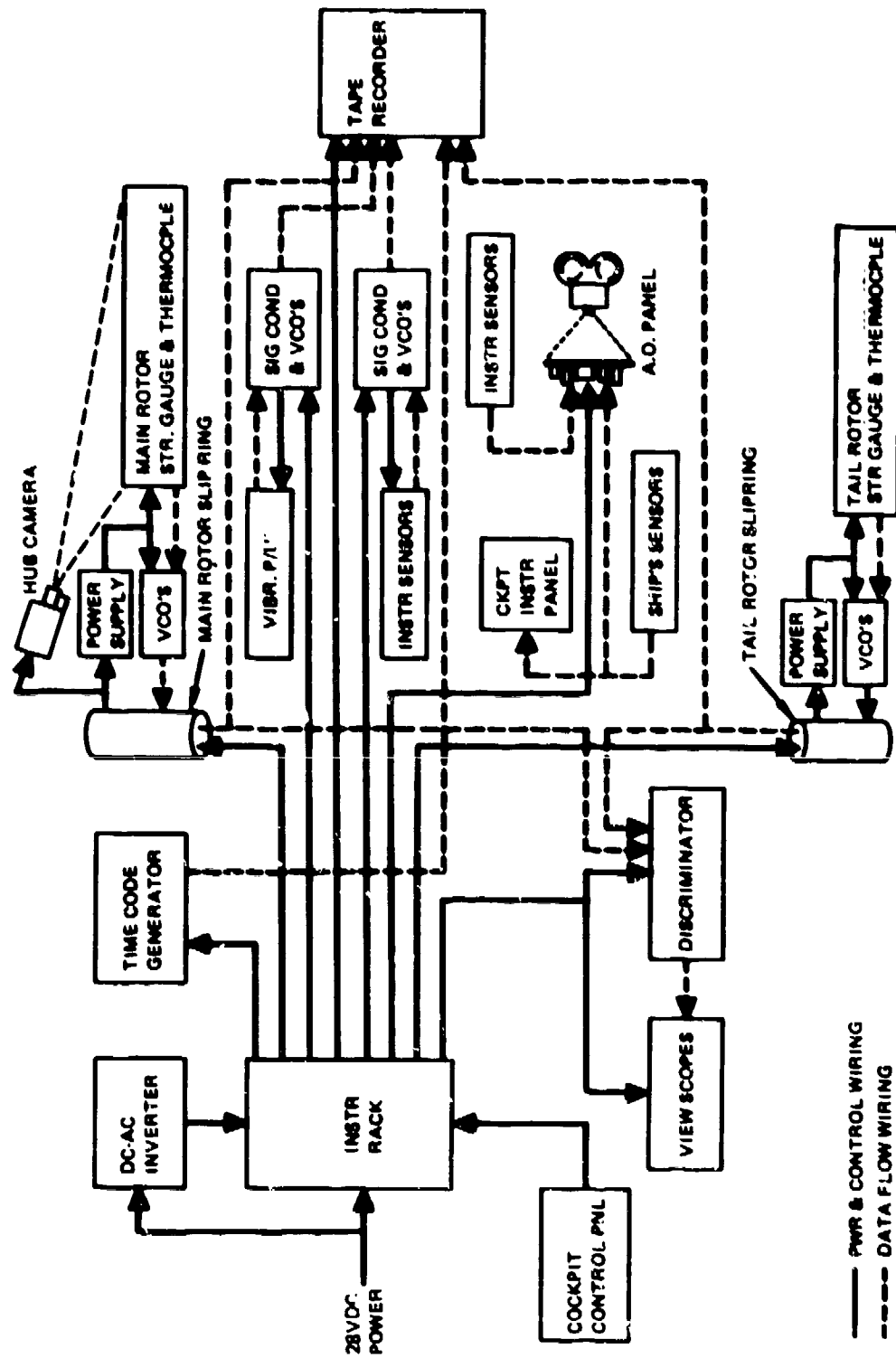
Figure 20. Block Diagram of Data Acquisition System.

- The 14-track FM tape recorder.

- An 18 hole photorecording automatic observer (A.O.) panel.

The photopanel, scopes, tape recorder and all signal conditioners were mounted in standard instrumentation racks located in the left and right aft cabin portion of the aircraft (Figures 21 and 22).

The data acquisition system was controlled from a panel, added to the cockpit pedestal, on the left-hand side. Mounted with the instrumentation control panel was a time-code generator which provided a digital readout of elapsed time to the flight crew and an IRIG-13 format time code for recording on the magnetic tape. Figure 23 shows the installation of the control panel and time-code generator on the forward left-hand side of the pedestal.

Signals from the blade sensors were transmitted via flexibly mounted wire runs to the VCO's and their associated preamplifiers located on top of the hub. A small bracket at the root end of the rotor blade provided a mounting for chromel-constantan thermocouple reference junctions, strain gauge biasing resistors and the blade disconnect plug. The composite VCO output was in turn transmitted via sliprings and wires to the tape recorder and discriminators. Noise problem effects on the signal lines were minimized due to the high level output of the VCO's. Power supplies mounted in the rotating systems received their input power via one slipring pair and provided 10 volt dc stable excitation power for the strain gauges and thermocouple reference junctions.

The nonrotating measurements, such as voltages, current, and basic performance parameters, were fed directly to low level discriminators via simple L-pad type signal conditioning.

The inflight real-time structural loads monitoring system provided the flight crewmember/stress engineer with analog displays of critical
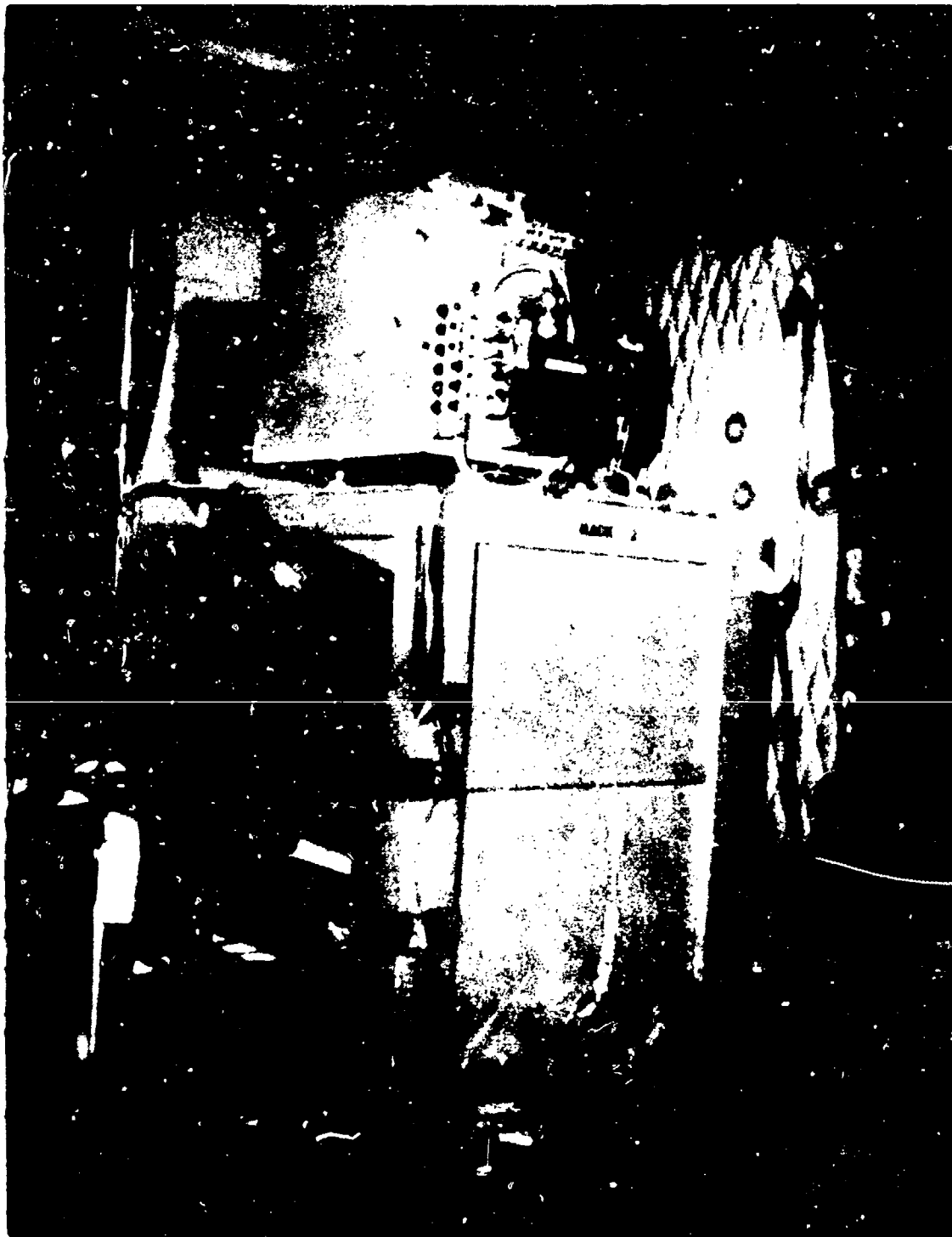
Figure 21. Left-Side Data Acquisition Equipment.
            (Photographs and Laser Monitor Scopes).

67
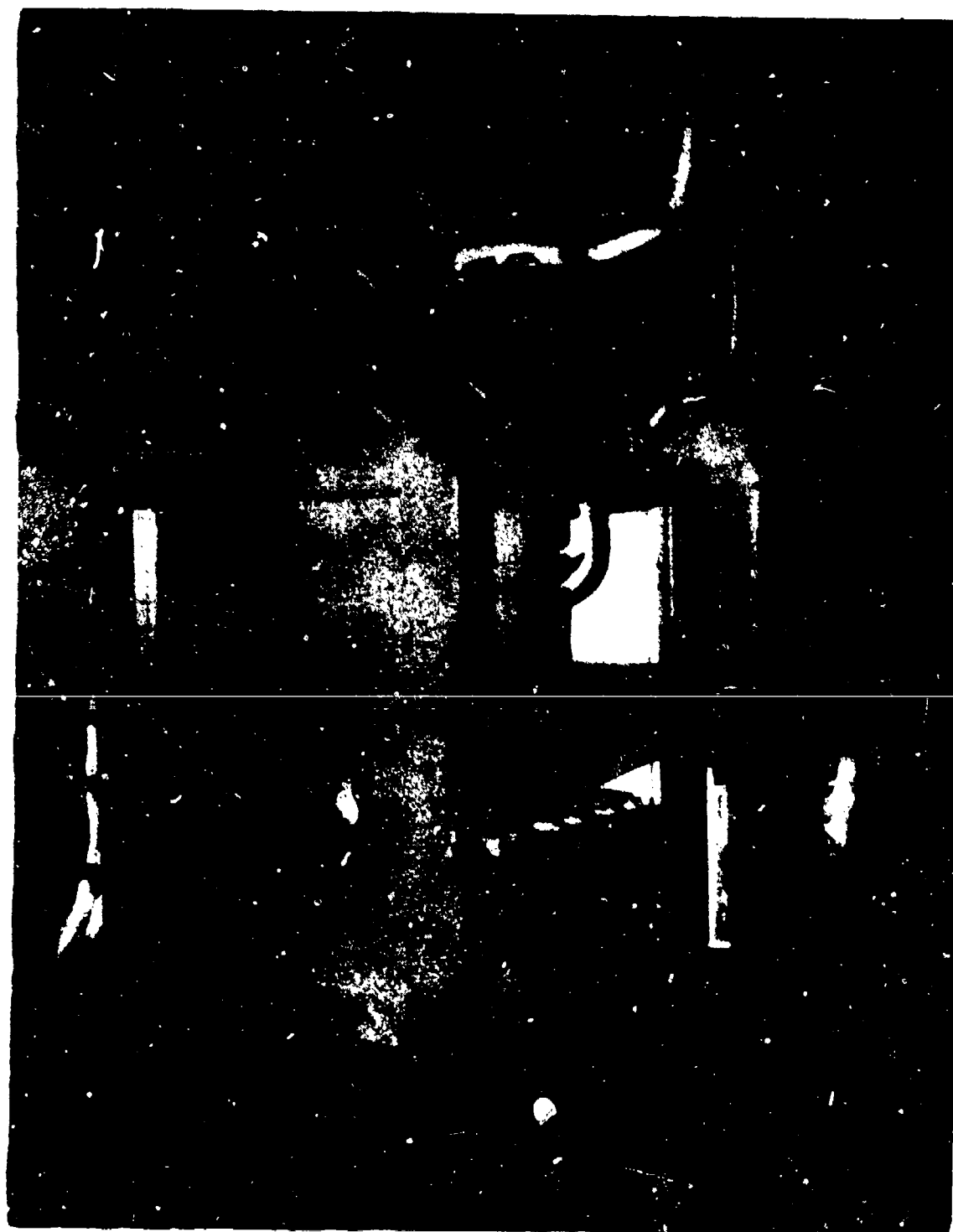
Figure 22. Right-Side Data Acquisition Equipment (Tape Recorder).
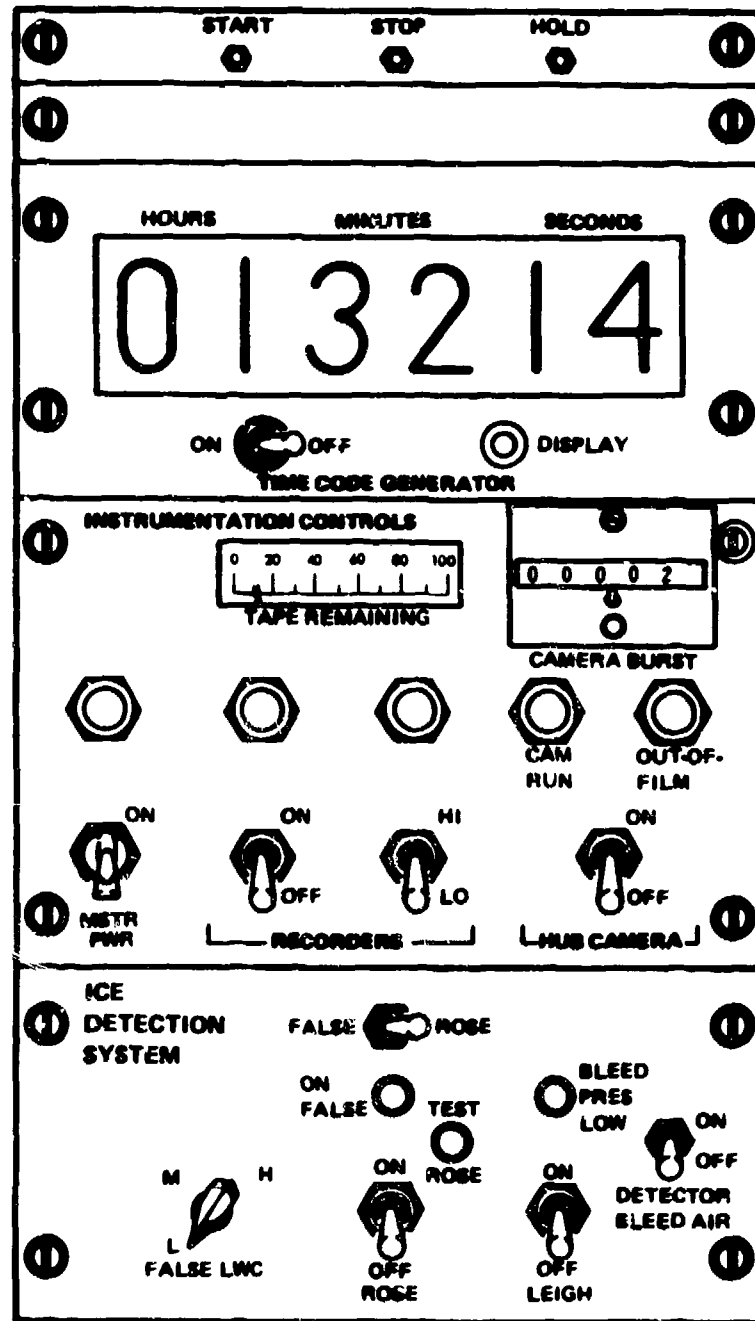
Figure 23. Cockpit Flight Test Instrumentation and Ice Detection Control Panel.

loads measurements. Typically the cathode-ray tubes received their input signal from strain gauges on the main and tail rotor blades and pitch links. The strain gauge signals were fed through VCO's and sliprings to discriminators, whence the analog signal was routed to the monitor scopes. Sweep generators allowed the observer to synchronize scope sweep rate with rotor blade rpm, enabling him to observe 1P and 2P load excursions and to make value judgements relative to safety-of-flight phenomena. Typically two oscilloscopes were used for each rotor system. On the main rotor system, flap and chordwise bending at blade station 35 were displayed jointly on one screen producing a lissajou figure, with the second scope displaying pitch link load. The discriminators for the lissajou pattern were built as a matched set. The tail rotor measurements displayed were chordwise bending @ blade station 11 and pitch link load. A fifth oscilloscope originally intended for vibration (at the c.g.) was never activated since discriminator space availability was relinquished to the temperature warning system. A block diagram of the real-time inflight monitoring system is presented in Figure 24.
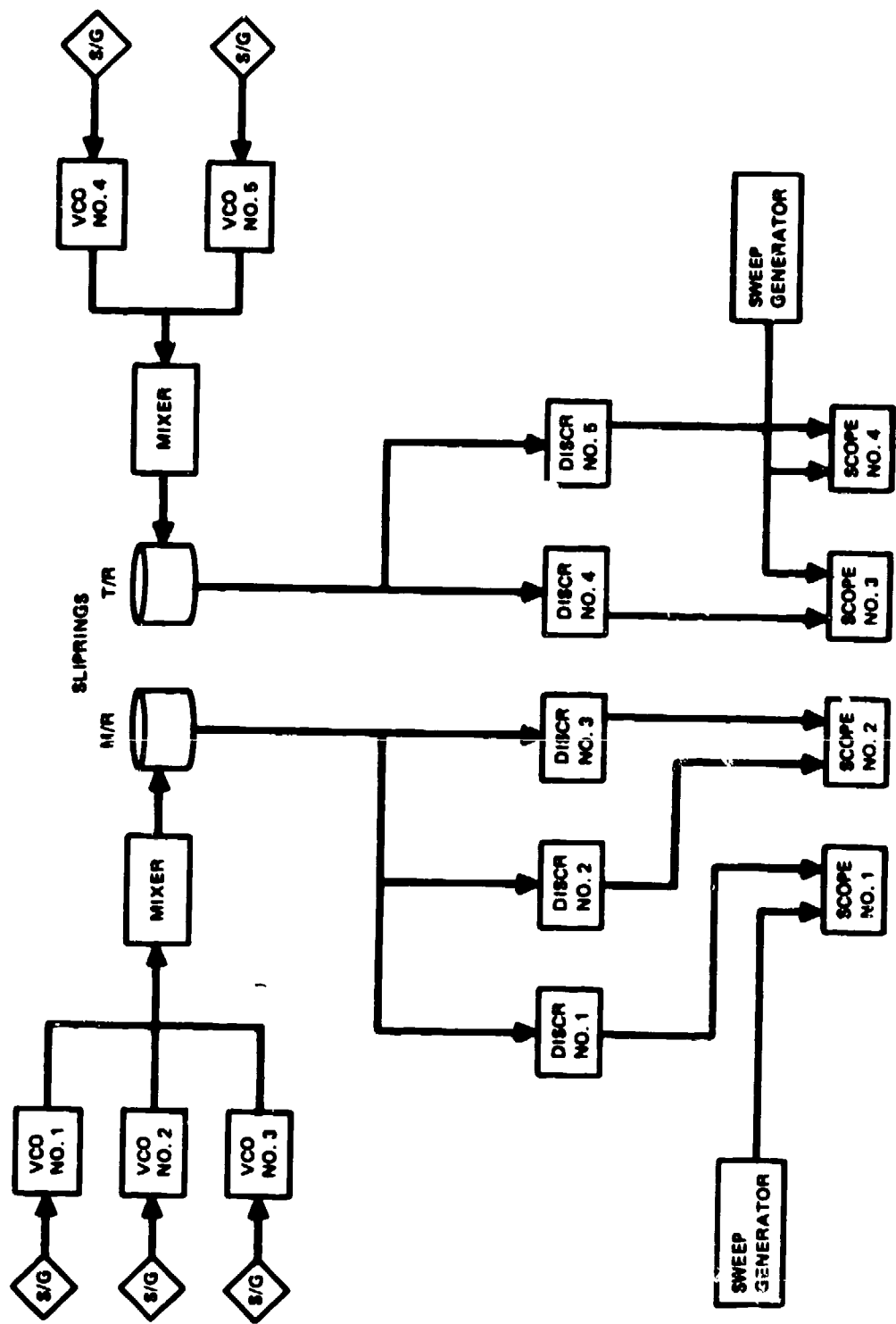
Figure 24. Real-Time Monitor Scope System Block Diagram.

71

4.0 AIRWORTHINESS TESTING

The first tests on the modified aircraft were to establish the airworthiness of the new configuration and to define an operating envelope. The tests included preflight tiedown testing equivalent to whirl tests of a new rotor; flight tests evaluating rotor loads, vibration characteristics, flying qualities; and complete ice protection system tests in clear air. A tctal of 34.4 operating hours were accumulated on the rotor blades and the other installed new systems. This included 1⁴ flights and 15.3 flight hours.

4.1 GROUND TESTS

Table 5 is a summary of the ground tests of the modified rotor system. Approximately 10 hours were accumulated prior to the start of flight testing.

For the rotor whirl tests the complete aircraft was installed in a fenced-in rotor whirl test area (Figure 25). The aircraft was restrained through the external sling load attachment point in the vertical force direction (rotor lift) and through a lateral attachment for yaw forces. Both the vertical and the yaw attachment were made through load cells with visual readout capability in the cabin. The yaw attachment point on the aircraft was a specially fabricated form collar surrounding the tail boom just forward of the 45-degree gearbox (Figure 26).

The vertical force to the external sling load attachment point was limited to 4000 pounds by reference to the load cell readout. Lift up to 70% collective was possible using this method combined with ballasting the aircraft to a gross weight of 9500 pounds.

			TABLE 5. LOG OF PREFLIGHT GROUND TESTS	
Date	Test	Hours	Purpose	Comments
12-12-74	1	0.1	First run with modified tail rotor blades	Satisfactorily accomplished
12-12-74	2	1.7	Envelope expansion of tail rotor	Satisfactorily accomplished
12-20-74	3	0.1	First run with modified main rotor blades	Instrumentation problems
1-4-75	4	0.5	Envelope expansion of main rotor	Satisfactorily accomplished
1-5-75	5	1.0	Envelope expansion including boost-off evaluation	Improved boost-off forces
1-7-75	6	2.2	Overspeed tests, ac generator tests vs load	Satisfactorily accomplished
1-8-75	7	4.3	Blocked engine air inlet and endurance running	Satisfactorily accomplished
		9.9	Total run hours on modified system	

The yaw force on the aft fuselage was maintained within 20 pounds of zero by varying tail rotor pedal position during main rotor torque changes. For full pedal sweeps both left and right, the tail rotor thrust was measured and reacted by a load cell and yaw restraint at the 45-degree gearbox.

No difficulty was experienced operating the aircraft over the full rpm and lift range. Monitoring of structural loads and dynamic characteristics was accomplished through the use of the real-time CRT scopes installed in the aft cabin area of the aircraft. The aircraft was manned and the testing conducted by a pilot and a flight test engineer in the pilot and copilot seats and a structural flight test engineer and a dynamics engineer in the main cabin where the scopes were located.

Figure 25. Test Aircraft Operating in the Tiedown Facility at Burbank.

Figure 26. Test Aircraft in Operation, Showing Lateral Bar/Load Cell at the Tail for Yaw Restraint.

The ground tiedown testing on a preflight rotor qualification program consisted of approximately 10 hours of operation. The purpose of this testing was to verify rotor stability and loads as well as to provide a reasonable operating background prior to flight testing of the modified configuration. Both the main and tail rotors were separately tested over a wide range of operating conditions. These included:

a. Engine overspeed to 6900 rpm or almost a 5% margin over normal flight operating rpm.

b. Tail rotor thrust over its full range of blade angle travel, and main rotor thrust up to approximately 13,500 pounds (70% collective). This is approximately 1-1/2g of lift.

c. Cyclic and collective pulses to check rotor stability and damping.

d. Speed sweeps from engine idle (4500 rpm) to maximum allowable overspeed (6900 rpm)

e. Testing at off-normal rotor rpm (315-338)

f. Endurance running at high thrust settings.

As previously noted in Section 3 (Table 4), load measurements were made at the following locations:

Main Rotor

a. Inplane bending moment, Sta. 35
b. Flapwise bending moment, Sta. 35
c. Inplane bending moment, Sta. 150
d. Flapwise bending moment, Sta. 150
e. Flapwise bending moment, Sta. 234
f. Pitch link axial load

Tail Rotor

g. Inplane bending moment, Sta. 11
h. Flapwise bending moment, Sta. 14
i. Pitch link axial load

4.1.1 Ground Loads and Dynamics

The main rotor loads measured during ground tests were well within limits, and all were below the levels measured during the flight tests. For this reason the ground measurements for the main rotor are not presented.

The tail rotor loads measured during the ground tests are presented because they give a good indication of the transient dynamic response during tail rotor pedal sweeps. Since the airframe is held in yaw during the ground test, full pedal sweeps can be made without considering the effect on aircraft attitudes. The cyclic loads measured during these sweeps are plotted against rpm and are shown in Figures 27 through 29. The three measured cyclic loads presented are below the maximum loads measured on a standard aircraft in level flight conditions and are also below the maximum design loads. These data are presented in Figures 30 through 32. (Unfortunately, directly comparable standard aircraft ground test data are not available.)

Vibration levels at several points on the airframe were recorded during rpm sweeps on the vehicle while in the tie down configuration. These runs were primarily made to identify blade and airframe or airframe component natural frequencies. The sweeps were made at a slow rate, and natural frequencies were identified by noting the frequencies where the recorded loads or vibration data reached a peak value in amplitude.

The frequency crossings identified on the main rotor are summarized in Table 6. These data were obtained on ground test No. 5. A comparison of the above frequencies with the predicted frequencies (for the cyclic or antisymmetric response and for the collective response) shows little difference. This is true for the 3P and 4P frequency crossings at 110 rpm, the 5P crossing at 234 rpm and for the 9P crossing at 238 rpm, which compare within 6 percent of the computed values. The 4P apparent
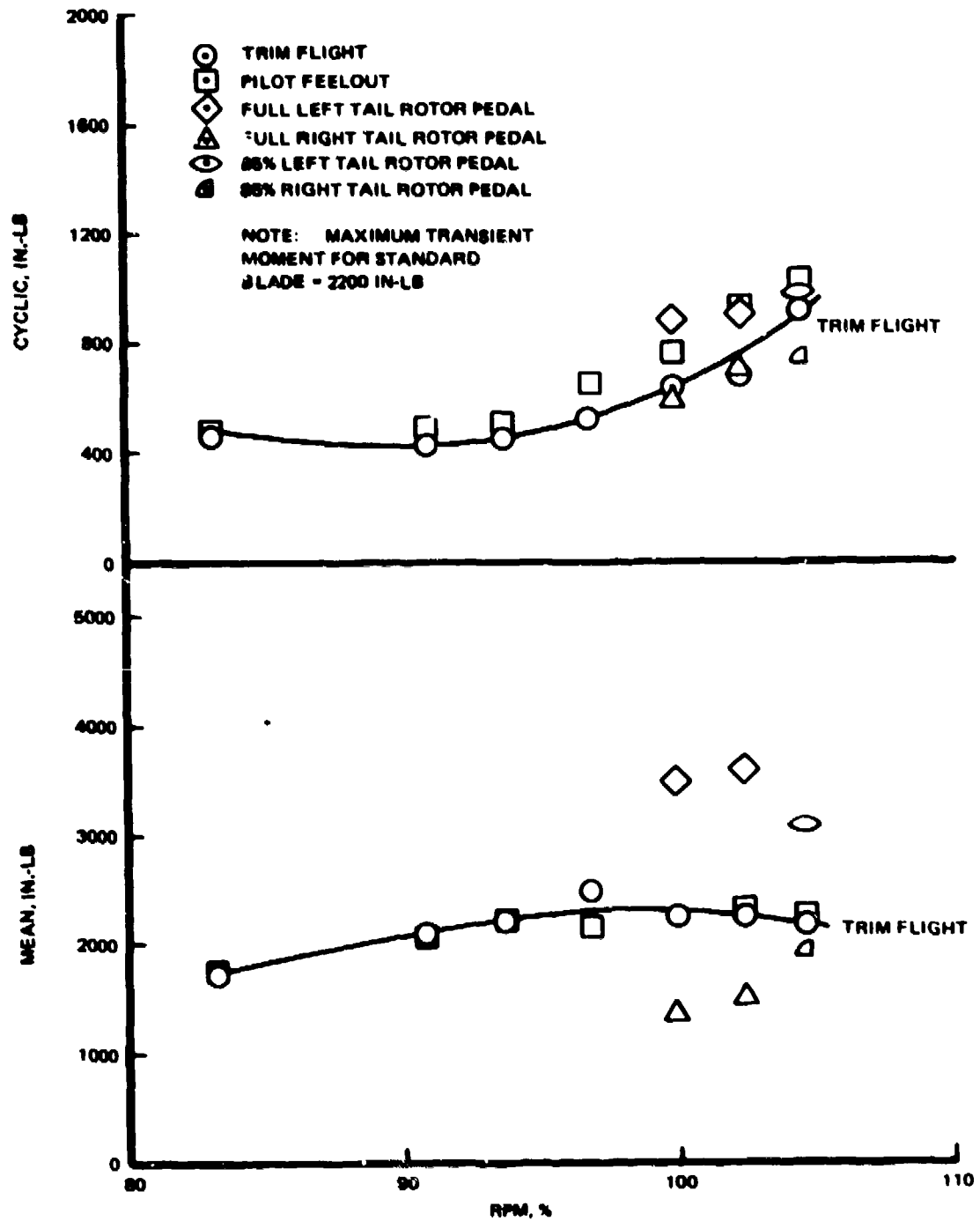
Figure 27. Tail Rotor Inplane Bending Moment at Station 11 During Ground Tests With Deicing Boots Installed.
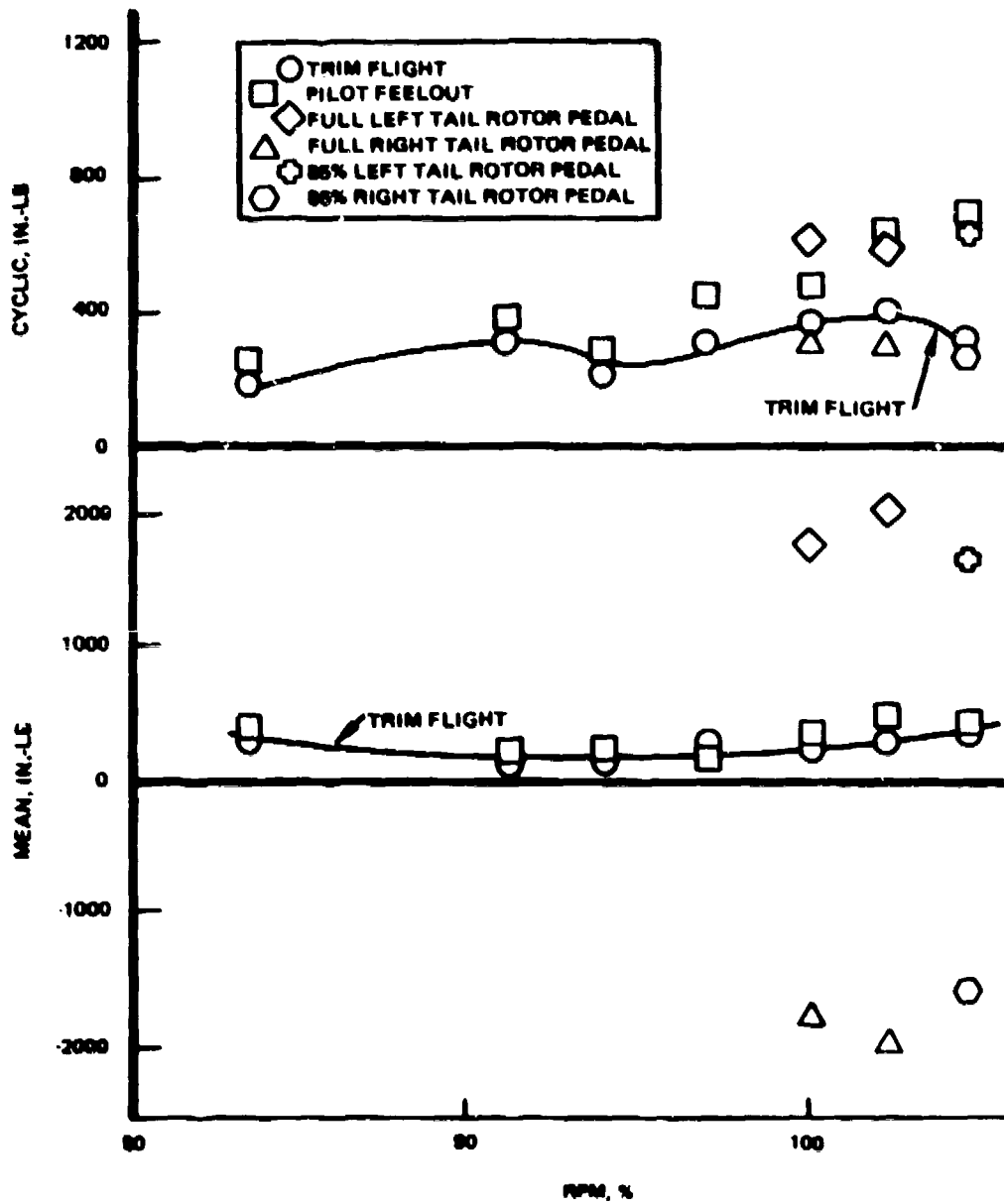
Figure 28. Tail Rotor Flap Bending Moment at Station 21.5 During Ground
Tests With Deicing Boots Installed
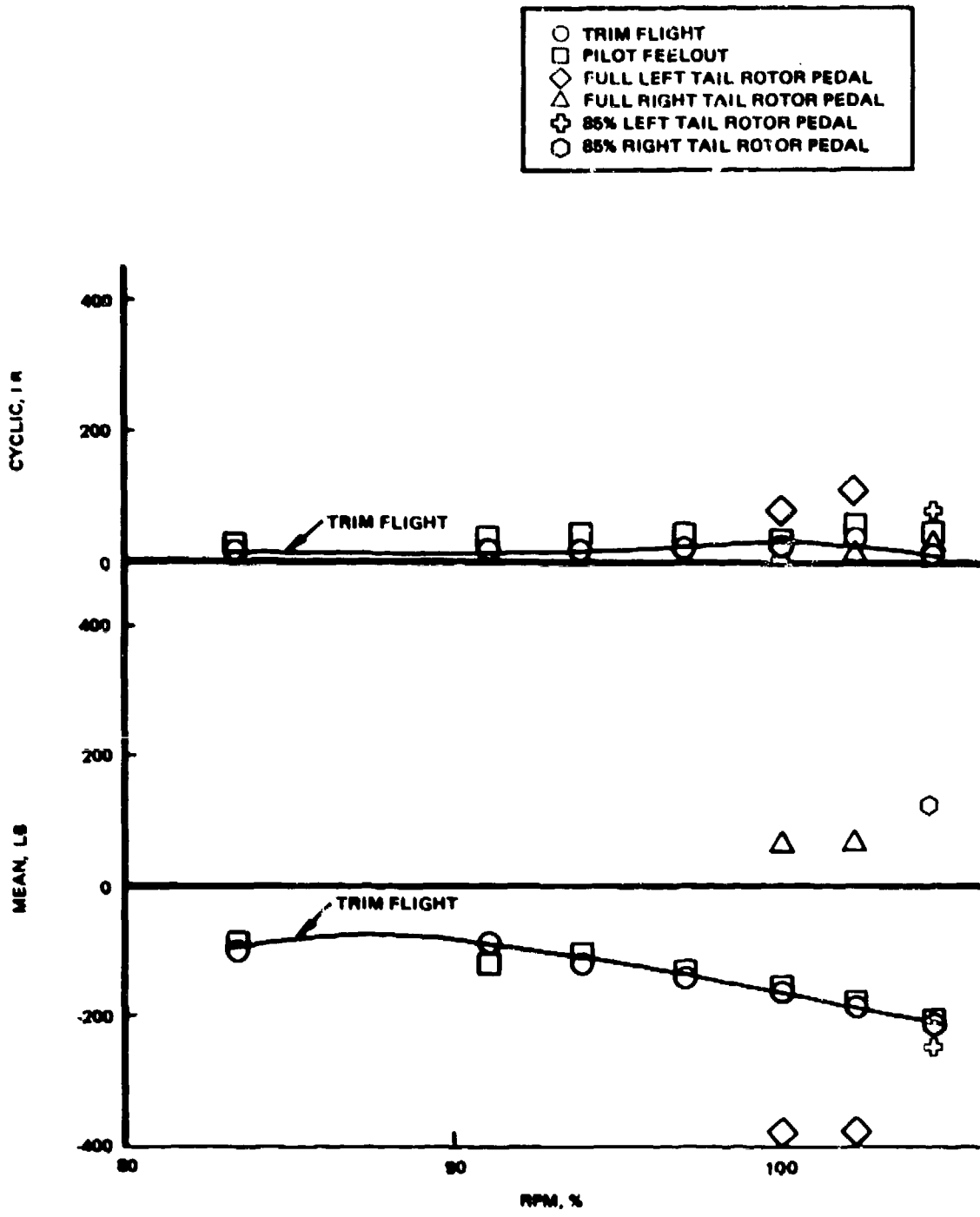
Figure 29. Tail Rotor Pitch Link Axial Load During Ground Tests With Deicing Boots Installed.
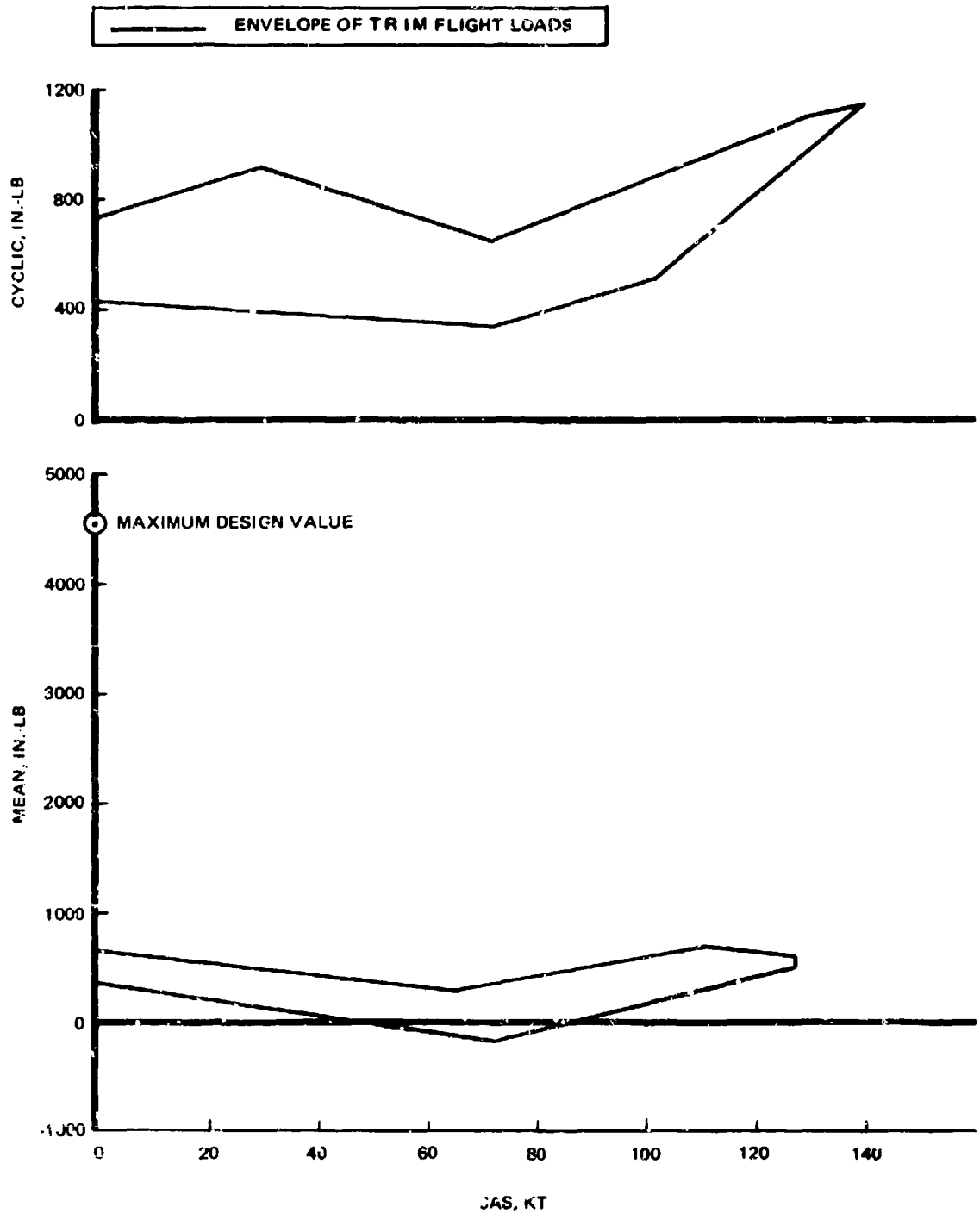
Figure 30. Tail Rotor Inplane Bending Moment at Station 11 With Standard Rotor.
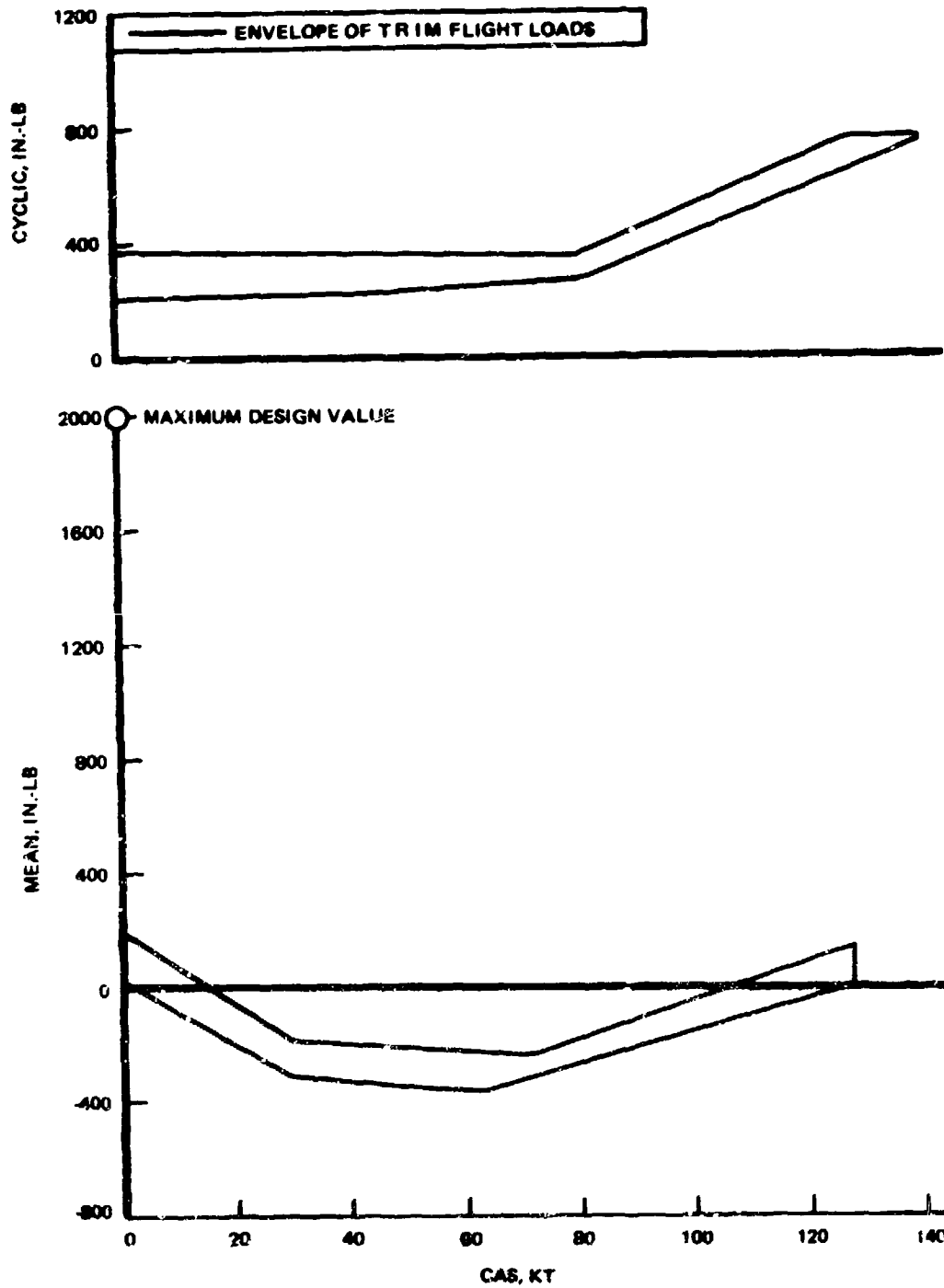
Figure 31. Tail Rotor Flap Bending Moment at Station 24 With Standard Rotor.
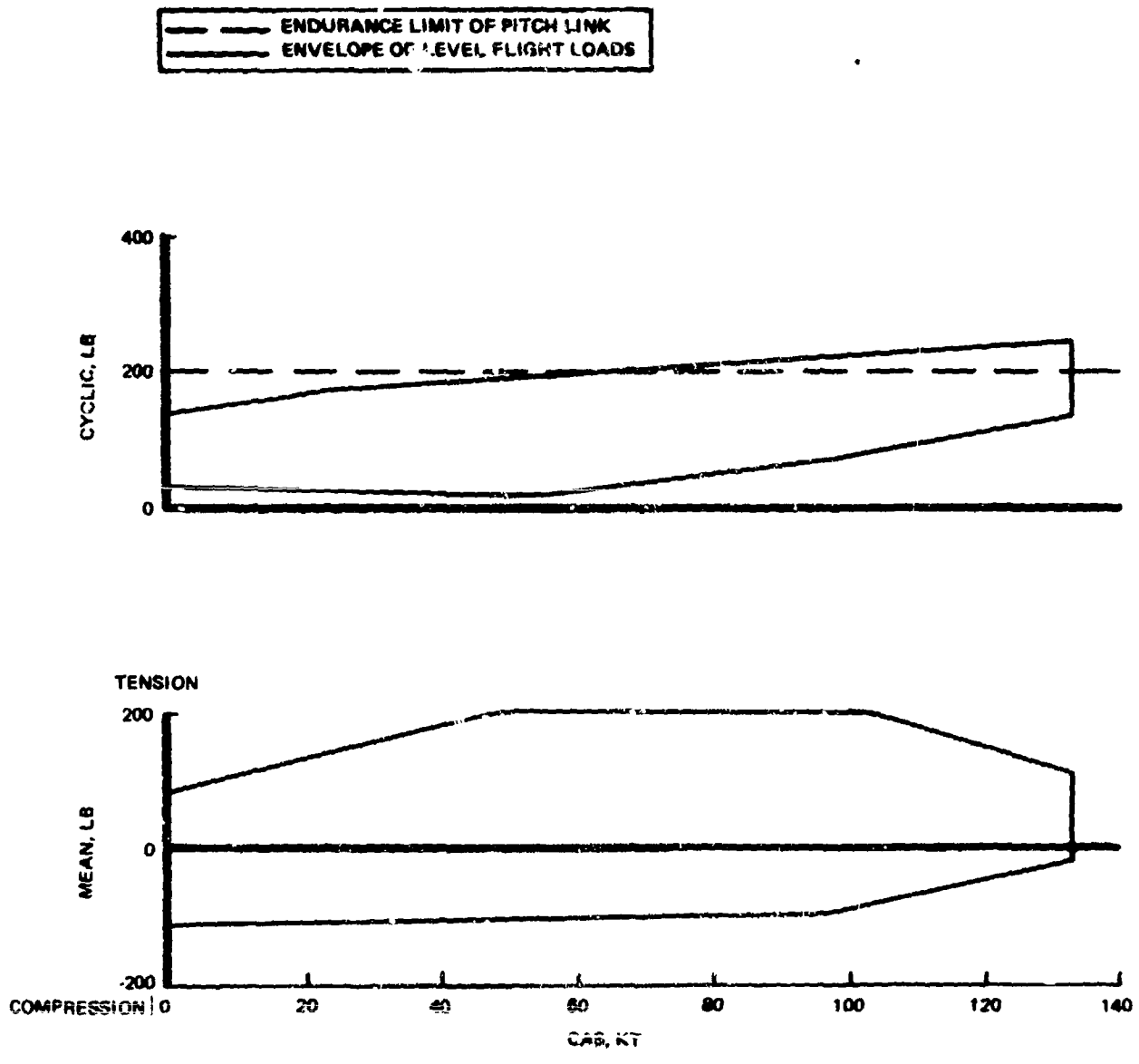
Figure 32. Tail Rotor Pitch Link Axial Load With Standard Rotor.

TABLE 6. MAIN ROTOR BLADE FREQUENCIES IDENTIFIED FROM SPEED SWEEPS

Frequency		Main Rotor RPM	Measurement	Comments
CPS	P			
11.0	2	220	Flap Bend @ Sta. 150	Antisymmetric Mode
14.67	4	220	Flap Bend @ Sta. 150	Collective Mode
19.5	5	234	Pitch link, F150 & F35	Antisymmetric Mode
22.0	4	330	Flap Bend @ Sta. 35	Very small response
35.7	9	238	Flap Bend @ Sta. 150	Antisymmetric Mode

crossing at 330 rpm, however, does not appear to have any bearing on predicted values. Due to the small indicated response, therefore, and subsequent flight tests which showed no undue response at 4P in the operating rpm range, it is expected that the 4P response at 330 rpm was not a true frequency crossing. From these tests, it is concluded that there are no significant main rotor blade resonances within the operational rpm range.

The RPM sweeps to identify the tail rotor natural frequencies are shown in Table 7.

TABLE 7. TAIL ROTOR BLADE FREQUENCIES IDENTIFIED FROM SPEED SWEEPS

Frequency		Tail Rotor RPM	Measurement	Comments
cps	P			
35.4	2	1060	Flap Bend @ Sta. 24	Collective mode
41.6	2	1250	Inplane Bend @ Sta. 11	Mode not identifiable
55.2	3	1100	Flap Bend @ Sta. 24	Antisymmetric mode
118.8	6	1190	Flap Bend @ Sta. 24	Collective mode

The 2P collective flap mode frequency at 1060 rpm is within 15 percent of the predicted value, and the 6P crossing at 1190 rpm is within 9 percent of the predicted frequency. The 2P response at 1250 rpm would exactly duplicate the analysis if the response were cyclic. The 2P response, however, is usually collective on a two-bladed rotor, and the instrumentation did not permit resolution of this question.

The 3P frequency crossing at 1100 rpm was within 20 percent of the predicted value. As would be expected, the tail rotor frequencies would be difficult to predict due to the influence of the aft fuselage dynamics. The test results do show, however, that the tail rotor is free from blade resonance within the normal operating speed range.

One additional observation is that during the tiedown test, the maximum tail rotor oscillatory load occurred in chordwise bending at or near the cyclic inplane natural frequency at nearly a steady-state amplitude. There was insufficient instrumentation to determine whether the response was cyclic or collective. The magnitude of the response was of the order of 700 to 800 inch-pounds and reached values of up to 1100 inch-pounds in pedal sweeps and transient pedal inputs. This is discussed further in Section 4.2.2.

Several frequency crossings were identified on the airframe, gearboxes and accessories during the speed sweeps, and these are summarized in Table 8. It should be noted that the lowest frequencies would be most influenced by the tiedown configuration. No effort has been made to identify the airframe modes excited since sufficient data were not available. No resonances were observed within or near the normal operating speed range during the ground runs and in subsequent flight tests, indicating that the modifications made to the aircraft have not adversely affected the airframe and airframe component dynamic response.

TABLE 8. AIRFRAME/ACCESSORIES VIBRATION RESPONSE FREQUENCIES IDENTIFIED FROM SPEED SWEEPS	
Frequency (cps)	Measurement Location
14, 30.7, 73	Tail Rotor Gearbox Longitudinal Acceleration
7.2, 13.8, 30.7	Pilot Vertical Acceleration
7.2, 13.7, 30.7	Copilot Vertical Acceleration
30.7	Pilot Longitudinal Acceleration
51	Tail Rotor Gearbox Lateral Acceleration
42	Generator Vertical Acceleration
80	Main Rotor Gearbox Lateral Acceleration
45	Generator Lateral Acceleration
23.2	Tail Rotor 90° Gearbox Vertical Vibration

4.2 FLIGHT TESTS

Table 9 presents a log of the flight tests conducted for airworthiness. Eleven flights and approximately 11 flight hours were involved.

Flight tests were conducted over the operational speed-altitude envelope at gross weights and c.g.'s to establish permissible loadings for the icing test program to cover:

a. Crew loading of four plus some added cargo -- forward c.g.

b. Crew loading of four (pilot, copilot and two observers), or equivalent cargo -- assumed icing test loading.

c. Crew loading of three (pilot, copilot, and one observer), or equivalent cargo -- mid c.g.

d. Crew loading of one (pilot only) -- aft c.g.

				TABLE 9. LOG OF AIRWORTHINESS FLIGHT TESTS	
Date	Test	Flight	Hours	Purpose	Comments
1-12-75	8	1	0.2	Hover and low-speed evaluation	Satisfactorily accomplished
1-12-75	8	2	0.6	Sideward and rearward flight	Satisfactorily accomplished
1-13-75	9	-	-	Deicing system check	Satisfactorily accomplished
1-14-75	10	3	0.6	Autorotation rpm check	Satisfactorily accomplished
1-17-75	11	4	1.6	Envelope expansion at mid c.g.	Satisfactorily accomplished
1-18-75	12	5	1.6	Maneuvering flight - mid c.g.	Satisfactorily accomplished
1-18-75	13	6	0.5	Low-speed evaluation - aft c.g.	Satisfactorily accomplished
1-18-75	13	7	1.5	Envelope expansion - aft c.g.	Satisfactorily accomplished
1-19-75	14	8	0.4	Low-speed evaluation - forward c.g.	Satisfactorily accomplished
1-19-75	14	9	1.5	Envelope expansion - forward c.g.	Satisfactorily acomplished
1-19-75	15	10	1.1	Envelope expansion - 10,000 feet - forward c.g.	Satisfactorily accomplished
1-20-75	16	-	-	Check run without hub camera on.	Satisfactorily accomplished
1-20-75	17	11	1.2	Envelope expansion without hub camera; first inflight deicing system operation; EMI checks	Elec. short to ground experienced in wiring to blade heater
			10.8	Total airworthiness flight hours	
			11	Total number of airworthiness flights	

87

The test aircraft was weighed, and the balance was checked prior to the start of the airworthiness flight testing. Table 10 defines the weight and c.g. for each configuration and the assumed icing test loading. These loadings and the travel of center of gravity with fuel usage are shown on Figure 33. Also shown on the curves are the start and end conditions of each of the airworthiness flights conducted. Tests were conducted to evaluate handling qualities and structural loads/ dynamic characteristics at each of the loadings identified as Configuration A, C, and D.

Figures 34 through 37 show each of the speed-load factor conditions tested. Noted on the curves are the operating conditions of rotor rpm and maneuver conducted. The load factor demonstrated is equivalent to a 45-degree banked level turn to 90 KCAS, decreasing to a 30-degree banked level turn at V_{max}. This is more than a practical usable maneuvering envelope for the UH-1H aircraft in normal operations. V_{max}

TABLE 10. AIRCRAFT WEIGHT AND BALANCE SURVEY			
	Pounds	C.G. Station	
Basic Weight of Test Aircraft (UH-1H S/N 70-16318 as Modified)	6199	144.1	
Plus Pilot, Engr. Observer and Aft C.G. Ballast	6661	141.4	
Plus Full Fuel	8020	143.3	Config. D
Plus Copilot and 1 Observer	8160	139.8	Config. C
Plus Copilot and 2 Observers	8480	137.7	Config. B
Plus Copilot, 2 Observers, and 340 LB.	8825	135.0	Config. A
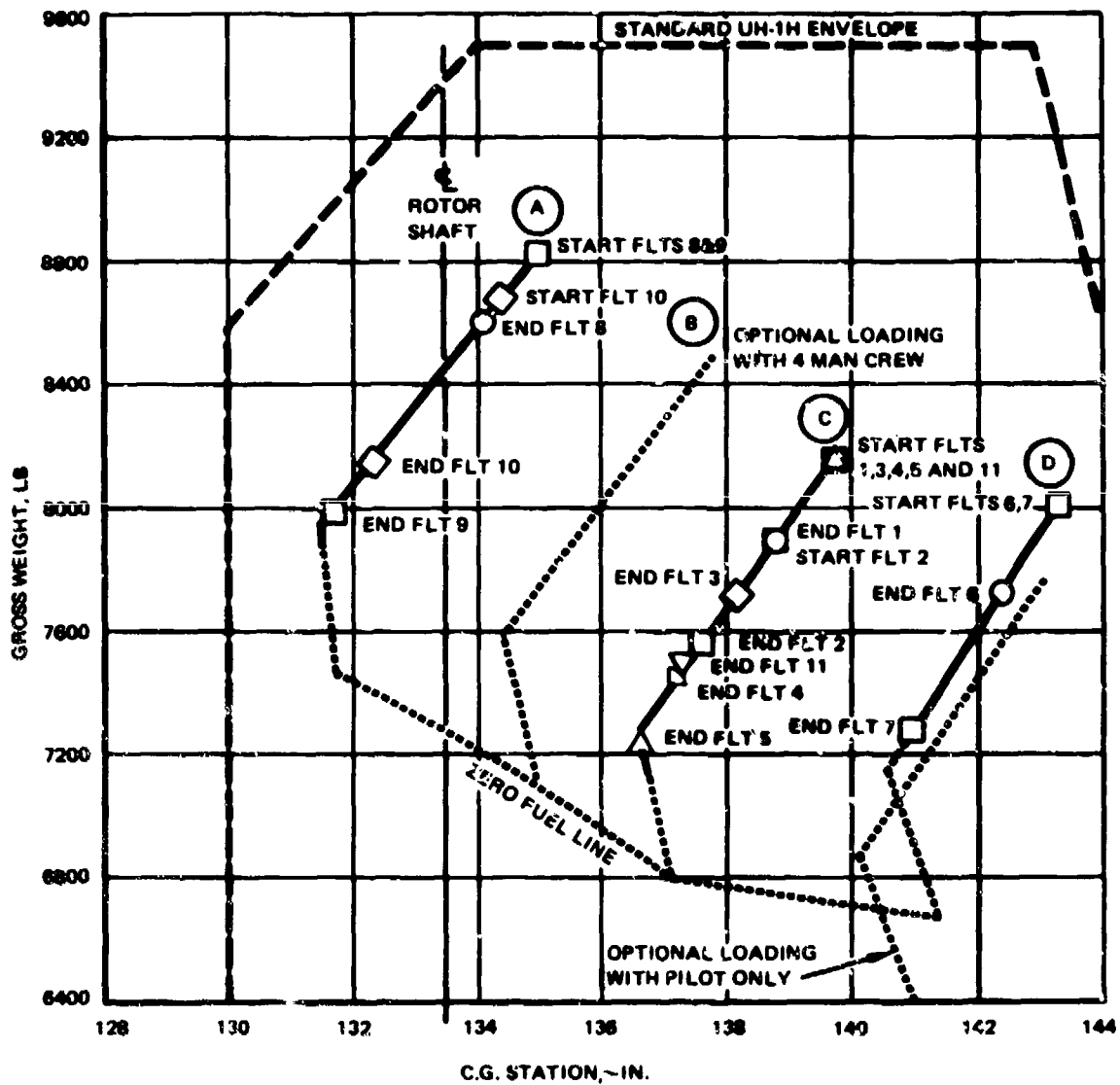
Figure 33. Gross Weight - C.G. Envelope for Airworthiness Tests.
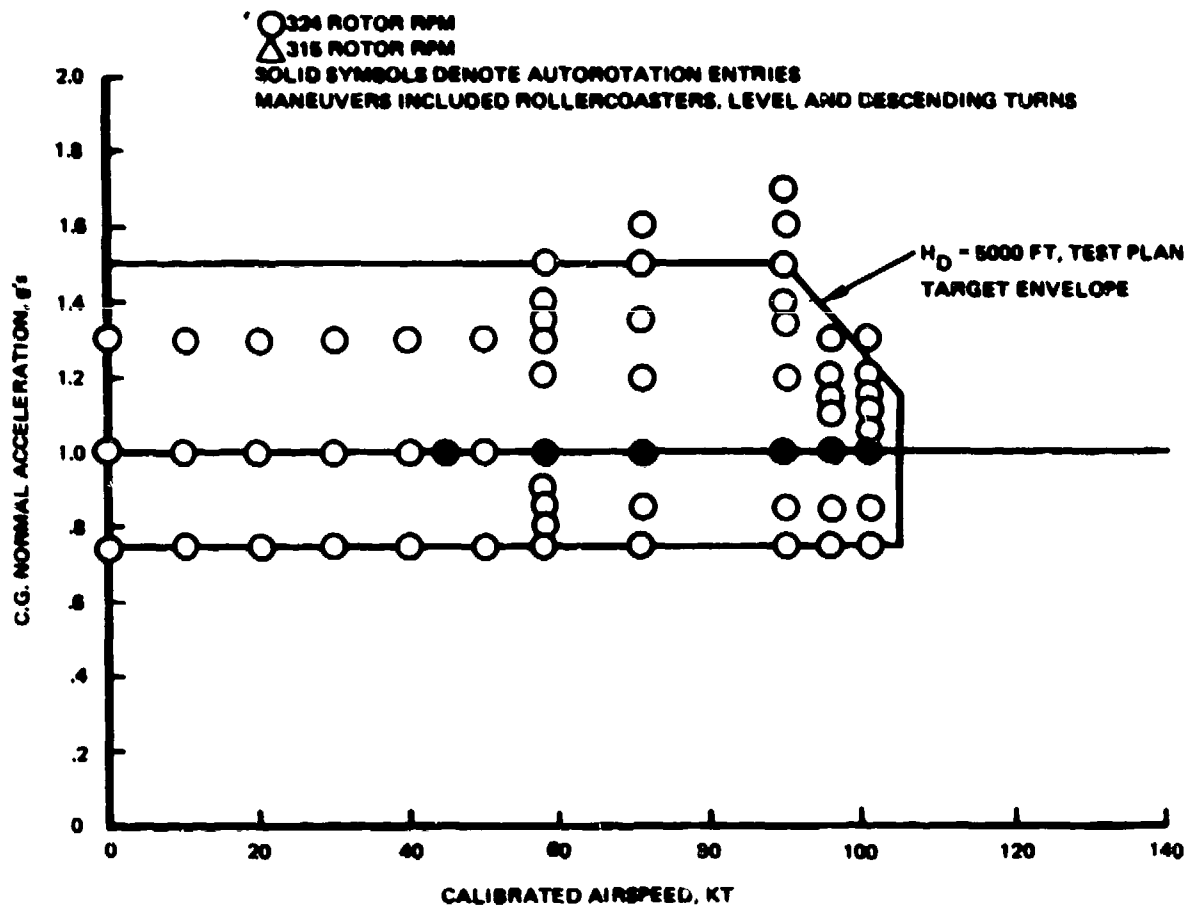
Figure 34. Airspeed - Load Factor Envelope - Configuration A.

Figure 35. Airspeed - Load Factor Envelope - Configuration C.

Figure 36. Airspeed - Load Factor Envelope - Configuration D.

W_{AVG} - 8425 LB   C.G. - 133.4 IN. (FWD)

H_{AVG} - 11,200 FT

○ ~ 324 ROTOR RPM

△ ~ 315 ROTOR RPM

SOLID SYMBOLS DENOTE AUTOROTATION ENTRIES
MANEUVERS INCLUDE ROLLERCOASTERS AND LEVEL TURNS

H_D 10,000 FT, TEST PLAN
TARGET ENVELOPE
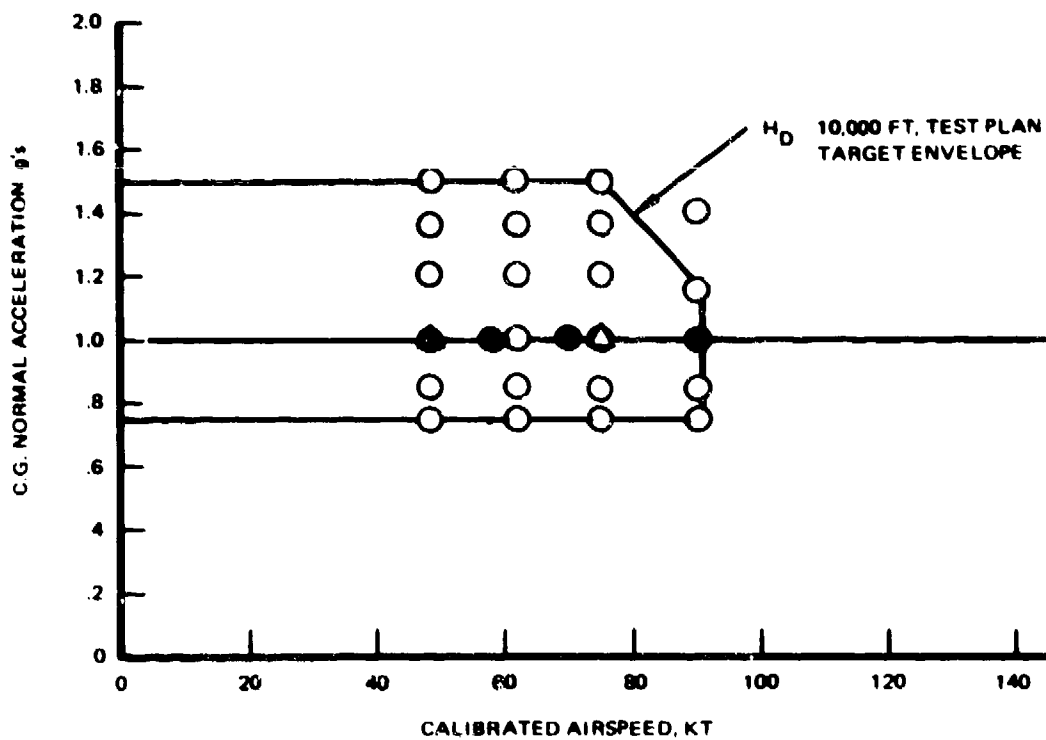
Figure 37.   Airspeed - Load Factor Envelope - Configuration A at 11,000 Feet.

demonstrated was equivalent to the published V_{NE} in the Operator's Manual[1]. Very little if any difference was noted in the handling/ dynamics characteristics from the basic (unmodified) UH-1H.

Data were obtained at a hover height of approximately 2 to 3 feet and were within the hover torquemeter check requirement tolerance of the maintenance check flight as set forth in the Maintenance Manual[2].

In level flight, data were obtained in the 70 to 90 KCAS range at an altitude of 5,000 feet. The results reflected some data scatter and indicated an increase in equivalent flat plate area of 2 to 5 square feet when compared with the level flight data presented in Reference (2). These data are considered to be semiquantitative since there was no performance baseline established with the unmodified UH-1H test aircraft. This drag increase does reflect approximately the increase in power required of the test aircraft due to the installation of modified main and tail motor blades, two sets of external sliprings, a hub camera, and two roof-mounted ice detectors.

Envelope expansion testing was basically conducted in two parts for each center of gravity location tested:

a. Hover and Low-Speed Flight: These tests were conducted from hover to approximately 50 KCAS at field elevation (2,350 feet).

(1) Anon. "Operator's Manual Army Model UH-1D/H Helicopters, TM 55-1520-210-10, 25 August 1971.

(2) Anon. "Organizational Maintenance Manual Army Model UH-1D/H Helicopters; TM 55-1520-210-20, 10 September 1971.

b. Inflight Tests: These tests were conducted at a pressure altitude of approximately 5,000 feet for all c.g.'s tested at speeds from 50 KCAS to V_{max}. At 10,000 feet, the tests were conducted at a c.g. location chosen on the basis of test results obtained at 5,000 feet. Since no c.g. loading was found to be critical, the tests were conducted at the heaviest normal loading and resultant c.g. location.

The actual conditions evaluated during hover and low-speed flight and for inflight testing are listed in Tables 11 and 12, respectively. All airworthiness tests in hover, low-speed, and forward flight were conducted in a buildup fashion, incrementally increasing the size of the control input in each axis until the response of the aircraft was more than sufficient to evaluate damping, controllability, and control margins. Sideward and rearward flight characteristics were evaluated using a calibrated pace vehicle to determine the actual speeds for configurations A, C and D. The control motions and response in transition and the control margins at speeds up to 30 knots in sideward and rearward flight are similar to those of a standard UH-1H helicopter. Autorotation entries were conducted over a speed range from 45 to approximately 106 KCAS at 5,000 feet for each c.g. configuration tested and from 40 to 90 KCAS at 10,000 feet, and rotor speed rpm control in autorotation was satisfactory at all conditions tested.

The assessment of handling qualities for the modified UH-1H helicopter was based primarily on qualitative evaluation by the pilot who received his familiarization training in the standard UH-1H helicopter just prior to this test program. As part of his training, the pilot flew the same basic flight cards that were used in envelope expansion testing of the modified UH-1H helicopter (this provided a baseline for comparison with each planned test condition). In areas where the pilot's comments could be compared with published test data, trends of control motion and response were verified. The pilot's comments on the modified configuration are contained in Section 4.2.2.

95

TABLE 11.   SUMMARY OF LOW SPEED CONDITIONS FOR FLYING QUALITIES EVALUATION

	RPM	\	FLIGHT NO.							
			1, 2	3	4	5	11	6 & 7	8 & 9	10
G.W. @ T.O.			8164	8164	8164	8164	8164	8021	8831	8681
C.G. @ T.O.			139.75	139.75	139.75	139.75	139.75	143.31	134.96	134.37
Configuration			C	C	C	C	C	D	A	A
Ground Feelout	315		X							
(Control inputs in all axes)	324		X							
Hover Feelout	315		X				X	X	X	
(Control inputs in all axes)	324		X				X	X	X	
Sideward Flight	324		15 KCAS	35 KCAS Rt 35 KCAS Lt			Rt & Lt to 25k	30 KCAS Lt 26 KCAS Rt	30 KCAS Rt 30 KCAS Lt	
Rearward Flight	324		15 KCAS	32 KCAS			To 25k	To 25k	30 KCAS	
Air Taxi	324		X	X			X	X	X	
Acceleration thru transition	315		X	X			X		X	
	324		X				X	X		
Acceleration to 50 KCAS	315		X	X				X	X	
	324		X	X			X			

TABLE 12. SUMMARY OF INFLIGHT CONDITIONS FOR FLYING QUALITIES EVALUATION

Flt	RPM	FLIGHT NO.							
		1 & 2	3	4	5	11	6 & 7	8 & 9	10
G.W. @ T.O.		8164	8164	8164	8164	8164	8021	8831	8681
C.G. @ T.O.		139.75	139.75	139.75	139.75	139.75	143.31	134.96	134.37
Configuration		C	C	C	C	C	D	A	A
Low Power Descents	324		58 KCAS						
Autorotations (including right and left turns)	324		58 KCAS	45, 58, 71 & 85 KCAS	96, 106 KCAS		45, 58 71, 90 96 & 106 KCAS	45, 58, 71, 90 96 & 106 KCAS	49, 58 71 & 90 KCAS
Forward Flight Feelout	315			58, 71 85 & 101 KCAS	106 KCAS	58, 71, 90 & 106 KCAS	58, 71, 90,101 & 106 KCAS	58, 71, 90 & 106 KCAS	49, 63, 76 & 90 KCAS
(Control inputs in all axes)	324			58, 71, 85 & 90 KCAS	106 KCAS	58, 71, 90 & 106 KCAS	58, 71, 90,101 & 106 KCAS	58, 71, 90 & 106 KCAS	49, 63, 76 & 90 KCAS
Rollercoasters	315 324			58, 71 & 90 KCAS	96 & 106 KCAS	58, 71, 90 & 106 KCAS	58, 71, 90, 96 & 106 KCAS	58, 71, 96 & 106 KCAS	49, 58 76 & 90 KCAS
Descending Turns (left & right)	315 324			58, 71 & 90 KCAC	96 & 106 KCAS		58, 71, 96 & 106 KCAS	58, 71, 90 & 106 KCAS	

97

TABLE 12. SUMMARY OF INFLIGHT CONDITIONS FOR FLYING QUALITIES EVALUATION (Cont)

Flt	RPM	FLIGHT NO.							
		1 & 2	3	4	5	11	6 & 7	8 & 9	10
Level Turns (Left & Right)	315 324			58, 71 & 90 KCAS	96 & 106 KCAS	58, 71, 90 & 106 KCAS	58, 71 90, 96 & 106 KCAS	58, 71 90, 96 & 106 KCAS	49, 58 80 & 90 KCAS
Operational Type Maneuvering Evaluation	324				X		X	X	X

98

The load factor - airspeed envelopes presented in Figures 34 through 37 were also expanded in an incremental manner. The load factors at each speed were obtained by performing rollercoaster, windup descending turns, and constant-altitude turns. No evidence of blade stall, as would be indicated by increasing vibration levels, was reported for any of the high positive load factor maneuvering conditions. Handling qualities were also evaluated during typical operational flight conditions such as climbs, powered descents, autorotations, power recoveries, rolling pullouts, boost-off operation, and point-to-point rolls. The flight qualities and control margins of the modified UH-1H helicopter are considered to be satisfactory over the tested flight envelopes for each weight and center of gravity configuration.

Measurements were made to evaluate the boost-off forces with the modified blades due to the relatively high forces of the basic UH-1H and the concern over the effect of blade c.g. shift due to the deicer boots. Design changes were incorporated in the modified blades to specifically achieve equivalent or lower collective forces.

Collective handle force versus collective position taken in flight at 70 knots is shown in Figures 38 and 39 for the standard blades and the modified blades, respectively. These data show the following comparison:

		Standard Blades	Modified Blades
a.	Collective Position for Zero Force	35%	30%
b.	Force Gradient (LB/percent θ)	23	14
c.	Pull Force To Reach 70%	86 lb	57 lb
d.	Push Force To Reach 0%	76 lb	42 lb
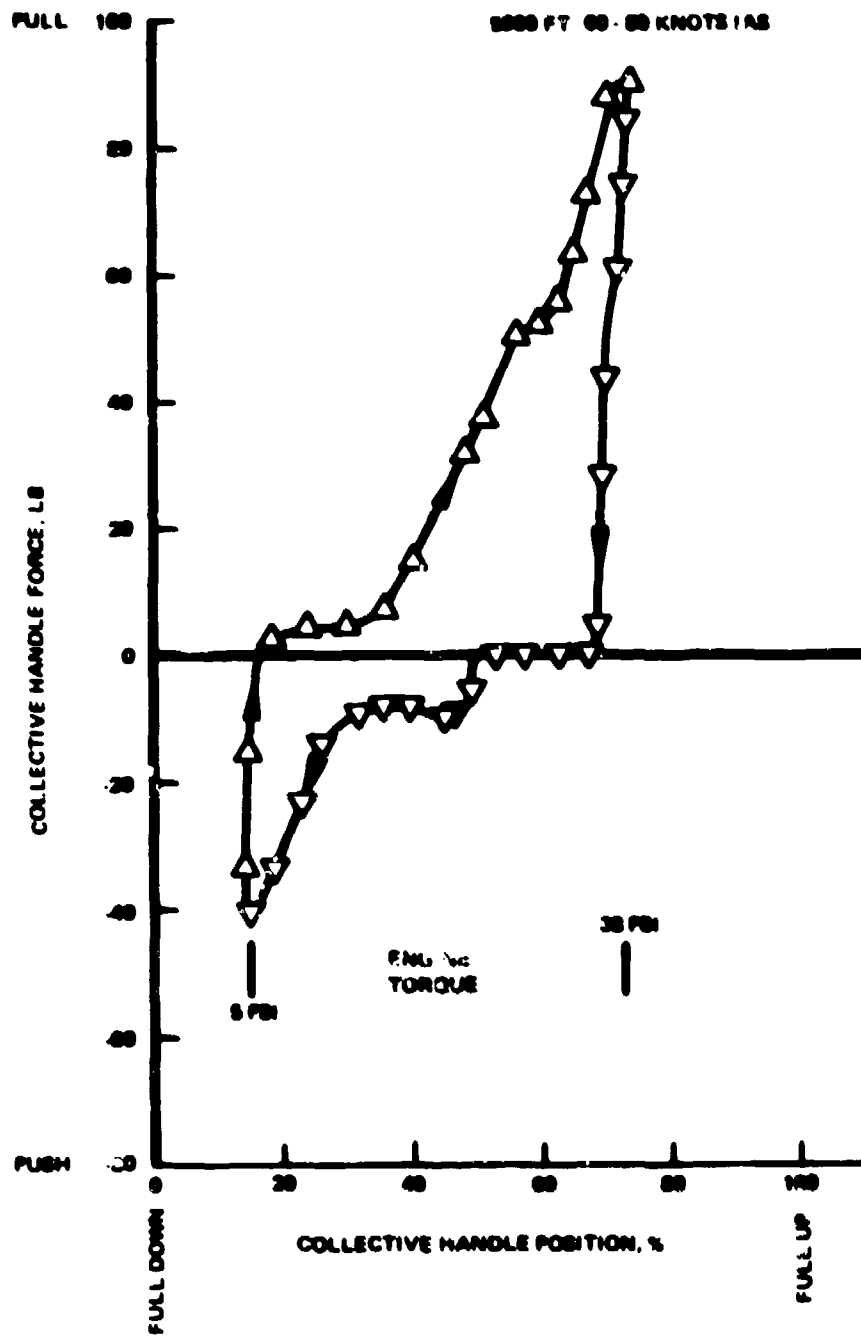
Figure 38. Inflight Boost-Off Collective Force With Standard Blades.
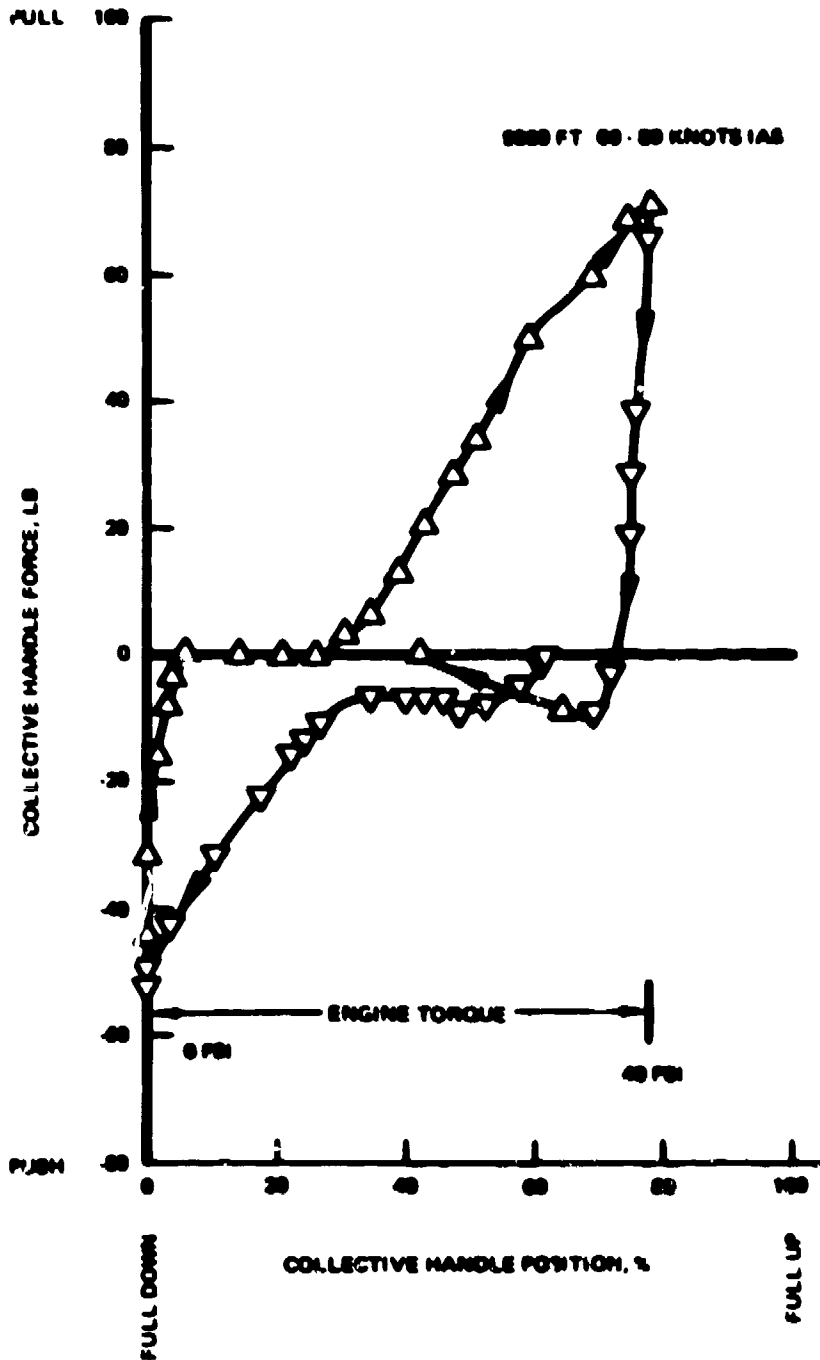
Figure 39.   Inflight Boost-Off Collective Force With Deicer
            Boots Installed.

101

Thus, the data show that the force gradient is reduced approximately
40%, and there is a reduction of the down (push) force required to reach
full-down collective of 45° (from 70 pounds to 40 pounds). The pull
force to reach 70% collective is reduced from 80 pounds to 57 pounds,
or a 24% reduction. Since the maximum practical pilot down effort seems
to be in the 40-60 pound range; the pilot alone cannot push to the full-
down position with standard blades, but he can with the modified blade.

Collective handle forces, as shown in Figure 44, were measured during the
tiedown tests. These data show an interesting comparison of the differ-
ence between ground and flight loading, which is the difference in rot -
coning and torque forces.

Modified Blades	Ground Tiedown	Inflight
a. Collective for Zero Force (pounds)	28	47
b. Force Gradient (lb/inch)	25	14

The unusual or hysteresis loop of the force versus position curves is due
to the lock and hold system of the UH-1H, which is designed to aid boost-
off operation.

4.2.1 Flight Loads and Dynamics

All the main rotor loads measured during the flight tests were well within
the loads measured on the standard unmodified rotor system. The tail
rotor steady and cyclic loads were different from those measured on the
standard aircraft (UH-1D) for which data were available. The comparison
showed the following relative to standard aircraft: (1) increase in
mean chord bending at station 11, (2) increase in oscillatory chord
bending at station 11 at a given speed, and (3) equal or slightly lower
flap equivalent bending at station 21.5.
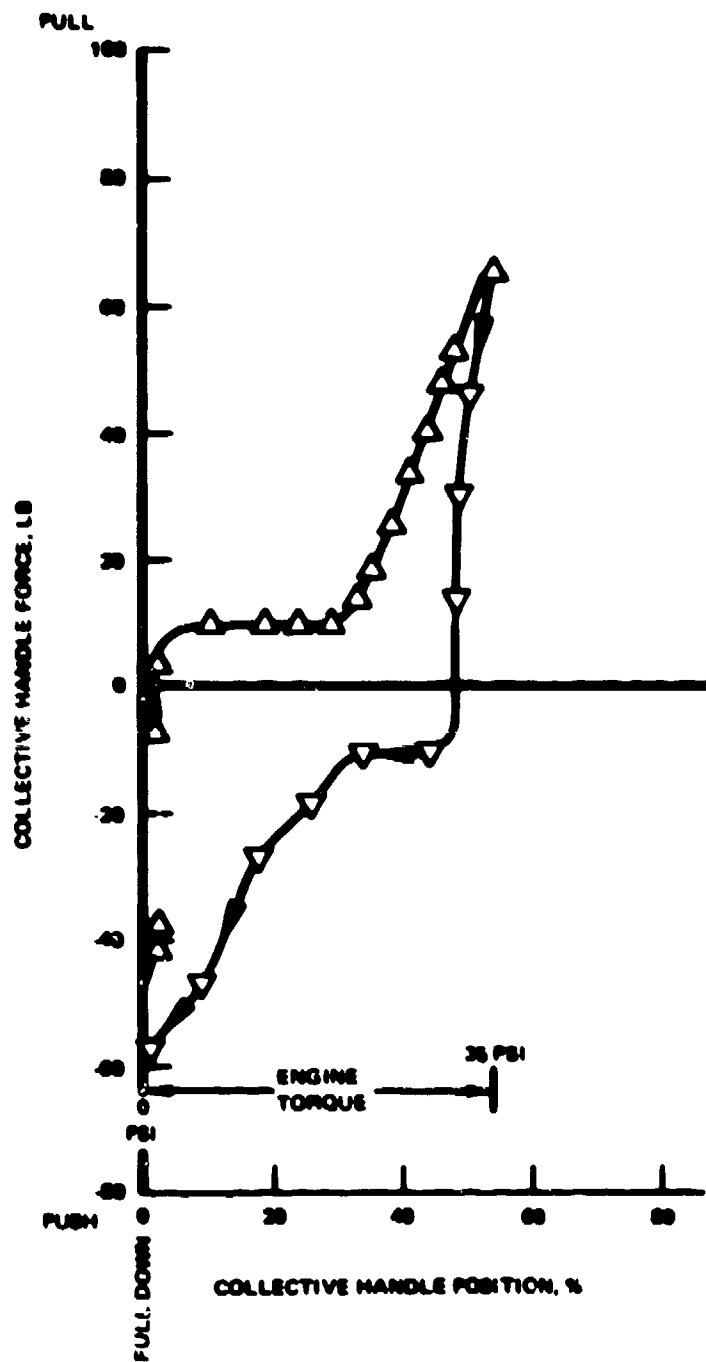
Figure 40. Boost-Off Collective Force During Ground Tiedown Test
With Deicing Boots Installed.

103

Since the deicer installation has a mass center location which is further forward than that of the standard tail rotor and since the blade is slightly heavier, a change in steady chord moment is to be expected. The cyclic moments would also be expected to change because of the slightly lower blade inplane frequency. A complete fatigue analysis was made of the highest loads, and all stresses were within all safe fatigue limits established for the standard blades. A review of other UH-1 model measurements using the same basic tail rotor structure (for the UH-1C and UH-1M) found that the cyclic moments in various flight maneuvers were well above those produced during the deicer test aircraft envelope tests. The load levels, therefore, while different from the standard UH-1H, are considered to be satisfactory. This is particularly true as the flap moments, which are the prime fatigue contributor, are actually lower.

The main rotor flap and inplane loads and pitch link loads for the forward cg are given in Figures 61 through 66. These loads are typical, as the mid and aft cg locations are essentially at the same level. The data for two altitudes (5000 feet and 15,000 feet) are presented. For comparison purposes, the loads measured on the standard blade are given in Figures 45, 46, 51, 5 , 55, and 57.

A direct overlay comparison shows that the cyclic loads are lower for the (deiced) modified blade.

The tail rotor loads are shown in Figures 69 through 84 (for comparison purposes, level-flight loads of standard aircraft are shown in Figures through 8). In all curves, a solid line is drawn between the level-flight points. The maximum level-flight speed and maneuver transient load obtained on the unmodified blade are marked on the figures. All cyclic loads are within the range experienced previously.
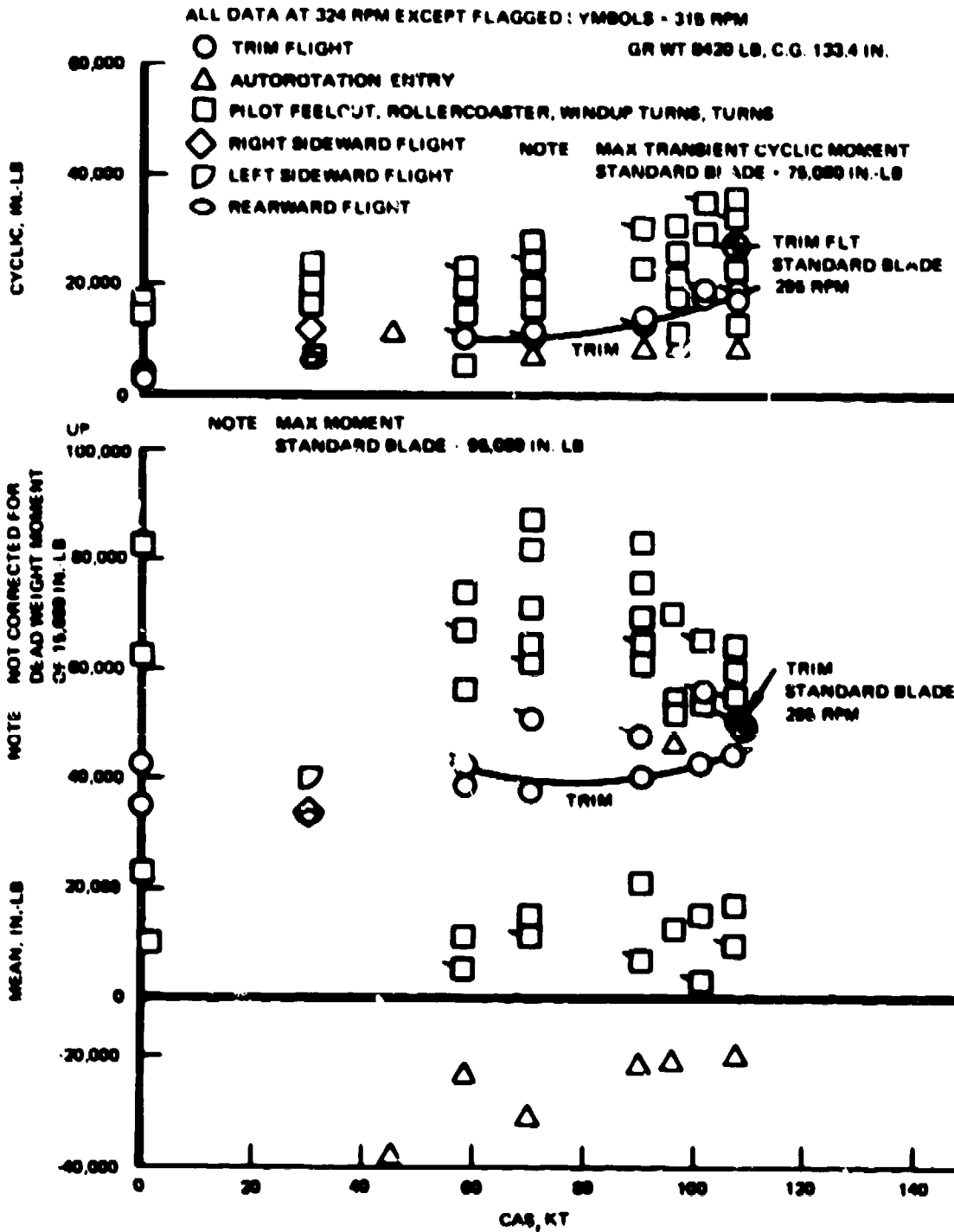
Figure 41. Main Rotor Flap Bending Moment at Station 35 With Deicing Boot Installed 5,000 Ft. Altitude.
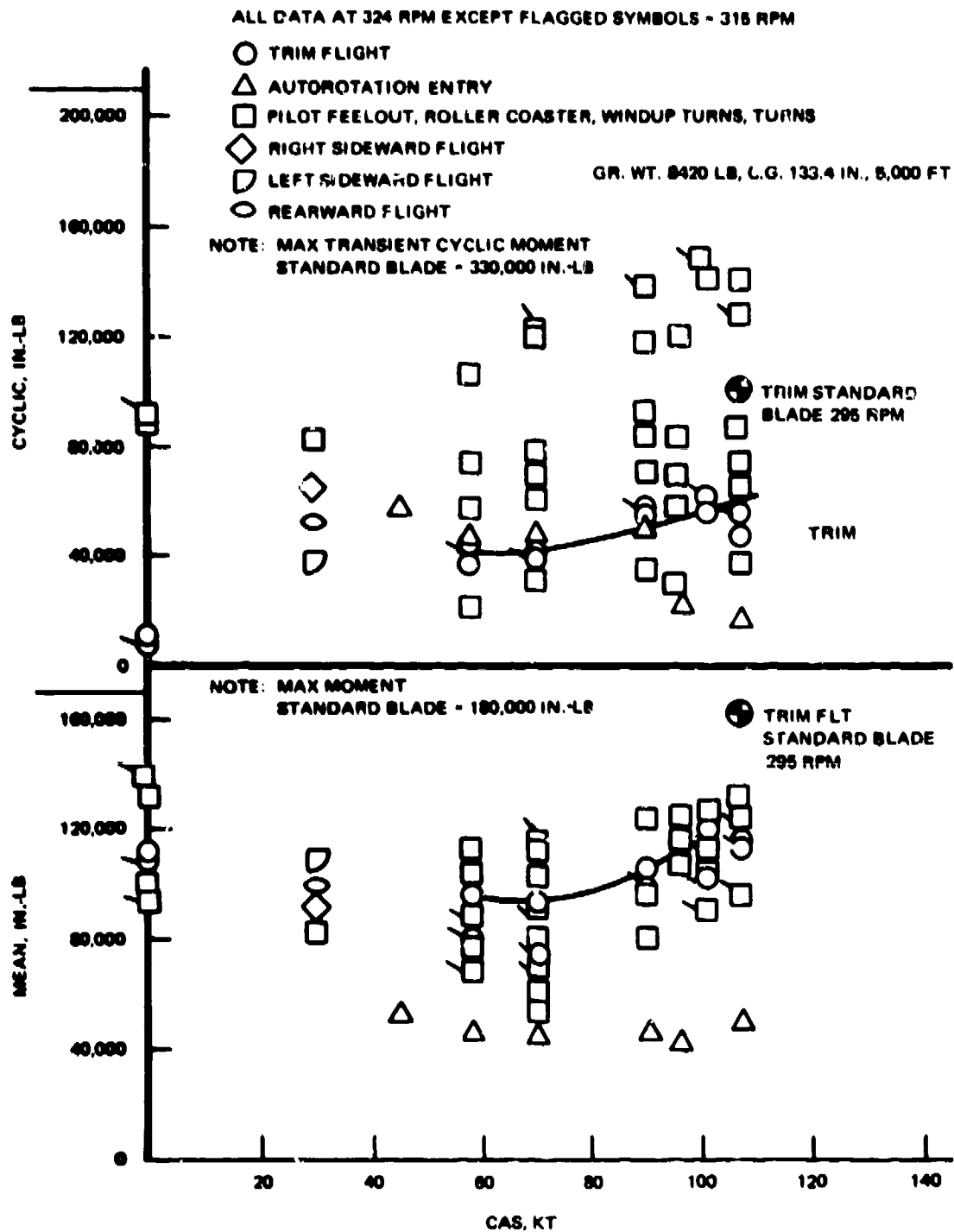
Figure 42. Main Rotor Inplane Bending Moment at Station 35 With Deicing Boot Installed - 5,000 Ft. Altitude.
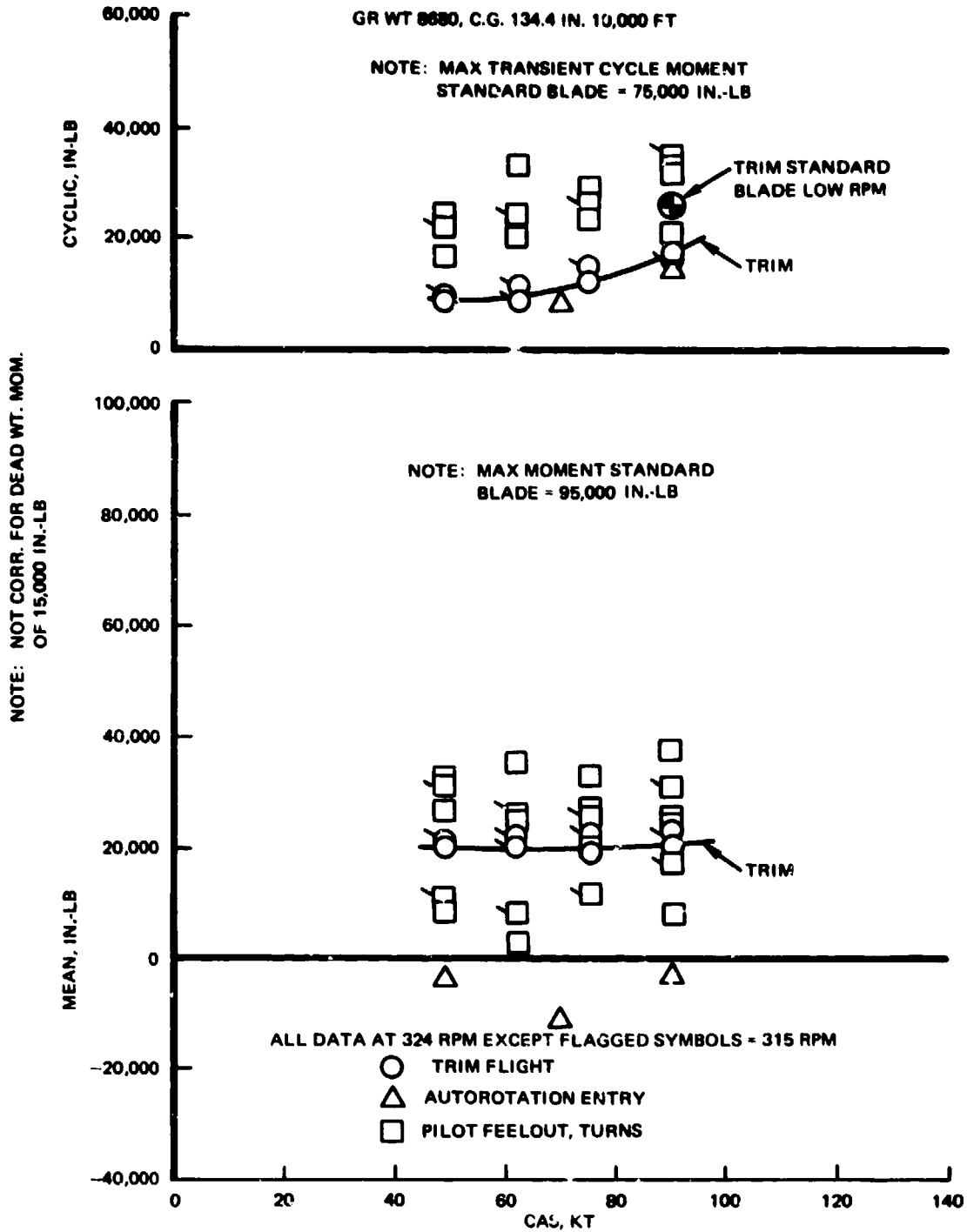
Figure 43. Main Rotor Flap Bending Moment at Station 35 With Deicing Boot Installed - 10,000 Ft. Altitude.
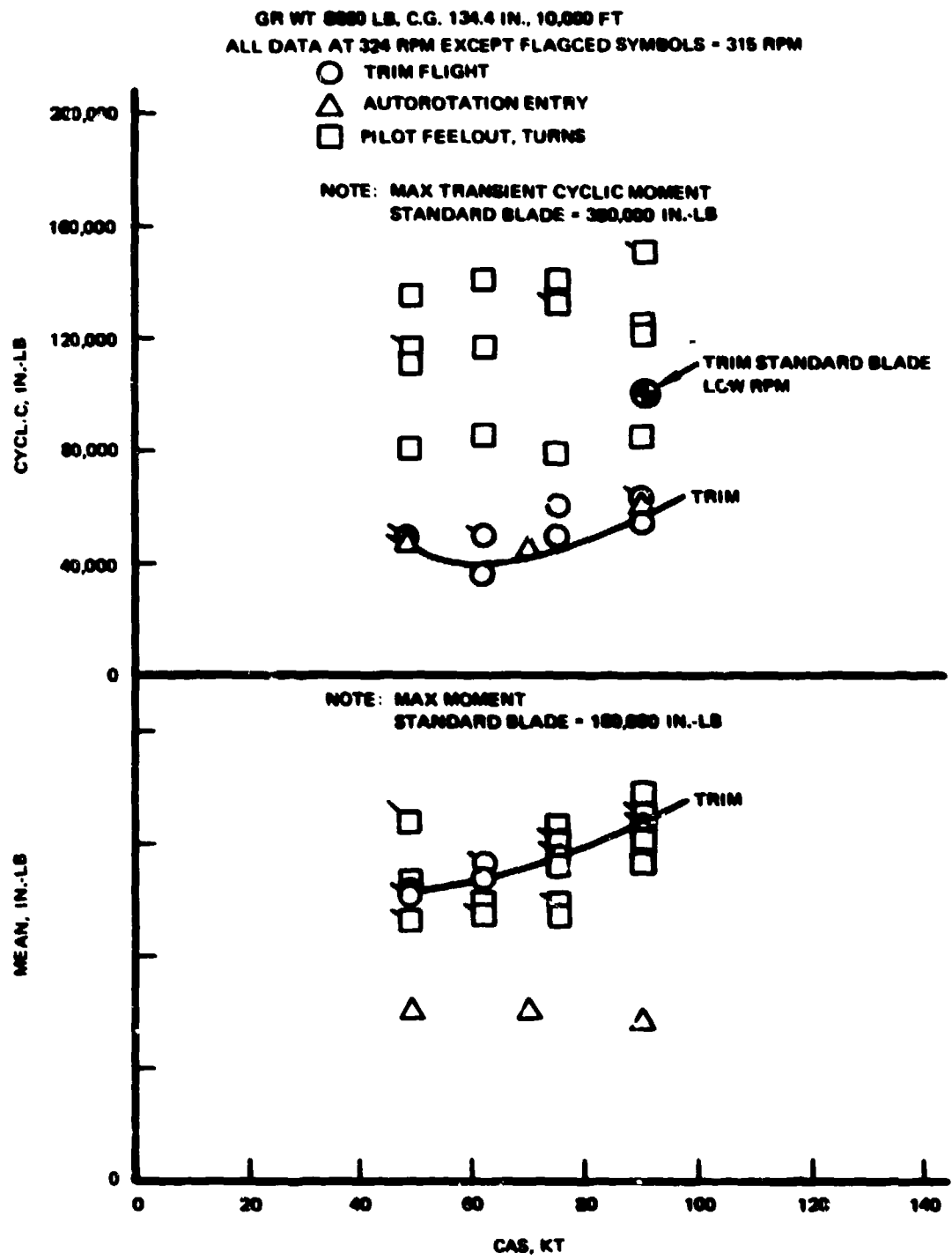
Figure 44. Main Rotor Inplane Bending Moment at Station 35 With Deicing Boot Installed - 10,000 Ft. Altitude.

108
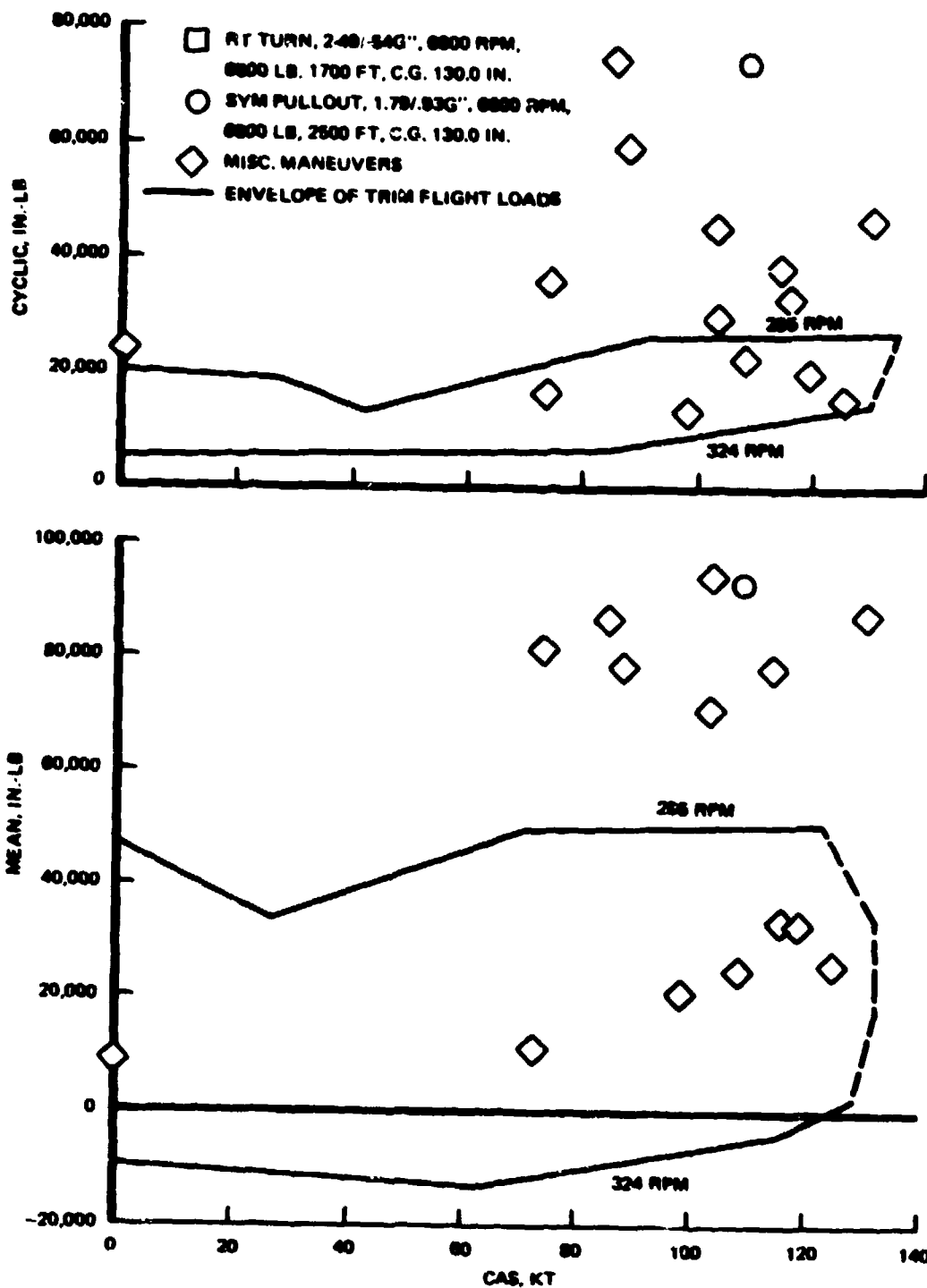
Figure 45. Main Rotor Flap Bending Moment at Station 35 With Standard Rotor.
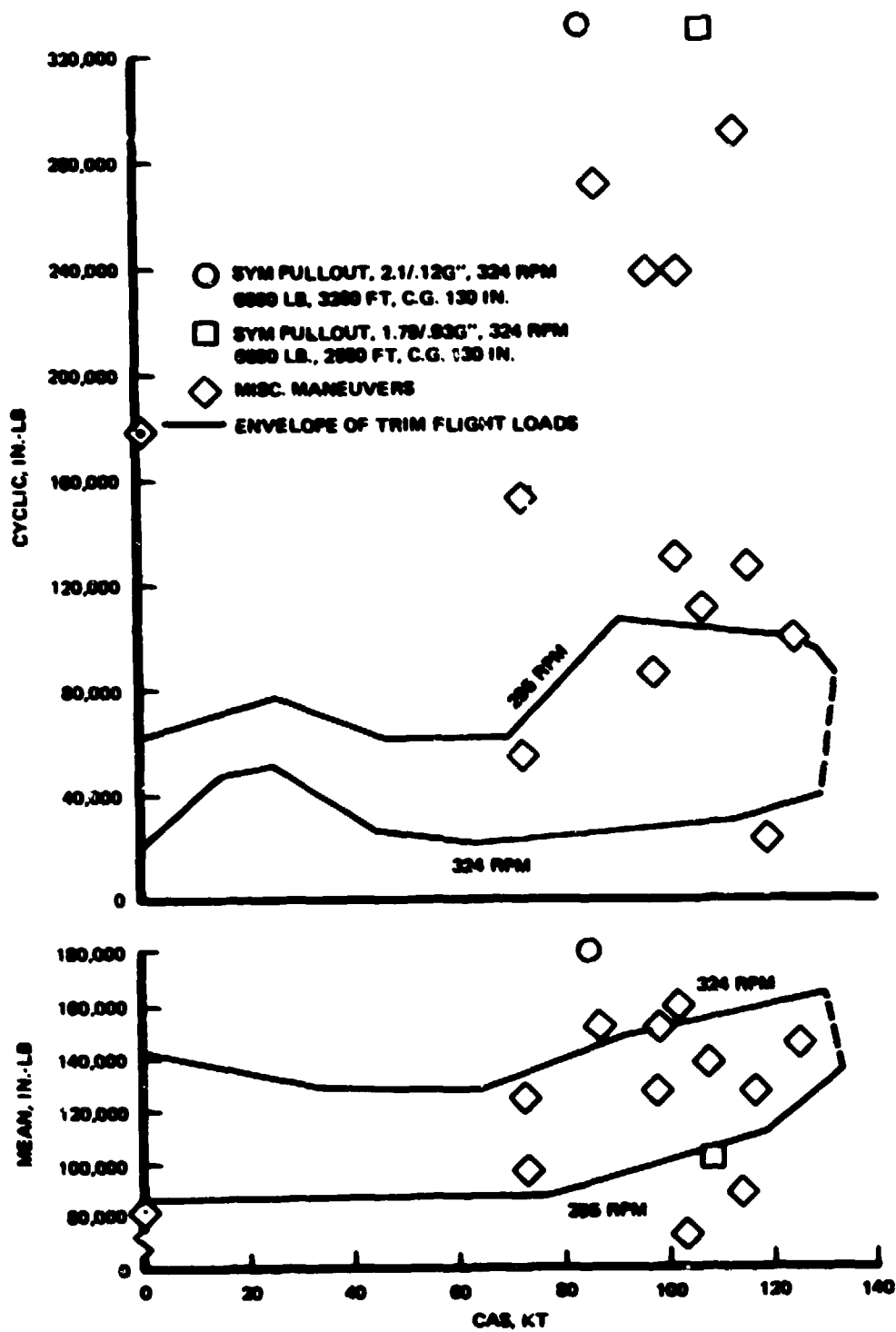
Figure 46. Main Rotor Inplane Bending Moment at Station 35 With Standard Rotor.

ALL DATA ARE 324 RPM EXCEPT FLAGGED SYMBOLS - 316 RPM

GR WT 8439 LB, C.G. 133.4 IN., 5,000 FT

O	TRIM FLIGHT
△	AUTO-ROTATION ENTRY
□	PILOT FEELOUT, ROLLERCOASTER, WINDUP TURNS, TURNS
◇	RIGHT SIDEWARD FLIGHT
▱	LEFT SIDEWARD FLIGHT
⬭	REARWARD FLIGHT

NOTE: MAX TRANSIENT CYCLE
BENDING MOMENT - 15,000 IN.-LB
STANDARD BLADE

TRIM FLT STANDARD
BLADE

CYCLIC, IN.-LB

40,000

20,000

0

TRIM

NOTE: NOT CORR FOR DEAD
WEIGHT MOMENT OF
3,000 IN.-LB

TRIM

MEAN, IN.-LB

20,000

0

-20,000

CAS, KT

0   20   40   60   80   100   120
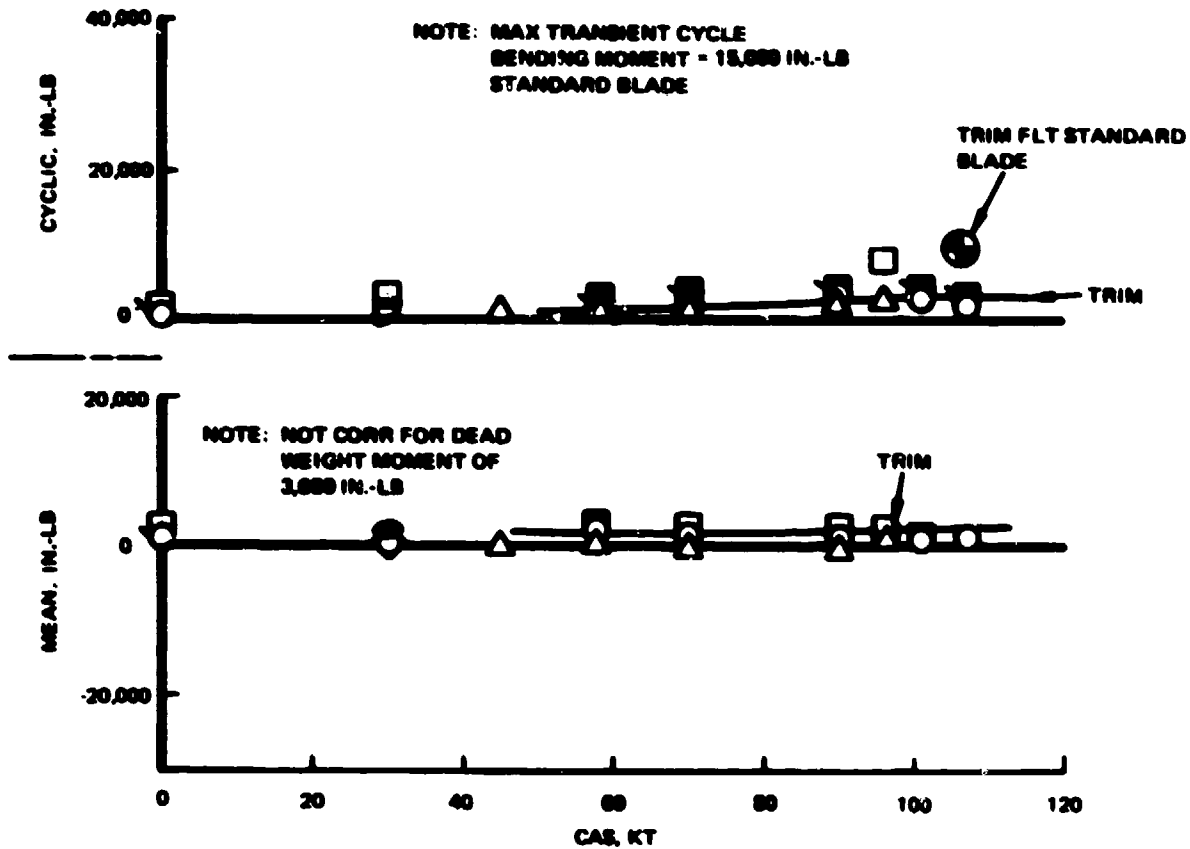
Figure 47. Main Rotor Flap Bending Moment at Station 150 With
Deicing Boot Installed - 5,000 Ft. Altitude.

111

Figure 48. Main Rotor Flap Bending Moment at Station 150 With Deicing Boot Installed - 10,000 Ft. Altitude.

ALL DATA ARE 324 RPM EXCEPT FLAGGED SYMBOLS - 315 RPM

O TRIM FLIGHT
△ AUTOROTATION ENTRY
□ PILOT FEELOUT, ROLLERCOASTER, WINDUP TURNS, TURNS
◇ RIGHT SIDEWARD FLIGHT
▽ LEFT SIDEWARD FLIGHT
⬭ REARWARD FLIGHT

NOTE: MAX TRANSIENT CYCLIC BENDING
MOMENT STANDARD BLADE - 198,000 IN.-LB

GR WT 8420 LB, C.G. 133.4 IN., 5,000 FT
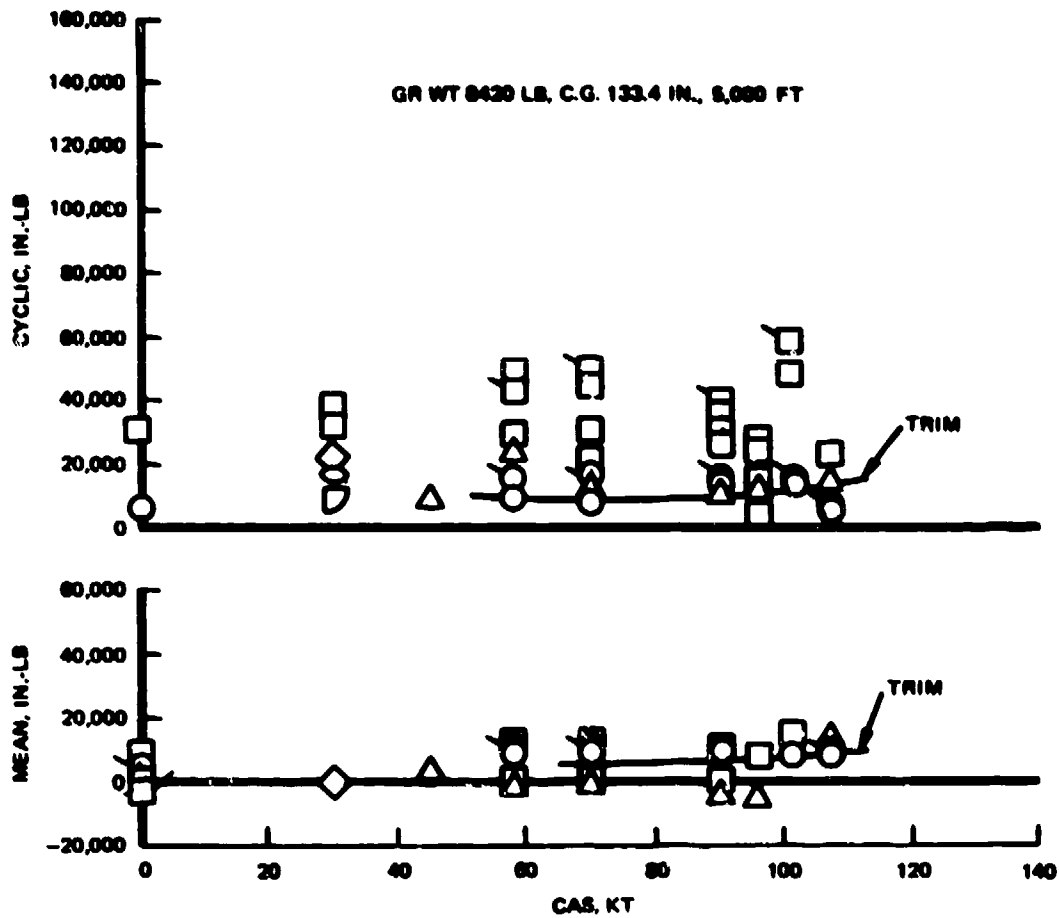
Figure 49. Main Rotor Inplane Bending Moment at Station 150
With Deicing Boot Installed - 5,000 Ft. Altitude.

113
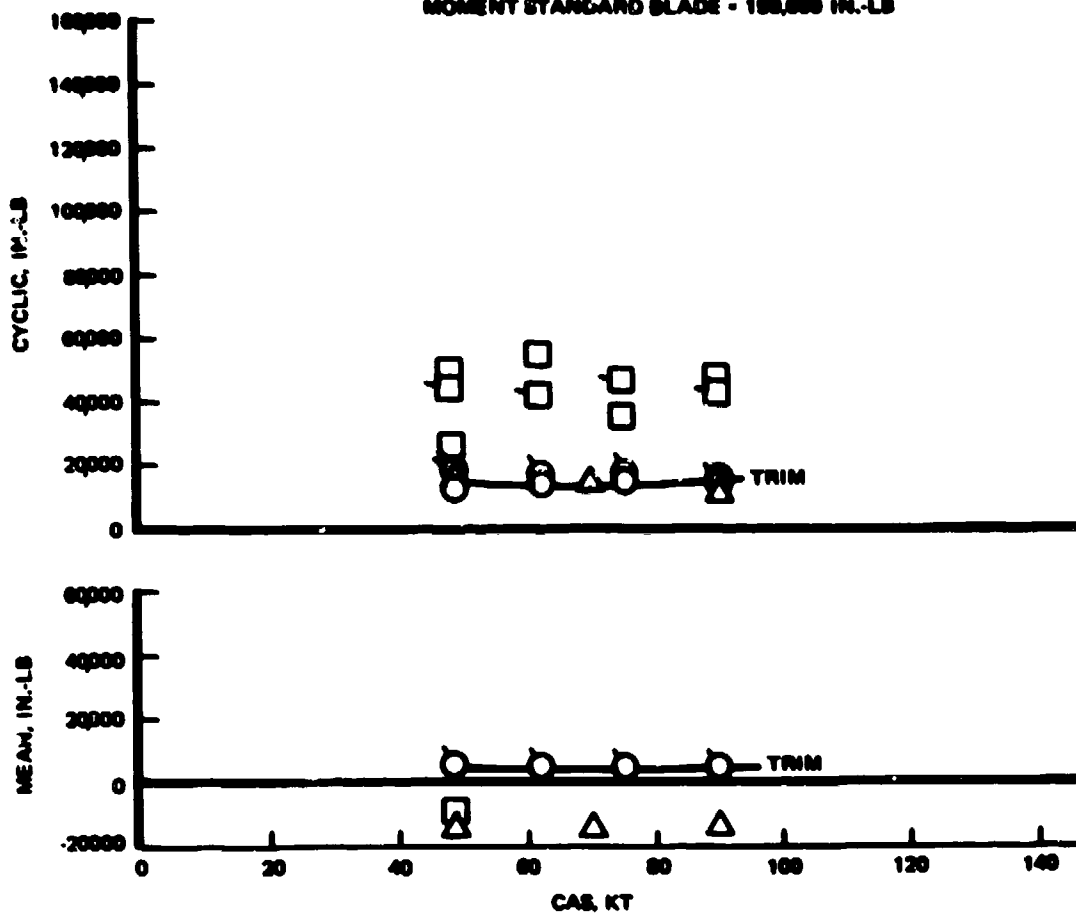
Figure 50. Main Rotor Inplane Bending Moment at Station 150 With
Deicing Boot Installed - 10,000 Ft. Altitude.

Figure 51. Main Rotor Flap Bending Moment at Station 150
With Standard Rotor.
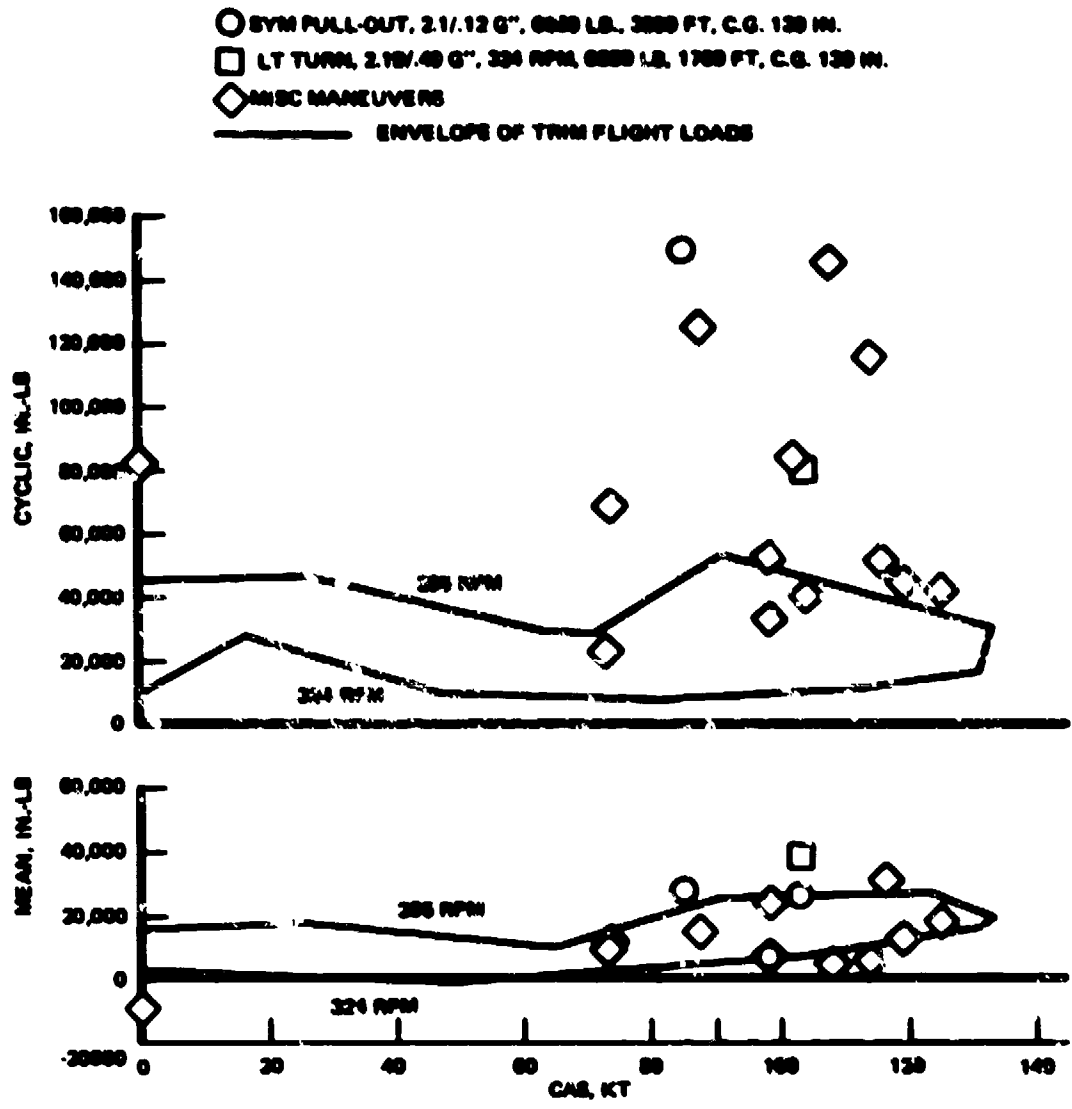
Figure 52. Main Rotor Inplane Bending Moment at Station 150 With Standard Rotor.

○ TRIM FLIGHT
△ AUTOROTATION ENTRY
□ PILOT FEELOUT, ROLLERCOASTER, WINDUP TURN, TURNS
◇ RIGHT SIDEWARD FLIGHT
▷ LEFT SIDEWARD FLIGHT
○ REARWARD FLIGHT

TRIM FLT STANDARD BLADE
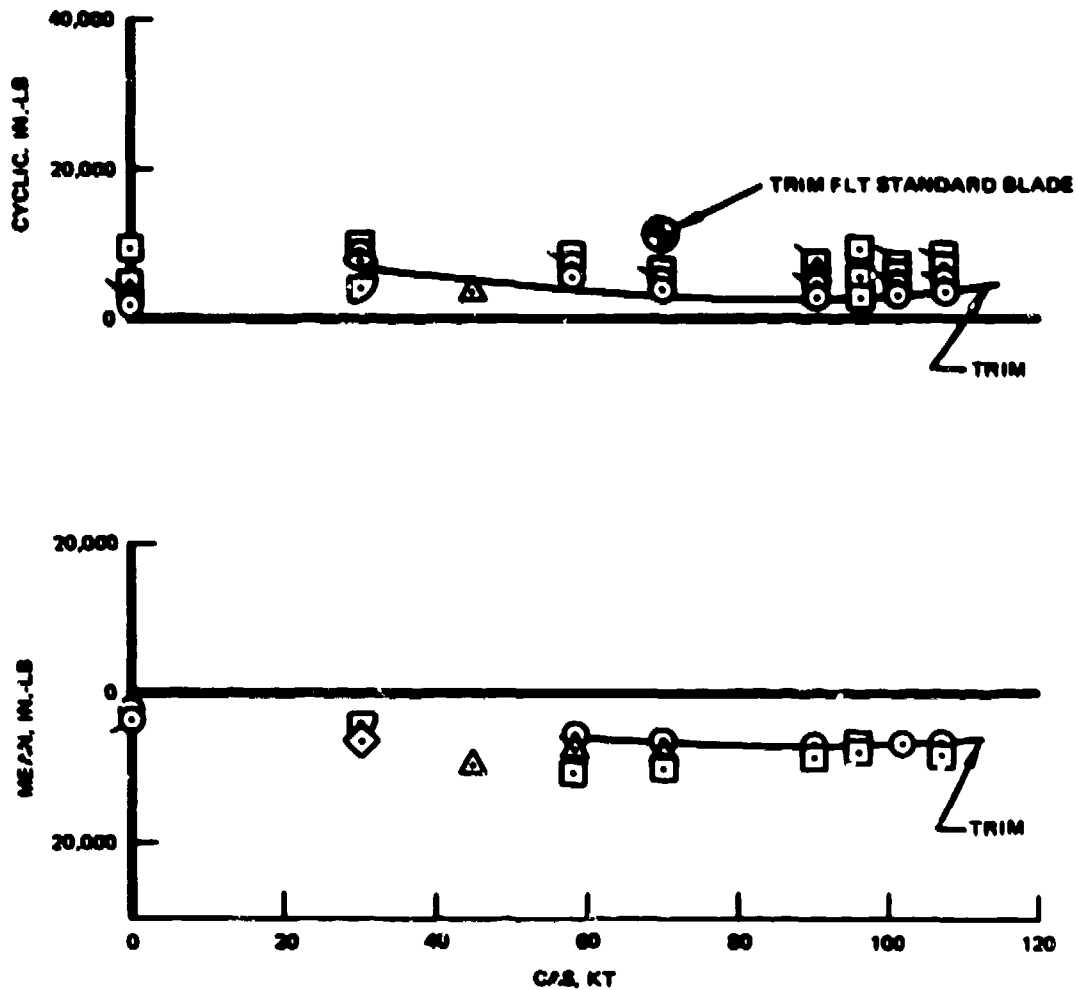
Figure 53. Main Rotor Flap Bending Moment at Station 234 With
Deicing Boot Installed - 5,000 Ft. Altitude.

117

GR. WT. 8888, C.G. 134.4 IN., 10,000 FT

ALL DATA ARE 324 RPM EXCEPT FLAGGED SYMBOLS - 315 RPM

○ TRIM FLIGHT
△ AUTOROTATION ENTRY
□ PILOT FEELOUT, TURNS
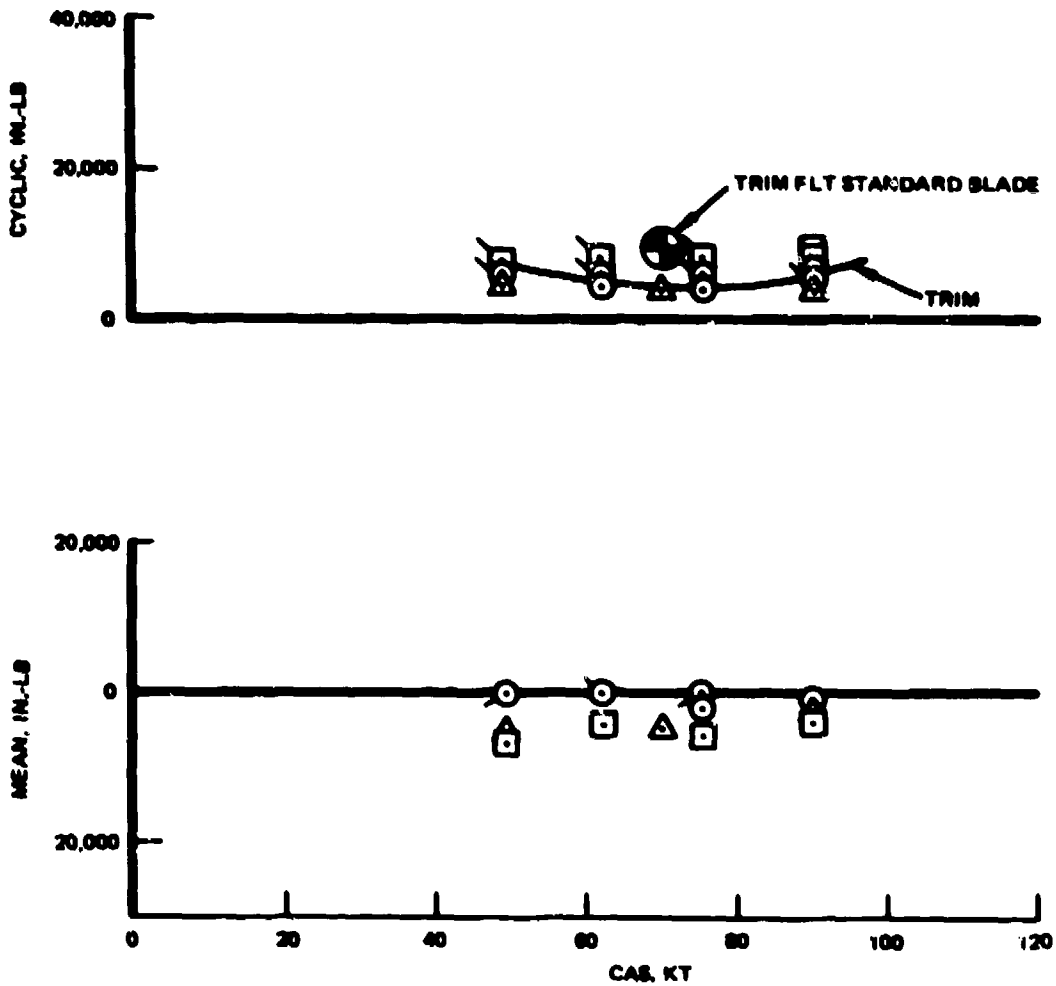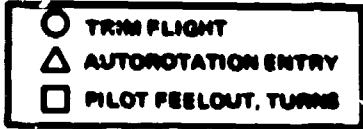
Figure 54. Main Rotor Flap Bending Moment at Station 234 With
Deicing Boot Installed - 10,000 Ft. Altitude.

118
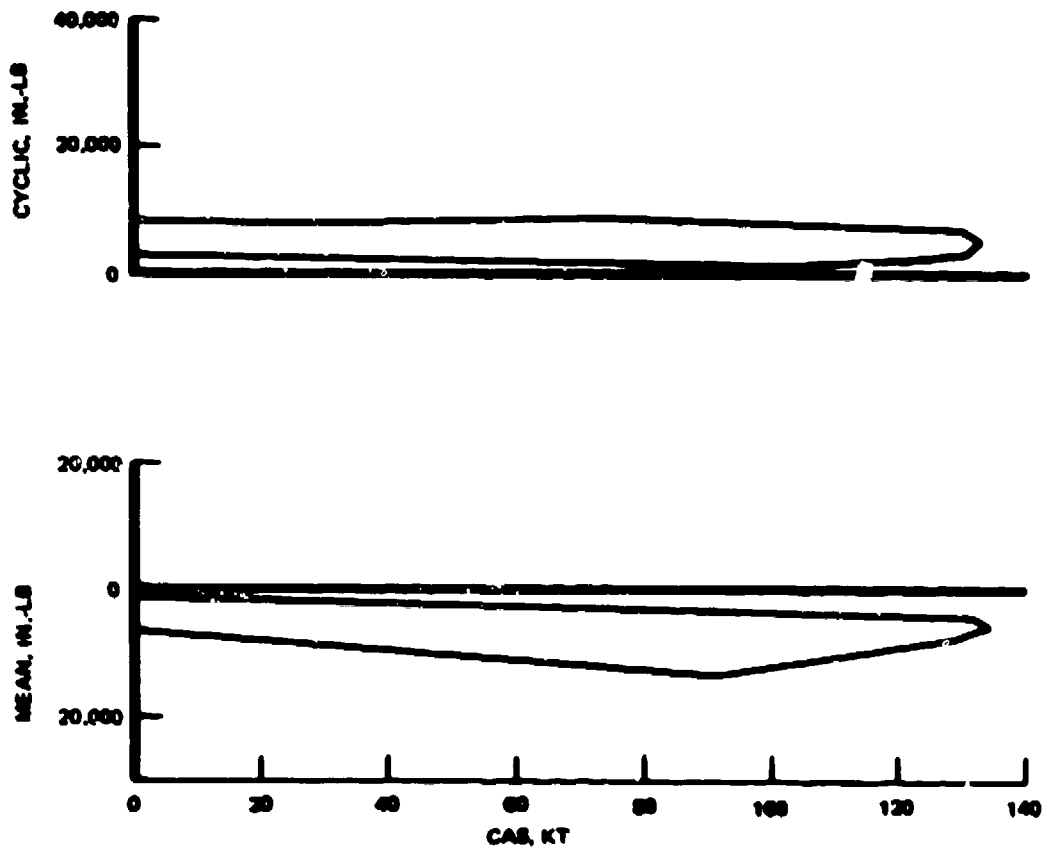
Figure 55. Main Rotor Flap Bending Moment at Station 234
With Standard Rotor.
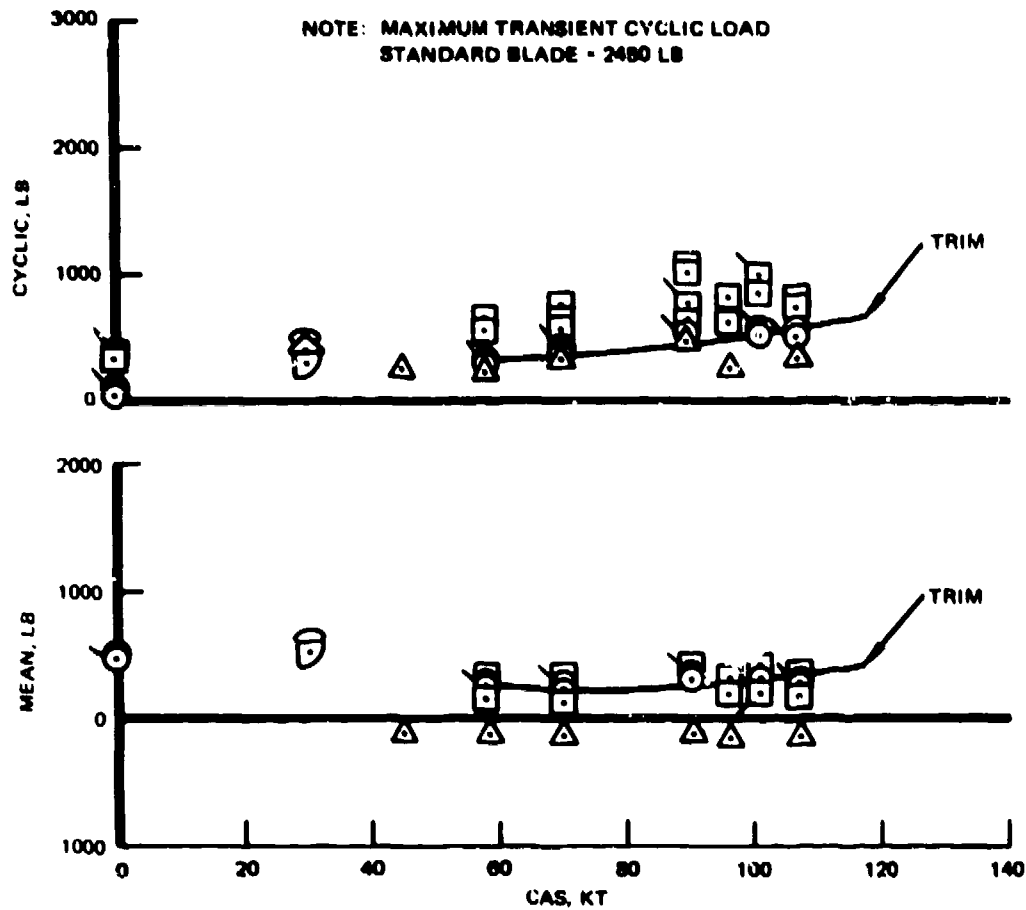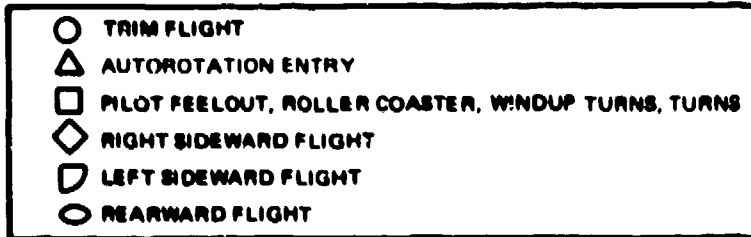
Figure 56. Main Rotor Pitch Link Axial Load With Deicing Boot
Installed - 5,000 Ft. Altitude.

GR WT 8680, C.G. 134.4 IN., 10,000 FT

ALL DATA ARE 324 RPM EXCEPT FLAGGED SYMBOLS = 315 RPM

O   LEVEL FLIGHT
△   AUTOROTATION ENTRY
□   PILOT FEELOUT, TURNS

NOTE: MAXIMUM TRANSIENT CYCLE LOAD
STANDARD BLADE = 2450 LB
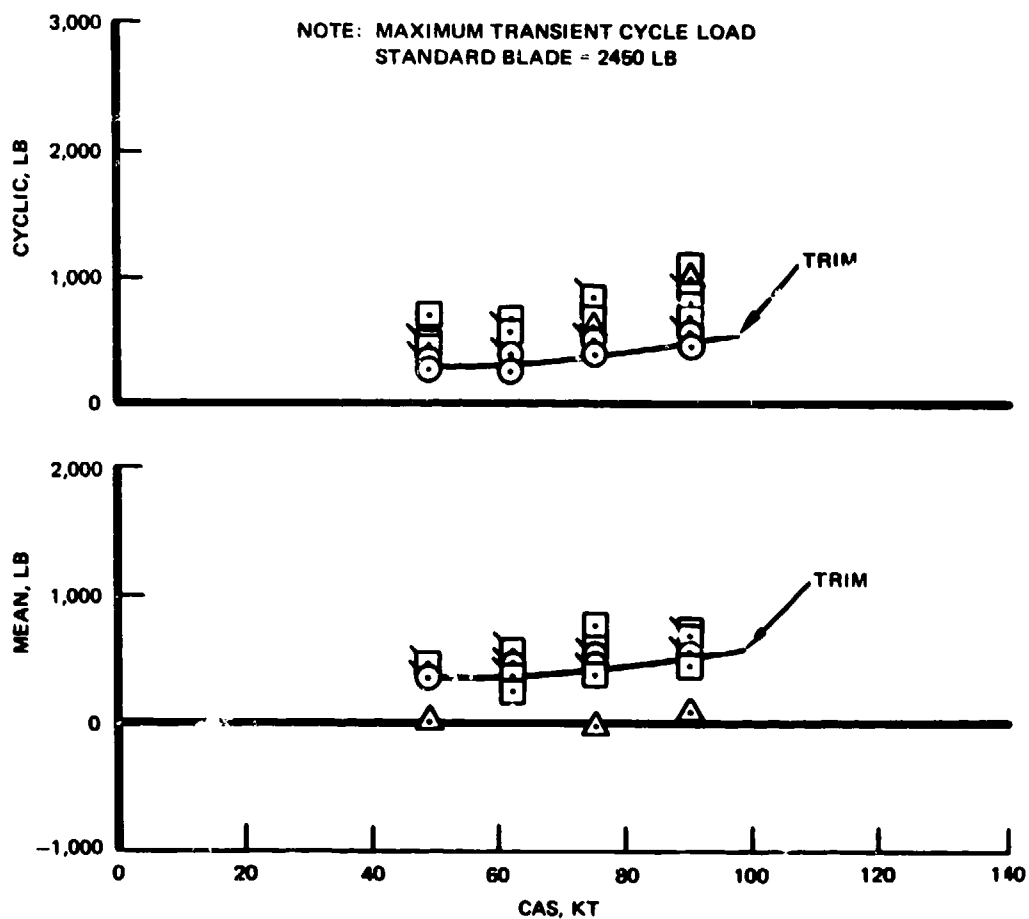
Figure 57.   Main Rotor Pitch Link Axial Load With Deicing Boot
Installed - 10,000 Ft. Altitude.

SYM PULL-OUT, 2.1/.12 G", 324 RPM, 8800 LB, 3200 FT, C.G. 130.0 IN.

SYM PULL-OUT DURING AUTOROTATION, 2.4/1.21 G", 8800 LB, 300 FT, C.G. 130.0 IN.

MISC. MANEUVERS
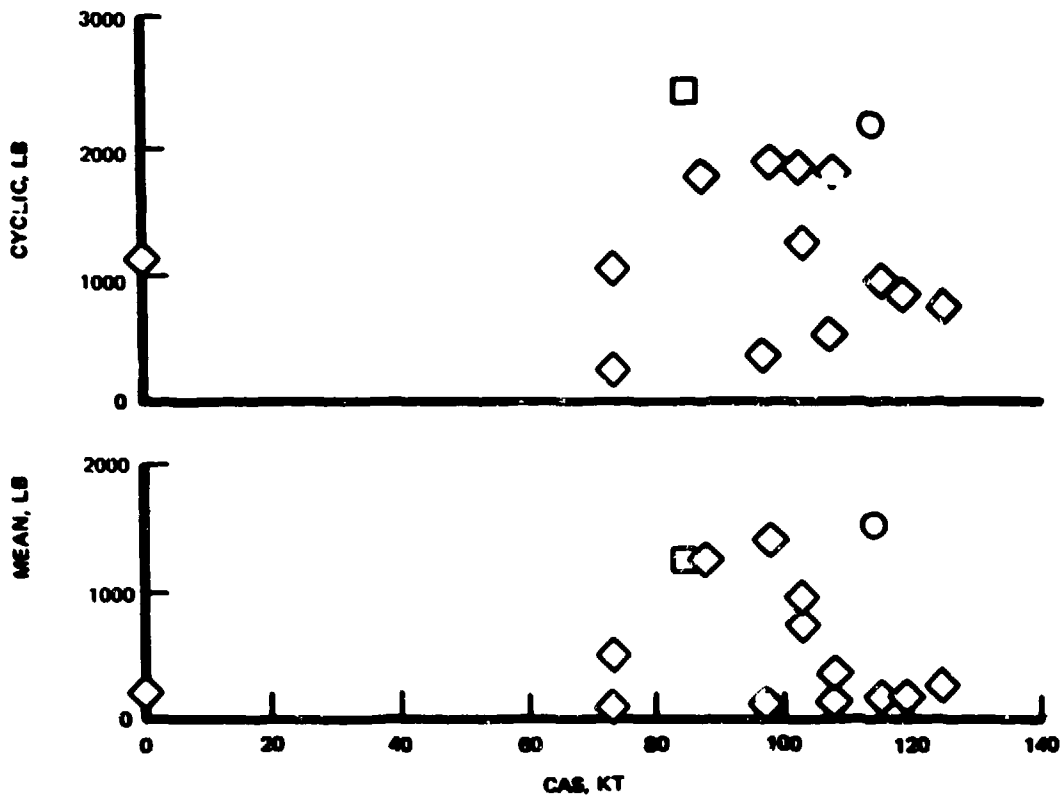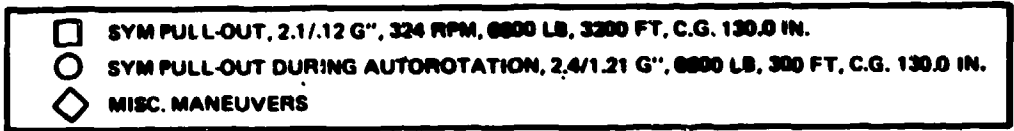
Figure 58. Main Rotor Pitch Link Axial Load With
Standard Rotor.
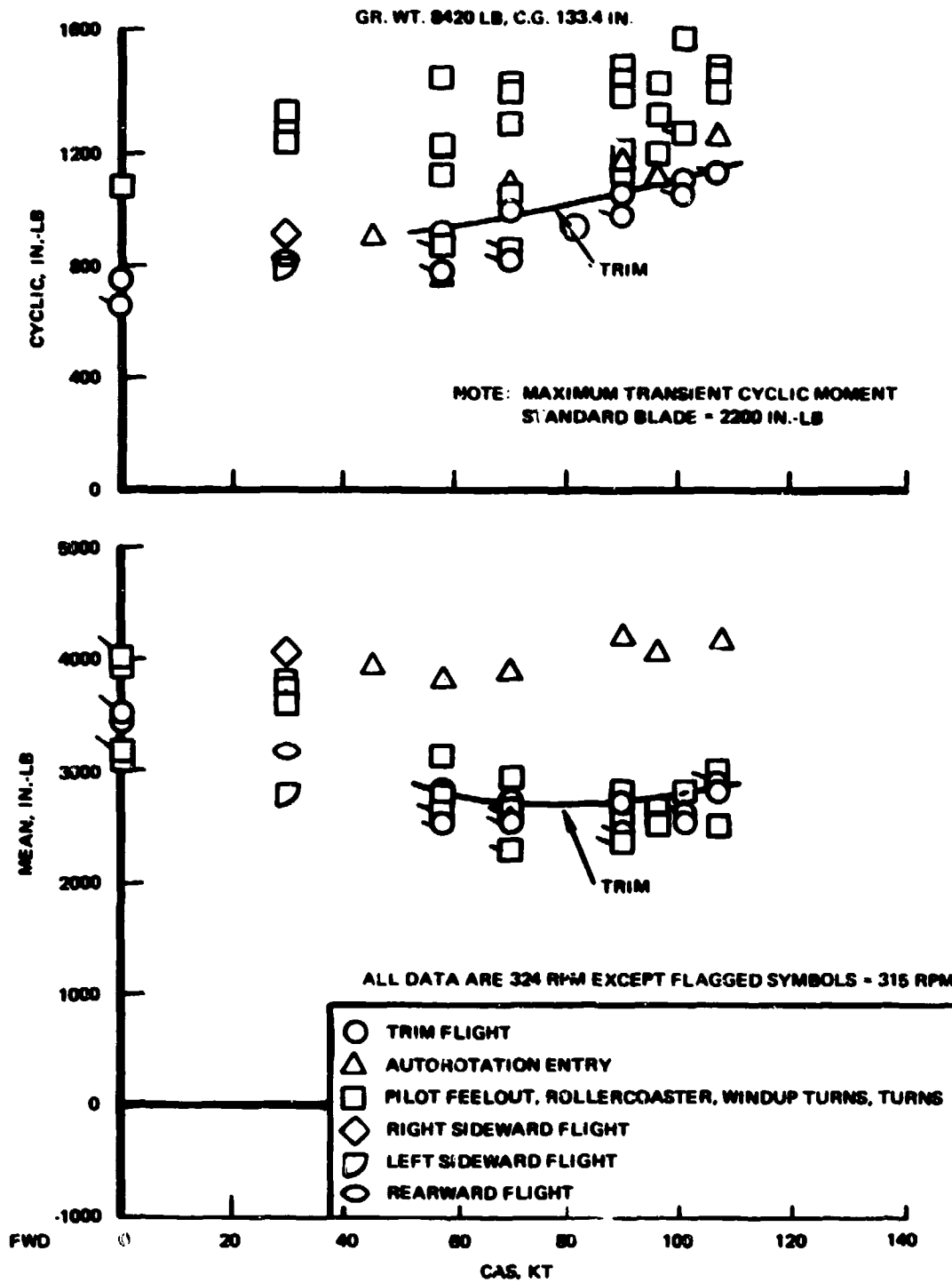
Figure 59. Tail Rotor Inplane Bending Moment at Station 11 With Deicing Boot Installed - 5,000 Ft. Altitude.

123
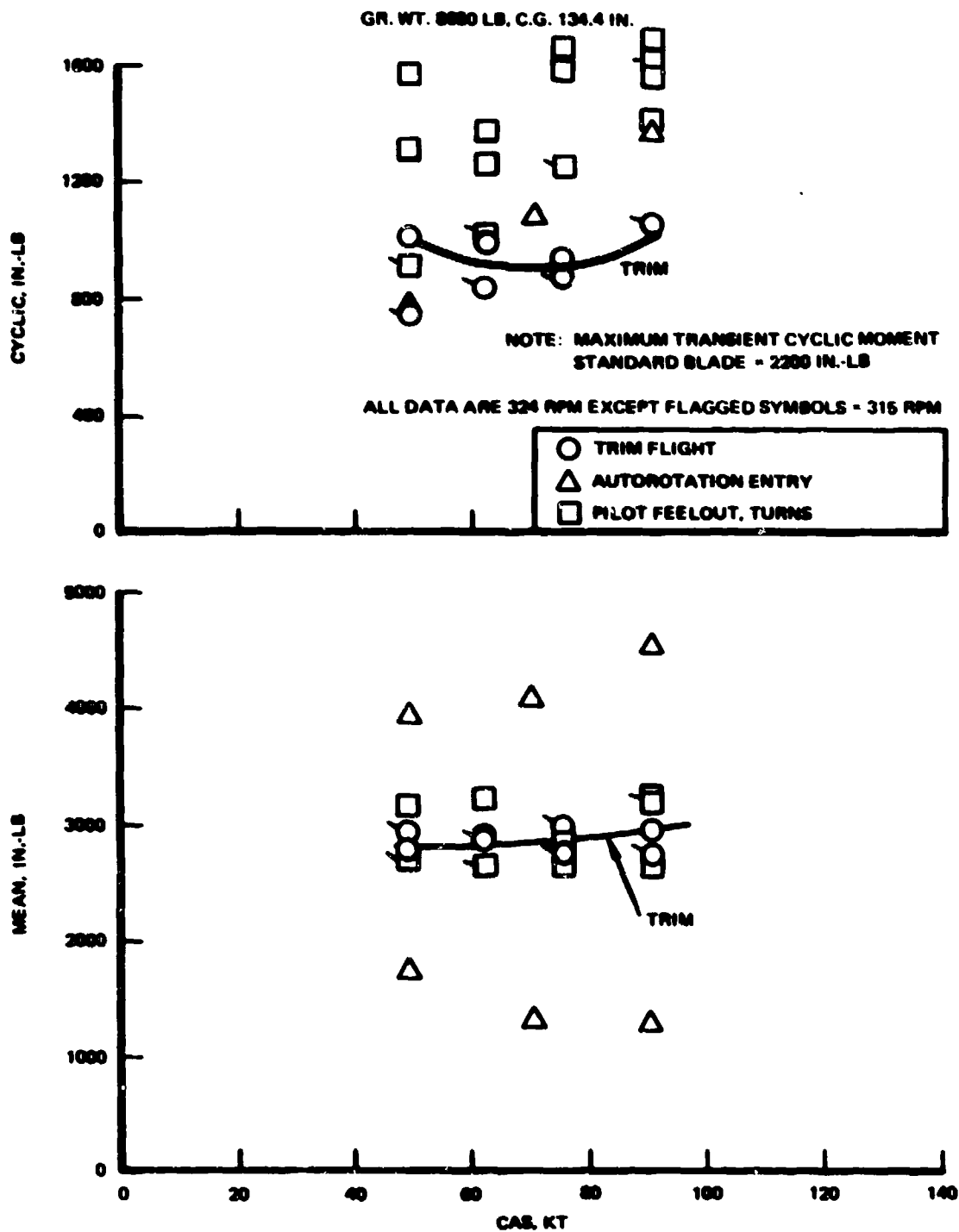
Figure 60. Tail Rotor Inplane Bending Moment at Station 11 With
Deicing Boot Installed - 10,000 Ft. Altitude.
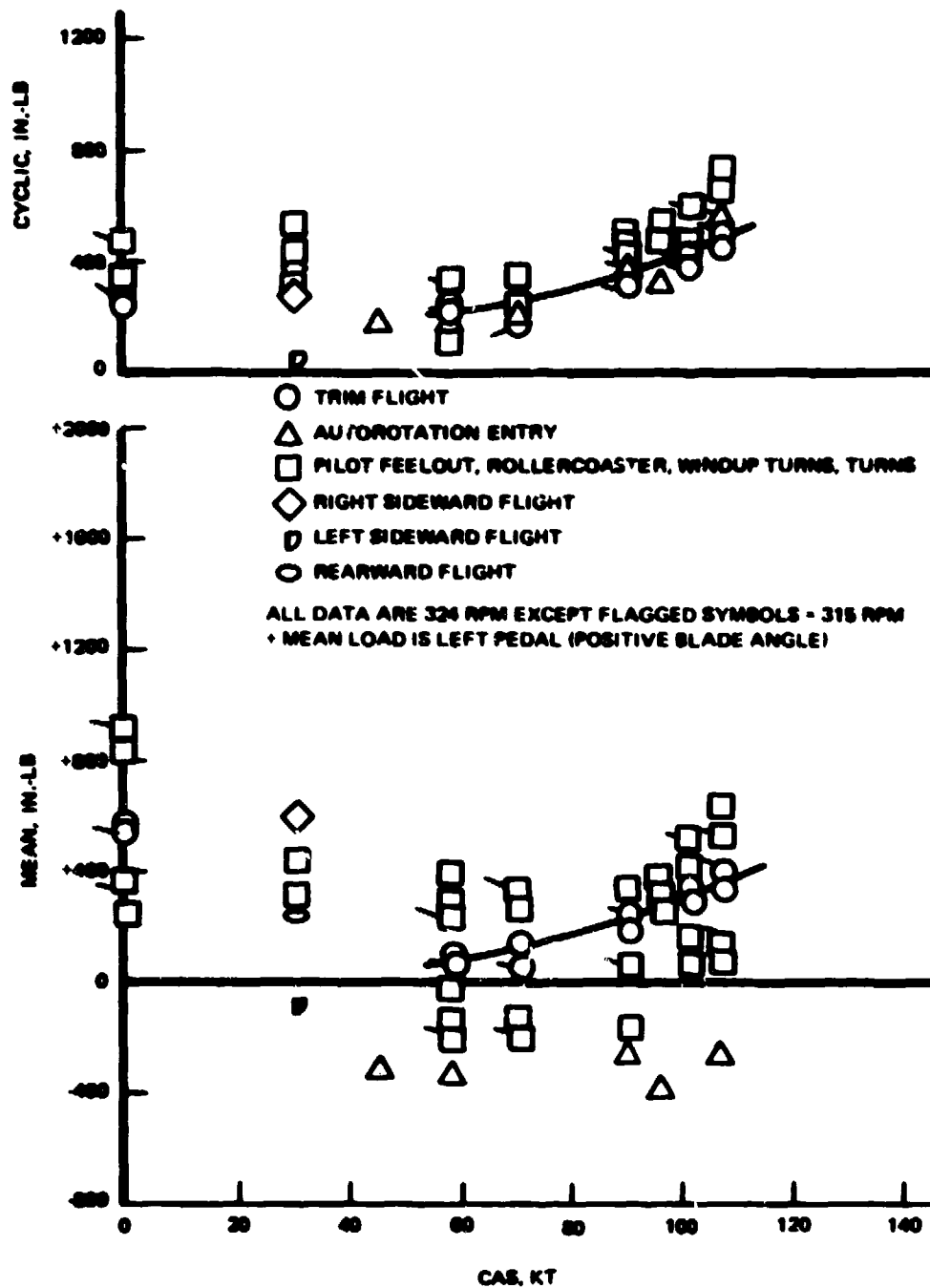
Figure 61. Tail Rotor Flap Bending Moment at Station 24 With Deicing Boot Installed - 5,000 Ft. Altitude.
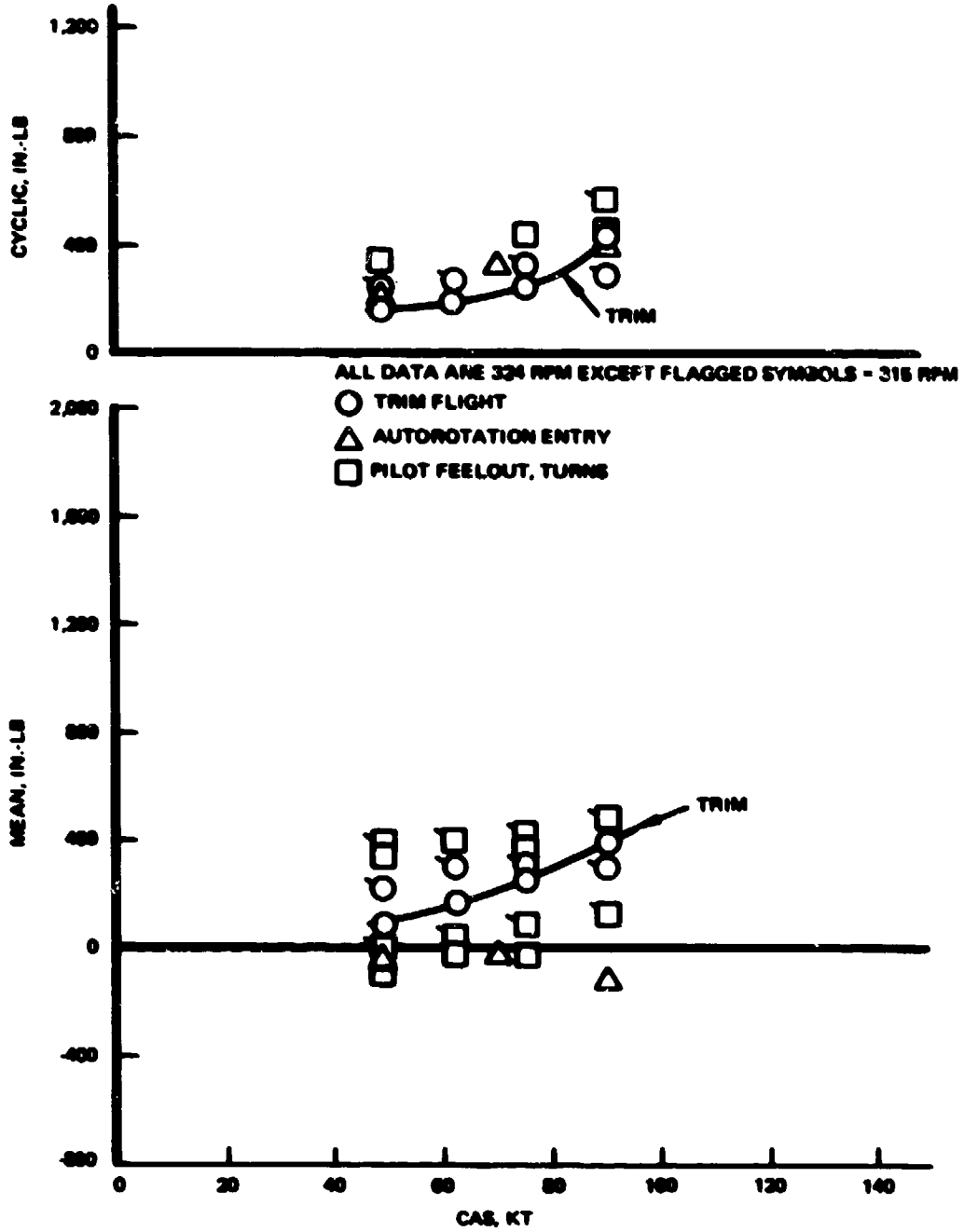
Figure 62. Tail Rotor Flap Bending Moment at Station 24 With
Deicing Boot Installed - 10,000 Ft. Altitude.
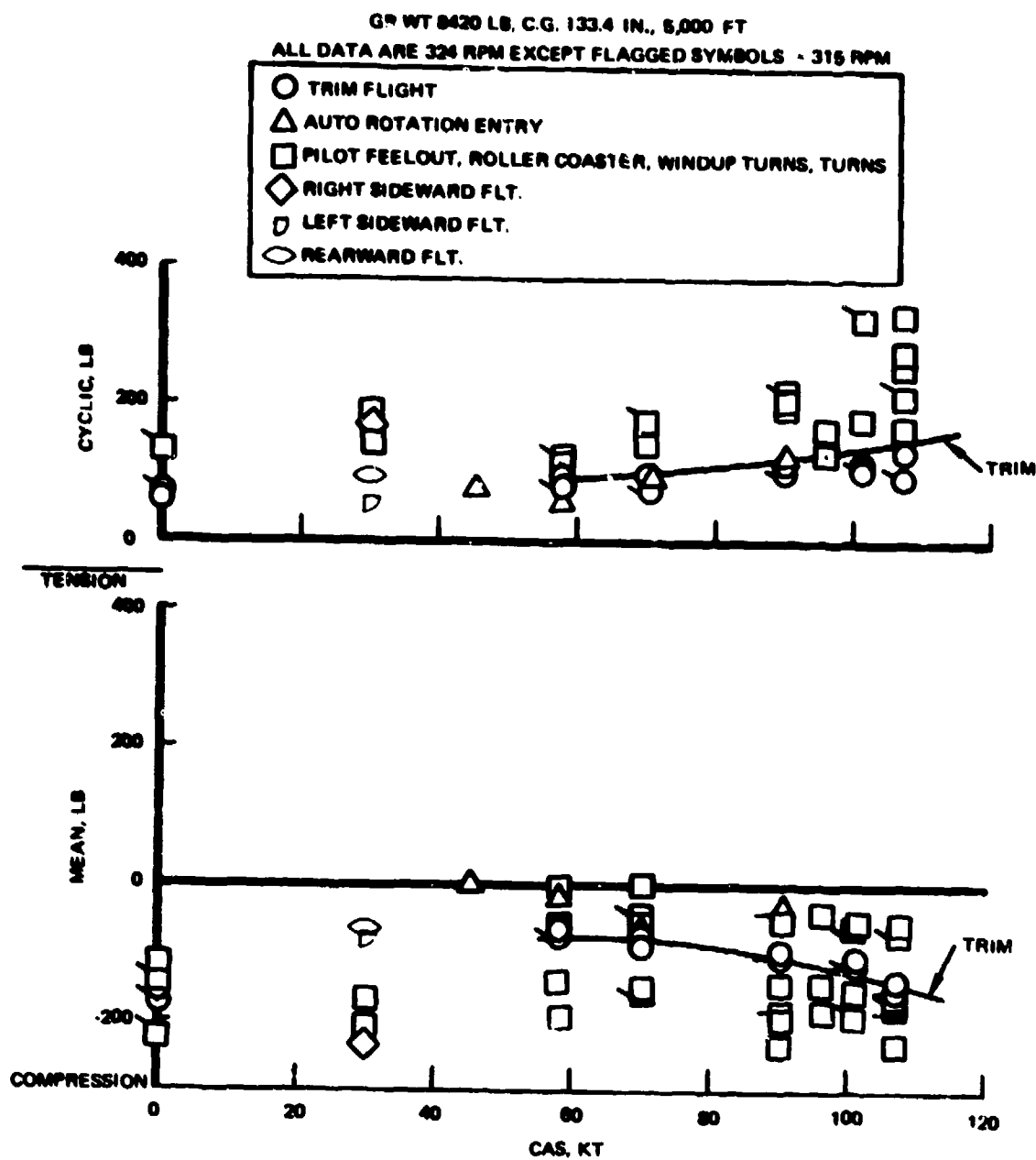
Figure 63. Tail Rotor Pitch Link Axial Load With Deicing
Boot Installed - 5,000 Ft. Altitude.

GR WT 8880 LB, C.G. 134.4 IN., 10,000 FT

ALL DATA ARE 324 RPM EXCEPT FLAGGED SYMBOLS - 315 RPM

○ TRIM FLIGHT
△ AUTOROTATION ENTRY
□ PILOT FEEL OUT. TURNS
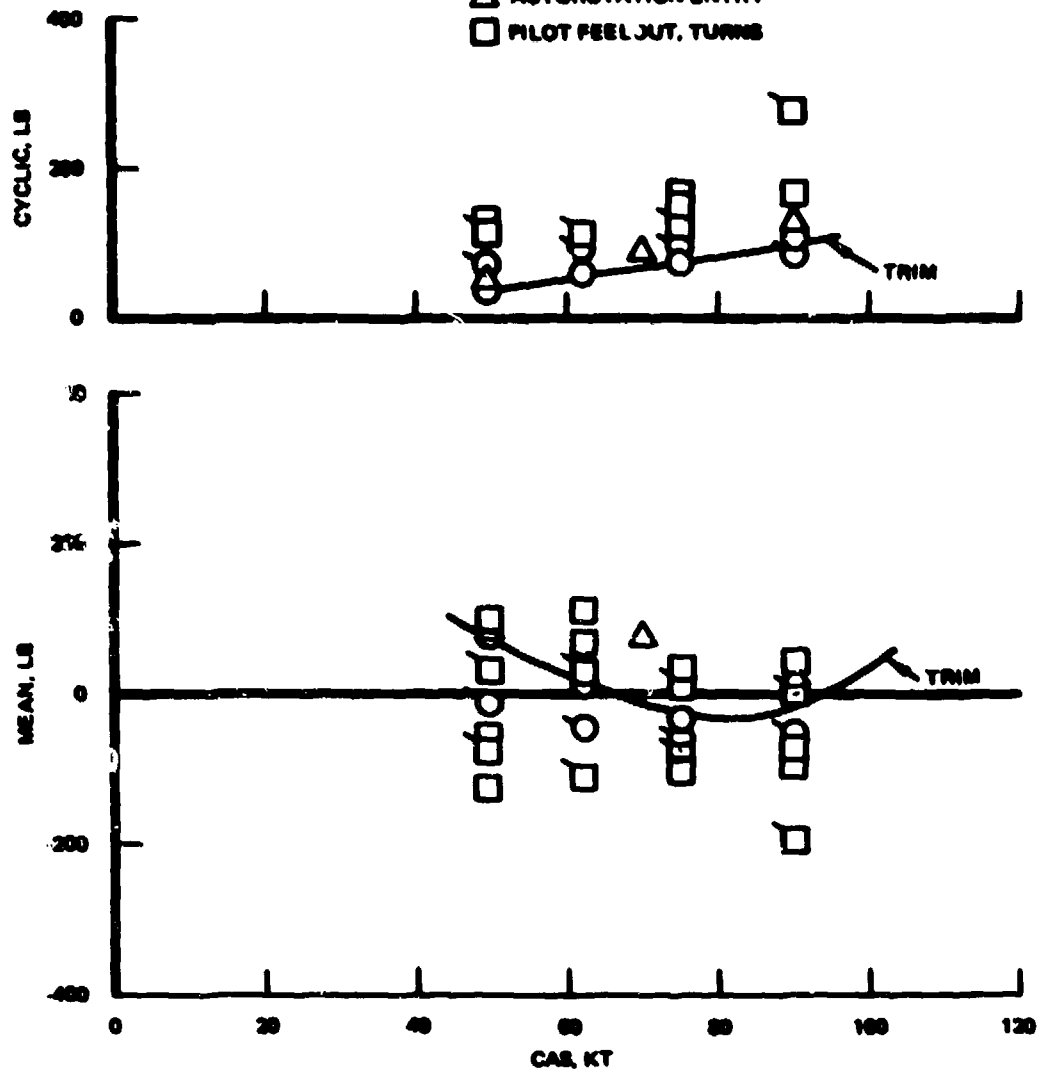
Figure 64. Tail Rotor Pitch Link Axial Load With Deicing Boot Installed - 10,000 Ft. Altitude.

Time histories of main rotor blade loads at 107 knots CAS are shown in Figure 65. The time histories show the harmonic content of the loads. A similar set of data for tail rotor pedal sweep inputs and level flight is shown in Figures 66 and 67.

Tail rotor dynamics were also evaluated during the airworthiness program. As indicated earlier, the predominant tail rotor chord moment response measured during the ground run was at or near the inplane natural frequency. Figure 68 is a comparison of time histories of measured chordwise bending moment response at three different airspeeds: hover, 50 KCAS, and 101 KCAS. It is seen that these data still exhibit some response at the inplane natural frequency of approximately 1.6P to 1.7P, but the response is predominantly 1P with some 2P. The source of the response at the 1.6 to 1.7P frequency has not been identified. However, there was no apparent change in its characteristic during the flight program at Edwards and at Moses Lake. The installation, therefore, is considered satisfactory.

The generator lateral and vertical vibration were also determined and found to be below the 5g limit for 0 to 40 Hz and the 10g limit for 40 Hz and above. The maximum vibration amplitude occurred at the rotational frequency of the generator (6600 rpm at normal rotor speed). The amplitude of response at this frequency was ± 1.5 g's. There were also bursts of vibration that occurred basically at one-half the rotational speed of the generator. These resulted in a maximum level of vibration response of the generator of ± 4 g's at infrequent intervals. The steady level of vibration due to both frequencies was of the order of ± 2 to ± 3 g's.

Lateral vibration on the top of the sliprings and on the hub below the sliprings was measured with the hub camera removed. The predominant vibratory response was at frequencies of either 1P (5.4 Hz), or 1P (5.4 Hz) and 7P (37.5 Hz) combined. The maximum 1P (5.4 Hz) vibratory response was encounted during transient pulse type maneuvers, and the maximum recorded vibration levels were 5.3 g's on the top of the sliprings,
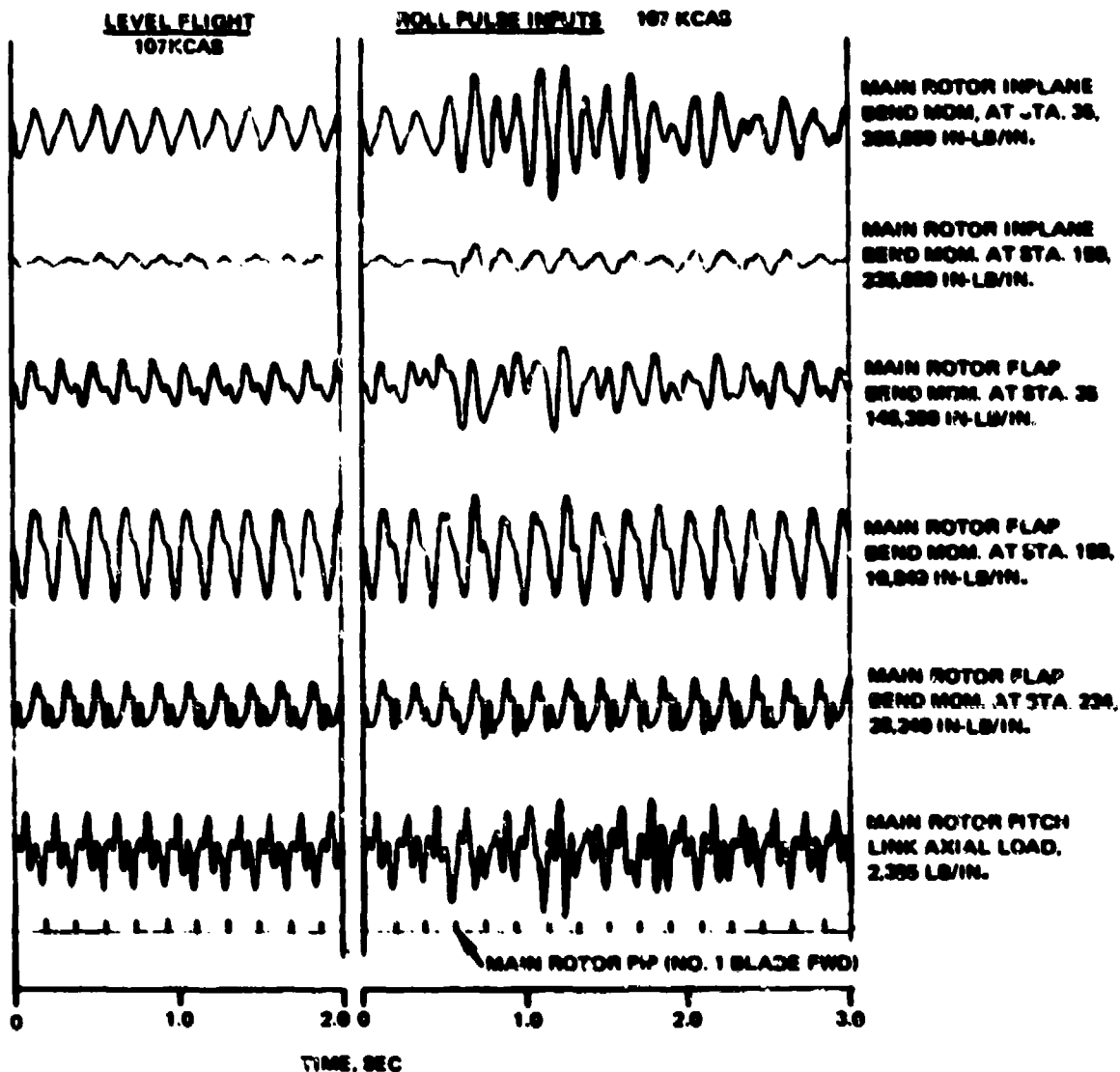
Figure 65. Tracing of Main Rotor Load During Level
Flight and Pulse Inputs.
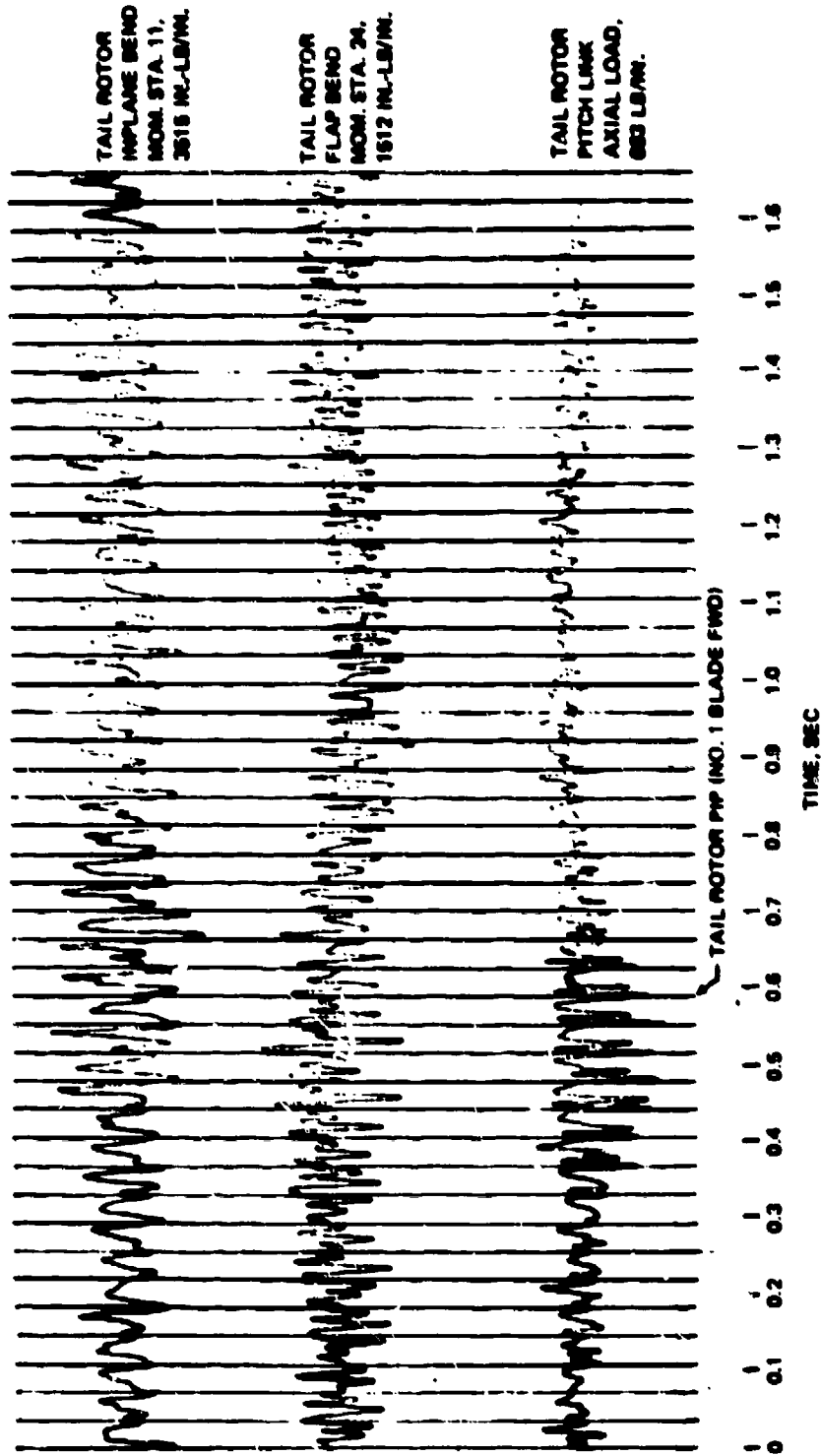
Figure 66. Tracing of Tail Rotor Loads With Deicing Boots Installed During Tail Rotor Pedal Inputs.

LEVEL FLIGHT 107 KCAS, 324 RPM, GR WT 8420 LB
C.G. 133.4 IN., TEST 14, FLIGHT 8, 1-19-76

TAIL ROTOR IN-PLANE BEND MOM STA. 11
3515 IN.-LB/IN.

TAIL ROTOR FLAP BEND MOM STA. 24
1512 IN.-LB/IN.

TAIL ROTOR PITCH LINK AXIAL LOAD
663 LB/IN.

T.R. PIP (NO. 1 BLADE FWD)

TIME, SEC

Figure 67. Tracing of Tail Rotor Loads With Deicing Boot
Installed During Level Flight.

132

HOVER

3615 IN.-LB/IN.
TEST 8 1-12-75

58 KCAS LEVEL FLIGHT

7030 IN.-LB/IN.
T14 1-19-75

101 KCAS LEVEL FLIGHT

7030 IN.-LB/IN.
T14 1-19-75

TAIL ROTOR PIP (NO. 1 BLADE FWD)

0   0.1   0.2   0.3   0.4   0.5   0.6   0.7   0.8   0.9   1.0

TIME, SEC
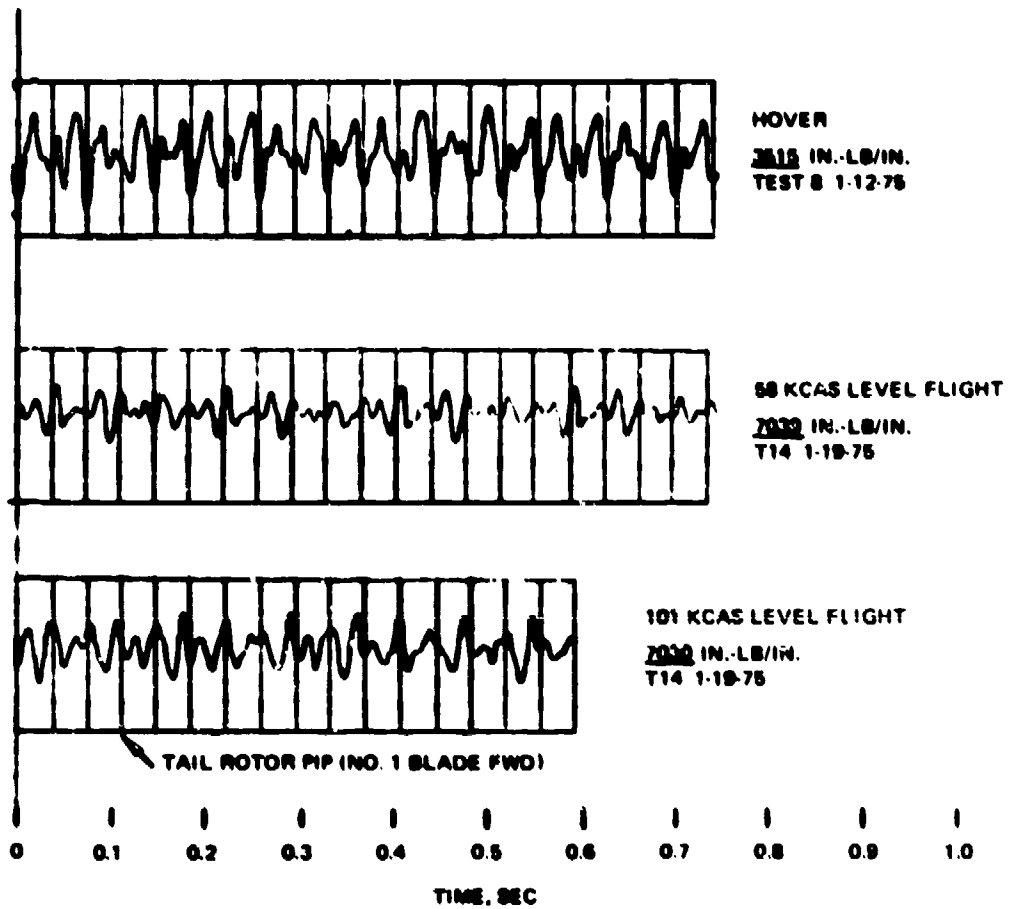
Figure 68.   Tail Rotor Inplane Bending Moment Dynamic
             Response With Deicing Boots Installed.

133

and 4.92 g's on the hub below the sliprings. The maximum combined 1P
(5.4 Hz) and 7P (37.5 Hz) vibratory response was encounted in normal
flight in the transition region. For this condition, the vibration
levels encountered on the top of the sliprings were 1.33 g's at
1P (5.4 Hz) and .05 g's at 7P (37.5 Hz) with the resultant combination
of the 1P and 7P of 3.90 g's. For this condition the maximum levels
on the hub below the sliprings were 1.03 g's at 1P (5.4 Hz) and 0.59 g's
at 7P (37.5 Hz). The vibration levels measured were less than the
established 6g limit.

In summary, the airworthiness load and vibration measurements demon-
strated that the structural and dynamic configuration of the modified
aircraft is satisfactory.

4.2.2 Pilot Comments

The Lockheed flight test pilot felt that overall general handling qua-
ities, vibration characteristics and general capabilities of the UH-1H
aircraft have not been noticeably affected by the installation of the
modified rotor blades. If anything, they are slightly improved in
that the vibration level during high-speed and maneuvering flight seems
to be reduced and does not increase with g loads as much as a basic
UH-1H. With the reduced boost-off forces, the pilot states that he
would not hesitate to attempt an autorotation landing if faced with a
double failure situation. The modified electrical system procedures do
not present any problem in operation. The following paragraphs present
the pilot's comments relative to the various flying qualities.

Handling Qualities

The overall handling qualities in all flight maneuvers, loadings and
c.g.'s tested are equal to those of a good flying UH-1H with the stan-
dard main rotor and tail rotor systems. The aircraft had ample control
margins in all flight maneuvers tested.

Vibration Characteristics

The vibration levels in all flight maneuvers, loadings, and c.g.'s tested are equal to those of a good flying UH-1H with the standard main rotor and tail rotor systems.

The increase in the vibration levels with an increase in "g" loads appears to be a little slower to build and not as severe with the modified rotor systems.

Boost-off Operation

Collective forces are much less with the modified rotor blades than with the standard blades. There were no problems in moving the collective control from flight position to 0 psi torque and up to 48 psi torque. Cyclic forces appear to be less and the feedback loads reduced, which gives a smoother movement of the cyclic control. Tail rotor forces appear to be a little higher, but no problem was experienced in obtaining full travel in both directions. Although the tail rotor forces are a little higher, the aircraft is much easier to fly than the standard UH-1H with boost-off and can be handled without requiring any assistance from a copilot (as a result of the reduced force requirements on the collective and cyclic controls).

Autorotation

Power chops were accomplished with all loadings and c.g.'s tested (from 45K to 111K) at 5000 feet and from OK to 90K at 10,000 feet with no problems in control of the aircraft or rotor decay.

By count, a 1- to 2-second delay was used before taking corrective action on the controls, and a moderate rate of movement was used to move the collective to the down stop. The rate of build in rotor rpm was good without having to load the rotor to increase the rate of build in

135

rotor rpm. At high gross weight, a small amount of up-collective has to be used to control the main rotor rpm in autorotation descents; this also appears to be a normal condition in the standard UH-1H.

Collective System Dither

On the ground and with the collective control on the downstop, the collective boost cylinder dithers and feeds a control input into the main rotor, causing what feels to be a moderate 2-cps vibration. The vibration will stop with a small amount of collective up off of the downstop. The vibration will stop when the hydraulic boost is turned off, and it will start up again when the boost is turned on if the collective has not been moved from the position that causes the dither to start. This condition was not encountered in flight with the collective on the downstop or with attempts to trigger it with small abrupt collective inputs.

4.2.3 Engine Inlet Screen Blockage

Also obtained during airworthiness testing was the effect on engine plenum pressure of a partial blockage of the engine inlet screen since it is expected that some ice would form on the screen based on past experience with the aircraft in icing. A baseline was obtained as a function of collective position for the unblocked UH-1H side air inlets. Then 50 percent of the side inlets were covered with heavy canvas on a diagonal from the upper aft corner to the lower forward corner (see Figure 69). The results of these tests, which are presented in Figure 70 and include the effect of inlet blockage on engine operation, show an increase in inlet screen differential pressure of 2.1 to 2.7 in. of H_2O.

In level flight, the unblocked engine inlet screen ΔP measured 6 - 7 in. of H_2O, and 8 in. of H_2O with climb power. A delta increase in engine inlet screen differential pressure from these values of 2 in. of H_2O would be an indication that an engine air inlet screen blockage equivalent to 50% of the side screen area was being experienced. It is
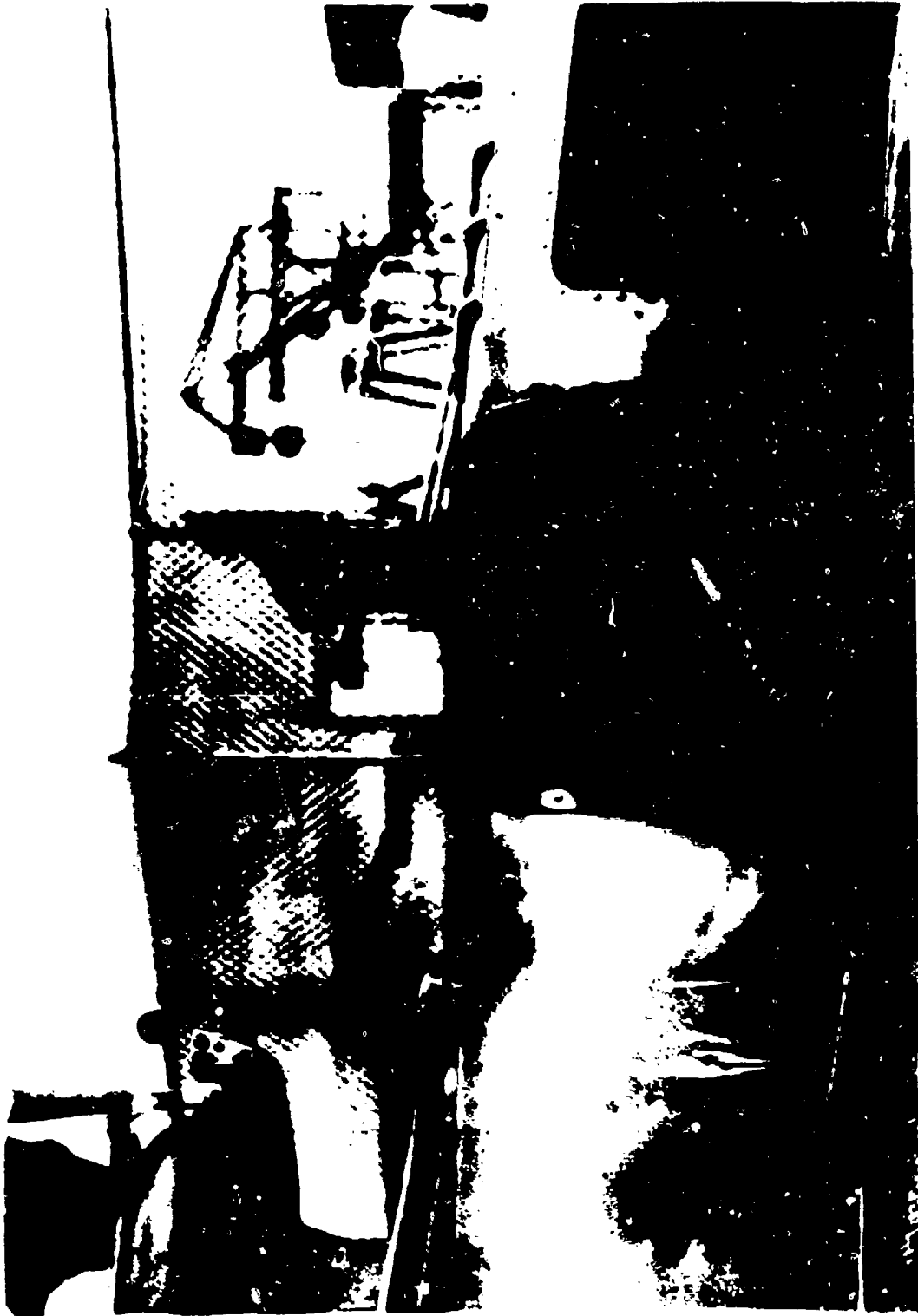
Figure 69. Closeup of Engine Air Intake Side Screens, Showing Partially Blocked Area.
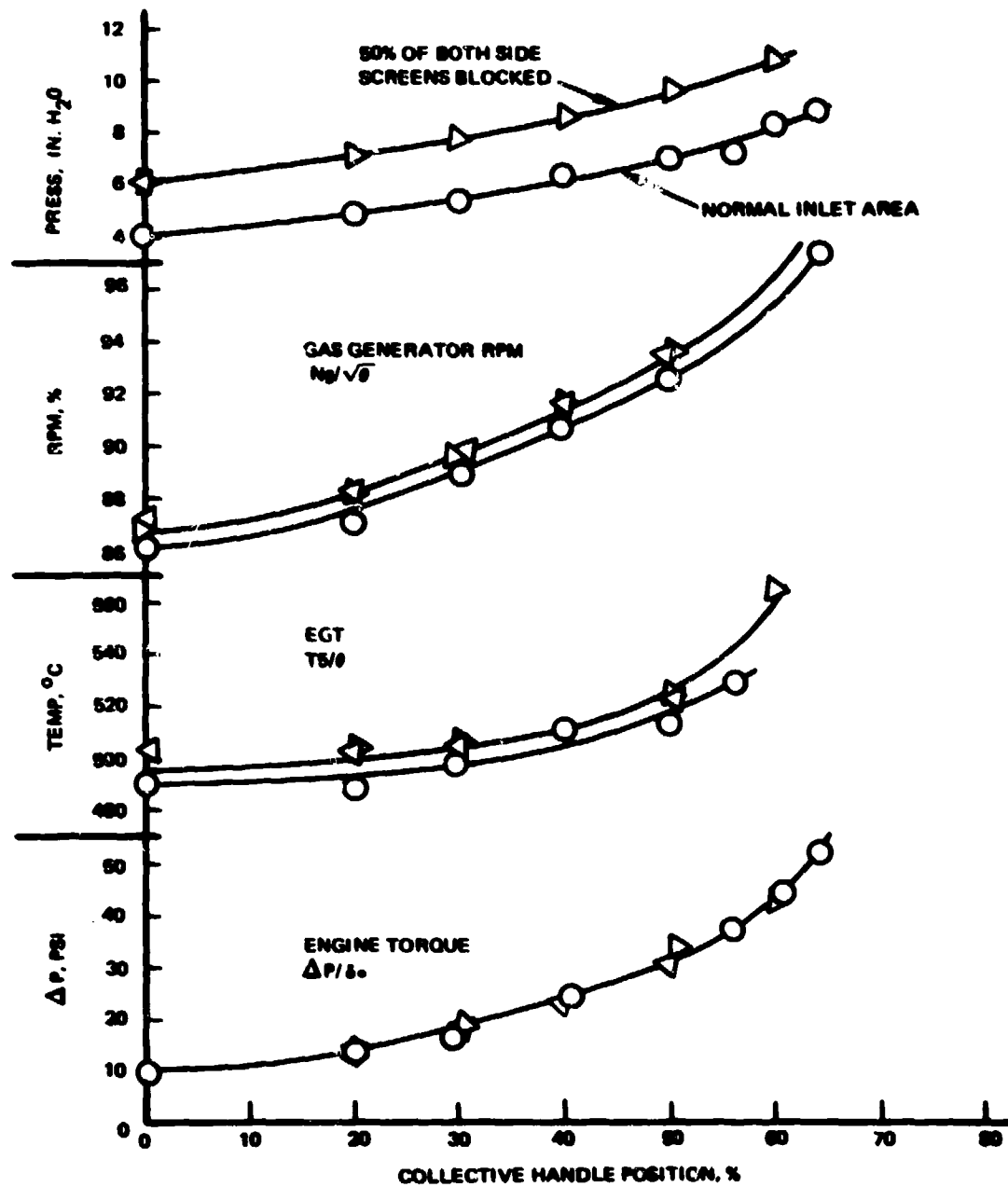
Figure 70.   Engine Inlet Screen ΔP Calibration.

estimated that the plenum pressure could be allowed to be 27 inches of H_2O (approximately 1 psi) below ambient before causing a structural problem, as the plenum bulkhead was reinforced for this program. (The structural limit would occur before a propulsion limit since a 1-psi reduction in compressor inlet pressure would cause only a 6 percent loss in power at sea level, or 10 percent at 10,000 feet.)

4.2.4 Ice Protection System Clear Air Testing

Tests were conducted in clean air as part of the airworthiness testing and prior to any tests to verify the functional and operational performance of the ice protection system. These tests included evaluation of the modified electrical system, windshield and stabilizer bar heater operation, and deicing system cycling tests. A log of the flights is shown in Table 13. These tests were conducted on the test number indicated in series with those shown in Table 9.

A discussion of general operation and problems encountered is covered in Section 6.6 and 6.7 for the electrical and deicing system.

4.2.5 Rotor Blade Thermal Performance

As part of the system functional performance testing in dry air and to assist with later correlation of icing tests, temperature-time histories were obtained for four main rotor blade stations and two tail rotor blade stations. These are presented in Figures 71 and 72. Also noted on these figures is the power ON schedule for each zone. A comparison with the predicted temperature use is also shown for these rotor stations. The agreement for main rotor stations 45 (zone VI) and 178 (zone III) is excellent and is fair at main rotor station 101.25 (Figure 71). This thermocouple is 0.1 inch from the zone boundary and is affected by conduction through the erosion shield to the adjacent zone. Hence, there is some preheating from zone IV; but, conversely, there is also heat dissipation to zone IV after it is deenergized. At station 83, there is

TABLE 13. LOG OF ICE PROTECTION SYSTEM CLEAR AIR TESTS					
Date	Test	Flight	Hours	Purpose	Comments
1-29-75	18	-	-	Deicing system check-out after blade wiring repair	Satisfactorily accomplished
1-29-75	19	12	1.7	Dry air cycling and EMI effects	Main rotor cycling o.k. but tail rotor not cycling
2-19-75	20	-	-	Deicing system testing	Overheated stab. bar heater-damaged boot
2-21-75	21	13	1.9	Deicing system dry air cycling	AC generator dropout problems
2-21-75	22	14	0.9	Mod. config. familiarization flight with Govt. pilot	Satisfactorily accomplished
2-24-75	23	-	-	Track and balance - standard blades installed	Satisfactorily accomplished
2-25-75	23	15	1.0	Functional check flight - Ferry config.	Satisfactorily accomplished
3-3-75	-	-	3.2	Ferry flight to Reno	Satisfactorily accomplished
3-4-75	-	-	5.8	Ferry flights, Reno to Moses Lake	AC generator reset problems
Total operating time on modified configuration					- 34.4 hours
Total number of flights on modified configuration					- 14
Total number of flight hours on modified configuration					- 15.3
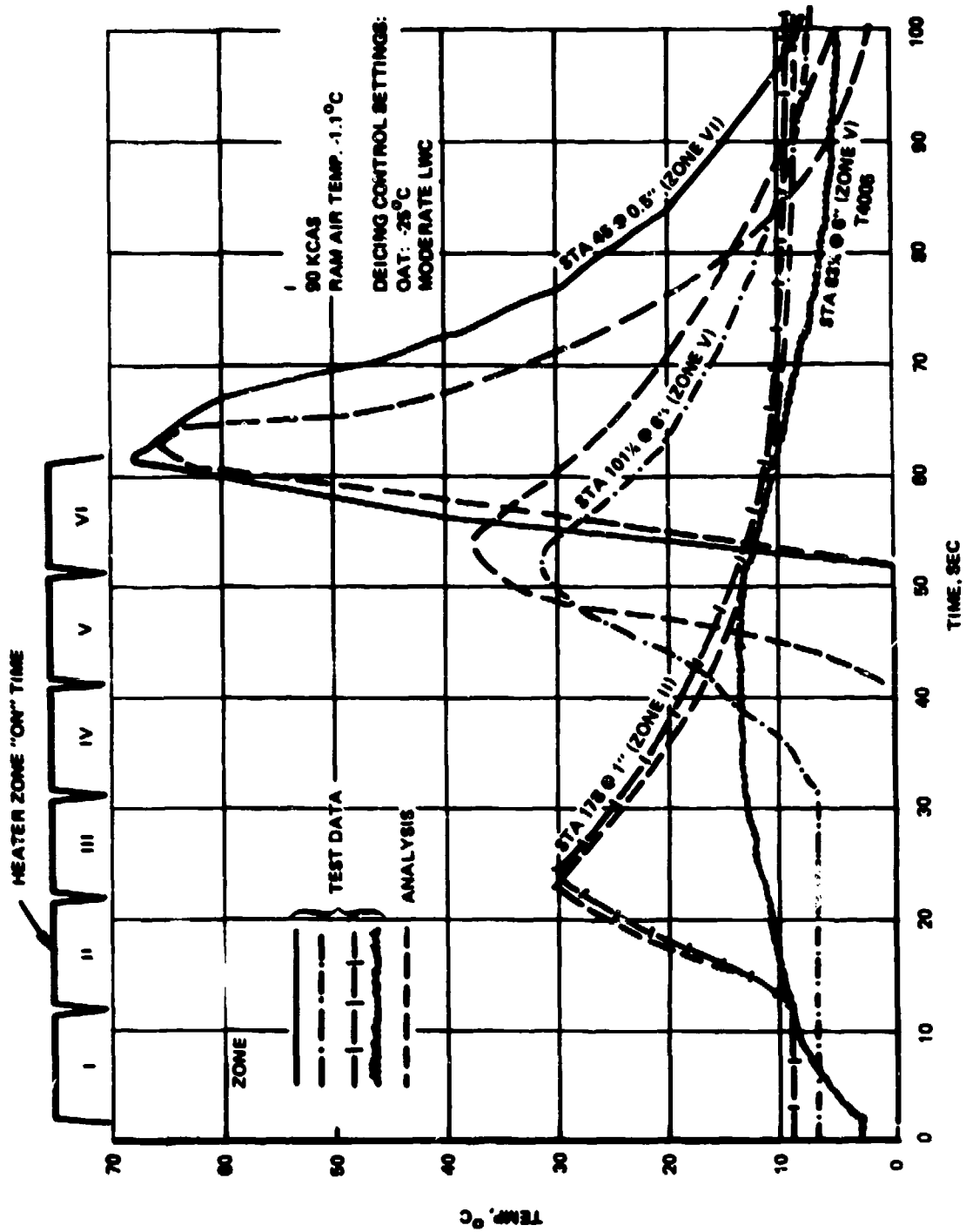
Figure 71. Main Rotor Blade Heater Skin Temperature During Dry Air Deicing System Test.
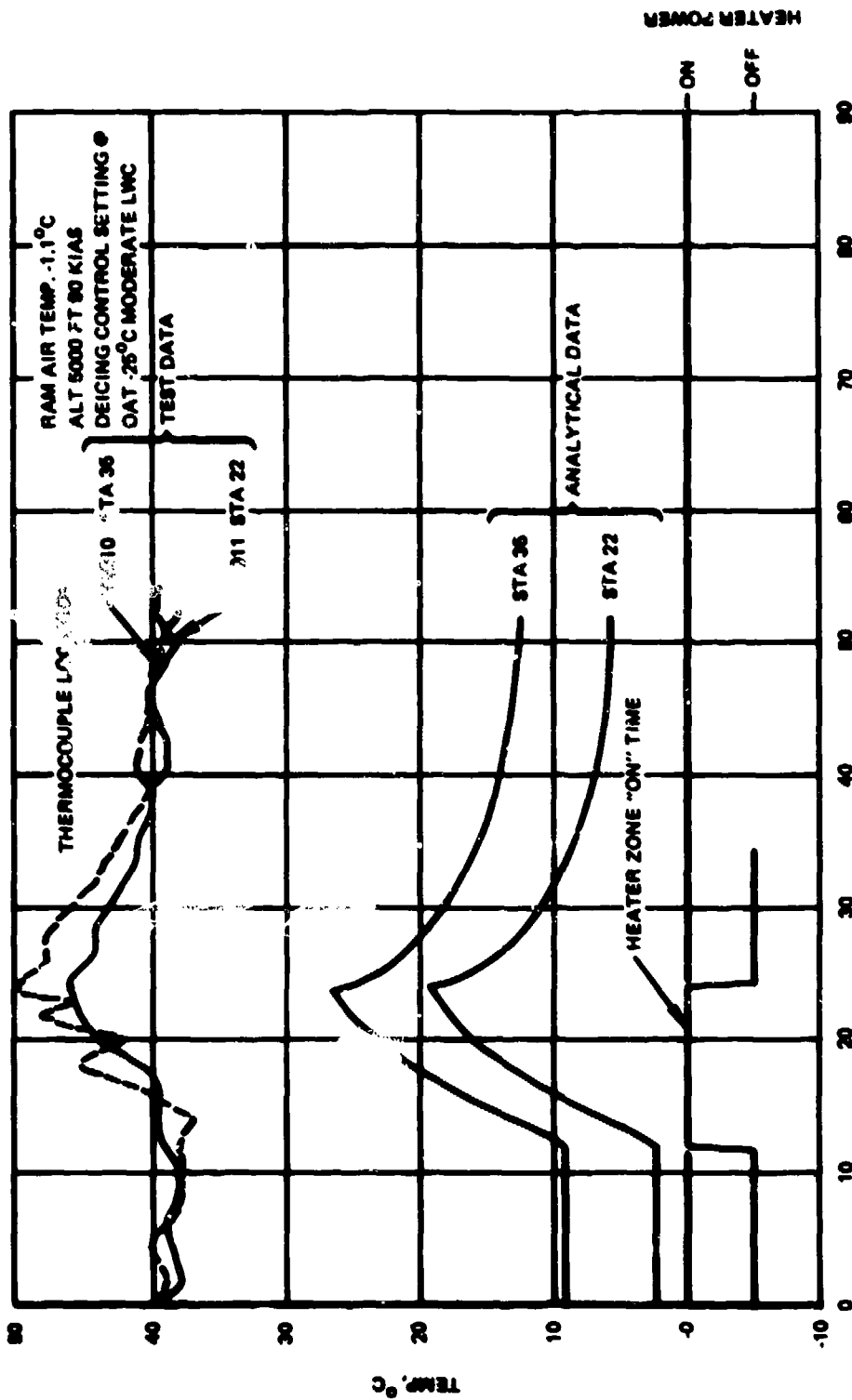
Figure 72. Tail Rotor Blade Heater Skin Temperatures During Dry
Air Deicing System Test.

a production break. Consequently, there is a 1/4-inch unheated area on either side of the production break (to provide a trim margin). This unheated area was accounted for in the design on the outboard side by a 1/2-inch-wide heating element which is energized by current from the common ground return, thus providing heat whenever any of the outboard zones are energized. The power density in this area is reduced to 33 percent of normal, however, to prevent overheat due to the relative long power ON time (equal to 5 zones). Thus, the temperature rise is over a relatively long period and is low relative to the other deicer areas.

The measured and predicted tail rotor temperatures are compared in Figure 72. Two factors can be noted with respect to the measured values: (1) the initial temperature level is significantly higher than predicted, and (2) the curves exhibit an irregular shape. Thus, it appears that the measurements were affected by electromagnetic interference (EMI), but it is not known how this influenced the signal strength. It is also believed that the tail rotor is heated to some extent by the engine exhaust, and this may account for some of the difference between measurements and predictions.

4.2.6 Windshield Operation

During the dry air testing at Edwards, the windshields were operated satisfactorily at 160, 200, and 230 volts ac during both ground and flight tests. The windshields appeared to cycle normally, and there were no instances of voltage shutdown due to an overheating condition.

The left windshield operates at a slightly higher temperature than the right windshield and has a slightly longer power ON cycle time. The temperature difference was noticeable to the touch and along with the different ON time is probably due to the difference in temperature sensor locations between the left and right windshields.

143

Ground tests to determine the minimum heating requirements of the left windshield were conducted at 50-, 100- and 160-volt settings of the Variac control. The results of these tests were considered to be inconclusive due to the longer time required to establish a stable ON/OFF cycle time at the high ambient temperatures during the ground tests.

5.0 SIMULATED ICING TESTS

Evaluation of the ice protection system was conducted in forward flight
under simulated icing conditions flying behind the USA AEFA CH-47
Helicopter Icing Spray System (HISS). The test program was conducted
at Moses Lake, Washington during the period of 12 March through 31 March
1975. A log of the test activities during that period is presented in
Table 14 and Appendix A and shows that 12 icing test flights and 14 main-
tenance flights were made. The maintenance flights were accomplished
for rotor tracking after blade change and troubleshooting intermittent
electrical ground problems. Deicing data points were obtained on nine
of the icing test flights. Icing test conditions ranged from $-5^{\circ}C$
to $-20^{\circ}C$ air temperature. Test temperatures were obtained by varying
the test altitude from approximately 4000 feet to 10,000 feet. The
liquid water content of the water spray from the tanker varied from
0.25 g/m^3 to 0.75 g/m^3. As the temperature was decreased, the maximum
liquid water content tested was decreased to encompass the probable
combinations of OAT and LWC.

In general, the ice protection system performance was considered satis-
factory. Windshield and stabilizer bar anti-icing appeared completely
effective. Although no tail rotor blade icing was experienced (page
163), the blade deicing heaters were cycled to gain operational
experience on the complete system. Main rotor deicing was complete
under most test conditions. Under some conditions, deicing of the
inboard 6 feet of the blade leading edge was not effected even though
the heaters operated properly (page 161).

TABLE 14. LOG OF ICE PROTECTION SYSTEM TESTING AT MOSES LAKE

Date	Test No. AEFA/ Lock- heed	Flt No. AEFA/ Lockheed	Flt Hr	Purpose of Test*	Comments
3-8-75	24	-	-	Ground run – system check-out of deicing system	M/R blade heater power supply line shorted
3-9-75	25			Ground run – system checkout after repair of M/R blade	Completed satisfactorily
3-10-75	26	2, 16	.5	Function check flight	Completed satisfactorily
3-12-75	27	2, 17	2.1	Functional flight behind tanker, deicing flight	Another M/R blade heater power supply shorted
3-14-75	28	3,4,5 18,19,20	1.2	M/R blade track and balance after replacement	Completed satisfactorily
3-15-75	29	2, 6, 21	.8	Deicing flight behind tanker	Flight aborted, P.M. antenna oscillating dur-ing icing flight
3-15-75	29	2, 7, 22	.5	Deicing flight behind tanker	Flight terminated due to weather
3-15-75	29	2, 8, 23,24,25	1.0	Functional flights due to 2P vibration	Completed satisfactorily
3-18-75	30	2, 9, 26	1.8	Deicing flight behind tanker	Completed satisfactorily
3-20-75	31	2, 10, 27	1.5	Deicing flight behind tanker	Completed satisfactorily

*See Appendix A for more details of test conditions

TABLE 14. LOG OF ICE PROTECTION SYSTEM TESTING AT MOSES LAKE (Cont)

Date	Test No. AEPA/ LAC	Flt No. AEPA/LAC	Flt Hr	Purpose of Test	Comments
3-20-75	3 / 32	11 / 28	0.8	Deicing flight behind tanker	Flight aborted due to weather
3-24-75	3 / 33	12 / 29,30	1.0	Functional flight for troubleshooting of deicing system short	M/R blade heater power supply wire found shorted
3-26-75	3 / 34	13 / 31	0.9	Deicing flight behind tanker	M/R blade short not identified, but found an open wire
3-27-75	3 / 35	14 / 32	1.2	Deicing flight behind tanker	Test aborted at altitude due to weather conditions
3-27-75	4 / 36	15 / 33	1.5	Deicing flight behind tanker	Completed satisfactorily
3-28-75	5 / 37	16 / 34	1.9	Deicing flight behind tanker	Completed satisfactorily
3-29-75	- / 38	17 / 35-39	0.6	Troubleshooting intermittent deicing & instru. elect. ground problem	Completed as planned
3-31-75	6 / 39	18 / 40	1.8	Deicing flight behind tanker	Completed satisfactorily

TABLE 14. LOG OF ICE PROTECTION SYSTEM TESTING AT MOSES LAKE (Cont)

Date	Test No.	Flt No.	Flt Hr	Purpose of Test	Comments
3-31-75	7 / 40	19 / 41	1.5	Deicing flight behind tanker	Completed satisfactorily

Total Icing Flights   12   Total Maintenance Flight Hours   4.3

Total Maintenance Flights   14   Total Icing Flight Hours   15.8

Total Operating Hours   29.1

148

5.1 OPERATIONAL TEST PROCEDURE

The following test procedure was used during the simulated icing tests at Moses Lake, Washington.

1. Each flight was preplanned with the icing conditions selected for evaluation, with a set of alternate conditions available if alterations to the flight became necessary.

2. Prior to the test flight the fixed-wing weather survey aircraft conducted a temperature-altitude check to find the altitude for the selected test ambient temperature.

3. A preflight briefing would be held for the test crew, chase aircraft crew, HISS tanker crew, and rescue helicopter crew, with other interested personnel in attendance.

4. After the briefing, the crews boarded their aircraft, took off, rendezvoused, and flew in formation to the test area.

5. Upon arriving in the test area, the HISS tanker stabilized at the altitude required for the desired ambient temperature and started the water flowing at the rate required to obtain the desired liquid water content.

6. The test aircraft then took a record in trimmed level flight before entering the icing cloud (Figure 73).

7. The test aircraft next entered the icing cloud behind the HISS tanker and stabilized at approximately 80 KCAS at a distance of 120-150 feet behind the tanker. This distance was monitored by a rearward-facing radar altimeter in the tanker, and the test aircraft pilot was informed of deviations from this distance by radio. Figure 74 shows the test aircraft operating in the spray cloud relative to the tanker.

Figure 73. Test Aircraft Establishing Trim Conditions Outside the Spray Cloud.

Figure 74. Test Aircraft Operating in Spray Cloud Behind the CH-47 Tanker.

8. After remaining in the cloud for the designated period of time, the test aircraft exited the cloud and took a record in trimmed level flight. The chase aircraft then moved in and observed the ice accumulated on the test aircraft, and the photographer took pictures prior to the deicing cycle. Figures 75 and 76 show the UH-1H in the spray cloud as viewed from the side and from the tanker.

9. When the external observations were reported, the deicing cycle was initiated. The observer in the chase aircraft visually noted any ice leaving the rotor, and this was also recorded by the photographer with a high-speed camera. If the chase aircraft reported that there was ice remaining on the blades, the deicing system was recycled.

10. After completion of the deicing cycle, the test aircraft took another record in trimmed level flight outside the cloud to establish a base for the next cycle.

11. The test aircraft reentered the cloud for the next test condition, and steps 7 through 10 were repeated.

12. After the completion of a given flight, the four aircraft returned to base.

5.2 ICING TEST CONDITIONS

The simulated icing tests were conducted in test envelope expansion fashion starting at just-below-freezing ambient temperature (23°F) and low liquid water content (0.25 gram per cubic meter). Information based on prior Army testing in simulated icing conditions indicated that 1/4 inch of ice would accumulate at the 40 percent rotor span point at this LWC and temperature in approximately 7 minutes. Using this as a guide, the initial deicing cycles were initiated after exposure times in the icing test condition of 2, 4, 6, 8, and 10 minutes to buildup to the 7 minutes and bracket it. After some deicing experience was obtained and the results were evaluated,

152

Figure 75. Test Aircraft Operating Wit. Rotor in Spray Cloud as Viewed From the Side.

Figure 76. Test Aircraft Operating in Spray Cloud as Viewed From the CH-47 Tanker.

8 minutes was selected as a reasonable OFF time for the 0.25 g/m^3 LWC, and this was used as a basis for selecting the change in power OFF time being inversely proportional to increases in LWC. No quantitative measure of blade ice thickness prior to deicing was made other than an attempt to keep the Δtorque increase in the area of 5 psi or 20% to be consistent with previous test recommendations. As lower temperatures and/or higher LWC conditions were tested, the exposure time or ice accretion time was increased in two steps to the established nominal OFF time. As mentioned under test procedures, each test condition of temperature and LWC was evaluated by conducting a deicing cycle in clear air after accreting ice first and then by evaluating two or more successive deicing cycles with the appropriate OFF time while flying continuously in the spray cloud.

The icing condition envelope that was the test target envelope is shown in Figure 77, which also indicates the incremental steps used in reaching envelope extremes. As can be seen, all but the high LWC and 23°F temperature corner of the envelope was achieved. Table 15 lists the specific test conditions attained and shows the time in the cloud and the deicing test cycle number. The cases where more than one cycle number is shown are the cases where flight in the cloud was continuous for the total time shown with deicing cycles accomplished every 8 minutes in light (L) LWC, 4 minutes in moderate (M) LWC, or 2 minutes in heavy (H) LWC conditions as appropriate.

The ice buildups which were obtained between deicing cycles can also be related to protection against intermittent maximum conditions, as defined in MIL-E-38453. The liquid water content associated with these conditions and 15-20 micron volume median droplet sizes is 2-2.5 g/m^3, depending upon ambient temperature. Since the deicing system is capable of completing a cycle every 36 seconds (with the heavy setting) even at -20°C, the ice buildup experienced in 4 minutes at 0.5 g/m^3 is more than representative of the ice buildup which might accrue during intermittent maximum conditions.
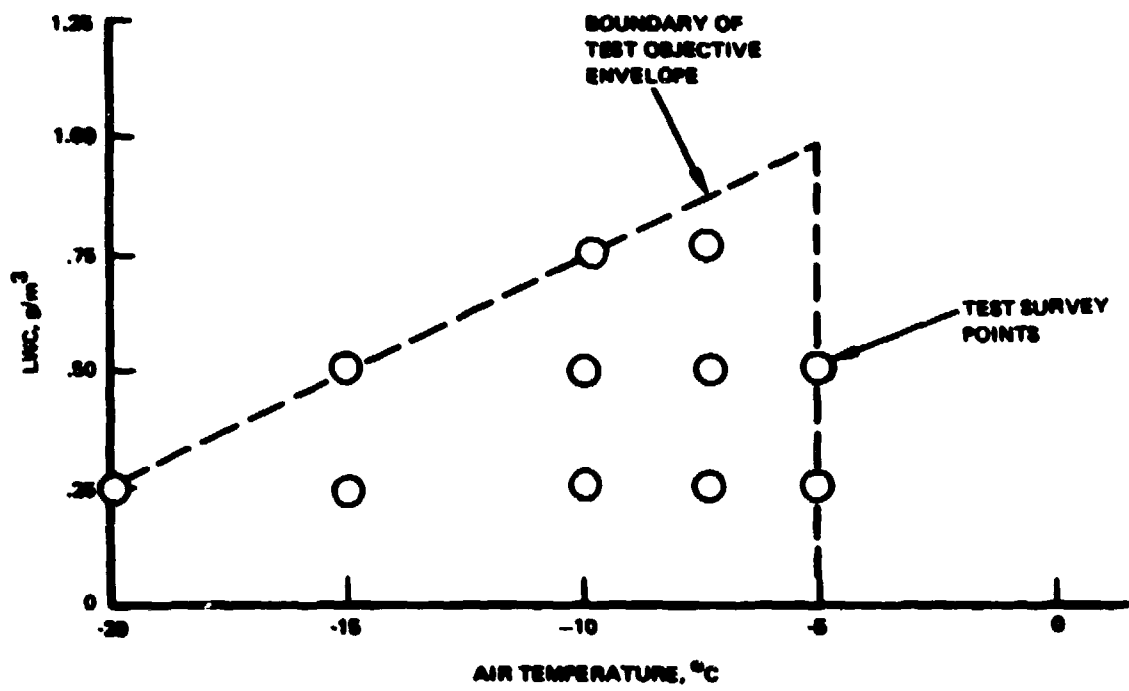
Figure 77. LWC Versus OAT Simulated Icing Test Envelope.

156

TABLE 15. DEICING TEST CONDITIONS AND GENERAL RESULTS

Lockheed Test/Flt. No.	Deicing Test Cycle No.	Tanker LWC, g/m^3	Test OAT (°C)	LWC Control Set	OAT Control Set, °C	Time in Cloud, (Min)	Chase Aircraft Comments
27/17	1	0.25	-5	L	-5	2	Ice accretion not evident.
	2	0.25	-5	L	-5	4	Need to repeat condition.
30/26	3	0.25	-5	L	-5	6	Blades clean after cycle.
	4	0.25	-5	L	-5	8	Shed incomplete.
	5	0.25	-5	L	-5	10	Good shed, less ice than 8 min.
31/27	6	0.25	-5	L	-5	8	Shed fairly complete. Nice shed - 3 distinct sheds.
	7	0.50	-5	M	-5	3	Not as good as 3 min.
	8	0.50	-5	M	-5	4	
34/31	9	0.25	-7.5	L	-5	8	1 shed only for zone 4 or 5.
	10	0.50	-7.5	M	-7.5	1	Aborted due to turbulence.
35/32	11	0.25	-7.5	L	-7.5	8	Zone 4 shed, 5 & 6 remained.
	12	0.50	-7.5	M	-7.5	4	Pretty good shed.
	13	0.50	-7.5	M	-7.5	4	Complete shed - excellent.

TABLE 15. DEICING TEST CONDITIONS AND GENERAL RESULTS (Cont)

Lockheed Test/Flt. No.	Deicing Test Cycle No.	Tanker LWC, g/m³	Test OAT (°C)	LWC Control Set	OAT Control Set, °C	Time in Cloud, (Min)	Chase Aircraft Comments
36/33	14	0.25	-10	L	-10	8	Full span ice, Inbd 6' kept ice. Good shed, zone 5 & 6 went together. 3 good sheds, Off time excessive.
	15	0.50	-10	M	-10	4	
	16 to 18	0.50	-10	M	-10	12+	
37/34	19	0.75	-7.5	H	-7.5	2.0	Cycled 6 times to clear all ice. Beautiful cycle; 4 cycles in cloud, 1 cycle in cloud, recycled to clean
	20	0.75	-7.5	H	-7.5	2.0	
	21 to 24	0.75	-7.5	H	-7.5	8.0	
	25	0.75	-10.0	H	-10	2.0	
39/40	26	0.25	-15	L	-15	8	Zone 1,2,3 good sym. shed. Ideal shed, real clean blade. Inbd 3 zones - no shed.
	27	0.50	-15	M	-15	4	
	28,29	0.25	-15	L	-25	16	
39/41	30	0.25	-20	M	-28	8.0	Zones 1,2,3 good, 5,6 small amount. Inbd 6' would not shed.
	31,32	0.25	-20	M	-30	16	

5.3 ROTOR BLADE DEICING

The effectiveness of the deicing system was determined during the test program primarily from visual inflight observations from the chase UH-1H aircraft. A main rotor hub-mounted movie camera was installed on the test aircraft as described in Section 3, but no blade pictures were obtained due to an obscured camera lens or the viewing window of the enclosure around the lens. The window had anti-icing provisions but successful operation with a clear window under low temperature and icing conditions was never obtained.

The blades were painted dull black with white stripes outlining the 6 heater zones to aid in the deicing evaluation, both visually and photographically. Figure 78 is a picture of the blade in flight taken from the chase helicopter that shows the zone boundary marking lines defining the six zones (zones are numbered I - VI starting from the outboard end and going inboard). Close inspection of the photographs shows ice formed on the blades on zones III, IV, V, VI, with the outboard edge just inside the zone III outer boundary line.

Although good photographic documentation is not available, the excellent observations of the USAAEFA engineering pilot/observer were detailed and specific. The right-hand column of Table 15 briefly summarizes pertinent observations/comments made by the chase helicopter on each deicing cycle. At all test conditions, good deicing shed results were reported, although the results were not always consistent. In general, the deicing of the blade occurred zone-by-zone as intended. The deicing was symmetrical in that the flight crew could not detect the shed except occasionally, and then only a barely perceptible low-level one-per-rev out-of-balance condition. Under conditions of -10°C and below, the deicing could be observed so distinctly that the chase observer could call off the shedding by zone number in sequence, and the test aircraft crew could correlate the zone sheds with the zone heater ON time

Figure 78. Main Rotor Blade, Showing Heater Boundary Lines.

lights in the control panel. These observations indicated that the ON time could be reduced approximately 2 seconds per zone. Thus a simple test procedure is feasible in future testing to use in optimizing the heater ON times.

At all temperature conditions, there was some residual ice near the inboard end of the blade. This residual ice varied from about 12 inches of span at -5°C to 60 inches (one-half of zone V and all of zone VI, the two inboard zones) at -10°C and colder. Repeated close internal cycles of the heaters generally failed to clear this ice even though the zone VI blade thermocouple readings showed that temperatures as high as 53°C were realized. (The temperature was increased by using longer ON times for succeeding heater cycles.) Figure 79 shows typical postflight residual ice formation at the root end of the blade. The blade heated area goes all the way in to within an inch of the root end. It appears that the large water droplets of the spray tanker cloud (150 microns) result in ice formation back of the heater (chordwise) and on the blade grip clevis fitting and essentially bridge the heated area and remain attached.

The 60-inch span corresponds to the doubler heater which extends from sta. 24 to 83, where there is a joint or juncture with the outboard blade heaters. The erosion shield material changes from aluminum to steel at this station. The joint in the heating element results in a 1/2-inch band which is unheated and which could provide sufficient ice bond strength to prevent the ice from there in to the grip clevis from shedding. Future testing should include checking the effect of this ice accumulation on autorotation rpm.

No positive indication of runback was evident on the outer portion of the blade. The inboard lower surface collected ice "drops", which are apparent on Figure 79 as far back as the trailing edge, as would be expected due to the large droplets behind the HISS.

161

Figure 79. Main Rotor Root End Residual Ice.

152

With respect to the tail rotor blades, the test results indicate that, at least for the conditions tested, ice protection is not required. The engine exhaust plume provided sufficient heat to anti-ice the tail rotor blades at all conditions tested. A review of high-speed camera film from the chase aircraft also showed no ice present on the tail rotor blades, although varying amounts of ice were present on the hub arms, slipring housing, vertical fin, and horizontal stabilizer.

Flying in the cloud behind the HISS tanker in level flight requires a power setting that would be used for climb. The higher exhaust gas temperature combined with the vortex pattern behind the tanker may result in a favorable anti-icing condition for the tail rotor, which would not be present under natural icing conditions at high liquid water content levels and low ambient temperatures. Therefore, tail rotor deicing capability for the UH-1H helicopter may still be required.

5.4 DEICING LOADS AND DYNAMICS

Main rotor and tail rotor loads were recorded prior to entering, while inside, and after leaving the deicing cloud created by the CH-47 spray tanker. Loads were recorded on magnetic tape, and the most critical structural loads were monitored in real time to maintain safety of flight.

Prior to the actual icing runs, the test helicopter was flown in the tanker wake at various locations to determine the effect of air turbulence from the tanker. Vertical passes were made through the wake in the center, to the left side, and to the right side. The center and left side vertical passes were made without any difficulty. The vertical pass on the right side was terminated when limit engine power was reached. The test helicopter was also flown in the "icing test position" behind the tanker. Main rotor blade loads for these wake turbulence survey tests are shown in Figures 80 through 86.
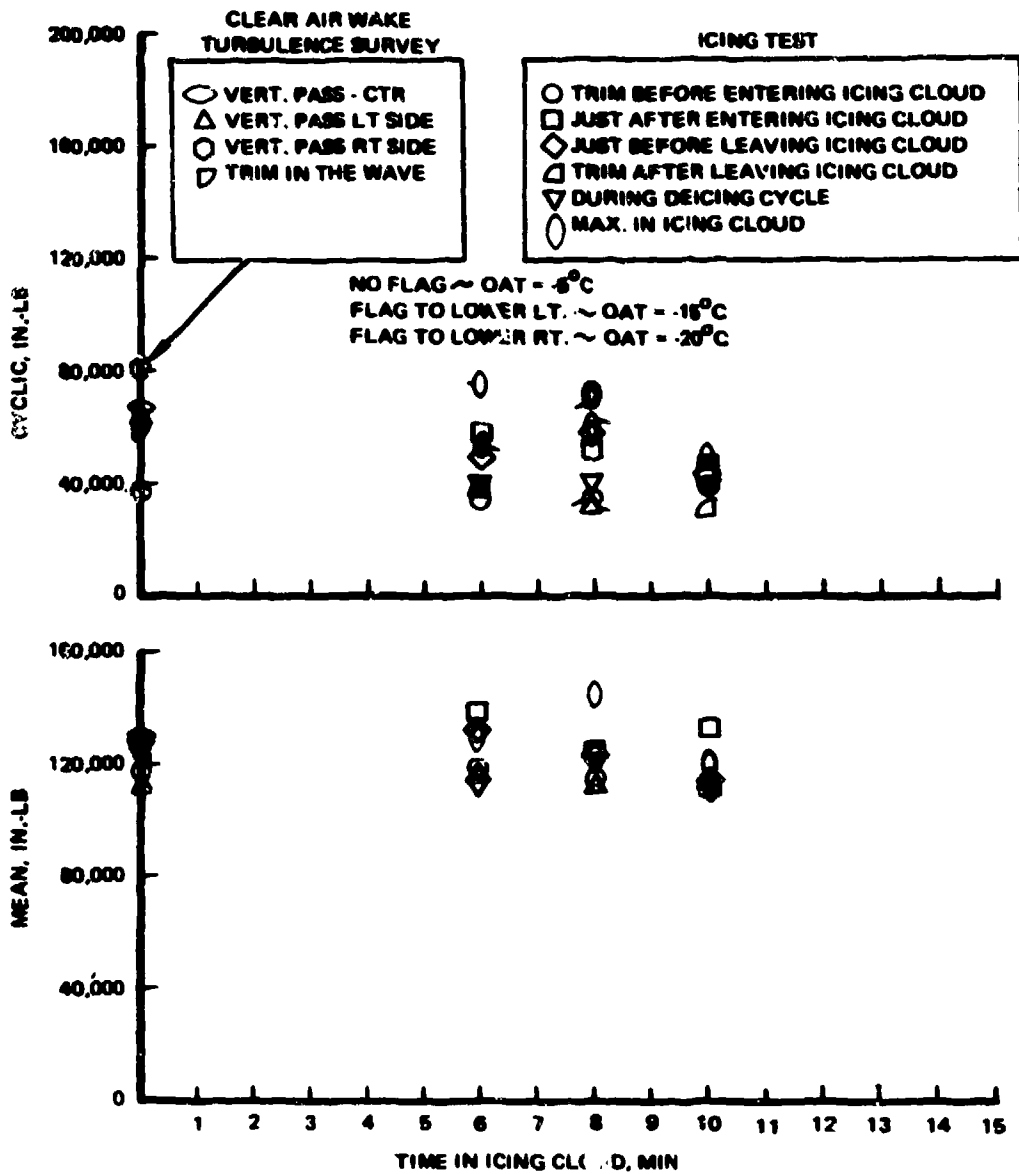
Figure 80. Main Rotor Inplane Bending Moment at Station 35 With Deicing Boot Installed, 80 KCAS

164
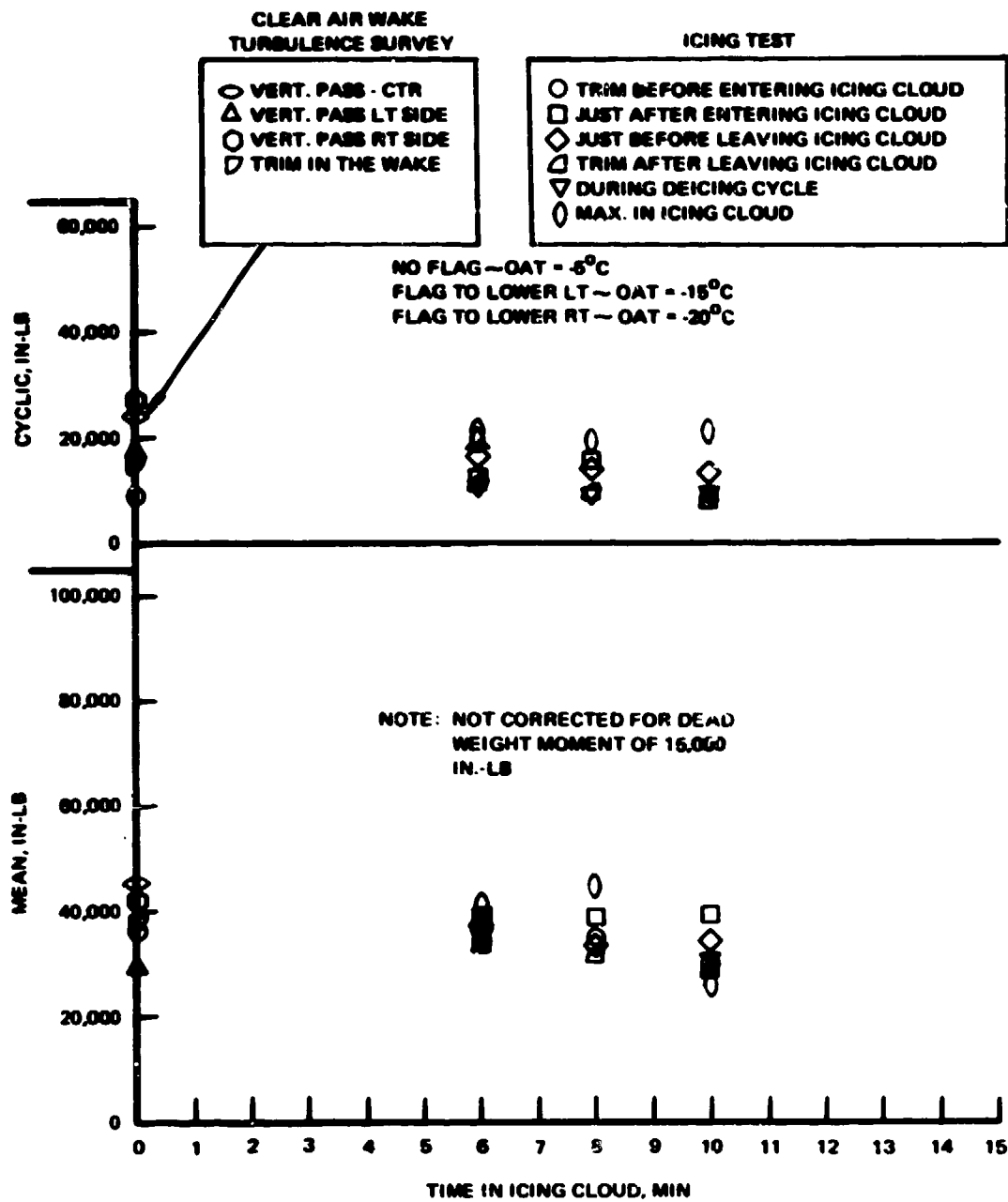
Figure 81.   Main Rotor Flap Bending Moment at Station 35 With Deicing Boot Installed, 80 KCAS
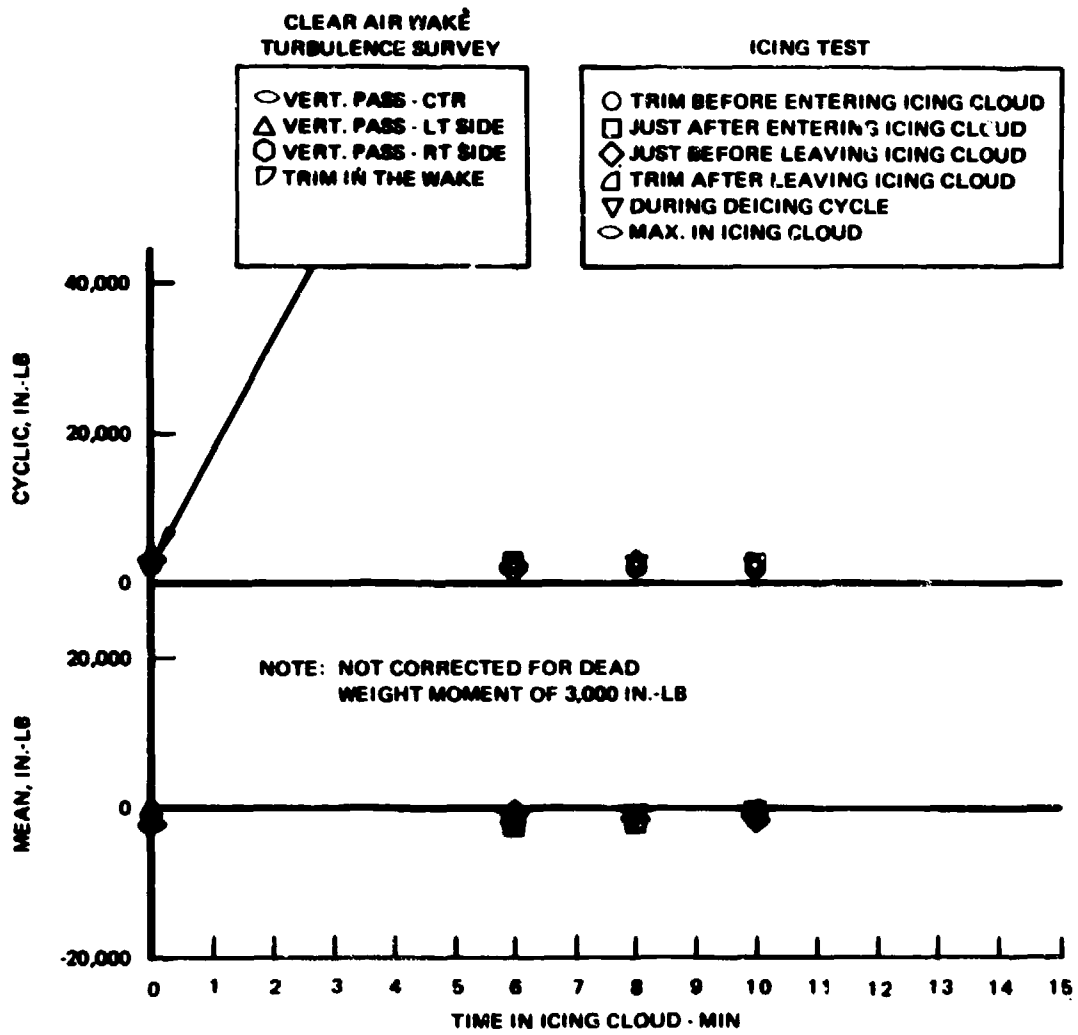
Figure 82. Main Rotor Flap Bending Moment at Station 150 With Deicing Boot Installed, 80 KCAS
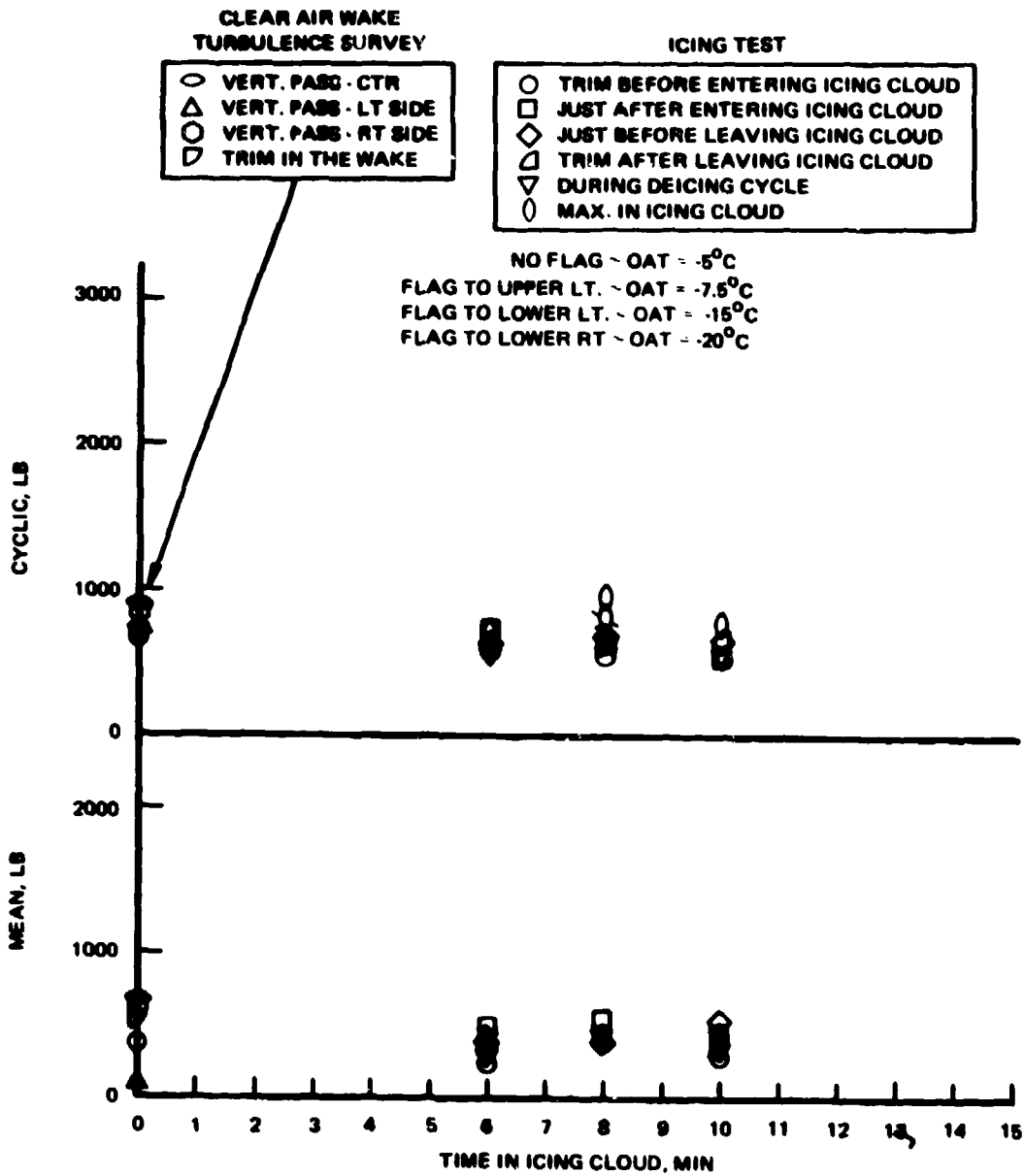
Figure 83. Main Rotor Pitch Link Axial Load With Deicing Boot Installed, 80 KCAS
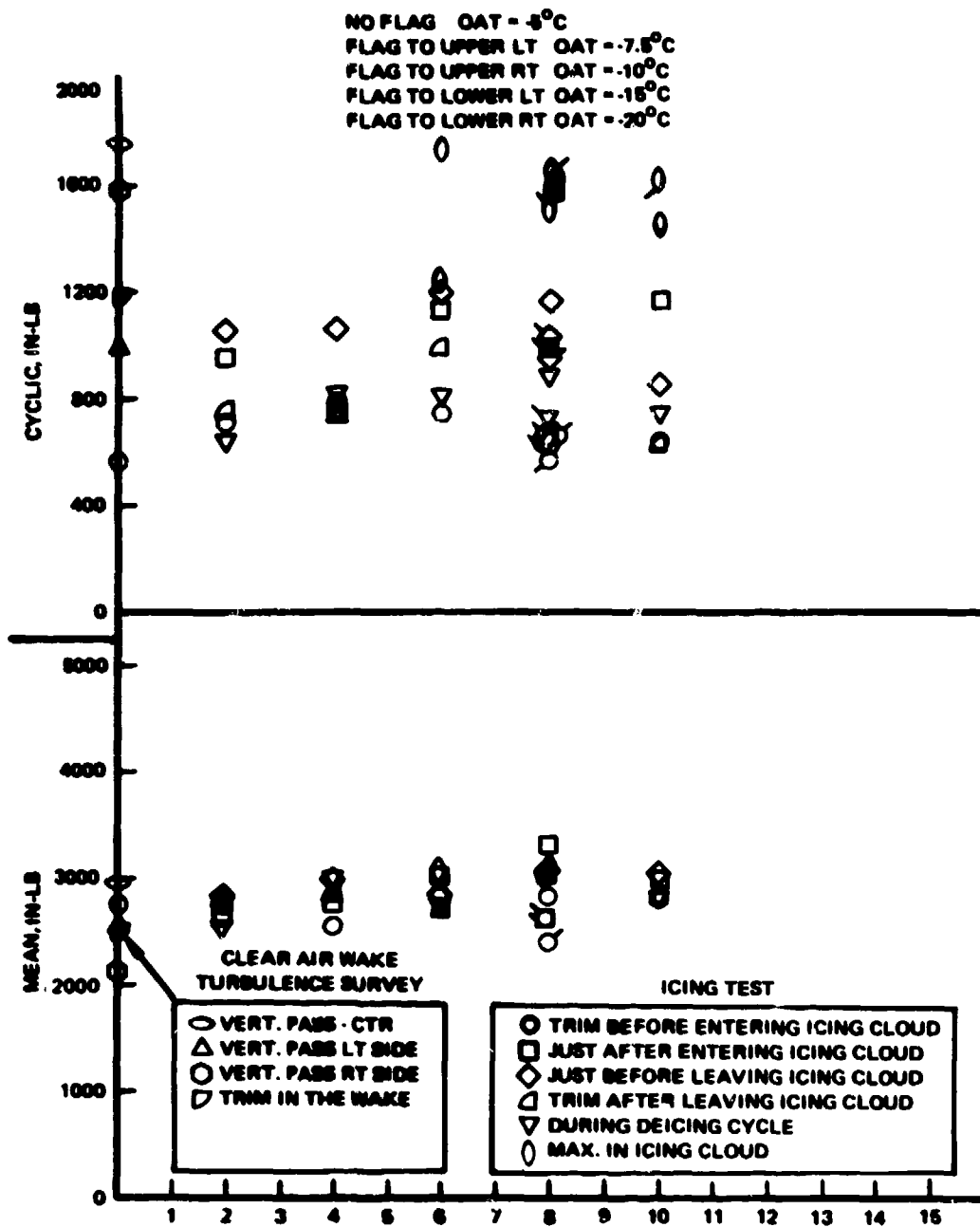
Figure 84.   Tail Rotor Inplane Bending Moment at Station 11 With
Deicing Boot Installed, 80 KCAS

168
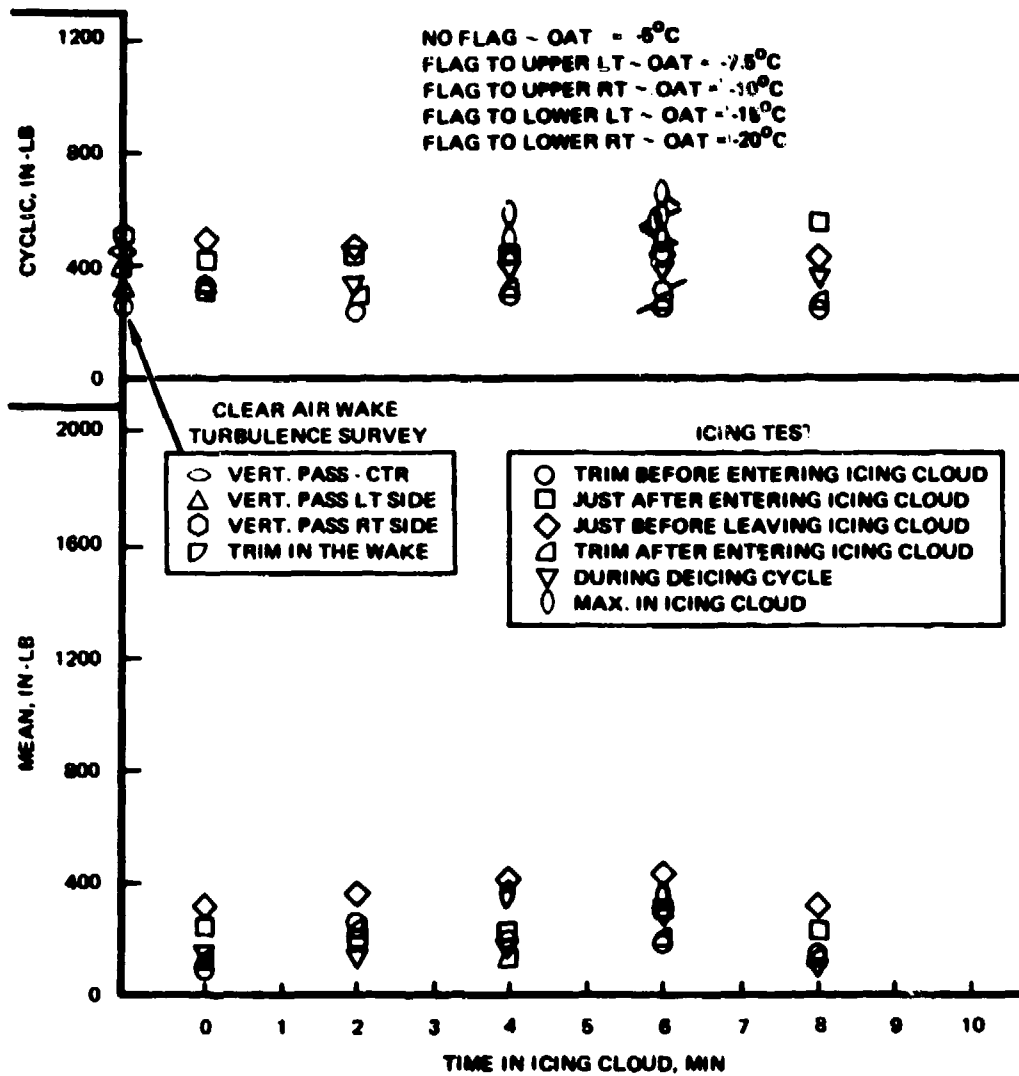
Figure 85. Tail Rotor Flap Bending Moment at Station 24 With Deicing Boot Installed, 80 KCAS
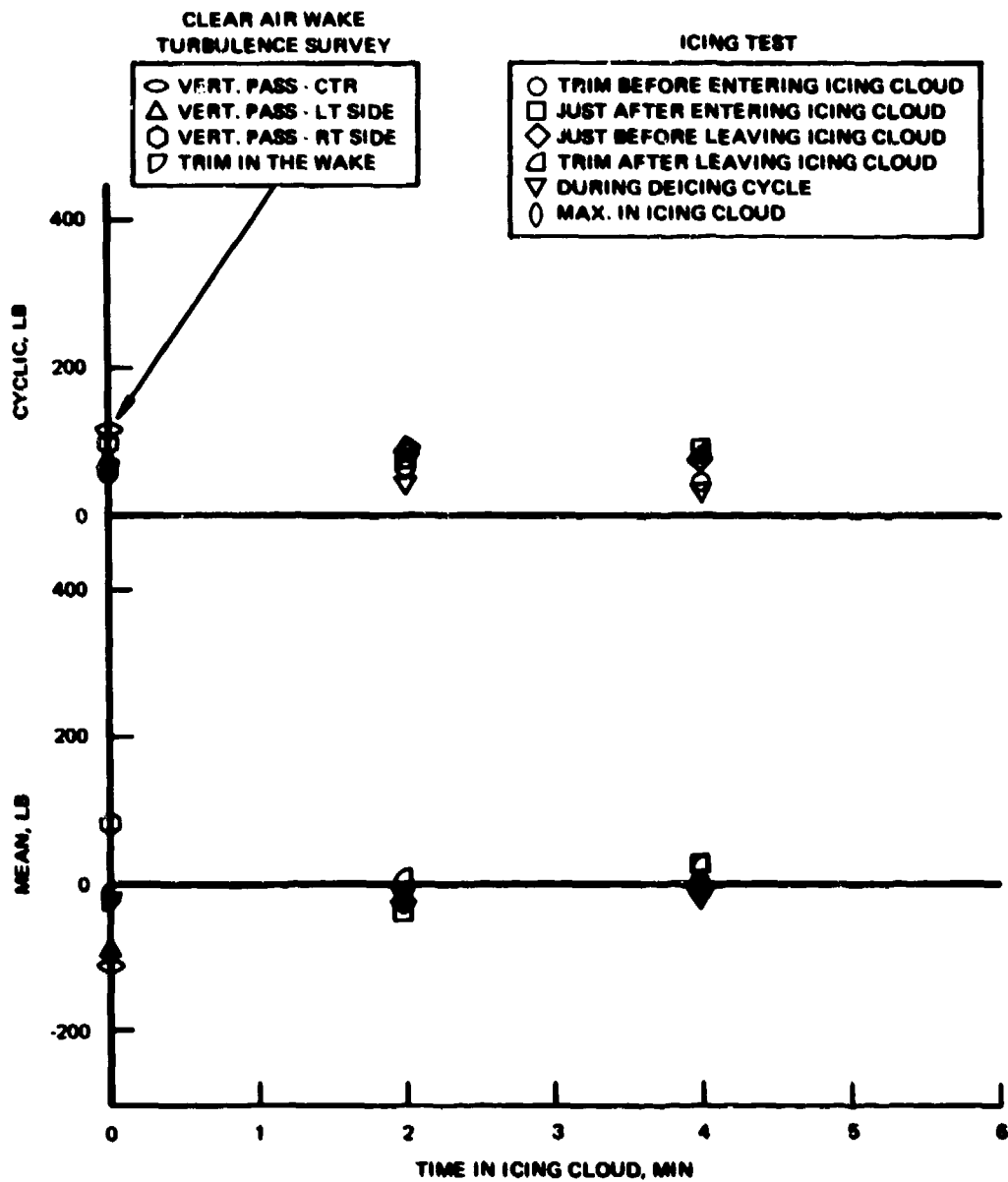
Figure 86. Tail Rotor Pitch Link Axial Load With Deicing Boot Installed, 80 KCAS

170

Ice accretion runs were conducted behind the tanker at three water spray flow rates of 0.25, 0.50 and 0.75 grams per cubic meter for various ice accretion times prior to deicing. The outside air temperatures varied **from 5°C to -20°C.** The structural loads are presented for the 0.25 and 0.75 g/m^3 flow rate in Figures 80 through 86 and Figures 87 through 91, respectively, as a function of the time spent in the cloud (i.e., the amount of ice on the blade).

The structural loads are plotted for each of the following conditions:

1. Trim before entering the icing cloud at the test altitude and speed, outside of the tanker turbulence.

2. After entering the icing cloud to obtain a base point in the tanker turbulence at the start of ice accumulation.

3. Maximum load in the icing cloud to determine the highest load obtained while in the icing cloud.

4. Prior to leaving the icing cloud to determine the structural loads in the tanker turbulence with the ice that had accumulated while in the icing cloud.

5. Trim out in clear air after leaving the icing cloud to establish the change in structural loads with the ice that had accumulated in the icing cloud so that it could be compared with the trim before entering the icing cloud.

6. During the deicing cycle to determine load changes as ice sheds from the main rotor blade.

A review of the plotted data shows that most of the increase in structural load was due to the downward flight operating condition and turbulent air behind the tanker. There was no significant change in loads due to ice accumulation. The data also shows that there was no significant change in loads during the deicing cycle as the blades shed the ice that

171
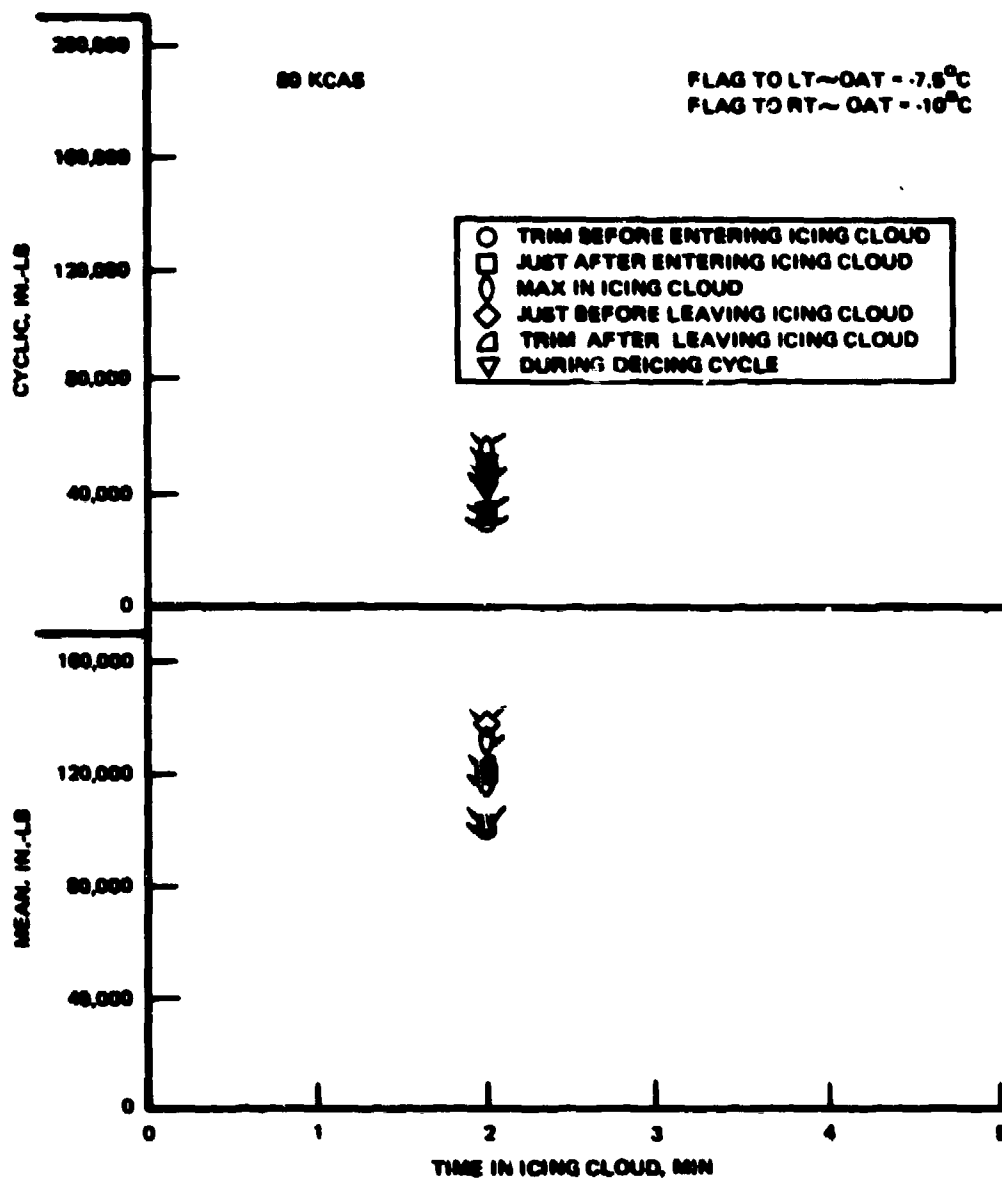
Figure 87. Main Rotor Inplane Bending Moment at Station 35 With Deicing Boot Installed, 0.75 g/m³.
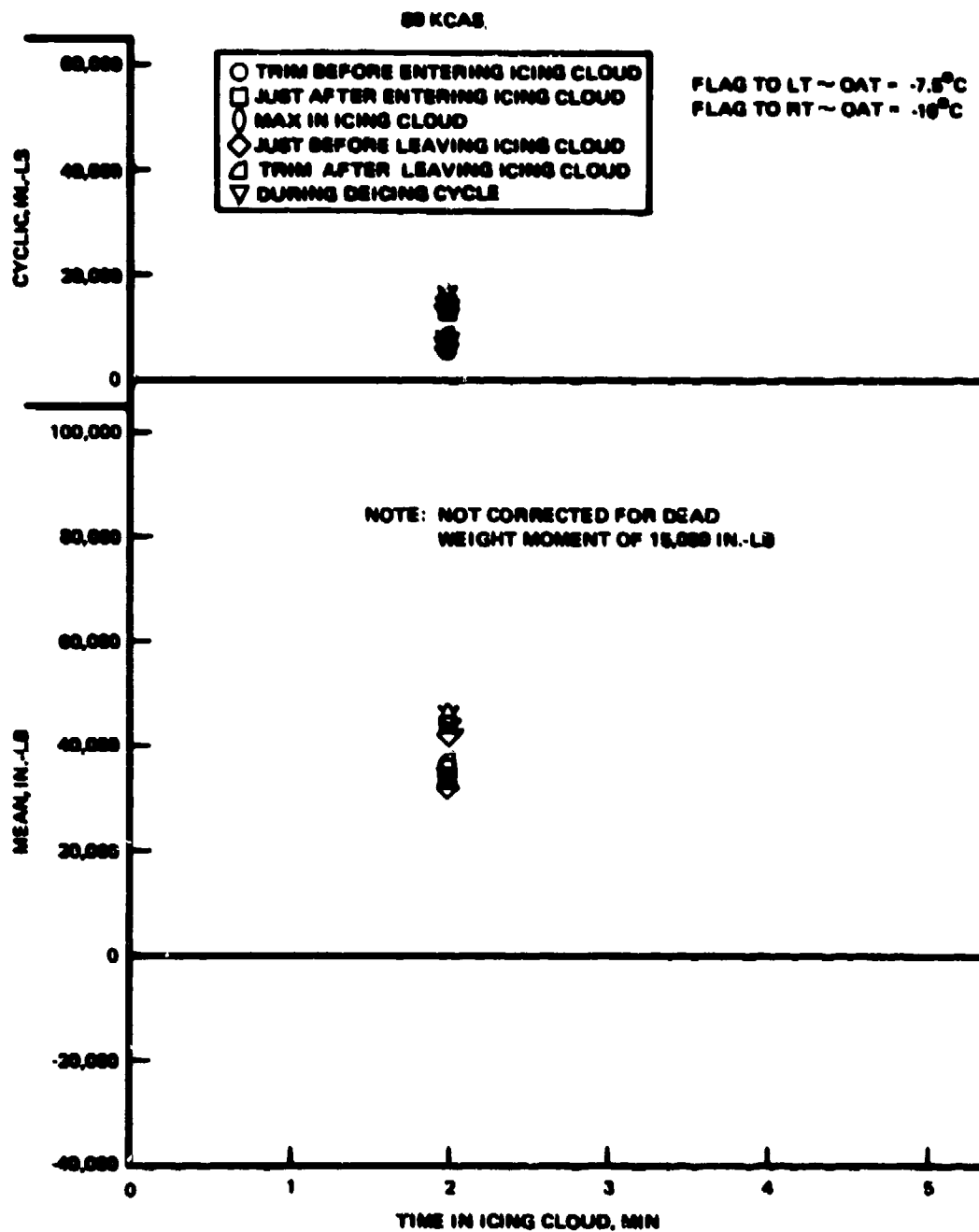
Figure 88. Main Rotor Flap Bending Moment at Station 35 With Deicing Boot Installed, 0.75 g/m^3.
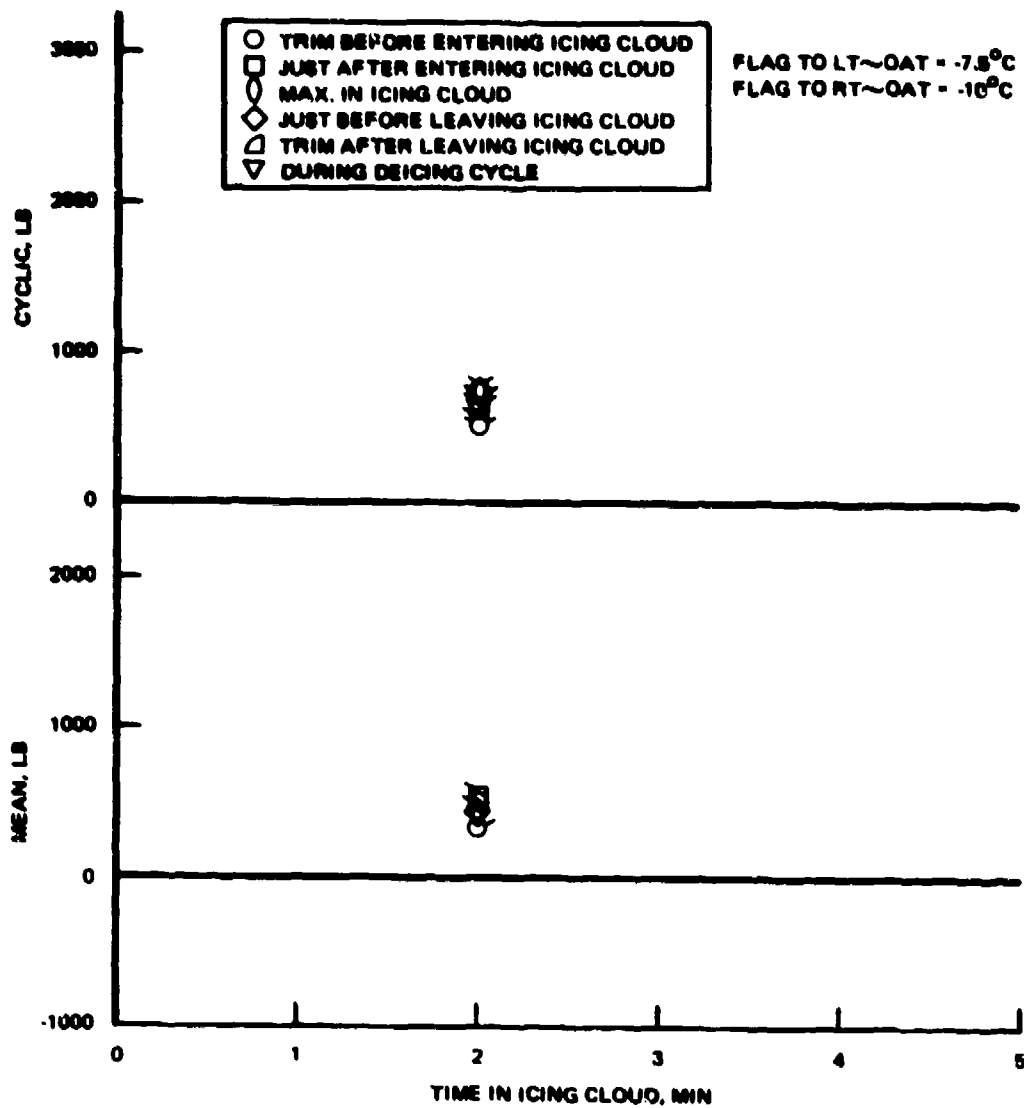
Figure 89. Main Rotor Pitch Link Axial Load With Deicing Boot Installed, 0.75 g/m³.

174
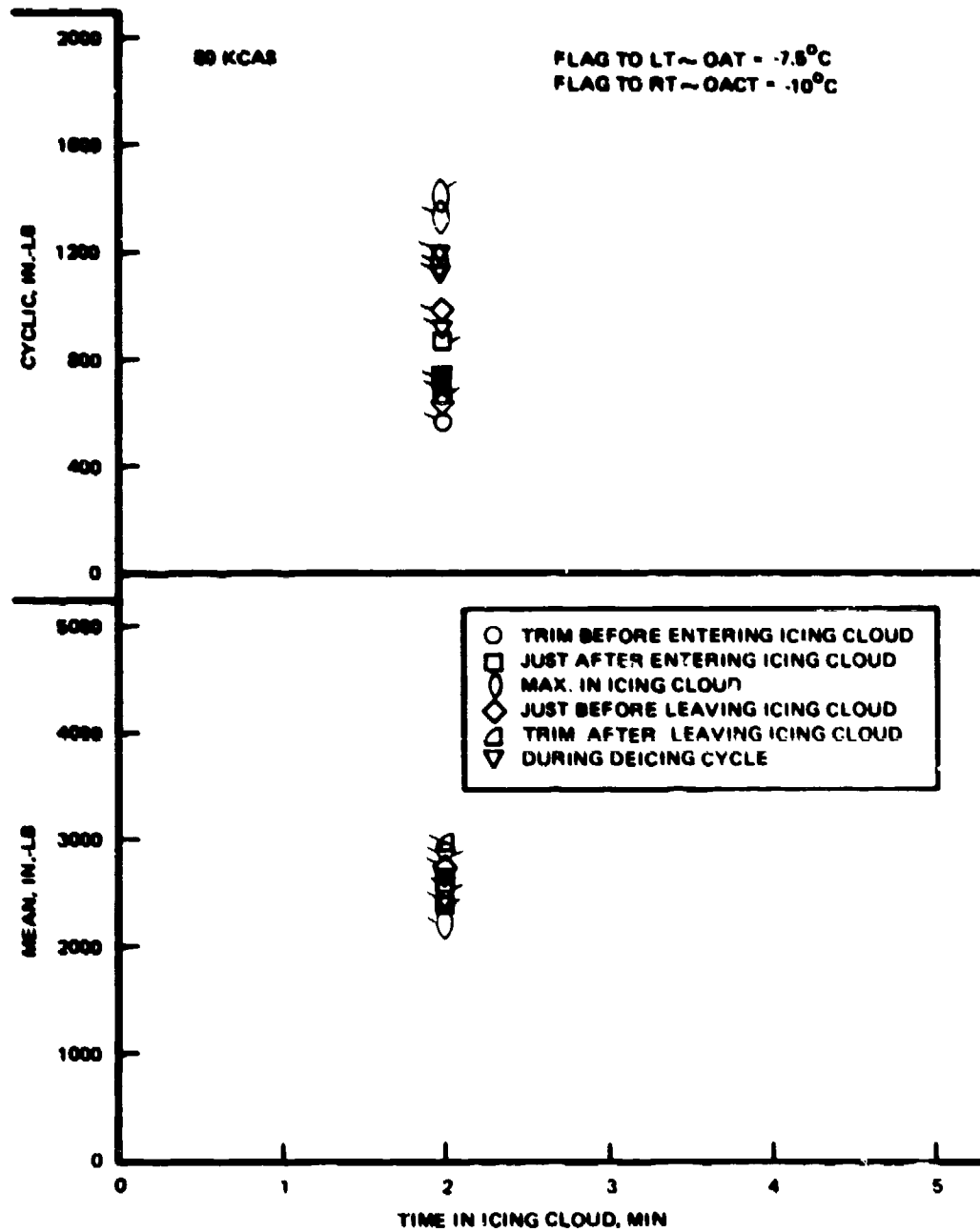
Figure 90. Tail Rotor Inplane Bending Moment at Station 11
With Deicing Boot Installed, 0.75 g/m³.
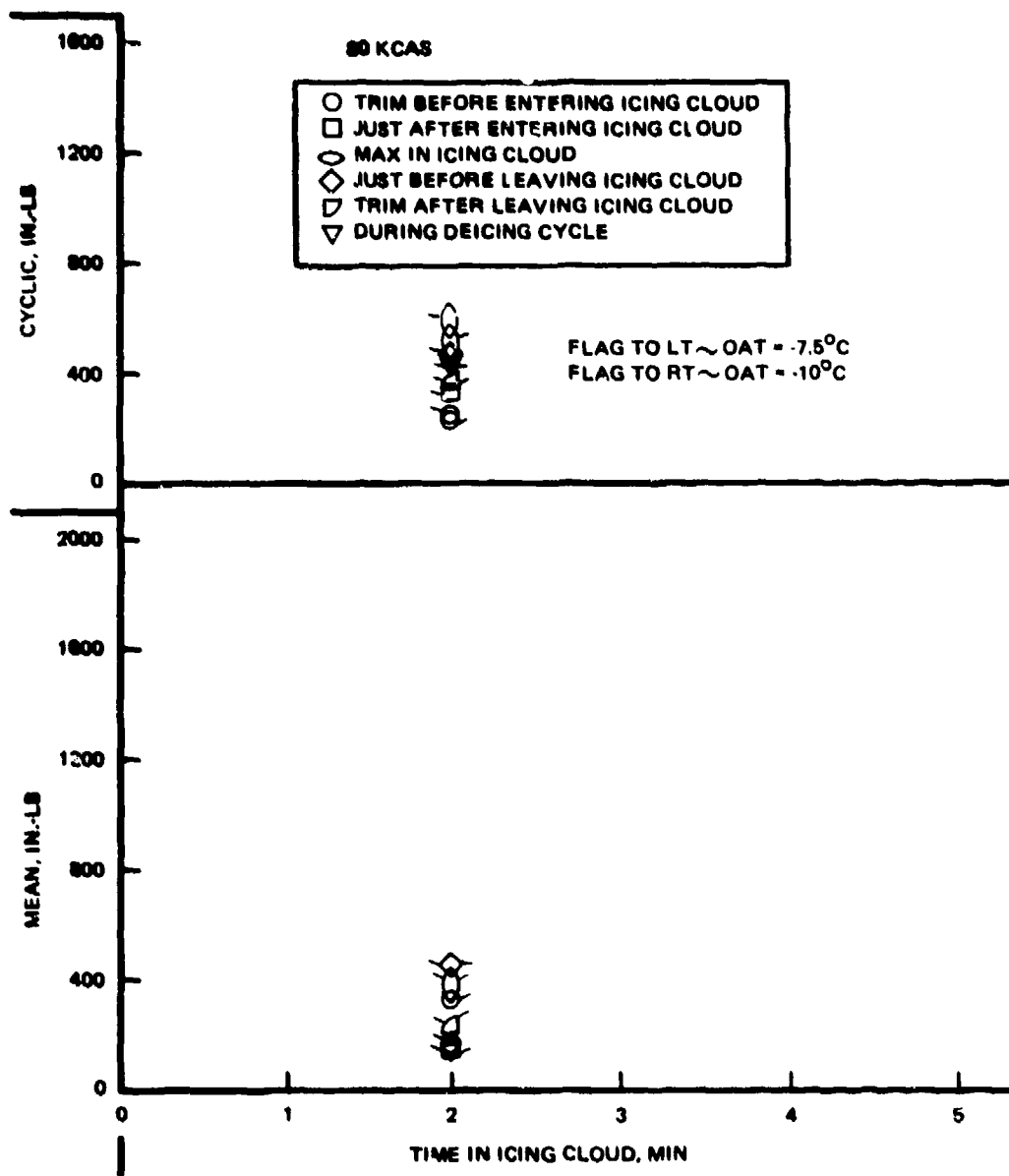
Figure 91. Tail Rotor Flap Bending Moment at Station 24 With Deicing Boot Installed, 0.75 g/m³.

176

had already accumulated. The loads measured were all within the flight loads measured during the dry air flight envelope expansion tests except for the tail rotor inplane bending moment at rotor station 11.

The tail rotor cyclic inplane bending moment reached a maximum value of 1750 in.-lb behind the tanker (Figure 84) as compared to the maximum of 1650 in.-lb that was measured during the envelope expansion tests at Edwards (Figure 60). This bending moment level is well within the structural capability of the tail rotor and below the maximum transient of 2200 in.-lb found in the measured records of the standard blade.

A time history of the main rotor flap bending at station 35 and the pitch link load during a typical deicing cycle is shown in Figure 92. These data are typical and show that there is no discernible change in loads before, during, and after the deicing cycle.

The tail rotor, because of the heat stream from the engine exhaust, was not in an icing environment. A difference in loads due to the turbulent wash from the tanker was evident.

Table 16 summarizes the predominant measured vibration response frequencies at the locations where vibration data were recorded and the approximate recorded response amplitudes. These data are presented for trim flight just prior to entering the cloud and while flying in the cloud.

The general vibration characteristics are not sensitive to being in the cloud or out of it. The only vibration that was significantly increased while in the cloud was the pilot's seat vertical 6P. This was probably due to the turbulence generated by the tanker helicopter.

The pilot's seat vertical vibration readings shown in the table appear to be high in general. It is not known whether these are real or due to a possible calibration error. In any event, the relative comparison, in and out of the cloud, would be unaffected.
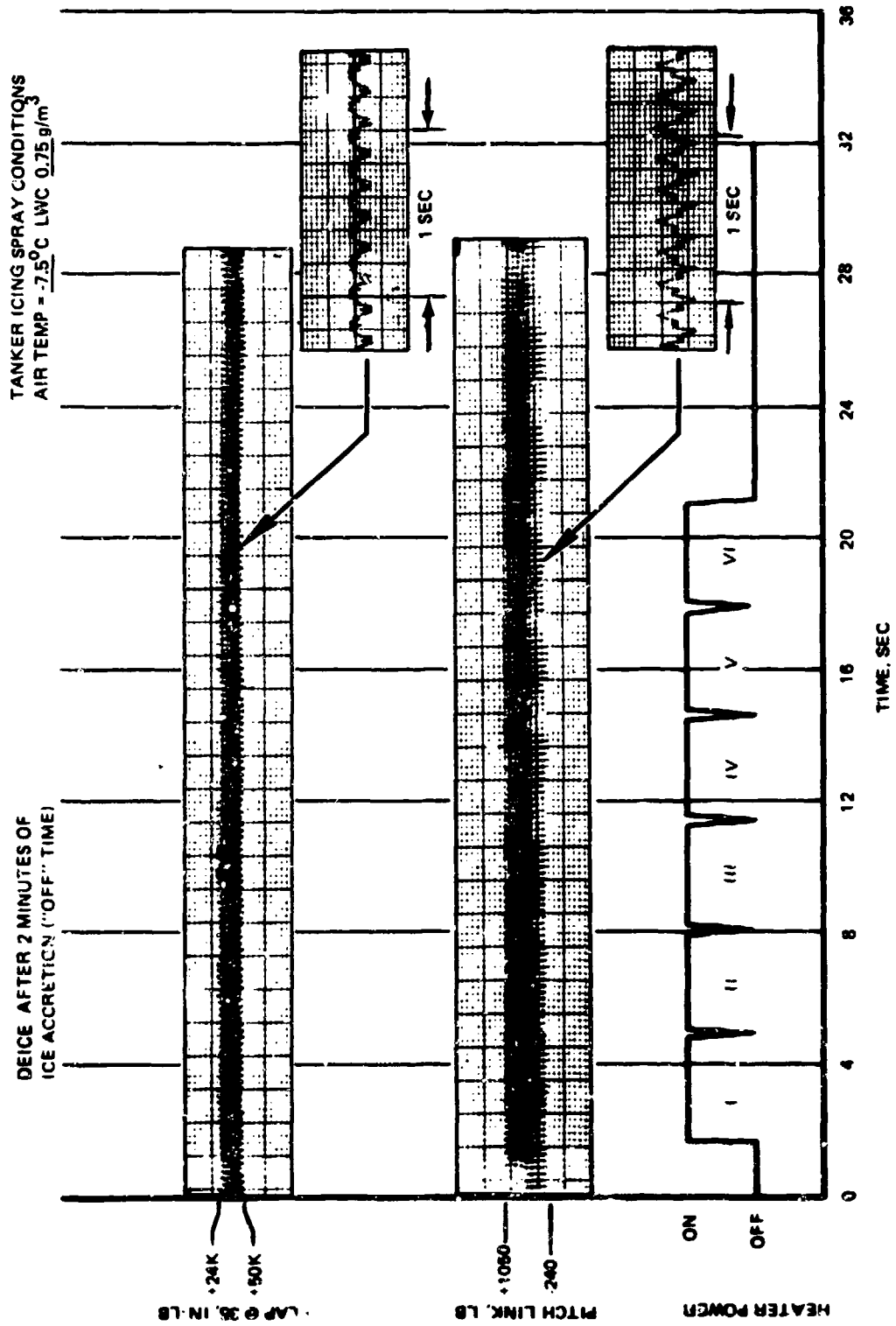
Figure 92. Main Rotor Loads During Deicing Cycle.

		Vibration Amplitude, g's	
TABLE 16. VIBRATION LEVELS RECORDED IN TRIM BEFORE AND AFTER ENTERING CLOUD			
Accelerometer Location	Vibration Frequency ω/Ω_R	Trim	In Cloud
Pilot's Seat Vert	1P	±0.2	±0.2
Pilot's Seat Vert	2P	±0.16	±0.15
Pilot's Seat Vert	6P	±0.1	±0.18
Pilot's Floor Long	2P	±0.12	±0.15
Pilot's Floor Lat	2P	±0.04	±0.07
Pilot's Seat Lat	2P	±0.02	±0.03
Pilot's Seat Long	2P	±0.05	±0.05
Pilot's Seat Long	10P	±0.3	±0.16
Tail Rotor Gearbox Vert	≈ 6P	±1.8	±1.8
Tail Rotor Gearbox Long	≈10P	±1.0	±1.2
Main Rotor Gearbox Lat	≈13P	±1.0	±0.7

A review of the vibration data was also made during the deicing sequence. The data, which was substantiated by pilot and observer comment, shows there was virtually no effect on airframe vibratory response during the deicing sequence at any of the vibration frequencies.

5.5 ROTOR BLADE THERMAL PERFORMANCE

A limited amount of blade temperature history data were obtained during the icing runs. Figure 93 shows, for example, the results of performing the deicing cycle in or out of the cloud (at -10°C). It is seen that the latent heat of fusion of the impinge had a slight effect on the blade unheated equilibrium temperature (the temperature pri
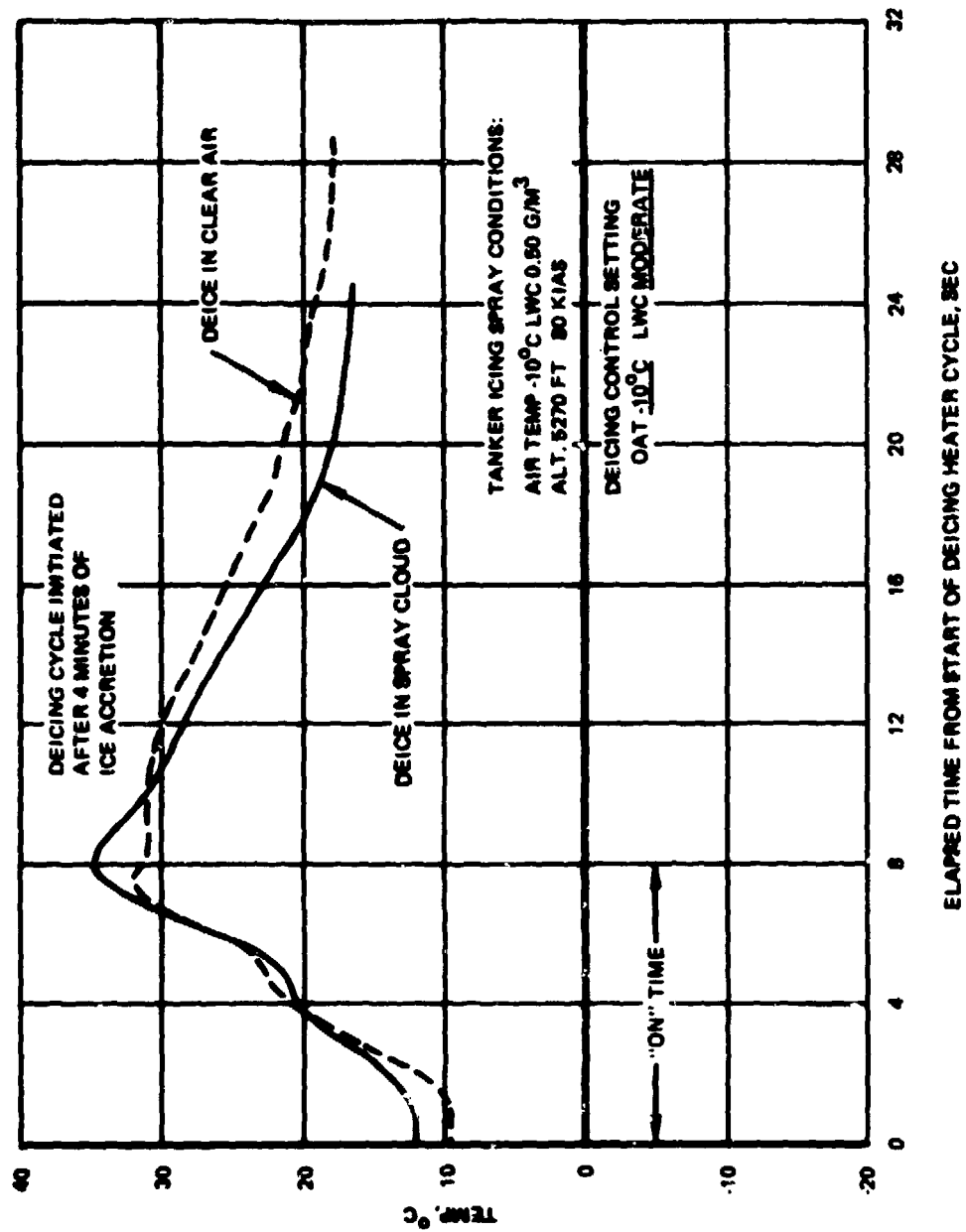
Figure 93. Comparison of Zone VI Heater Temperature During a Deicing Cycle in and out of the Icing Spray.

to the start of deicing); i.e., the blade temperature in the cloud is higher since the impinging droplets which freeze release their latent heat of 144 Btu/lb. The cooldown in the cloud, on the other hand, is faster since the droplets impinging on the surface (above freezing) absorb heat since they are sensibly heated to the surface temperature. The absolute magnitude of the blade temperature level, however, appears to be incorrect since all the temperatures are noted as being above freezing. In addition, there is a change in the temperature-time slope at 4 seconds, which corresponds to the time of ice release (presumably at 0°C).

Figure 94 shows the temperature-time history for four main rotor stations at an ambient of -5°C. This curve clearly shows the effect of kinetic heating along the rotor span. At this ambient temperature the blade will be ice free along the outboard 50 percent of the span due to the kinetic heating. Ice shedding is discernible only at station 45, as a change in temperature slope.

Figure 95 is a summary of the measured temperature rise at station 45 as a function of semiautomatic OAT control setting for light (160 volts) and moderate (200 volts) icing intensity settings. The clear air temperature rise is, as would be expected, higher than during icing. The temperature rises during icing for both the light and moderate settings indicate a satisfactorily conservative level above the ambient temperature datum.

Figure 96 is a correlation of predicted and measured temperature rise at station 45 for an ambient temperature of -10°C. This run consisted of three consecutive deicing cycles. It was reported by the space plant that it appeared that the ice had not shed inboard on the first cycle; therefore, two subsequent cycles were performed in an attempt to clear the residual ice. On the first cycle, the measured temperature shows a flat spot for 2 seconds (at an indicated temperature of ....). Allowing for the probability of instrumentation EMI problems, ...
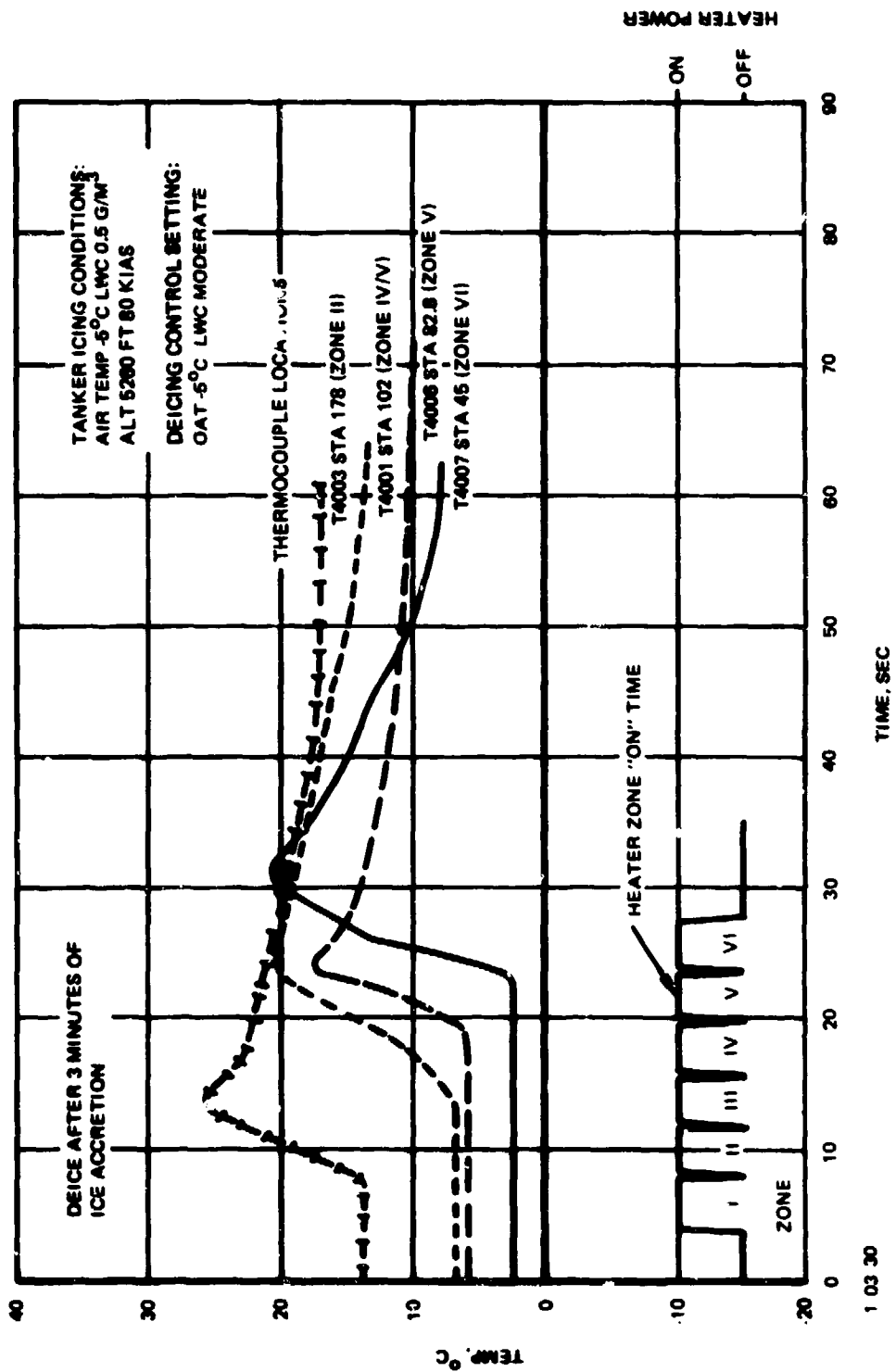
Figure 94. Main Rotor Blade Heater Skin Temperatures During Deicing System Test.
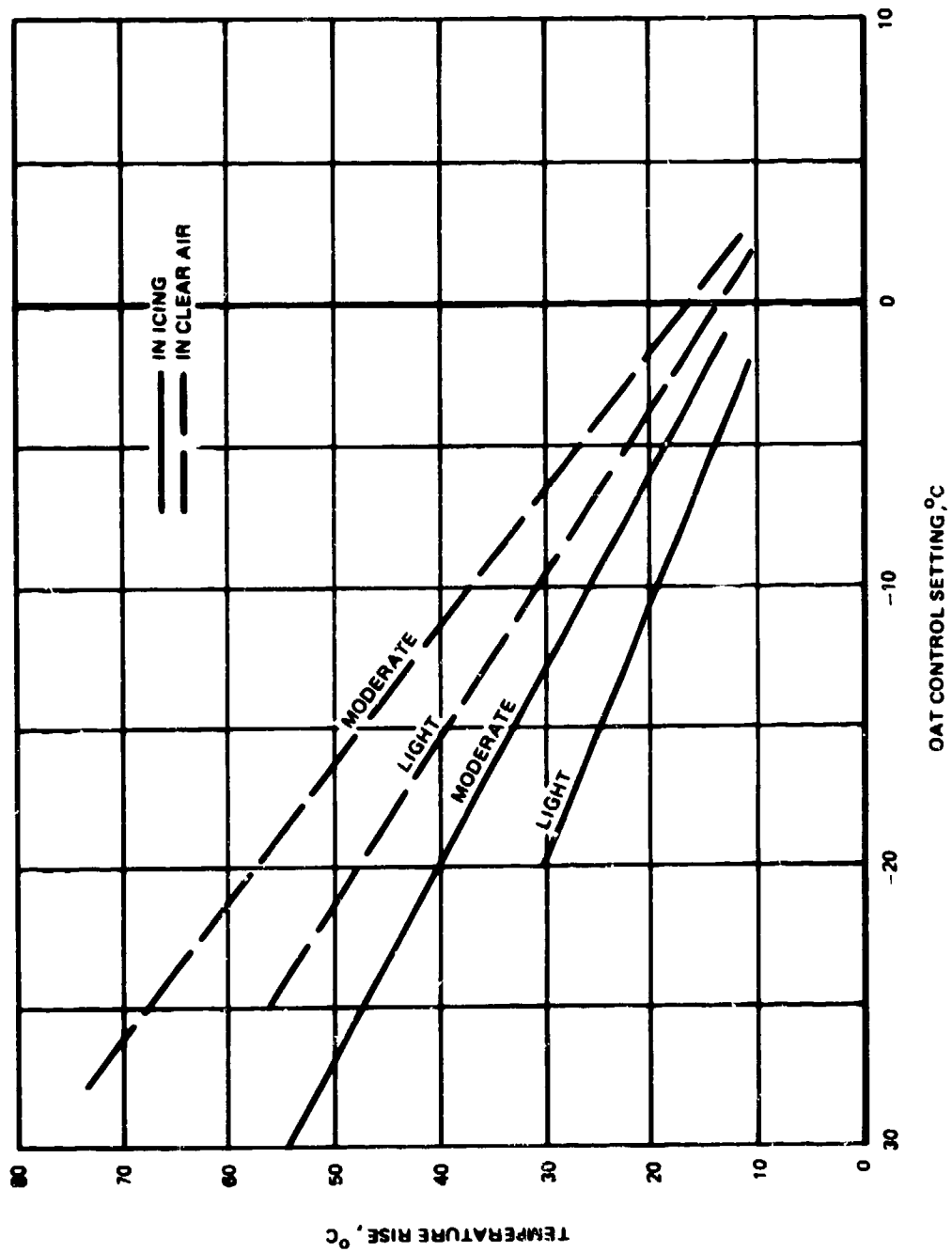
Figure 95. Skin Temperature Rise of Main Rotor Blade at Station 45 With Varying OAT Control Setting.
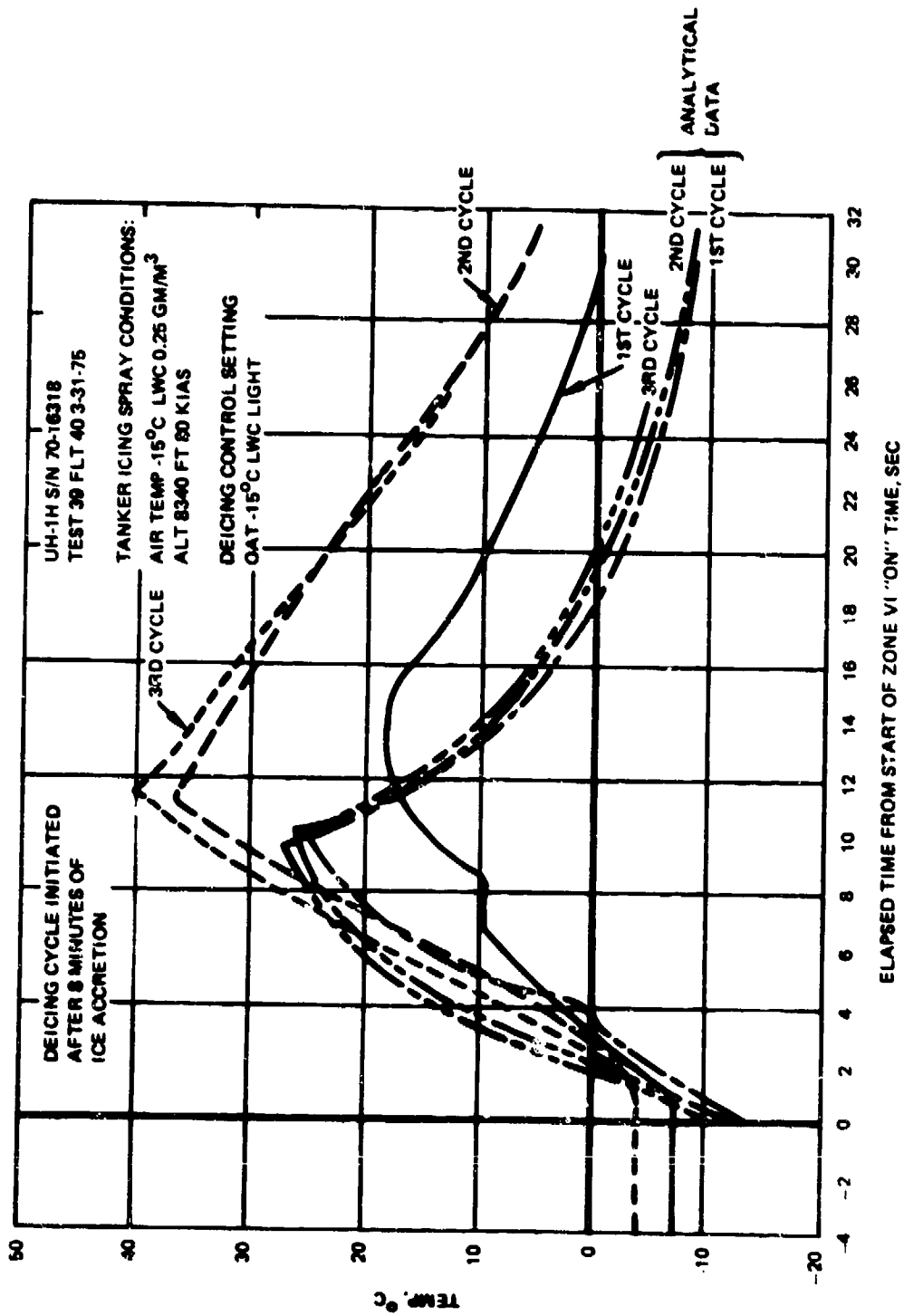
Figure 96. Comparison of Zone VI Deicing Heater Temperature During Repeated Cycles in Clear Air To Deice Zone VI.

since the correct initial temperature should be -14°C, the flat spot
can be attributed to the melting of an ice layer (at 0°C) and the
subsequent formation of a cavity under the ice. It is to be noted
that the subsequent measured temperature rises are higher than the
predicted values. This would occur as a result of the insulating
effect of a layer of ice over the surface. The thermal model used
for the analysis accounted for thermal capacity of the ice and its
thermal conductivity but presumed that the ice shed at 0°C.

Unfortunately, none of the movies or still photographs that were taken
indicated the extent of ice which failed to shed during the -20°C
condition (shedding was reported by observers in the chase plane as
being complete during the -15°C test conditions). There are two
phenomena which could have contributed to the reported incomplete
shedding:

1. An ice ridge at the station 83 production break. This can
   be corrected in a heating element redesign either by locally
   increasing the power density or by using a continuously heated
   parting strip on either side of the break.

2. The ice anchoring to the unheated area inboard of station 50.
   The heated area inboard of station 50 extends only 1 inch on
   either side of the leading edge, whereas the ice catch with the
   large (150-micron volume median diameter) droplets from the
   HISS extends substantially further aft of this point.

Figure 97 presents a comparison of the expected water catch distribu-
tion on the main rotor blade as would be experienced in natural icing
with that occurring behind the tanker. It is seen that the large
droplets result in double the total catch rate per foot of span for a
given liquid water content; alternatively, the leading-edge catch
rate is approximately 40 percent higher (for equal liquid water contents),
and impingement extends approximately 100 percent further aft behind the
HISS than would be experienced in natural icing. Although the catch rate
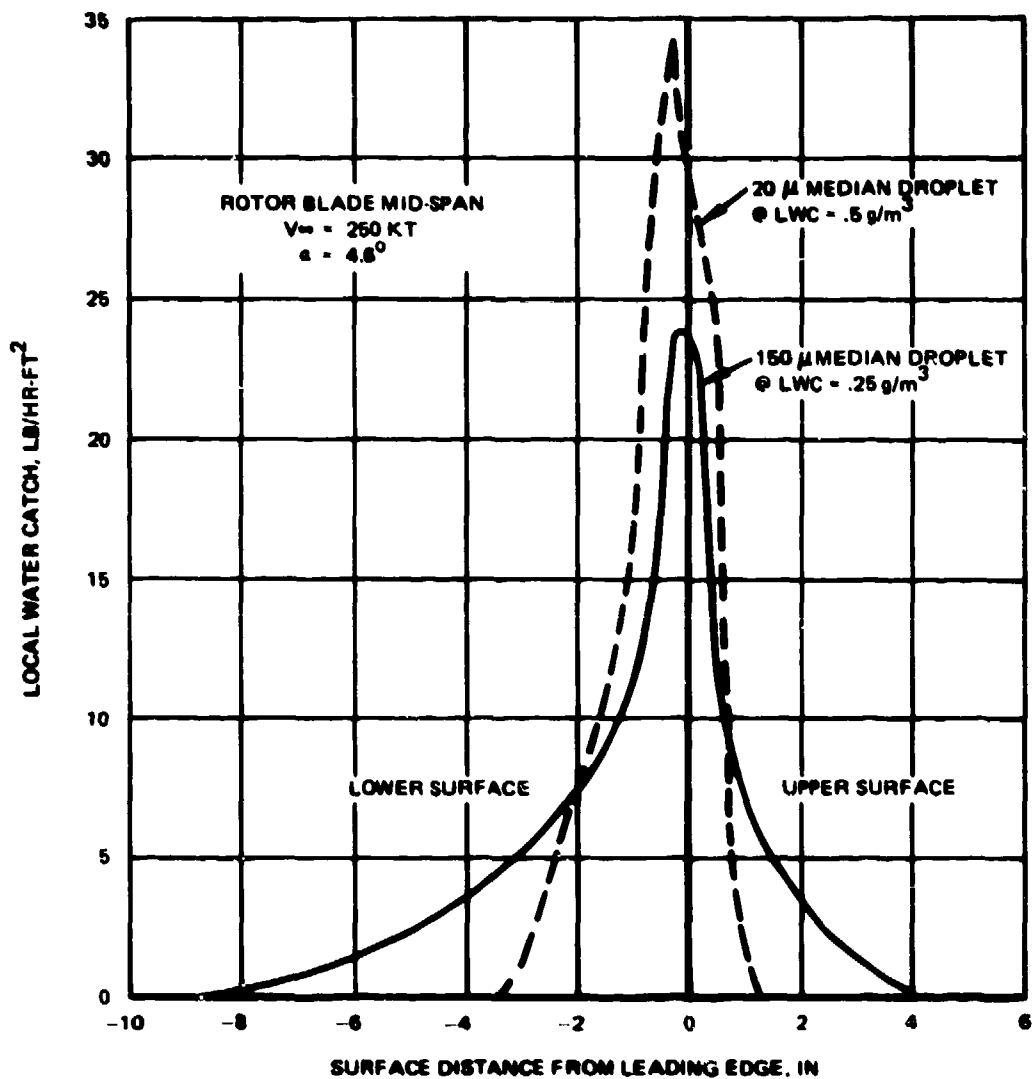
Figure 97. Local Water Catch Distribution for Two Droplet Sizes at the
Liquid Water Content Required for Equivalent Total Water
Catch.

behind the HISS is double that for natural icing, the severity of icing
is generally evaluated at the leading edge; and thus tanker icing could
be taken as at least 40 percent more severe than natural icing.

5.6 WINDSHIELD ANTI-ICING

The anti-icing characteristics of the windshields were considered to be
satisfactory at each combination of liquid water content and ambient
temperature tested. At no time was there any evidence of ice clinging
to either windshield within the heated areas. Accumulations of ice
were outside the heated areas and on the wiper blade assemblies. The
thickness of this ice varied with liquid water content, temperature,
and time duration within the icing cloud. The wiper blades were
effective in keeping the windshields clear of water film when they were
used to improve the pilot's view of the HISS tanker during flight in the
spray cloud. (An annoyance, however, was the wiper travel onto the ice
outside of the heated area. It is concluded that the wiper travel should
be modified to eliminate this problem.) An example of typical ice
accumulation outside the heated windshield areas can be seen in Figure 16.

The pilot's windshield cycled normally at 160, 200 and 250 volts during
both dry air and icing operation. The copilot's windshield had a slightly
longer ON time than the pilot's windshield at 200 and 250 volts. At
160 volts, in cold air and in icing conditions, the ON time of copilot's
windshield increased substantially and at temperatures below -10°C stayed
on almost continuously.

During the initial tests at Moses Lake, the variable voltage control
(Variac) to the copilot's windshield failed and a replacement was not
available; therefore, it was not possible to determine the voltage
required by the copilot's windshield to obtain an ON-OFF cycle similar
to the pilot's windshield at 160 volts, although the copilot's wind-
shield was satisfactorily anti-iced at all "Variac" (low-volt) condi-
tions tested down to -20°C.

5.7   ICE DETECTOR/SEVERITY METER PERFORMANCE

As discussed in Section 2.4, two ice detector sensing units were
mounted on top of the fuselage (Figure 16). Fundamentally, these
units are ice detectors, with their output signals processed as
appropriate to provide indications of liquid water content. Figures 98
and 99 show the response of the ultrasonic unit in several different
spray cloud densities. As previously noted, the HISS cloud has a ver-
tical extent of the order of 5 feet; this results in the ice detectors'
normally being positioned near the edge of the cloud when the main
rotor is positioned near the center (Figure 75).

Thus, the detectors will indicate a below-average cloud liquid water
content. Figure 98 does show the effect of a penetration of the
sensor through the cloud and provides a measure of the vertical
distribution. The nominal liquid water content noted on the figures
is obtained from the calibration data for the HISS.

These data show that the ultrasonic unit provides a very rapid response
to local icing severity conditions and that it apparently yields at
least a good measure of relative icing severity. Further testing under
natural icing conditions is needed to establish its usefulness in pro-
viding signals for the modulation of the rotor deicing system.

Only one problem was experienced with the ultrasonic system during
the icing tests: the probe and mounting strut generally failed to
deice automatically, and it was necessary periodically to deice the
unit manually (by pressing the test button, which activates the
heating unit).

Unfortunately, no data were obtained with the infrared sensing system
as the icing severity circuitry was not operable, and all icing
signals from the sensor were being processed through the LWC
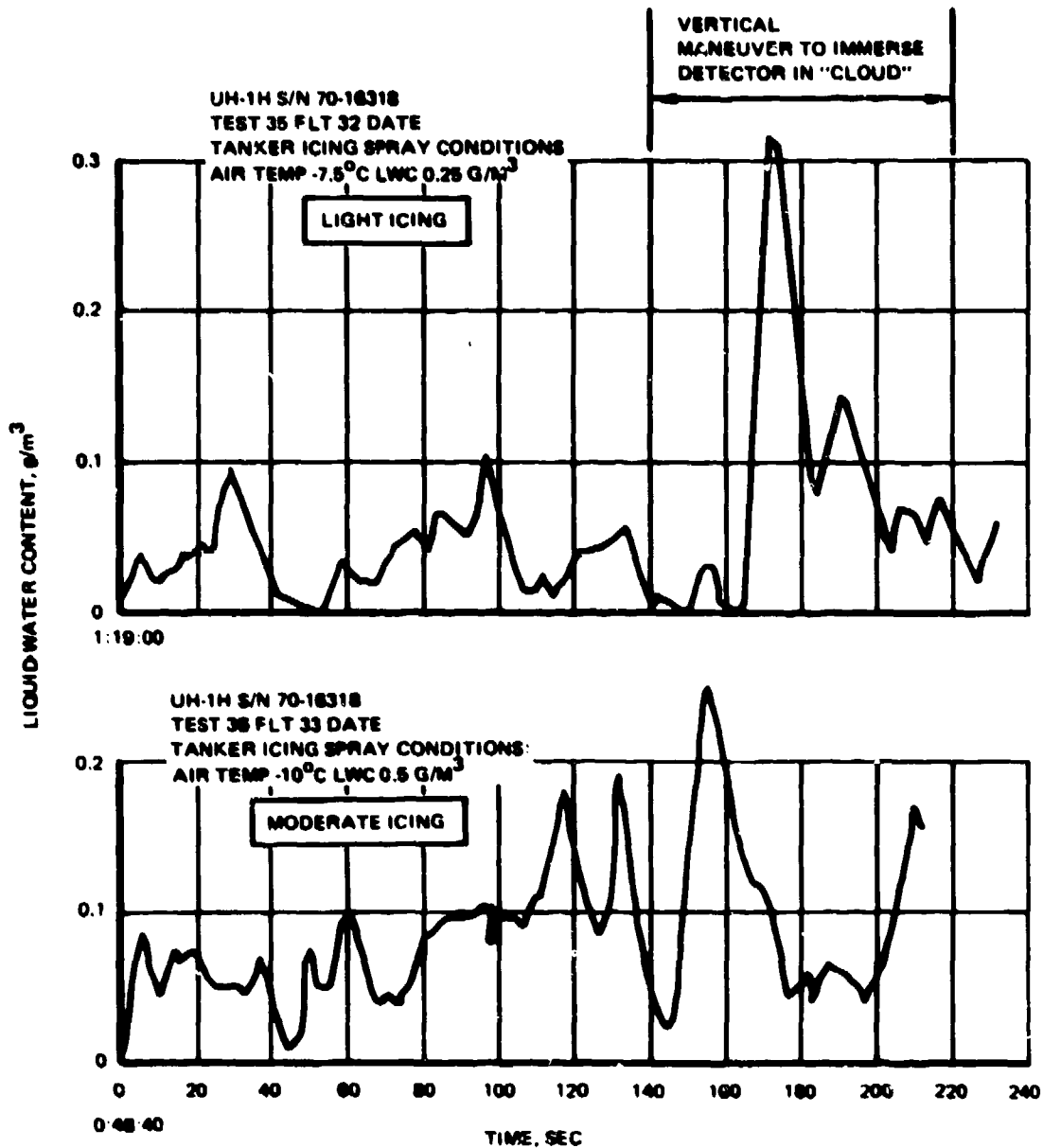
Figure 98.   Liquid Water Content Meter Performance.
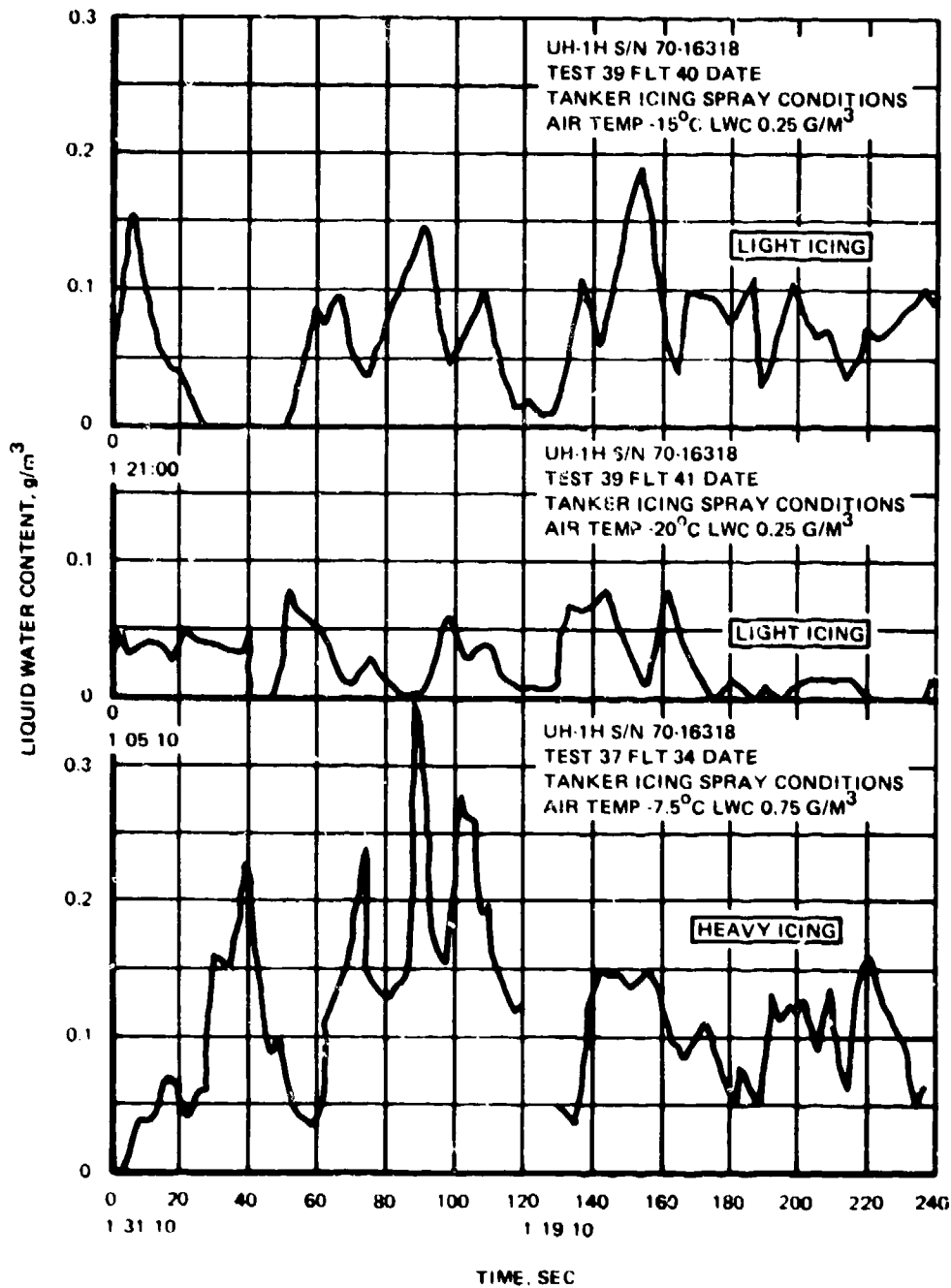
Figure 99. Additional Liquid Water Content Data.

component. Ground checkouts indicated that the detector portion of
tne system was apparently functioning properly.

Figure 16 shows the ice accumulation on the ice detector masts on top
of the cabin roof after a typical test flight. It can be seen that the
ice accretes well down on the supporting mast, implying that for tanker
spray tests, at least, the masts need not be so high; however, the
smaller droplet size in natural icing clouds might produce different
results. A change in mast height should be deferred, therefore, until
completion of natural icing investigations.

5.8 STABILIZER BAR

The energy levelc which were established and used for stabilizer bar
anti-icing proved to be effective in preventing the formation of ice
on the heated area of the arm and tip weight (Figure 100). Actuation
of the system, however, is currently tied into the ice detector signal:
heat is not applied until icing is encountered. The transient response
of the assembly is such that, based on analysis, the coldest heater sur-
face temperature (midway between the heater wires) does not reach 0°C
(from -18°C) until approximately 8 minutes after the application of heater
power. Thus, it is concluded that the stabilizer bar anti-icing system
should be actuated prior to entering the icing condition and that the
ice detector signal requirement should be deleted. This is the procedure
that was used in the test program to obtain proper anti-icing.

5.9 UNPROTECTED AREAS

Some of the unprotected areas on the aircraft that experienced significant
ice buildups during the testing (although the ice didn't cause any problem
or generate any concern during the program) are potential problems. They
could be FOD sources for the tail rotor or adjacent aircraft in formation
flight and, therefore, should be monitored in future testing.
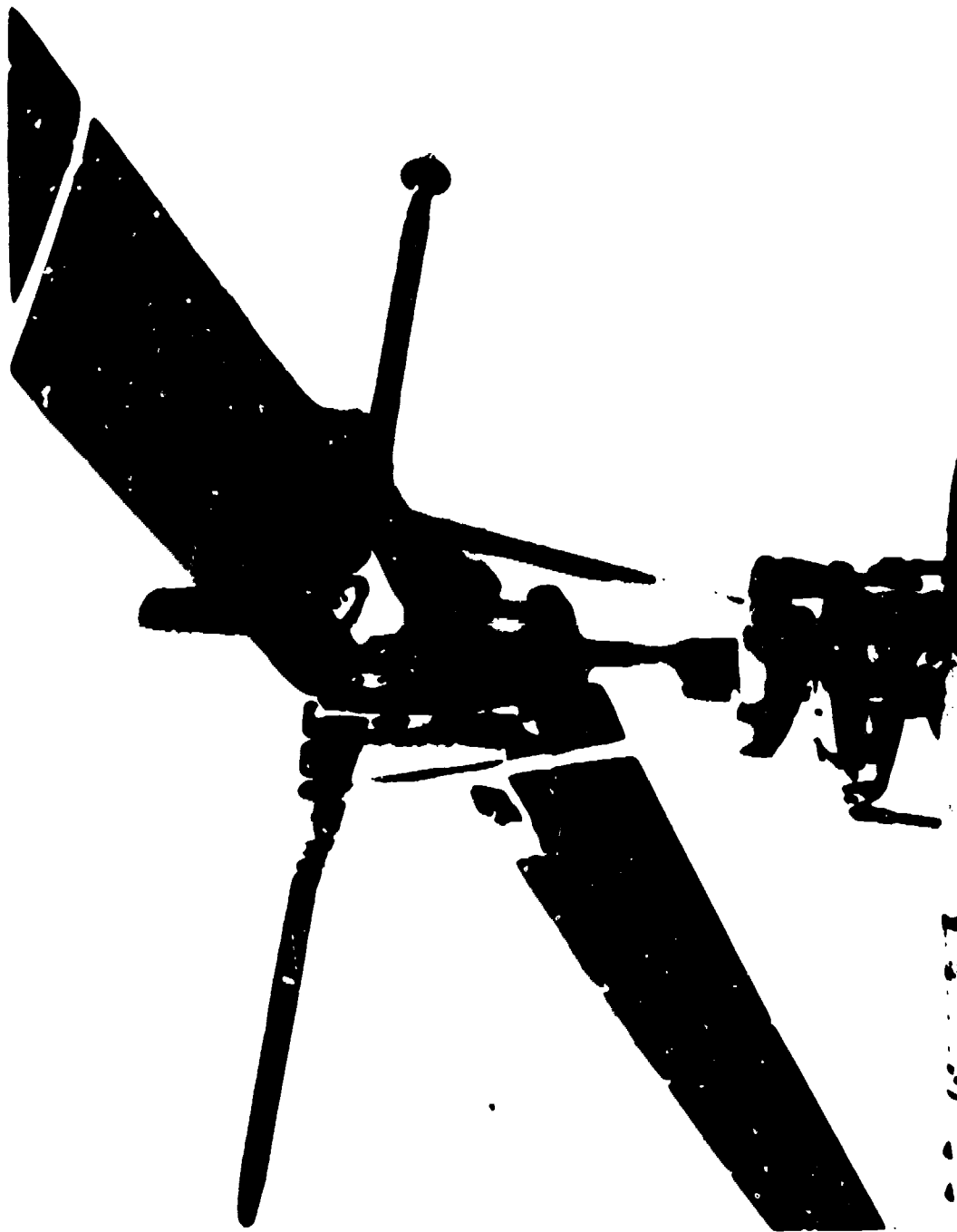
Figure 100. Typical Stabilizer and Rotor Head Condition at the Completion of an Icing Test Flight.

a. R. H. synchronized horizontal stabilizer

b. Aft fuselage vertical pylon

c. Battery vent

d. Rotor control Rods

e. Fuselage nose

f. FM whip antenna

Figure 101 shows the ice buildup remaining on the horizontal stabilizer and vertical fin after return to base. Observation of the movies taken from the chase plane indicate ice accretion over the entire upper surface of the horizontal stabilizer. (This is to be expected because of the relatively large water droplets from the HISS and the increased negative angle of attack.) The ice buildup on these surfaces was not noted to cause any problems but does serve as an indication of the total accumulation on an airfoil. The maximum leading-edge accumulation observed on the ground was 1 inch on the right hand horizontal stabilizer and approximately 1/4 inch on the vertical fin. The left hand horizontal auto-stabilizer appears to be kept ice-free by engine exhaust heat.

Figure 102 shows typical ice buildup on the battery vent. In one instance, the ram air inlet was almost closed. It is recommended, therefore, that the system be redesigned to incorporate a different type of ventilation such as an internal fan or a much larger scoop or a baffle.

Figure 100 shows typical ice collection on the main rotor control rods. Although a substantial amount of ice built up on the control rods, swashplate and pitch links, there was no problem with aircraft control. Ice thicknesses of 1/2 inch were measured on the blade attach fittings. The ice texture which was seen at all ambient temperatures was of the glaze variety and closely matched the description of freezing rain, which can be found on pages 21 and 22 of Volume I of this report.

Figure 101. Horizontal Stabilizer and Vertical Fin Icing.
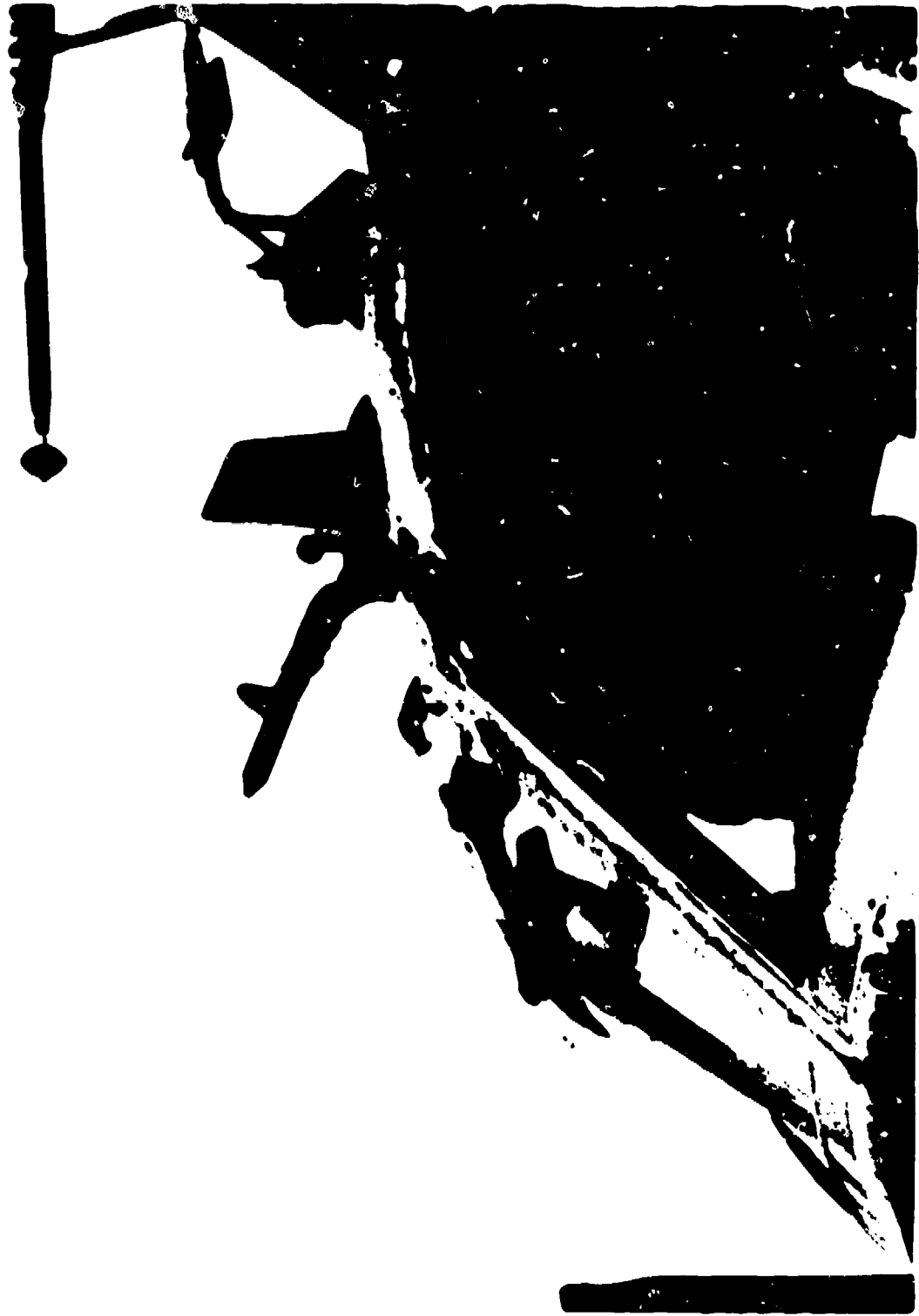
Figure 70. Icing of Battery Vent on Fuselage Vent.

Much of the helicopter nose was covered with ice and this, too, is symptomatic of the large droplets existing behind the tanker. The principal effect of nose icing would be the icing of the chin bubble window. The test crew, however, did not believe that the icing which was experienced represented a potential operational problem or hazard. It is also to be noted that the much smaller water droplets associated with natural icing would only impinge close to the immediate stagnation area of the nose and are not likely to cover the entire window.

Previous icing of the UH-1H[3] showed that the FM whip antenna oscillated violently with ice on it, and several inches were broken off by the tail rotor. The recommendation was made (reference 3) that the antenna be canted an additional 12.5 degrees by a wedge; and this was done for this program. Observation from the chase aircraft on the first icing flight were that the antenna continued to whip violently due to ice changing its natural frequency; therefore, the antenna was removed for the remaining test flights. It is recommended that the antenna be moved to a new location or that a flush antenna be used if it is available.

There was no icing of the engine air inlet screen of any significant magnitude. On one flight, ice buildup on the right-hand side was noted (Figure 103), but this condition was not consistent.

5.10 EFFECT OF ICE ACCRETION ON AIRCRAFT PERFORMANCE

Data were recorded during the testing to assess the incremental changes in power required due to flight operations under icing conditions. The parameters recorded at each trim point by test and flight number are presented in Table A-1 in the Appendix of this report.

(3) Mittag, Maj. Carl F., UH-1H HELICOPTER NATURAL ICING TESTS, US Army
     Aviation Engineering Flight Activity Report 74-77, Volume I of Rotary
     Wing Icing Symposium, 4-6 June 1974.

Figure 103. Engine Inlet Screen Icing.

For a deicing cycle, the change in torque pressure between the trim point provides a measure of the change due to ice accretion. These changes are considered approximate as in the case of repeated ice accretion and deicing cycles there is no way to account for the ice remaining on the blade resulting from an incomplete ice shed after a deicing cycle. In addition, the chase aircraft observers reported many instances of ice leaving the aircraft after exiting the cloud and before the deicing cycle (during ambients of -7.5°C and warmer), thus affecting the delta change measurements.

The torque changes due to main rotor and fuselage ice buildup have been summarized in Table 17. The average torque increase for the main rotor icing above that required for level flight is shown to be 12.3 percent and varied between 0 and 28.3 percent for all conditions tested. The average torque increase due to ice buildup on the fuselage and approach rotating components was 5.7 percent and varied between 0 and 9.7 percent. The average value of the combined torque increase for the main rotor and fuselage ice buildup was 18.6 percent and varied between 0 and 31 percent.

The wake and vortex pattern behind the tanker result in the test aircraft flying in a simulated climb condition to maintain its position in the icing cloud. From nonicing test data, the torque increase was found to be 44 percent when flying behind the tanker. During the icing tests, torque pressures of 42 to 50 psi were reported under some test conditions and reflect torque increases of 58 to 78 percent, respectively. This higher level of power required in the cloud with resultant increase in exhaust gas temperature (55-65°F) may also contribute to anti-icing of the tail rotor by the engine exhaust wake. Natural icing tests will have to be conducted before this effect can be confirmed.

TABLE 17. SUMMARY OF ENGINE TORQUE INCREASES DUE TO ROTOR AND FUSELAGE ICING

6.0 NEW INSTALLATION PROBLEM AREAS

6.1 MODIFIED ROTOR BLADES

Visual inspection procedures for all new installations were prepared and utilized during the test program to assure flight safety. These inspections included preflight, daily, and 25-hour inspections.

The modified rotor blades were given special attention because of the limited testing and number of blades fabricated (a total of four main and three tail blades were modified for use in the test program) prior to flight operations. Before any testing, the main and tail rotor blades were inspected by the "C" scan ultrasonic method to verify bonding integrity and to document their initial or zero time signatures as described in Section 5.2 of Volume I. In addition, the first main rotor blade that was modified was used as a teardown specimen to verify bonding procedures. The initial "C" scan and visual inspection of the teardown blade cross-sectional cuts indicated low bond strength where the heater element braided wires ran under the erosion shield along the span of the blade. Therefore, shear and tension coupon specimens were cut from portions of the actual test blade as well as fatigue test specimens, and tests were conducted that established adequate structural integrity of the "good" bonded area. This is discussed in detail in Sections 5.2 and 5.3 of Volume I.

To further augment this aspect of the test program, a second "C" scan ultrasonic inspection was performed after the airworthiness testing and prior to the simulated icing tests. The blades had 34.4 total operating hours and 15.3 flight hours accumulated to that point. There was no change in the "C" scan recordings between that signature and the zero time signature, thus verifying the daily "coin" tap test indications. To minimize flight time usage of the modified blades, they were removed

200

for the ferry flights from Edwards AFB to Moses Lake, Washington, and
return. Daily "cold" tap tests and visual inspection of the blades were
also performed to monitor bonding integrity throughout the program. No
problems were experienced or discrepancies noted.

6.2 OTHER NEW INSTALLATION

In addition to the blade inspections and as mentioned above, all new
installations were monitored closely during the test program. No
problem areas were found until the end of the testing at Moses Lake,
when a postflight inspection revealed that the instrumentation conduit
standpipe wire guide that routed the deicing and instrumentation wires
up through the main rotor shaft to the slipring had failed at the top
end and had been in that condition for an unknown number of flight hours.
Teardown and inspection showed that the insulation had worn through sev-
eral of the deicing wires, and some instrumentation wires were actually
severed at the tube failure point. These exposed wires were obviously
the source of intermittent short-to-ground warning light indications
and instrumentation grounds that plagued the icing flight testing for
many of its hours. Figure 104 shows the condition of the wiring as
found during the teardown inspection investigating the tube failure.

Another problem found at the very conclusion of the program was a
loss of torque on the tail rotor retention nut. Design changes will
be required to preclude this situation as well as the main rotor wire
guide tube discussed above prior to any further testing.

No other problem areas in the test installations were identified. The
25-hour preventative maintenance check (performed twice during the pro-
gram) showed no problem with the ac generator drive or other new instal-
lation aspects.

In addition to the visual inspections of the generator and the main rotor
slipring installations, vibration pickups were mounted on the units to

check dynamic characteristics. No problems were indicated. The results of the measurements are discussed in other sections of this report.

6.3 BLADE HEATER WIRING

The major problem experienced during the program was several occurrences of short-to-ground electrical wiring failures in the power lines to the blade heaters on the main rotor blade. A total of four "short" failures were experienced and one "open." All of the failures were repaired at the test site by the test crew with a minimum loss of aircraft availability time. Four of the failures occurred on one blade at blade station 83 in the area where the power leads pass under the inboard edge of the steel erosion shield, and the fifth failure was at blade station 262 (26 inches from the blade tip). The failures are attributable to design and manufacturing details that can be corrected relatively easily on future blade/heater assemblies.

There are eleven flat braided power leads which run along the upper blade surface from the root end connector to the blade heaters at the outboard zones. At the station 83 production break, the eleven wires are routed under the steel erosion strip on their way out to the various heater zones. The first short to ground occurred between wire No. 2 (the second from the last toward the trailing edge of the erosion shield) and the erosion shield edge. It was detected by the ice protection system's fault detection circuitry and displayed a ground fault warning light in the cockpit. The failure was caused by a breakdown of the dielectric material between the sharp edge of the erosion shield and the wire braid. The breakdown occurred after 10.8 flight hours and approximately 25 total operating hours on the blades. Blade flexing in flight apparently had caused the sharp edge of the inboard end of the steel erosion shield to cut into the insulating material. When 230 volts of deicing electrical power was applied, arcing occurred.

Figure 105 shows the external evidence of the failure. Repair was made by trimming the corner of the steel erosion shield off and splicing in a piece of braid to replace the burned section. No structural damage to the basic blade was evident. The repaired area was covered with a non-conductive potting adhesive to restore blade contour.

The erosion shield edge is pressed hard against the dielectric material during the heater/shield assembly bonding operation. It apparently pressed harder than normal on th's one particular blade (the first flight heater assembly to be manufactured) because of the added thickness to the wire braids due to the solder rplice joints of the power supply lead wires and the erosion shield/heater assembly wires. This undesirable condition was noted on the first heater assembly and was changed by the deicer manufacturer relocating the splice 1-1/2 inches further inboar' and well away from the edge of the erosion shield.

Two of the other failures on this blade and station were similar in nature and cause. Figure 106 shows the external evidence of a short in the No. 1 wire (the end wire) which burned out approximately a 1-inch-long section of braid. Figure 107 shows the replacement braid splice soldered into place and the fiberglass cloth tape added underneath for better insulation. This failure was apparently a soldered splice that opened and caused the arcing across the gap. Figure 108 shows the repaired area closed with sealing compound.

Figure 109 shows the strap of braided wires in the Station 81-83 area after the outer insulation material was carefully removed to locate and repair another "open" that was experienced. It was found that each of the braids had a spliced-in section in this area and several of the solder joints were loose and/or questionable in addition to the one that initiated the problem. All of the questionable solder joints were repaired, and the area was covered over with a clear insulating and protective sealing compound as a final repair.

Figure 104. Main Rotor Slipring Wiring Condition Found on Disassembly
Investigation of Wire Guide Tube Failure.
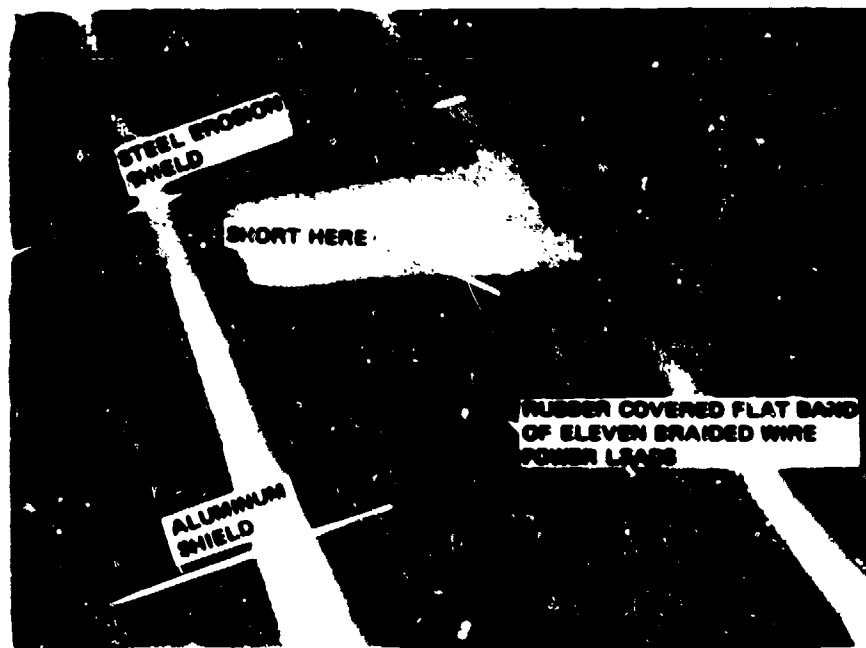
Figure 105. External Evidence of Wiring Short Failure No. 1,
Blade Station 83, Top Surface.

Figure 106. Electrical Short at Station 83 of No. 1 Wire.

Figure 107. Repair of Failure Showing Replacement Braid
Splice Section.
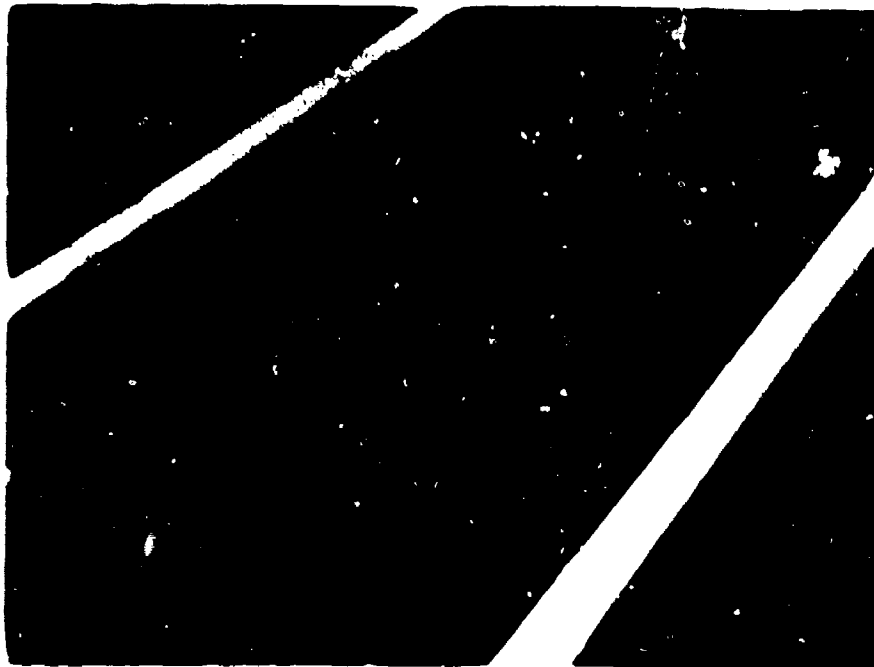
Figure 108. Station 83 Repair Area Covered With Sealing
Compound and Ready for Further Flight.
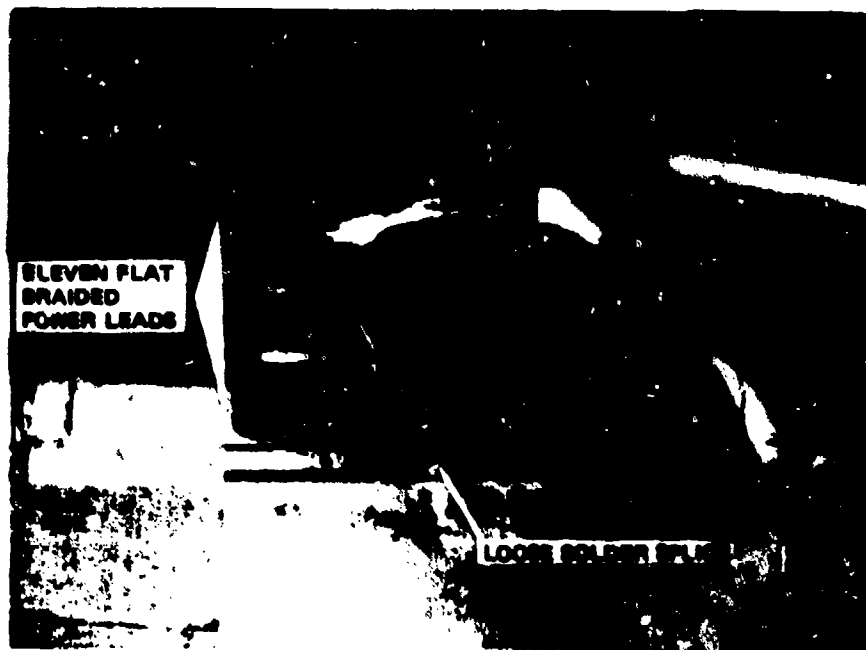
Figure 109. Station 80-83 Wiring Insulation Removed, Showing
Spliced Wires and "Open" Joint That Were Found.

The short at Station 262 was on a different blade and was on the underside of the blade. This short was also between the wire braid and the erosion shield. It was repaired by carefully removing a semicircular piece of the erosion shield at its trailing edge to uncover the braid. Physical evidence indicated that the braid was just under the edge of the erosion shield at this point instead of 1/8 inch in from the edge. This location apparently permitted moisture to penetrate a pinhole in the epoxy and fiberglass shield fairing and provide a path to ground. Figure 110 shows the repair area with the "sliver" of erosion shield removed thus exposing the braid. Careful manufacturing indexing techniques will prevent mislocation of the assembly in future assemblies as well as precautions to assure moisture sealing of any porosity in the shield/fairing joint.

6.4 BLADE HEATER DIELECTRIC STRENGTH

In the process of the troubleshooting investigations of the blade wiring short problems discussed in the previous paragraphs, measurements of the heater to blade/erosion shield dielectric integrity became routine. The results of these measurements showed a wide variation in dielectric strength between the three main rotor blades used in the program and in any one blade from time to time. It is hypothesized that this is due to moisture paths, admitting moisture into the blades. This is an area that warrants further investigation and action on a complete modified blade assembly prior to further development testing.

6.5 STABILIZER BAR HEATER ASSEMBLIES

The stabilizer bar is anti-iced (continuously heated), and its operation was checked during the system functional tests. Its power density is proportional to the generator voltage and, as discussed in Section 2, is 5 watts/in.^{2} at 200 volts. Operation was satisfactory at 160 and 200 volts. At 230 volts, however, one of the balance bar tip weight heaters burned out during one of the ground runs. It is believed that the failure

Figure 110.   Station 262 Failure Area After Steel Shield
Material Was Removed.

was a "simple" overheating of the part (Figure 111). The location of the
failure is surprising since the least cooling would occur at the inboard
end of the arm (least tangential velocity). Although the other parts
showed no visual damage, a "feel" inspection indicates that there was
substantial sponginess in the rubber indicating that some outgassing had
occurred. As a precaution, all heating elements were then replaced. A
thermal analysis was then performed to establish temperature limits for
a thermostatic control system. This analysis showed tha the heating
element could achieve a temperature of approximately 600°F in dry air (the
wires are spaced approximately 3/16 inch apart). This compares to an
allowable temperature of approximately 425°F based upon the char properties
of rubber. An overheat control system should limit the heater element to
approximately 300°F (the sensing element would be .010" behind the heating
element, and the temperature differential at 230 volts is 130°F to the
average temperature in the plane of the sensing element). It has also
been concluded that an etched foil heating element design would be superior
and would have prevented the burnout.

208

Figure 111. Stabilizer Bar Tip Weight - Failed Heater.

Operation with the second stabilizer bar heater assembly at Moses Lake revealed that after a very short operating period, a bonding separation between the heater and the tip weight was experienced. This could have contributed to the failure during the dry air ground tests but in any case implies that an improved bonding material such as a hot bond as opposed to the present cold bond should be used on future assemblies.

6.6 ELECTRICAL SYSTEM OPERATION

AC Electrical System

Incorporation of the ac electrical system in the UH-1H was accomplished with a minimum impact on the normal helicopter operating procedures. The electrical system, including the ac generator, the regulator and protection panel, ac generator/external power contactor, external ac power

monitor and ac bus, performed throughout the flight test program with only a minor problem occurring in the regulator and protection panel. Both the original flight regulator and protection panel and the spare unit developed a delay in energizing the ac bus after the engine had come up to normal operating rpm. Both malfunctions occurred after several hours of normal operation. Delays in energizing the ac bus varied from 5 minutes for the spare unit to as long as 20 minutes for the original flight unit. Subsequent laboratory testing established that the circuitry was temperature sensitive and would not actuate below 32°F. This problem has been corrected by the manufacturer.

Analysis of the ac electrical system performance showed satisfactory coordination between aircraft-generated ac power and external ac power and operation with a floating neutral. Further design resolution may be required in the use of certain external power carts which connect their ac system neutral to the control pins in the external ac power connector through a relay coil. This feature ties the ac system neutral to the aircraft's dc system (which uses the aircraft structure as dc return) and consequently removes the floating neutral.

Performance of the dc electrical system proved to be satisfactory throughout the flight test program. Use of the starter-generator as both the starter and the main dc generator required only minor modification to the startup procedure and coordinated well with the transformer-rectifier as the standby dc source. At light dc system loads, however, the dc generator did not automatically pick up the dc bus from the transformer-rectifier standby source. This feature can be corrected by slight design changes to the standby source reverse-current relay circuit.

Ground tests were conducted using a load tank to evaluate the cooling characteristics of the ac generator under varying electrical loads at voltage levels of 160, 200 and 230 volts. The results of these tests are presented in Figure 112 and indicate that the maximum temperature rise
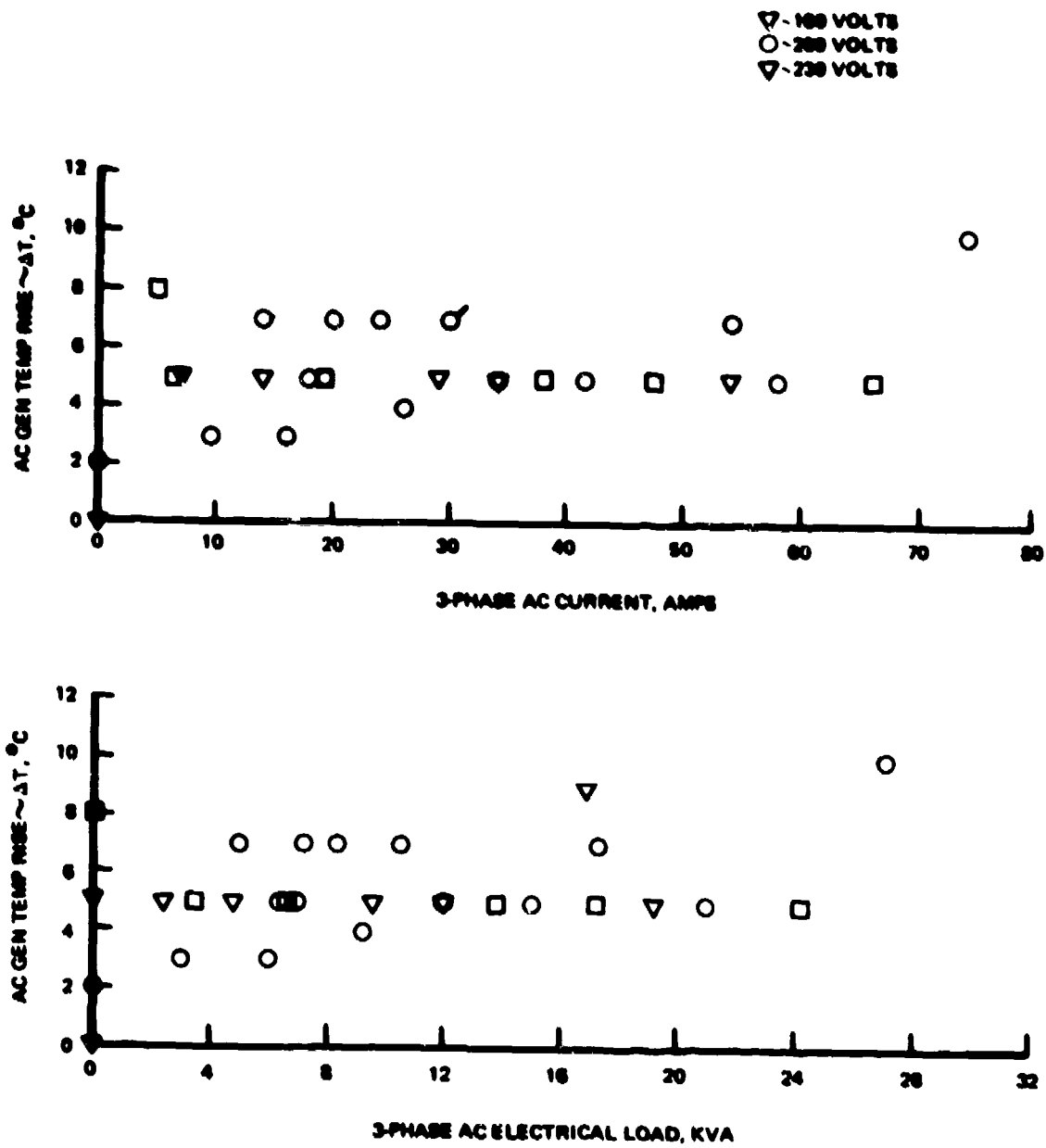
Figure 112. Temperature Rise of AC Generator Cooling Air
With Varying Electrical Load.

211

experienced was 18°F. The maximum inflight temperature rise experienced during this period of testing was 27°F. It would be expected that the temperature rise is proportional to the generator output instead of being almost independent. The measured inlet temperature was noted to be 20-30°F above ambient, and it may be that this reading for some reason is too high.

No problem of overheating is expected with such a small temperature rise during operation under heavy load. The ac generator is rated for satisfactory operation with its outlet air temperature at 300°F, and no condition of this type will be experienced during deicing system operation.

6.7 DEICING CONTROL SYSTEM OPERATION

The basic design concept of the deicing control system proved to be effective in satisfactory deicing of the main and tail rotors. Flexibility in the operational characteristics of the system allowed adjustments of the deicing energy to be made very simply and quickly.

Several problems were encountered in the initial operation of the control system. Most of these, however, were resolved during the early system flight tests. The various types of system problems and effected corrections were:

Electromagnetic Interference (EMI)

Electromagnetic interference and noise triggering of the control systems protection circuits comprised the most prevalent malfunction. Unsuppressed relays and other magnetic circuits in the basic UH-1H provided the basic source of interference; however, some capacitive coupling from the windshield power wires during switch-on of the windshields also occurred.

Protection circuits most susceptible to EMI were main and tail "open,"
main and tail "short," and controller "fault." All of these susceptible
circuits were immunized to EMI from the normal system operational sources
by the addition of ceramic bypass capacitors at key points in the circuit
cards of the control panel and deicing controller.

After addition of the bypass capacitors, no further EMI malfunctions
occurred until the mechanical failure of the wire guide tube inside of
the main rotor mast was experienced at Moses Lake. Failure of the tube
caused chafing of the heater power wires to the main rotor blades and
stabilizer bar and resulted in intermittent shorts of phase voltage to
structure. This was indicated by flickering at the "heater ground"
light on the control panel. The intermittent faults to structure were
a new, stronger source of EMI and cause triggering of the controller
"fault," main "short" and zone 6 shutoff circuits. Further addition of
bypass capacitors desensitized part of the susceptibility, but some still
remained at the end of the flight test program.

Controller Fault Overvoltage Sensing

Overvoltage protection in the control system (to shut the deicing system
off if the generated voltage were higher than that commanded by the
controller) tripped when a new ac voltage regulator was installed and
the copilot's windshield was switched on. The protection circuit toler-
ances were determined to be too tight for normal operation of the reg-
ulator and voltage variations due to unbalanced loading. The overvoltage
trip point was increased by 7 percent by changing calibration resistors
in the controller.

7.0 FLIGHT TEST CONCLUSIONS AND RECOMMENDATIONS

1. An ac electrical system can easily be installed on the UH-1H.

2. The fully heated pilot's and copilot's windshields provided very effective anti-icing to the minimum flight test temperature of -4°F. The windshield wiper travel, however, should be compatible with the heated area so that the blades do not stroke over ice beyond the heated area.

3. No main or tail rotor blade structural or dynamic problem was encountered over any part of the flight envelope investigated.

4. Main rotor boost-off control forces are reduced compared to a standard UH-1H aircraft.

5. Engine power increases of 15 - 20 percent (trimmed level flight) were noted due to icing of the main rotor blades under simulated icing conditions created by the HISS tanker. The ice buildup is typical of that allowed between deicing cycles under **natural icing conditions.**

6. The main rotor blade deicing system controls ice shedding in a manner that precludes perceptible vibration effects.

7. The rotor blade deicing system appears to be capable of providing protection throughout the range of continuous maximum and intermittent maximum icing conditions, although some modifications of the heating element design may be desirable around the production break at station 83 to assure complete deicing inboard of that station at the extreme cold temperature conditions.

8. No problems due to icing of the engine inlet screen or other unprotected surfaces other than the battery vent and the FM whip antenna were noted.

9. The battery vent should be relocated or redesigned, and the FM antenna should be relocated to prevent it from striking the tail rotor due to ice buildup changing its dynamic response or fatiguing the mounting.

10. The failures that occurred in the main rotor blade deicer power feed lines were repairable in the field. The failures, however, do emphasize the need for the highest degree of quality control throughout the manufacturing process to assure reliability.

11. The dielectric strength of the main rotor deicer assemblies (as measured at the cable connector) between the heating element and the blade deteriorated with time at Moses Lake. It is believed that the problem is due to moisture penetration at some point(s) in the circuit. It is recommended that humidity testing be performed in the laboratory to determine the cause of the problem and thus effect a permanent repair.

   No problem was noted with the tail rotor deicers, and the dielectric strength was measured at a minimum of 500 megohms (compared to a requirement of 3 megohms).

12. The timer/controller system performed well after the initial development bugs and EMI problems were eliminated. The fault sensing provisions were extremely useful and accurate in providing reliable fault indications.

13. The ac generator voltage regulator has some minor problems which have been corrected.

14. Further flight testing in natural icing is required to evaluate the effectiveness and necessity of an ice detector/icing severity system and also to establish a recommendation on system design. Both systems tested (the ultrasonic and the infrared) had problems but offer promise.

15. The icing cloud generated behind the CH-47 HISS tanker was too limited in size, particularly height, to achieve an adequately uniform cloud over the test aircraft. Also, the downwash generated by the tanker on the test aircraft resulted in an increase in vibration, structural loads, and power requirements.

Table A-1. UH-1H DEICING TEST PROGRAM TRIM POINT DATA

Test Condition	Acft's OAT(°C)	Test OAT(°C)	Sys OAT(°C)	CAS (kts)	Alt. (ft)	Inlet ΔP (in. H₂O)	Torque (psi)	N₁ (%)	EGT (°C)	Fuel Coll. Pos(%)	RPM (lb)
LCC Test 27 Flight 17											
Trim (baseline)	-4	-4.3	0	81.5	6200	6.5	29	92.2	490		1075
Trim (in tanker)	-4	-4.1	0	79.0	6200	8.0	37	95	523		925
Trim (downwash base-line repeat)	-4	-4.4	-1	81.5	6280	6.5	29	92.2	489		820
Trim (with 2 min ice)		-4.2	-5	80.5	6100	7.0	31	93.0	496		760
Trim (after deicing)	-4	-4.4	-2	84.0	6200	7.0	31	92.8	494		700
Trim (with 4 min ice)	-4.5	-4.5	-2	85.0	6220	7.0	33	93.2	500		610
LCC Test 30 Flight 26											
Trim (baseline)	-4.1	Inop	-1	75	8320	6.0	26	92.2	492	52	1190
Trim (with 6 min ice)	-4.1	Inop	-5	75	7920	6.0	30	93.0	500	53	1100
Trim (after deicing)	-4.1	Inop	-5.5	75	8020	6.0	27	92.2	494	50	1040
Trim (with 8 min ice)	-4.1	Inop	-6	75	8130	6.0	30	93.5	500	50	940
Trim (after deicing)	-4.0	Inop	-1	75	7860	6.0	25	92.0	486	50	725
Trim (with 10 min ice)	-4.0	Inop	-1	76	7620	6.0	25	91.8	488	48	580
Trim (after deicing)	-3.0	Inop	+1	74	7190	6.0	25	92.0	488	47	440

Table A-1. UH-1H DEICING TEST PROGRAM TRIM POINT DATA (Cont)

Test Condition	Acft's OAT(°C)	Test OAT(°C)	Sys OAT(°C)	CAS (kts)	Alt. (ft)	Inlet ΔP (in. H₂O)	Torque (psi)	N₁ (%)	EGT (°C)	Fuel Coil. Pos(%)	RPM (lb)
LCC Test 31 Flight 27											
Trim (baseline)	-4.1	Inop	-1	75	5300	6.0	25	90.5	476		1125
Trim (with 8 min ice)	-5.0	Inop	+1	72	5260	6.5	27	91.2	482	45	1010
Trim (after deicing)	-4.5	Inop	+1	75	5300	6.0	25	90.8	480		950
Trim (with 3 min ice)	-5.0	Inop	+1	75	5260	7.0	32	92.3	492	45	880
Trim (after deicing)	-4.0	Inop	+1	75	5230	6.5	26	91.0	482		825
Trim (with 4 min ice)	-4.1	Inop	+1	75	5280	6.75	32	92.2	494		760
Trim (after deicing)	-4.0	Inop	+1	74	5300	6.5	26	91.0	482		515
LCC Test 34 Flight 31											
Trim (baseline)	-5.6	-6.2	-5	71	4350	6.0	25	90	470	41.0	975
Trim (with 8 min ice)	-7	-6.4	-6	78	4390	7.0	40-30	91.1	478	46.0	830
Trim (after deicing)	-6	-5.6	-5	77	4430	6.5	24	89.5	468	44.0	760
LCC Test 35 Flight 32											
Trim (baseline)	-6	-5.9	-6	75	4260	6.5	25	20	470	44	1150
Trim (with 8 min ice)	-7	-6.1	-6	75	4280	7.0	30	91	478	46	1050
Trim (after deicing)	-6	-6	-6	75	4280	6.5	26	90.1	472	42	980
Trim (with 4 min ice)	-7	-5.8	-6.5	75	4190	7.1	33	92	478	45	910
Trim (after deicing)	-6	-5.8	-6	75	4220	6.9	27	90.1	472	44	860

Table A-1. UH-1H DEICING TEST PROGRAM TRIM POINT DATA (Cont)

Test Condition	Acft's OAT(°C)	Test OAT(°C)	Sys OAT(°C)	CAS (kts)	Alt. (ft)	Inlet ΔP (in. H₂O)	Torque (psi)	N₁ (%)	EGT (°C)	Fuel Coll. Pos(%)	RPM (lb)
LCC Test 36 Flight 33											
Trim (baseline)	-8.5	-8.5	-7.5	75	5160	6.5	26	90.1	470	44	1200
Trim (with 8 min ice)	-9.0	-8.5	-8.0	74	5170	6.5	29	91.0	474	45	1090
Trim (after deicing)	-9.0	-8.6	-7.5	75	5160	6.5	26	90.0	470	45	1000
Trim (with 4 min ice)	-9.0	-8.4	-8.0	75	5250	7.0	32	92	482	45	910
Trim (after deicing)	-9.0	-8.4	-7.5	75	5150	6.5	26	90	470	44	850
Trim (after 3 deicing in cloud)	-8.0	-9.0	-9.0	75	5290	7.1	32	91.5	480	48	670
LCC Test 37 Flight 34											
Trim (baseline)	-7	-6.3	-6.5	75	4680	6.5	27	90.2	472	45	1180
Trim (with 2 min ice)	-7	-6.1	-7	75	4640	7.5	34	92.2	488	47	1120
Trim (after deicing)	-7	-6.4	-6	75	5850	6.5	26.5	90.8	476	47.5	1030
Trim (with 2 min ice)	-7	-6.3	-6.5	75	6020	7.5	35	93.1	496	49.5	1000
Trim (after deicing)	-7	-6.1	-6.0	75	6000	6.5	27.5	91.0	476	47.5	925
Trim (after 4 deicing cycles)	-10	-8.5	-8.25	75	8180	7.0	28	92.0	484	52	730
Trim (after deicing 2 min of ice)	-9	-8.4	-8.9	75	8940	7.0	31	93.0	494	55	610

Table A-1. UH-1H DEICING TEST PROGRAM TRIM POINT DATA (Cont.)

Test Condition	Acft's OAT(°C)	Test OAT(°C)	Sys OAT(°C)	CAS (kts)	Alt. (ft)	Inlet ΔP (in. H_2O)	Torque (psi)	N_1 (%)	EGT (°C)	Fuel Coll. Pos(%)	RPM (lb)
LCC Test 39 Flight 40											
Trim (baseline)	-13	-13.7	-12.5	75	8370	6.0	27	90.9	466	48	1160
Trim (with 8 min ice)	-14	-13.6	-12.5	75	8340	6.5	31	92.0	478	53	1050
Trim (after deicing)	-14	-13.5	-12.25	75	8280	6.5	28.5	91.2	472	50	975
Trim (with 4 min ice)	-13	-13.9	-12.5	75	8400	7.0	37.5	94.1	500	55	890
Trim (after deicing)	-17	-18.6	-16.0	75	10265	6.5	34.0	93.5	486	56	810
LCC Test 39 Flight 41											
Trim (baseline)	-18	-18.6	-16	75	10800	6.0	30	92.4	474	54	960
Trim (with 8 min ice)	-18	-17.3	-16	75	10400	6.5	34	93.9	490	57	840
Trim (after deicing)	-17	-17	-15	73	10330	6.25	30	92.3	476	53	775
Trim (after 2 deicing cycles in cloud)	-18	-19	-17	75	10950	6.2	32	93	479	55	575

12867-75